SEISMIC BEHAVIOR AND RETROFIT OF OUTRIGGER KNEE JOINTS

By

NASIM KHALIL SHATTARAT

A dissertation submitted in partial fulfillment of the
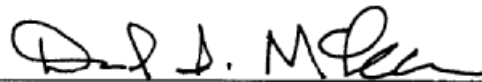requirements for the degree of

DOCTOR OF PHILOSOPHY IN CIVIL ENGINEERING

WASHINGTON STATE UNIVERSITY
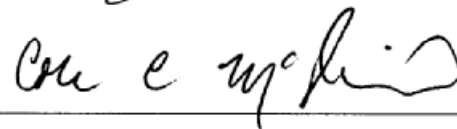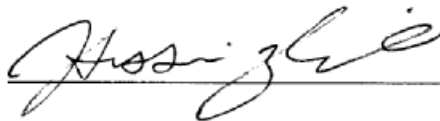Department of Civil and Environmental Engineering

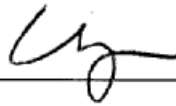AUGUST 2004

To the Faculty of Washington State University:

The members of the Committee appointed to examine the dissertation of NASIM KHALIL SHATTARAT find it satisfactory and recommend that it be accepted.

<div style="text-align: center">Chair</div>

ACKNOWLEDGMENTS

All praise belongs to God (Allah), the Lord and Cherisher of the universe, who made it possible for me to accomplish my goals.

SEISMIC BEHAVIOR AND RETROFIT OF OUTRIGGER KNEE JOINTS

ABSTRACT

By Nasim Khalil Shattarat, Ph.D.
Washington State University
August 2004

Chair: David I. McLean

The seismic vulnerability of outrigger knee joint systems in older bridges was demonstrated in the 1989 Loma Prieta, California earthquake and in the 2001 Nisqually, Washington earthquake. This research was conducted to obtain a better understanding of the seismic behavior of existing outrigger bents that incorporate deficiencies as present in the Spokane Street Overcrossing in western Washington State and to develop and evaluate the effectiveness of retrofit measures for improving their performance in an earthquake.

In this study, seven knee joint specimens were tested under simulated seismic loading. Three as-built specimens were tested, two under in-plane loading and one under out-of-plane loading. The as-built specimens failed at low ductility levels due to shear distress, low torsional strength of the beam, and reinforcement bond failures within the joint. Retrofit measures using steel jacketing were developed and applied to the remaining four knee joint specimens. Three of the specimens were retrofitted with circular steel jacketing around the joint and the beam; two were tested under in-plane loading and the third under out-of-plane loading. The fourth retrofitted specimen

represented a knee joint in a split outrigger bent and was upgraded with D-shaped steel jacketing and tested under in-plane loading. All retrofitted specimens performed well, achieving enhanced strength, ductility, drift ratio, and energy dissipation capacities.

Threshold principal tension stress values for evaluating existing outrigger joints with similar steel arrangement to those present in the Spokane Street Overcrossing were established. Principal tension stress values of $4.5\sqrt{f_c'}$ psi ($0.38\sqrt{f_c'}$ MPa) and $6.0\sqrt{f_c'}$ psi ($0.50\sqrt{f_c'}$ MPa) were set as limits beyond which joint shear cracking and joint failure, respectively, are expected.

The retrofit measures proposed in this study incorporate the use of an elbow-shaped steel jacket around the beam and the joint. Design and detailing guidelines for retrofitting outrigger bents were proposed, including for split outrigger bents. The guidelines include equations for the jacket thickness required to form a stable force transfer mechanism between the beam and the column reinforcement, to avoid anchorage failure of the column longitudinal bars, and to restrain the hooks on the beam bars.

TABLE OF CONTENTS

LIST OF TABLES

LIST OF FIGURES

To
My Mom and Dad
My Beloved Wife Abeer
& My Gorgeous Daughter Lana

CHAPTER ONE

INTRODUCTION

1.1 INTRODUCTION AND BACKGROUND

Several earthquakes have played a role in the development of seismic provisions for highway bridges. Earthquakes of particular significance are the 1933 Long Beach earthquake, 1940 EL Centro earthquake, 1971 San Fernando earthquake, 1989 Loma Prieta earthquake, 1994 Northridge earthquake and the 1995 Kobe earthquake in Japan. Each of these earthquakes tested the state-of-the-art for seismic engineering and led to improvements in the then-current practice.

Prior to the March 1933 Long Beach earthquake, there were no special provisions for the seismic design of highway bridges and buildings. Brick buildings with unreinforced masonry walls, including many of the school buildings in Long Beach and nearby areas, failed disastrously during this earthquake. As a direct result of the structural failures of unreinforced masonry schools, earthquake-resistant design and construction were mandated for public schools in California (Wood, 1933).

After the May 1940 El Centro earthquake, the bridge design office of the California Department of Transportation (Caltrans) specified minimum seismic design requirements for bridges which formulated the first code requirements in the United States for seismic design of bridges (Housner, 1990). The American Association of State Highway Officials (AASHO), the agency responsible for the development of bridge design specifications in the United States, adopted Caltrans seismic design specifications in 1961. The name of the agency was changed in 1973 to the American Association of

State Highway and Transportation Officials (AASHTO).

The February 1971 San Fernando earthquake, also known as the Sylmar earthquake, resulted in severe damage to hospitals and public utilities and the collapse of newly constructed highway overpasses (Roberts, 1996). Shortly after this catastrophic event, Caltrans, in 1973, issued new seismic design criteria for bridges introducing the effects of fault proximity, site conditions, dynamic structural response, and ductile details for reinforced concrete construction. Furthermore, Caltrans initiated a three-phase Bridge Seismic Retrofit Program for upgrading older, non-ductile bridges following the 1971 San Fernando Earthquake. The first phase of the program involved installation of hinge and joint restrainers intended to prevent deck joints from separating (Roberts, 1992).

The October 1989 Loma Prieta earthquake and resulting bridge damage led to acceleration of the Bridge Seismic Retrofit Program adopted by Caltrans. The damage to the China Basin and the I-880 freeway, and collapse of the Cypress Viaduct, the dropped span in the east crossing of the San Francisco-Oakland Bay Bridge, and the collapse of Struve Slough Bridge near Monterey highlighted weaknesses in the joints within bents, lack of ductility in beams and columns, and poor resistance to longitudinal loads (EERI, 1990). Consequently, there was an increased call for retrofit activities commensurate with the enormity of the problem.

Since then, Caltrans identified 860 structures that required retrofit, 122 of which had been strengthened at the time of the January 1994 Northridge Earthquake. Furthermore, Caltrans sponsored a number of research studies investigating the seismic response of reinforced concrete knee joints at the University of California at San Diego and at the University of California at Berkeley. While the 1994 Northridge earthquake

resulted in the collapse of 11 overpasses on some of the busiest freeways in Los Angeles and the San Fernando Valley, it showed the enhanced performance of new and retrofitted bridges during the earthquake, in which all 122 strengthened structures were undamaged.

The seismic behavior of beam-column joints in buildings has been extensively researched since the late 1960's (Wallace et al., 1996). However, the cyclic behavior of knee joints found at the top of multi-storey building frames and in bridges only received attention after the 1989 Loma Prieta earthquake, specifically focusing on the behavior of outrigger bridge knee joints (Megget, 2000).

Typically, bridge structures consist of a stiff bridge deck spanning between transverse bents. In most cases, the columns of the bent are close to the deck, resulting in a regular bent with an integral cap beam between the deck and the beam-column joint (Stojadinovic and Thewalt, 1995). In cases where geometric or right-of-the way constraints prevent the use of regular bents, one or more of the columns may be moved outwards and the cap-beam extended to form an outrigger bent. Under seismic loading, outrigger bents are subject to gravity forces combined with both in-plane and out-of-plane lateral loads, resulting in complex bending, shear and torsion within the bents. Past experience has demonstrated the vulnerability of the knee joints in outrigger bents, particularly in older, poorly detailed joints, but even in relatively recent construction, as was the case in the 1989 Loma Prieta earthquake.

Outrigger knee joints are present in a number of concrete bridges nationwide. In Washington State, outrigger bents are present in several important bridges such as the Alaskan Way Viaduct, the I-90/I-5 interchange, and the SR 99 Spokane Street Overcrossing. Figure 1.1 shows an outrigger bent from the SR 99 Spokane Street

Overcrossing.

Figure 1.1 Outrigger Bent in the SR 99 Spokane Street Overcrossing

A complicating factor present in a number of bridges with outriggers in Washington State, including in the Spokane Street Overcrossing, is the presence of splits in some of the bents. Expansion joints are located at the ends of every fourth bent, with a split column being common to both bents in order to accommodate longitudinal movement within the bridge. Typically, a 2-in. (5-cm) gap is incorporated into the split columns. In the outrigger bents, this split carries through the outrigger beams and knee joints, making the development and installation of effective retrofit measures challenging.

After the April 29, 1965 Seattle earthquake, significant cracks were observed in a number of the split columns in the SR 99 Spokane Street Overcrossing. Horizontal

flexural cracks on the exterior surfaces opposite the split were reported at many locations, while vertical cracks starting from the bottom of the split were reported at two column locations (Zhang et al., 1996). Concern was expressed in regard to the possibility of collapse of the split columns had the earthquake been stronger. A previous study performed by Kramer and Eberhard (1995) found similar potential vulnerabilities in the split columns present in the Alaskan Way Viaduct.

Following the February 28, 2001 Nisqually earthquake, there was notable structural damage to a curved bridge unit in the Alaskan Way Viaduct. Major concrete cracking in the knee joints of this unit was observed in the vicinity of welded reinforcing bar laps. Furthermore, there was concrete cracking in the transverse floor beams at one of the bents (T. Y. Lin International, 2001). Figure 1.2 shows damage to a knee joint in the Alaskan Way Viaduct.

Figure 1.2 Damage to a Knee Joint in the Alaskan Way Viaduct

While California is considered to be the national leader in bridge seismic retrofit, the need to seismically retrofit older bridges has been recognized by departments of transportation in other states where seismic considerations exist. The Washington State Department of Transportation (WSDOT) has funded several research projects to better understand the seismic performance of bridges following the 1989 Loma Prieta earthquake. Several studies in 1995 and 1996 at the University of Washington were conducted to investigate the seismic vulnerability of the Alaskan Way Viaduct (T. Y. Lin International, 2001). Other studies were performed by the WSDOT on the SR 99 Spokane Street Overcrossing. These studies included probabilistic seismic hazard analysis, geotechnical considerations, pushover analysis of a typical bridge unit, bridge load rating, inspection of structural damage and crack gages, design of seismic retrofit measures, and replacement and retrofit cost estimates. In addition, a recent experimental study was completed at Washington State University (McLean, El-Aaarag and Rogness, 2001) that investigated the seismic performance of split columns and developed retrofit strategies for such columns. However, none of the previous studies was directed to evaluate the seismic performance of the outrigger knee joints under in-plane and out-of-plane motions.

Both the SR 99 Spokane Street Overcrossing and the Alaskan Way Viaduct were built in the early 1950's with little or no seismic considerations as part of the design. These bridges provide an important part of the transportation system in downtown Seattle, and there is no viable detour for traffic if they are closed, as was the case during 2001 Nisqually earthquake. Replacing the SR 99 Spokane Street Overcrossing and the Alaskan Way Viaduct with less vulnerable structures is desirable, but the SR 99 Spokane

Street Overcrossing replacement cost was estimated at $46.7 million in 1996 (Zhang et al., 1996), while the replacement of the Alaskan Way Viaduct cost was estimated at $879 million in 2001 (T. Y. Lin International, 2001). The necessary funds to replace these bridges are unlikely to become available in the immediate future. Consequently, it is imperative that the WSDOT maintain and strengthen the bridges to the extent that funds permit. WSDOT has implemented a first phase of retrofitting for the Spokane Street Oversrossing, including retrofitting the columns with steel jackets and installing joint restrainers. For the split columns, "D" shaped steel jackets were used in order to maintain the gap in the split columns, as shown in Figure 1.3.
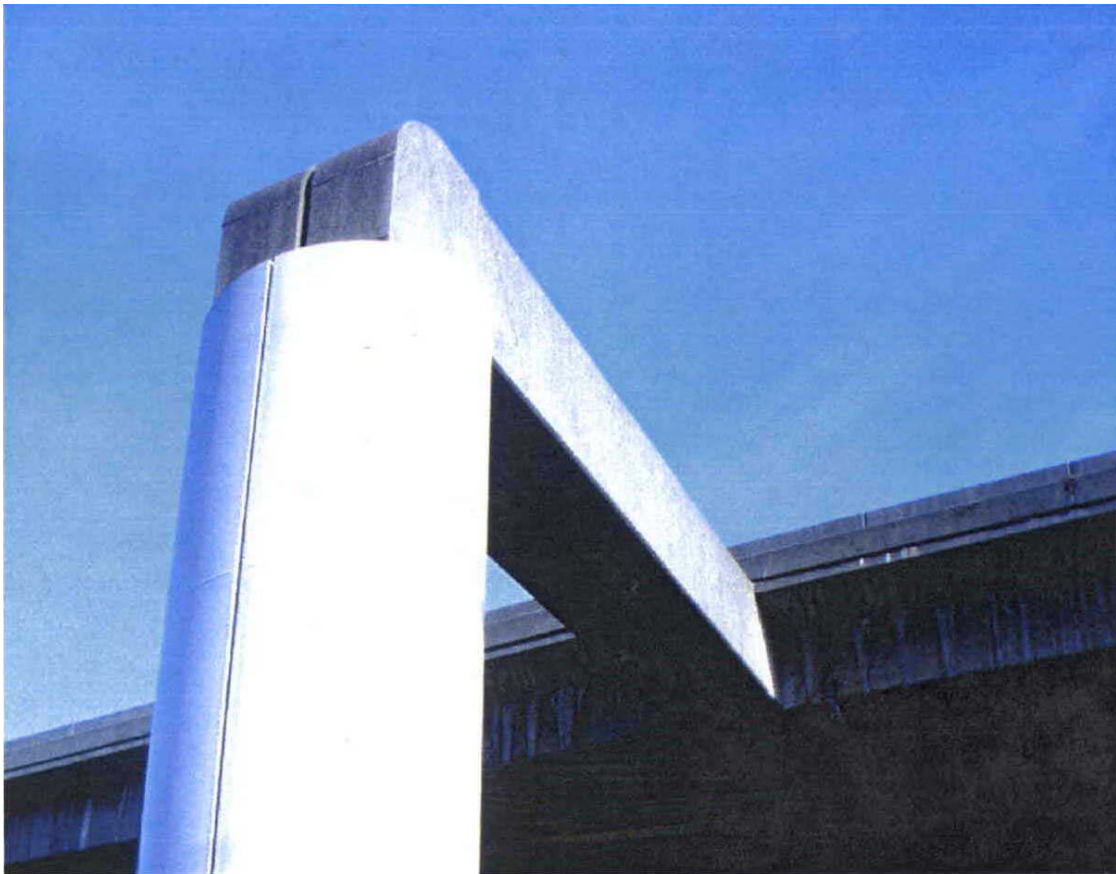
Figure 1.3 Retrofitted Split Columns in the SR 99 Spokane Street Overcrossing

The behavior of the knee joint systems in the SR 99 Spokane Street Overcrossing was selected as the focus of this study. The bridge is one of two major north-south highways through downtown Seattle. It begins in Fife at I-5 Exit 137 and ends near the Everett Mall at I-5 Exit 189. The bridge carries an average of 63,000 vehicles per day and was designed in 1957 (Zhang et al., 1996). The bridge was probably designed in accordance with the 1953 AASHO Standard Specifications for Highway Bridges. Construction of the bridge began in March 1958, and it was opened to traffic in September 1959. Part of the structure consists of cast-in-place reinforced concrete box girders. The other two parts of the bridge consist of steel plate girders, which span over Spokane Street, and timber stringer-trestle approach spans at the south end. The reinforced concrete box girders are supported on forty-three bents, of which twelve have outrigger knee joints. A typical view of an outrigger knee joint is shown in Figure 1.1.

Several previous studies have investigated the seismic behavior and retrofit of outrigger bents. However, these studies did not address all of the deficiencies present in the outrigger bents of the Spokane Street Overcrossing. Further, the retrofit measures proposed in these earlier studies are expensive to implement and hard to directly apply to split columns. Therefore, the behavior of as-built outrigger knee joints under both in-plane and out-of-plane lateral loadings needs further investigation, and new retrofitting methods need to be developed and evaluated for application to the outrigger knee joints present in Spokane Street Overcrossing, including application to the split outrigger joints.

1.2 OBJECTIVES AND SCOPE

The overall goals of this research are to obtain a better understanding of the seismic behavior of existing knee joints and to develop and evaluate the effectiveness of the retrofit measures for improving their performance in outrigger bents. To achieve these two goals, five objectives were established:

1) evaluate and define the vulnerabilities of outrigger bents under seismic and gravity loadings;

2) develop appropriate retrofit measures for outrigger knee joints that address the identified vulnerabilities;

3) evaluate through experimental testing the feasibility of and benefits resulting from retrofit measures applied to outrigger knee joints;

4) develop recommendations for the seismic assessment of the existing outrigger knee joints; and

5) provide design and detailing guidelines for a practical retrofit method for improving the performance and safety of outrigger bents in bridges.

1.3 ORGANIZATION OF DISSERTATION

This dissertation is organized as follows. A background of the current knowledge about the behavior of knee joints under seismic loading is presented in Chapter Two. This includes discussion of damage to knee joints in previous earthquakes, a review of previous experimental investigations into cyclic behavior of knee joints, and joint design recommendations.

The development of the experimental program is presented in Chapter Three. This chapter includes the selection of the prototype, dimensional scaling, test configuration and specimen variables, specimen reinforcement details, material properties, experimental setup, loading system, and instrumentation.

In Chapter Four, the results of the experimental program are presented. Three 1/3-scale specimens replicating the existing outrigger knee joints and four retrofitted specimens were tested. Observed specimen behavior and test results are discussed first, followed by a comparative overview of the test results, including force-displacement response envelopes, specimen ductility and drift ratios.

Chapter Five gives procedures for the seismic assessment of existing knee joints. Recent recommendations by other researchers, provisions in design documents and the results of the current study are used to propose assessment procedures for existing knee joints.

Chapter Six provides retrofit guidelines for outrigger knee joints. A review is made of possible failure modes in existing knee joints and vulnerabilities in outrigger knee joints. This is followed by a discussion of the retrofit design and detailing requirements to enhance the seismic performance of outrigger knee joint systems in the opening and the closing directions.

Lastly, conclusions and recommendations resulting from this study are presented in Chapter Seven.

CHAPTER TWO

LITERATURE REVIEW

2.1 INTRODUCTION

In this chapter, current knowledge about the behavior of outrigger knee joints under cyclic loading is reviewed. This review includes discussion of damage to knee joints from past earthquakes, previous tests on as-built bridge knee joints and on retrofitted joints, and joint design recommendations.

2.2 KNEE JOINT FAILURES

In 1989, a major earthquake struck northern California causing severe damage to San Francisco's highway system. The most lethal damage occurred on Interstate 880, when that highway's upper deck collapsed onto its lower roadway, as shown in Figure 2.1, killing 43 people, (Priestley et al., 1996). Joint shear failure was identified as the major contributor to this collapse.

Clear evidence of joint shear failure of outrigger knee joints was first recognized in the 1989 Loma Prieta earthquake (Priestley et al., 1996). The damage was not limited to joints in older bridges; knee joints in newly designed and constructed bridges also experienced distress. The main reasons for damage to outrigger knee joints in that earthquake were unsatisfactory detailing of the column and beam reinforcement extensions into the joint, lack of a force transfer mechanism between the members meeting at the joint, especially in the opening direction, and lack of joint horizontal and

vertical reinforcement (Priestley et al., 1996). Figures 2.2 through 2.4 show some examples of joint failures that occurred during the Loma Prieta Earthquake.

Figure 2.1 Cypress Viaduct After Loma Prieta Earthquake
http://www.sfmuseum.org/1989/89photos.html

Figure 2.2 Damage to an Outrigger Bent in the I-280 China Basin Viaduct, 1989
Loma Prieta Earthquake (Adapted from Priestley et al., 1996)
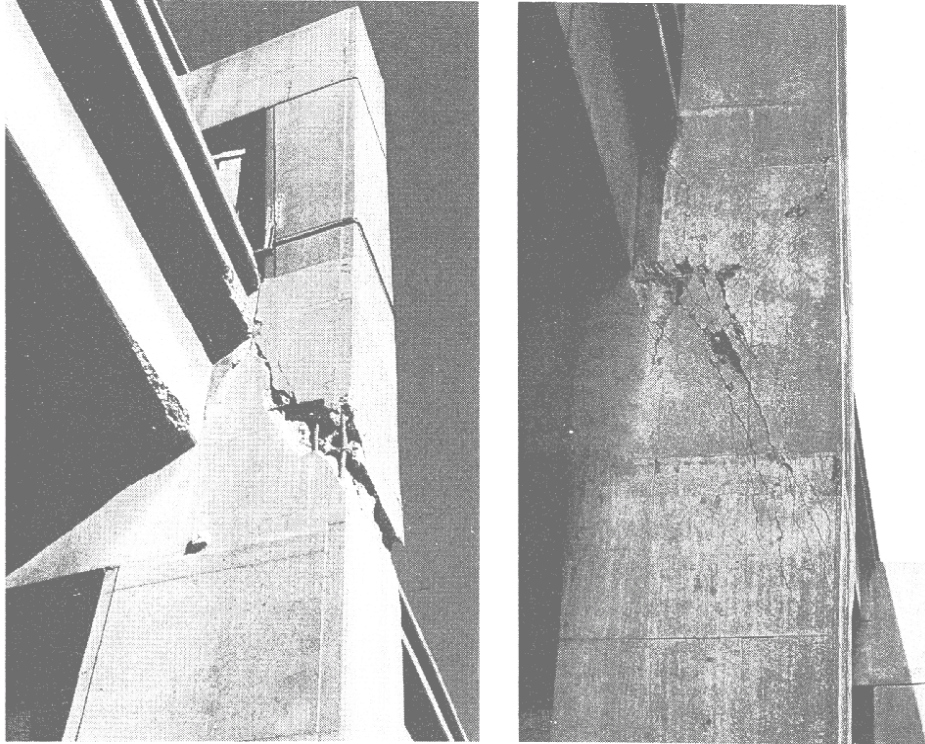
Figure 2.3 Joint Shear Failure, 1989 Loma Prieta Earthquake (a) I-880 Viaduct, (b) Embarcadero Viaduct (Adapted from Priestley et al., 1996)

Figure 2.4 I-980 Joint Failure , 1989 Loma Prieta Earthquake (Adapted from Ingham et al., 1994a)

In 2001, a significant earthquake occurred in the Puget Sound area of western Washington State, referred to as the Nisqually earthquake. In general, bridge structures performed very well during that earthquake, attributed to the retrofit efforts put forth by WSDOT (Filiatrault et al., 2001). However, there was observed damage in the outrigger bents of several bridges. Figures 2.5 and 2.6 show the damage to knee joints in the Spokane Street Overcrossing and in the Alaskan Way Viaduct near South Washington Street, respectively.

Figure 2.5 Cracks in Outrigger Knee Joints

Figure 2.6 Cracking on Outrigger Beams, 2001 Nisqually Earthquake (http://www.wsdot.wa.gov/projects/viaduct/deis/chapter1_1.htm)

2.3 SEISMIC BEHAVIOR OF AS-BUILT AND RETROFITTED BRIDGE OUTRIGGER KNEE JOINTS

The 1989 Loma Prieta earthquake highlighted the need for improved understanding of the performance and design of bridge knee joints. In response, two significant research studies were conducted in California. As-built specimens modeling the actual damaged bridges were tested, and retrofit strategies were then proposed and evaluated through further testing.

2.3.1 Ingham, Priestley, and Seible (1994a, 1994b)

Researchers at the University of California at San Diego investigated the in-plane behavior of outrigger knee joints using eight one-third-scale test specimens. These specimens represented an as-built knee joint followed by a repair, a retrofit and a redesign for two basic member configurations. The first test focused on a rectangular

column configuration representing a bent in the I-980 southbound connector in Oakland, California, a bent that performed poorly during the 1989 Loma Prieta earthquake. The second test considered a circular column configuration modeling a bent in the I-105 in Los Angeles, California, a structure having joint reinforcement detailing typical of the 1991 practice in the state of California.

The test setup shown in Figure 2.7 modeled the knee joint, outrigger beam, and the upper section of the column. To ensure proper simulation of the seismic forces in the beam and the column, the actuator was inclined so that its line of action passes through the point representing the base of the column. Replication of the prototype dead load forces was achieved using prestressed tendons applied at a location corresponding to the cap beam point of contraflexure for a uniformly distributed load.
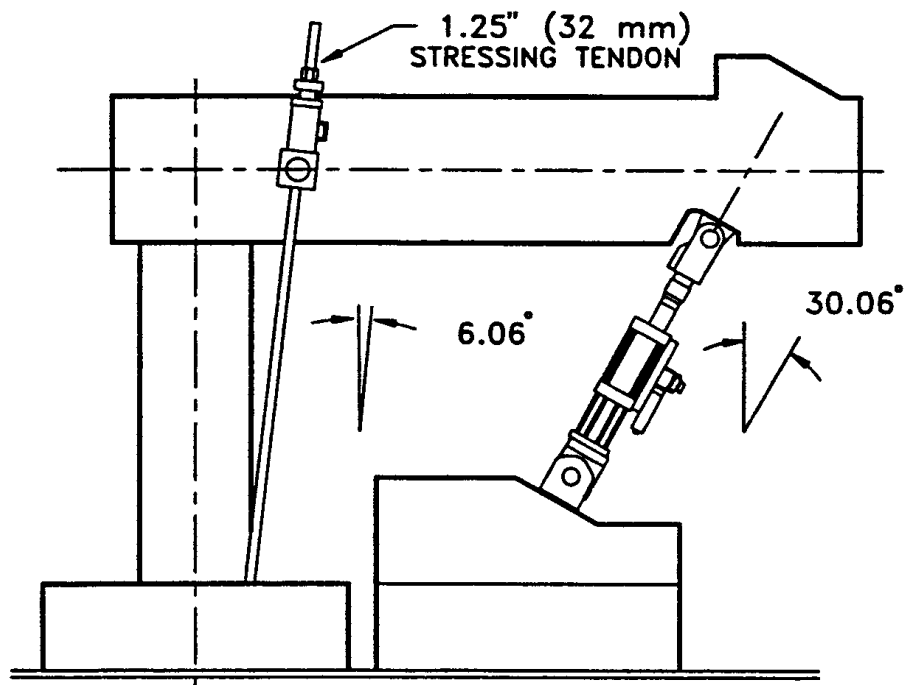
Figure 2.7 Test Configuration (Adapted from Ingham et al., 1994b)

As-built specimen with a rectangular column

Reinforcement details of the as-built specimen with a rectangular column configuration are shown in Figure 2.8. Experimental test results showed that the test specimen performed poorly in the joint-closing direction. Extensive diagonal splitting occurred before attaining the target displacement during cycling to a displacement ductility level (μ_Δ) of -0.8 in the closing direction. Following attainment of this displacement level, bond failure of the unconfined lap-splice between the vertical tails of the top cap beam reinforcement and the embedded longitudinal column reinforcement occurred, as shown in Figure 2.9.
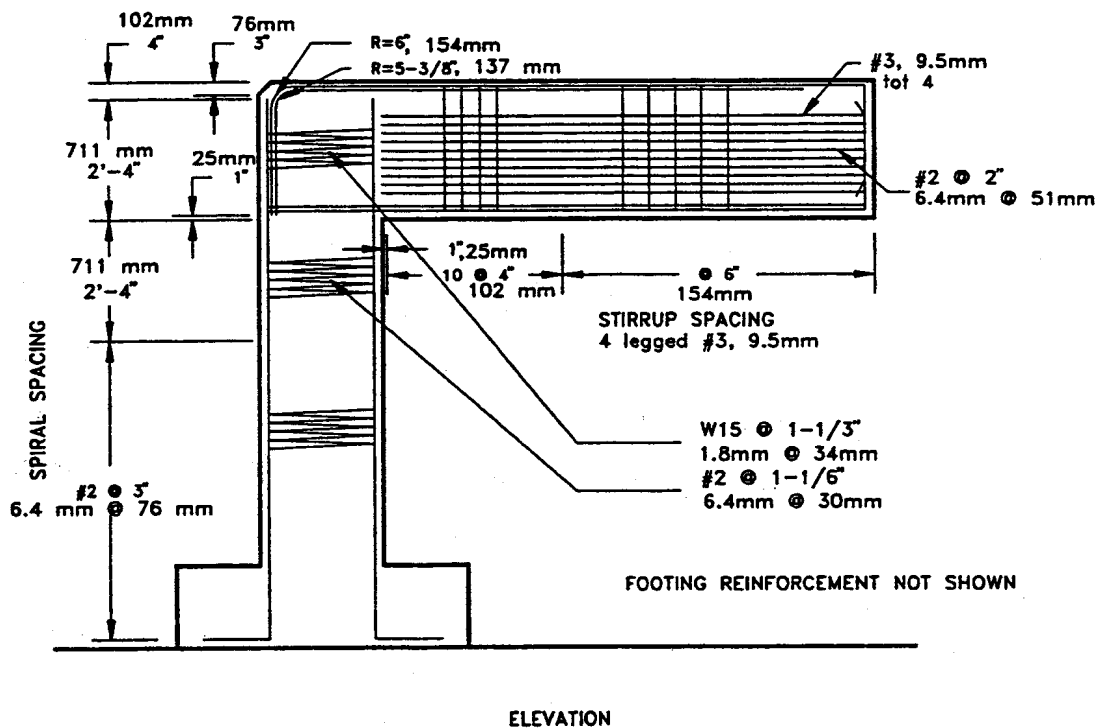
Figure 2.8 Reinforcement Details of as-Built Specimen with a Rectangular Column Configuration (Adapted from Ingham et al., 1994a)

17
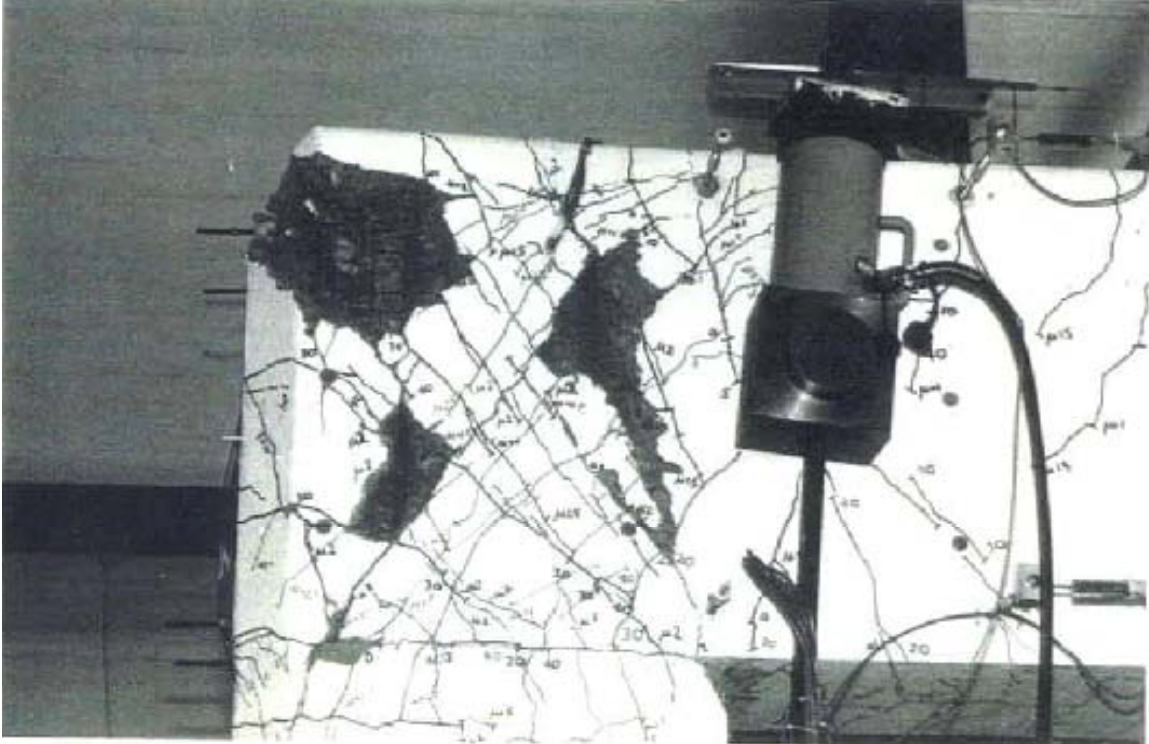
Figure 2.9 Joint Status at the End of the Test (Adapted from Ingham et al., 1994a)

The force-displacement history, shown in Figure 2.10, indicates that the test specimen failed to support the calculated theoretical yielding strength in the joint opening and closing directions. The measured flexural strength of the as-built test specimen was approximately 75% of the predicted strength using conventional flexural analysis. Joint principal tension stress reached a maximum of around $5.8\sqrt{f_c^{'}}$ psi ($0.48\sqrt{f_c^{'}}$ MPa) in the closing direction before failure, while the compression tensile stress reached a maximum of approximately $0.15 f_c^{'}$, with $f_c^{'}$ being the measured compression strength of the concrete used in the specimens. The principal stresses were determined using a simple Mohr's circle analysis, as discussed by Priestley et al. (1996). Vertical displacement

ductilities of 2.4 and –1.2 were reported for opening and closing directions at the end of the test, respectively.
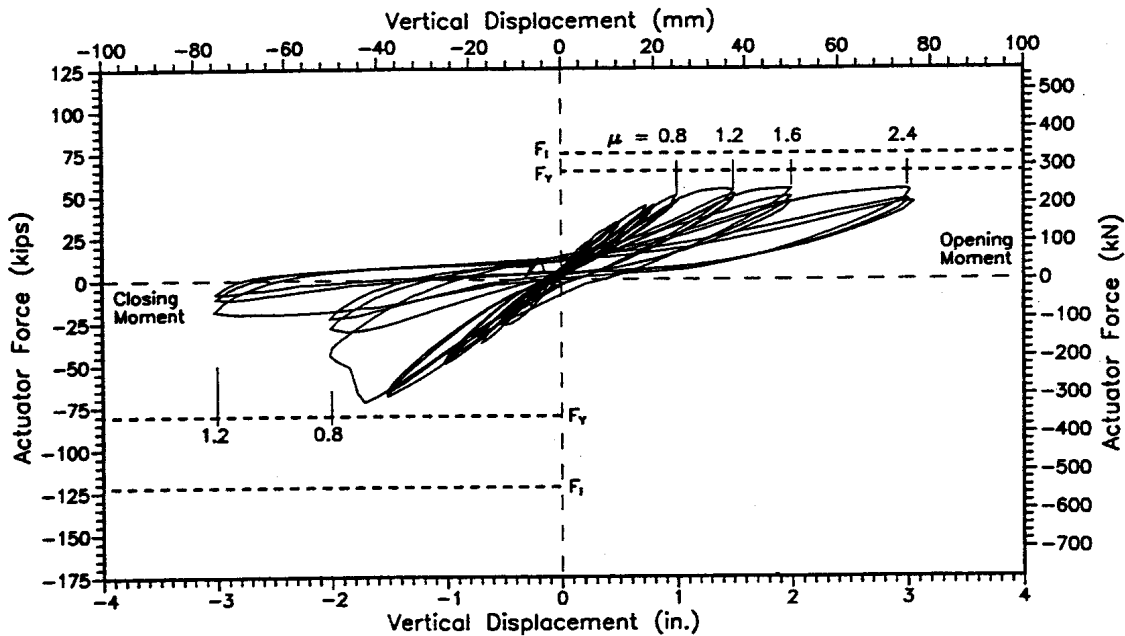
Figure 2.10 Actuator Force-Beam End Vertical Displacement History (Adapted from Ingham et al., 1994a)

Retrofit of as-built specimen with a rectangular column

Following the test of the as-built specimen, a retrofit strategy was adopted which utilized external prestressing of the cap beam and joint incorporating bolsters on the back face of the joint, as shown in Figure 2.11. The aim of the retrofit measure was to force plastic hinging in the column under positive and negative moments. Thus, the level of the prestressing force was chosen to ensure sufficient flexural strength of the cap beam, provide confining pressure to the lap splice between the longitudinal column reinforcement and the vertical tails of the top cap beam reinforcement, and to provide hook restraint for the top cap beam reinforcement.

19
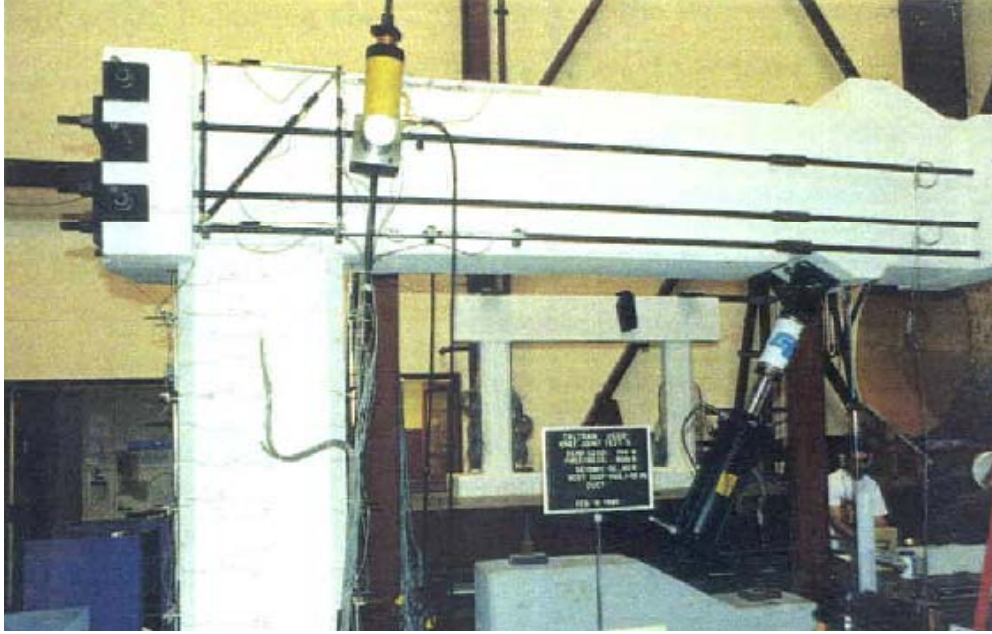
Figure 2.11 Retrofitted Technique Using External Prestressing (Adapted from Ingham et al., 1994a)

The retrofit strategy was shown to be an effective retrofit technique as it assisted in overcoming the identified deficiencies and provided higher strength and ductility than in the as-built specimen. However, tests on the retrofitted specimen revealed that the principal compression stress in the joint became the dominant stress influencing the joint behavior due to prestressing forces. This resulted in a decay of the joint integrity due to crushing of the compression diagonal struts under cyclic loading, which in turn provided poor anchorage for the embedded longitudinal reinforcement. Crushing of the diagonal compression strut is shown in Figure 2.12. Furthermore, the researchers pointed to the impracticality of applying this retrofit scheme to existing outrigger bents because of obstruction from the superstructure of the bridge.

At the end of the test, the specimen was able to attain a displacement ductility level of ±3 in both directions. The maximum calculated joint principal tension stress was

approximately $9.0\sqrt{f_c'}$ psi $(0.75\sqrt{f_c'}$ MPa), while the maximum principal compression stress was around $0.25\,f_c'$, which is significantly higher than that obtained in the as-built specimen, $0.15\,f_c'$
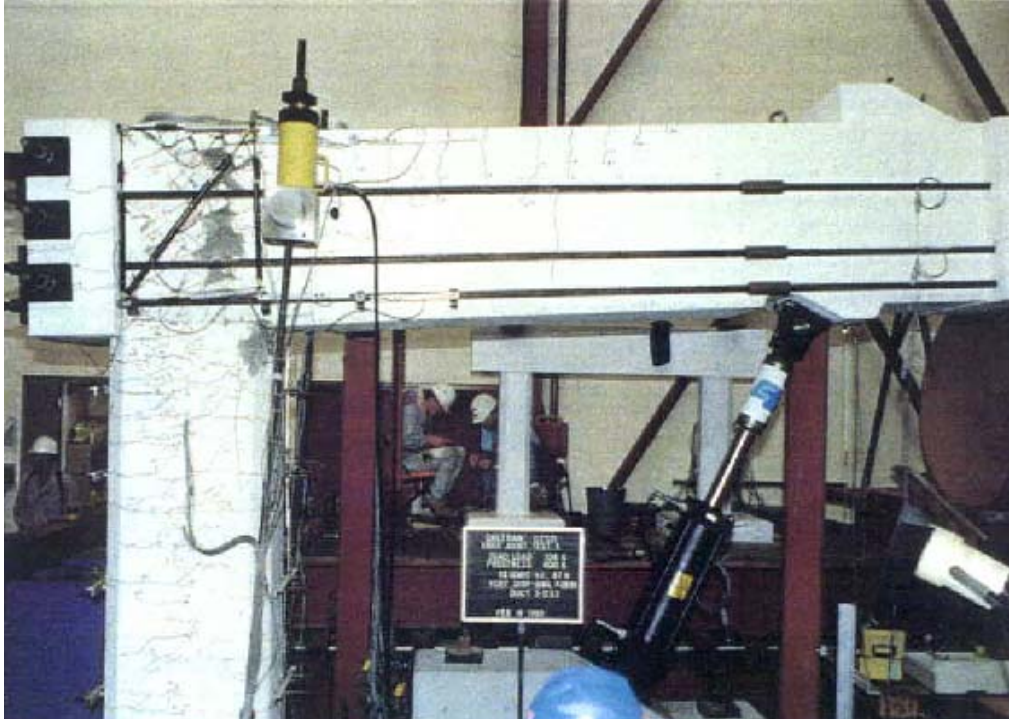
Figure 2.12 Crushing of the Diagonal Compression Strut (Adapted from Ingham et al., 1994a)

As-built specimen with a circular column

The second one-third scale as-built specimen was designed with different reinforcement details than the first one. The specimen had a circular column and connected positive and negative longitudinal outrigger beam reinforcement with vertical and horizontal joint stirrups, as shown in Figure 2.13. The actuator force-vertical beam end displacement history is shown in Figure 2.14. The history demonstrates that the specimen was not able to attain the ideal strength in both directions and had limited

energy dissipation capacity. The behavior exhibited by the second test specimen indicated a failure to develop a stable joint-opening force transfer mechanism due to bond failure along the column longitudinal reinforcement because of inadequate embedment length. However, the specimen performed better than the first as-built specimen due to the presence of joint vertical and horizontal reinforcement and the effective detailing of the beam reinforcement extending into the joint. The specimen achieved a vertical displacement ductility of 2.8 and -3.0 in the opening and the closing direction, respectively, and the maximum joint principal tension stress was $10.0\sqrt{f_c'}$ psi $(0.83\sqrt{f_c'}$ MPa). Figure 2.15 shows the test specimen at final stages of the test.
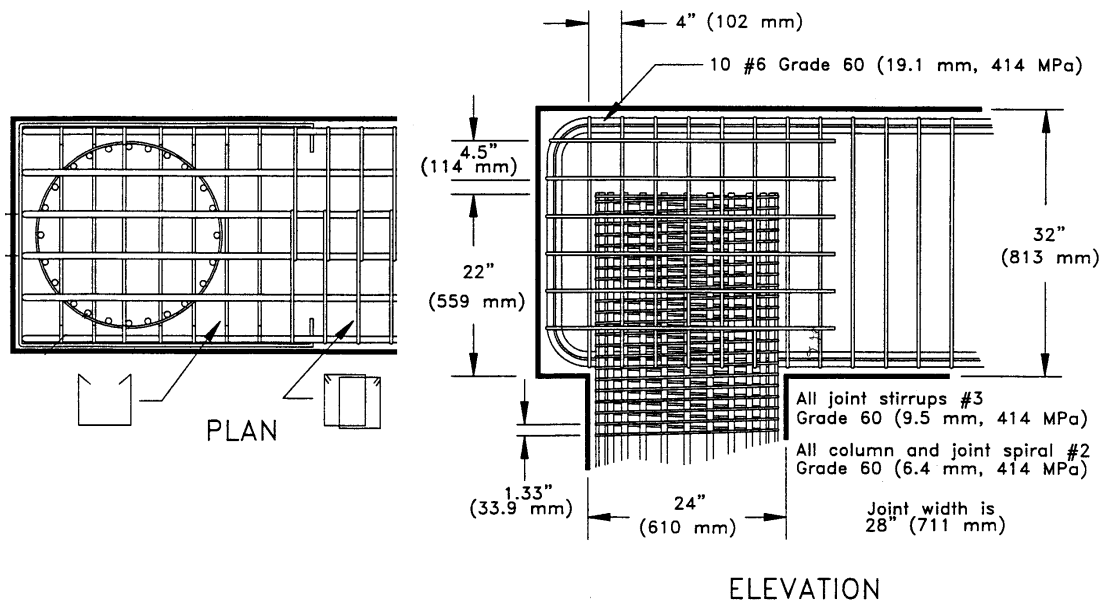
Figure 2.13 Joint Reinforcement Details of as-Built Specimen with a Circular Column (Adapted from Ingham et al., 1994b)

22
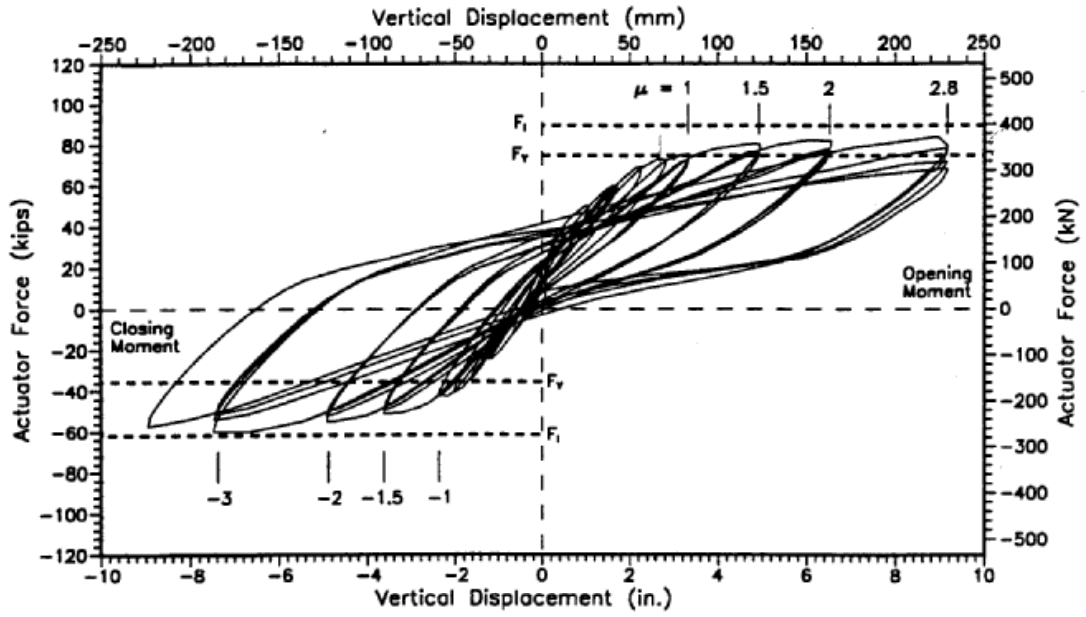
Figure 2.14 Actuator Force-Beam End Vertical Displacement History (Adapted from Ingham et al., 1994b)
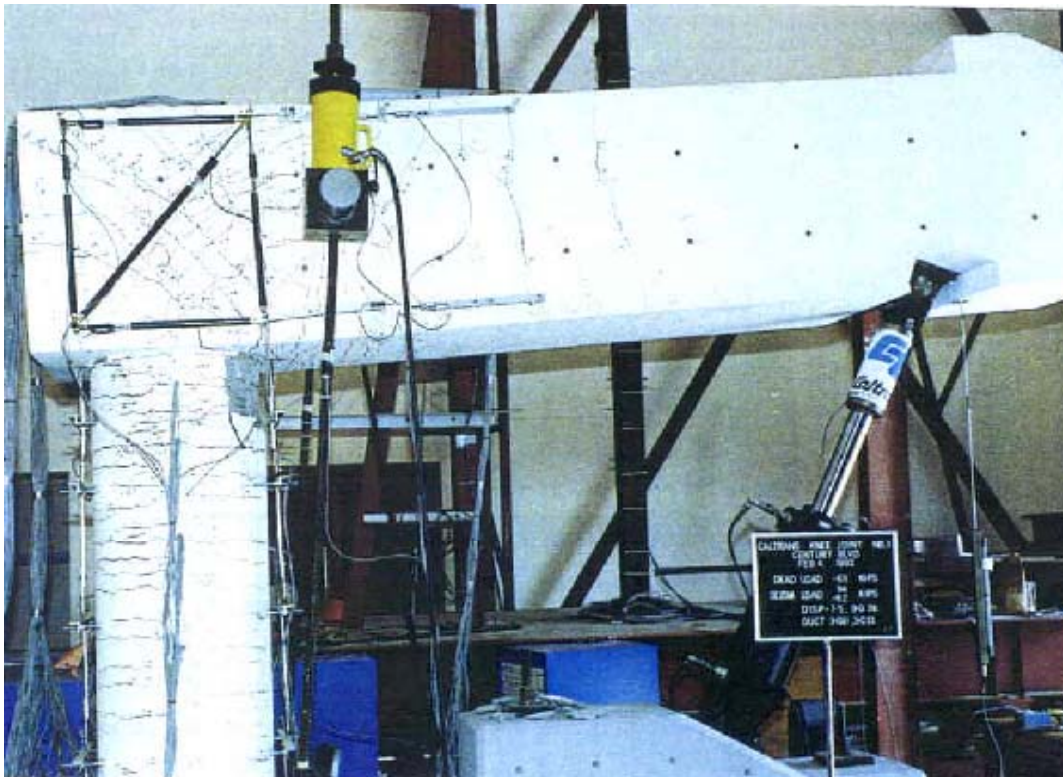
Figure 2.15 Test Specimen at a Ductility of 3 in the Joint Opening Direction (Adapted from Ingham et al., 1994b)

Retrofit specimen with a circular column

The retrofit measures for the second as-built specimen incorporated the use of a lightly reinforced concrete jacket encasing the joint. The main objectives of this retrofit scheme were to support a mechanism for which the column tension force is transferred to the vertical cap beam tails in the closing direction, ensure elastic behavior of the joint for both the retrofit jacket and the as-built reinforcement at the most final stages of the test, improve the confinement upon the vertical tails of the beam reinforcement, and to ensure adequate embedment length for the longitudinal column reinforcement. The latter was achieved through a haunch in the joint. Reinforcement details of the retrofitted joint are shown in Figure 2.16.
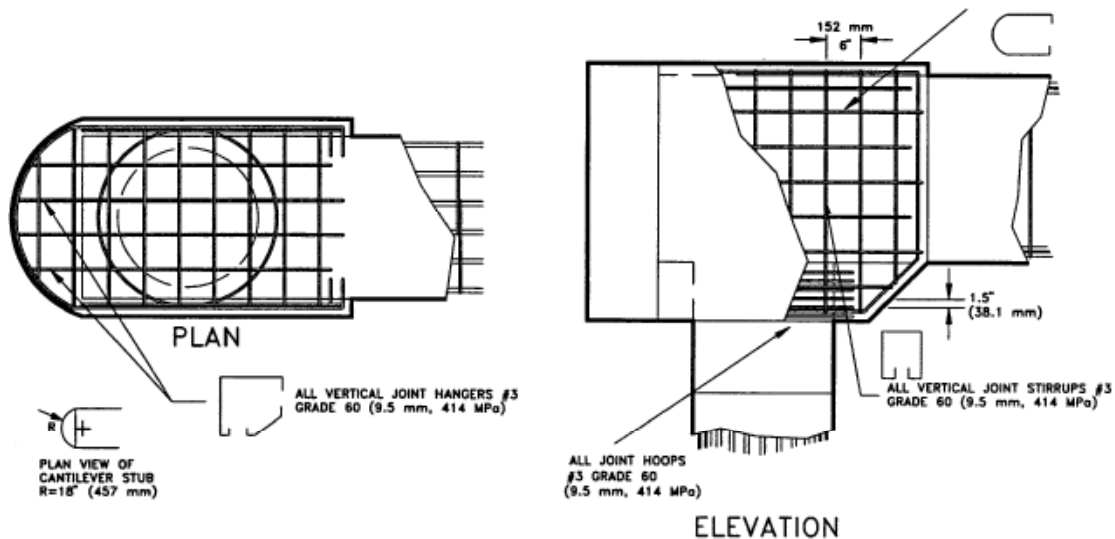
Figure 2.16 Joint Reinforcement Details of the Retrofitted Specimen (Adapted from Ingham et al., 1994b)

Testing showed that the retrofit strategy satisfied the targeted goals and the specimen reached the calculated ideal strength in both directions. In comparison to the as-built specimen, Figure 2.17 demonstrates that the retrofit specimen had more displacement ductility capacity and regular hysteretic behavior. The haunch in the joint effectively engaged the as-built joint reinforcement as the joint responded in essentially an elastic manner, as intended. The maximum principal tension stress in the joint was around $10.0\sqrt{f_c^{'}}$ psi ($0.83\sqrt{f_c^{'}}$ MPa).
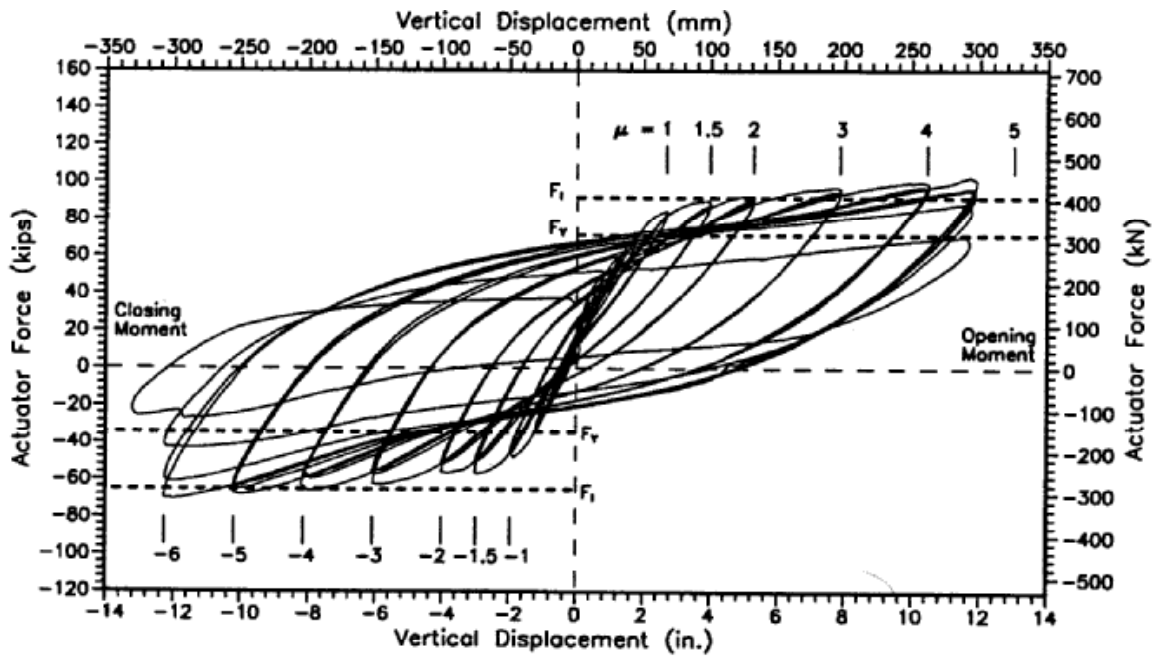
Figure 2.17 Actuator Force-Beam End Vertical Displacement History (Adapted from Ingham et al., 1994b)

2.3.2 Stojadinovic and Thewalt (1995)

Researchers at the University of California at Berkeley investigated the performance of as-built outrigger knee joints under in-plane and out-of-plane seismic loading simultaneously. Two as-built half-scale models, one with a long and one with a short outrigger beam, were constructed and tested to evaluate the performance and establish the failure mechanism of existing systems. A simultaneous bi-directional displacement pattern simulating the anticipated motion of the prototype under the effect of an earthquake was applied using a pair of horizontal 150-kip (667-kN) actuators positioned at an approximately 40-degree angle to the beam axis. Vertical loading simulating the changes in the column axial load caused by the outrigger bent frame action, and the gravity load was applied using a pair of 50 kips (224 kN) vertical actuators. Figure 2.18 shows the test setup utilized in the study.

Elevation   Side View

Plan
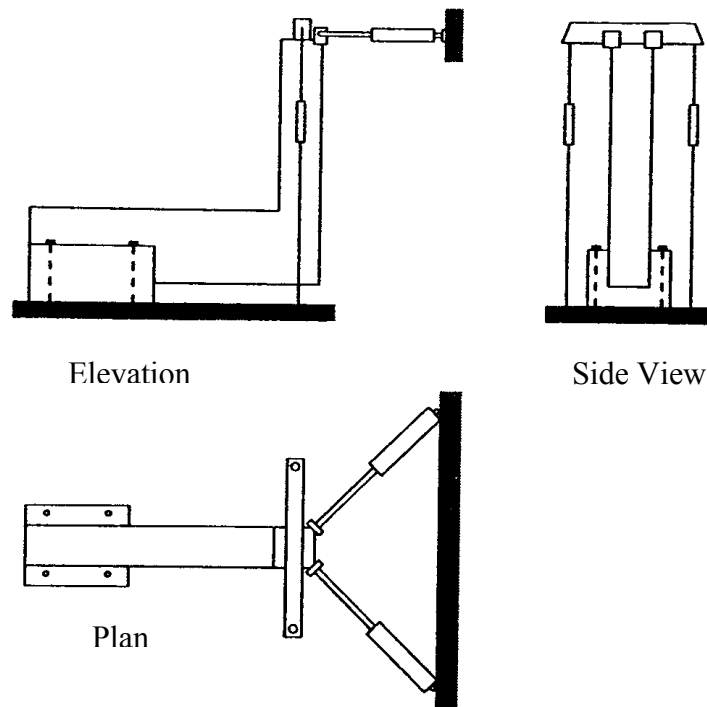
Figure 2.18 Test Setup (Adapted from Stojadinovic and Thewalt, 1995)

As-built specimens

The specimen with the long outrigger beam was a replica of bent B20 on the I101/I280 Interchange at Alemany Boulevard in San Francisco, while the specimen with the short beam was a model of a typical knee joint system found on elevated highway structures. Both of the specimens had inadequate joint confinement and detailing. The beam transverse reinforcement consisted of open U-shaped stirrups topped with U-shaped caps. Figures 2.19 and 2.20 show the reinforcement details of the as-built short and long specimen, respectively.
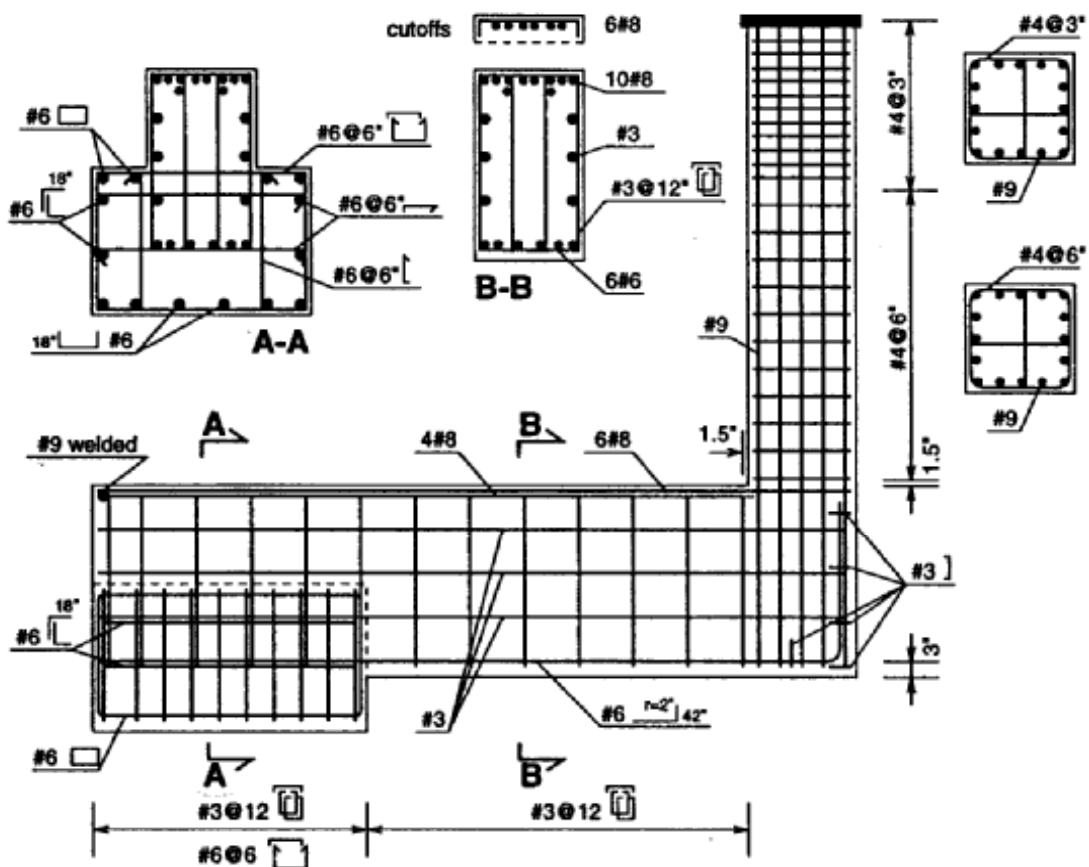
Figure 2.19 Reinforcement Details of the As-Built Long Beam Specimen (Adapted from Stojadinovic and Thewalt, 1995)

Figure 2.20 Reinforcement Details of the As-Built Short Beam Specimen (Adapted from Stojadinovic and Thewalt, 1995)

Both as-built specimens performed in a brittle manner with low force and displacement capacity. Analysis of the measurements collected from the specimens showed an initial yielding drift ratio of 0.7% and 0.5% for the long and the short outrigger beam specimens, respectively. Shortly after yielding, a splitting bond failure was observed in the region where the outside column bars overlapped with the beam bottom bar hook extensions. The bond split failure, which occurred at a drift ratio of approximately 1% in both specimens, was evident in the sudden drop in strains measured at three locations along a column bar in the exterior corner of the column and the abrupt

drop in the capacity, as evident in the force displacement responses shown in Figures 2.21 and 2.22. Further loading of the specimens showed a significant loss in transverse joint opening strength due to the deterioration of the anchorage of the interior column bars.

The as-built specimens with long and short outrigger beam attained displacement ductilities, defined using the column tip transverse displacement, of 1.5 and 2.0 respectively. The joint shear stress coefficient, defined according to ACI-ASCE C-352 85, at the point of specimen failure was 4.43 and 5.90 for the as-built long and short outrigger beam specimens, respectively. Strains measured in column bars and hoops as well as measured and computed moment-curvature response of both specimens showed that the columns had enough shear strength to yield the critical column cross section in bending. Behavior of the tested specimens under joint opening showed a better performance than under joint closing because the column reinforcement was better anchored at the inside of the knee joint. Furthermore, both specimens showed a different response in the longitudinal direction. The long outrigger beam torsion capacity was inadequate due to the lack of closed stirrups, while the short specimen showed a higher force capacity with very small torsional deformations for the beam functioning as an extension of the knee joint. Figures 2.23 and 2.24 show the status of the as-built short and as-built long specimens, respectively, at the end of the test.
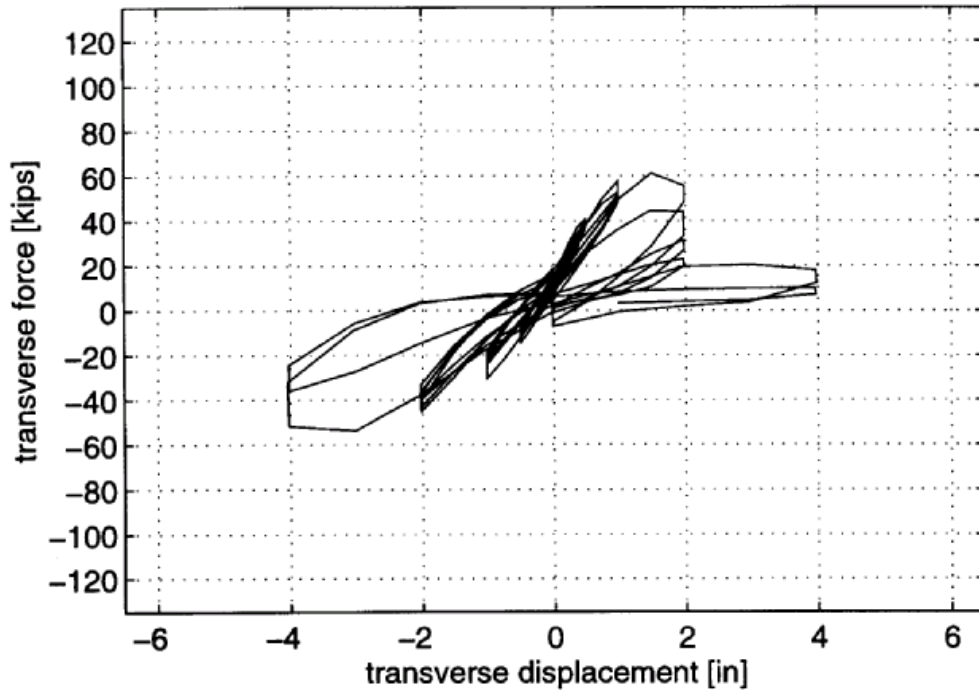
(a)
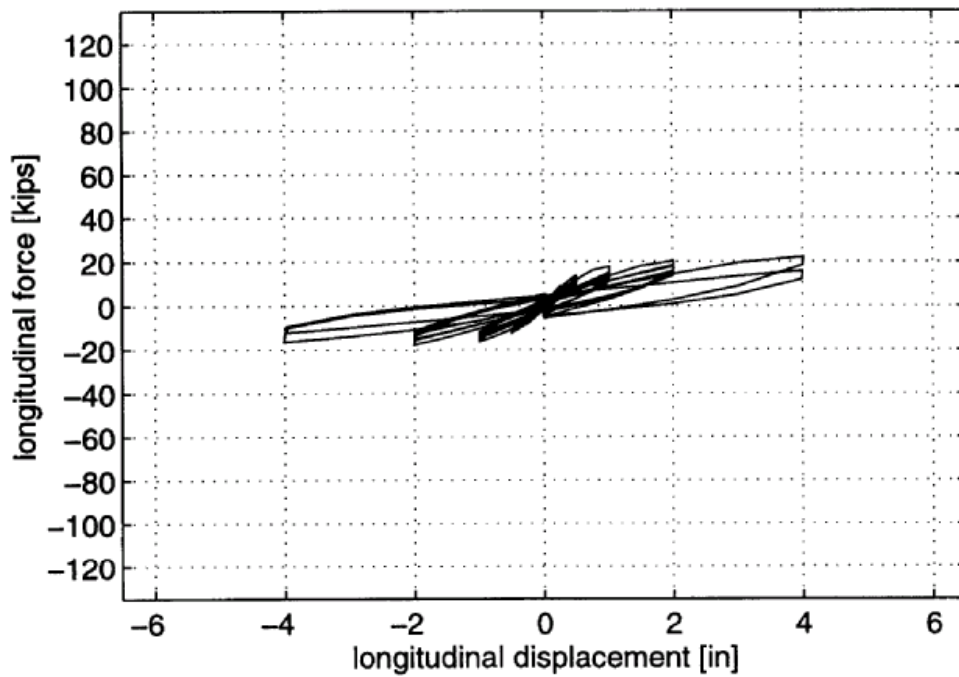
(b)

Figure 2.21 Force-Displacement Responses of the As-Built Long Specimen. (a) Transverse Direction (b) Longitudinal Direction. (Adapted from Stojadinovic and Thewalt, 1995)

30
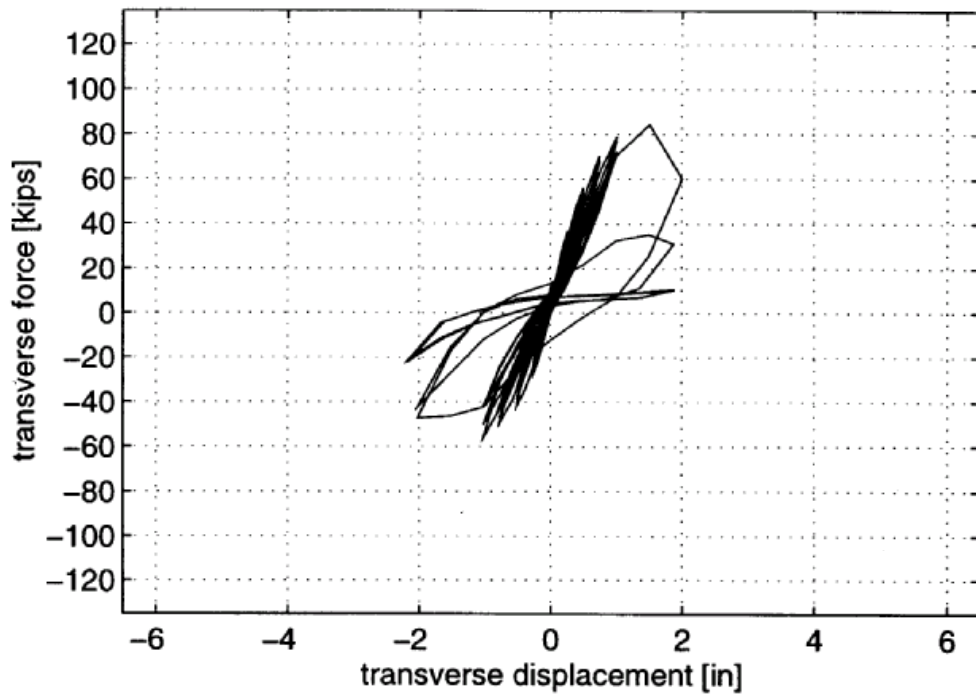
(a)
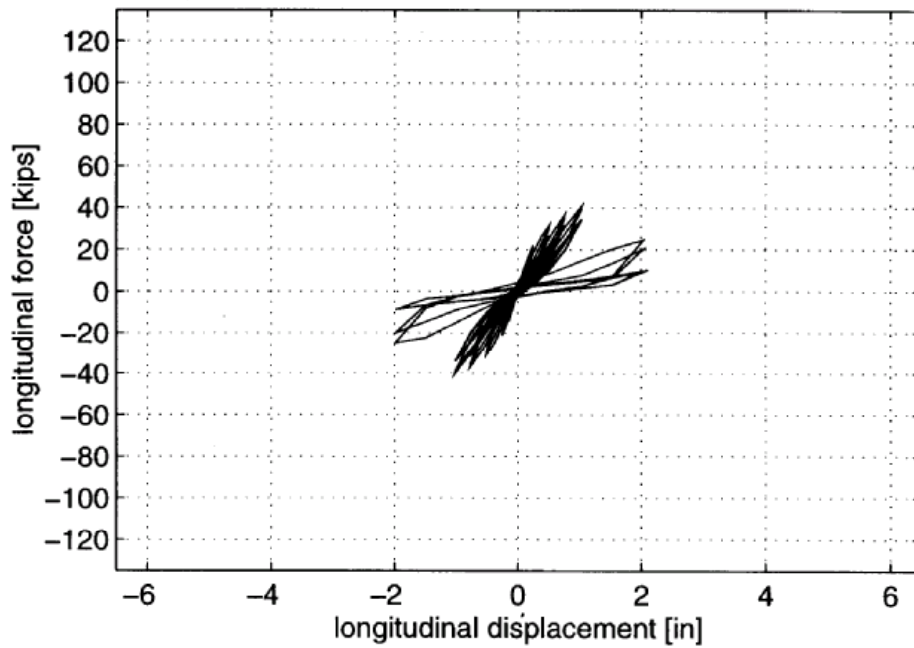
(b)

Figure 2.22 Force-Displacement Responses of the As-Built Short Specimen. (a) Transverse Direction (b) Longitudinal Direction. (Adapted from Stojadinovic and Thewalt, 1995)

Figure 2.23 Bond Split Failure of the Knee Joint in the As-Built Short Specimen(Adapted from Stojadinovic and Thewalt, 1995)
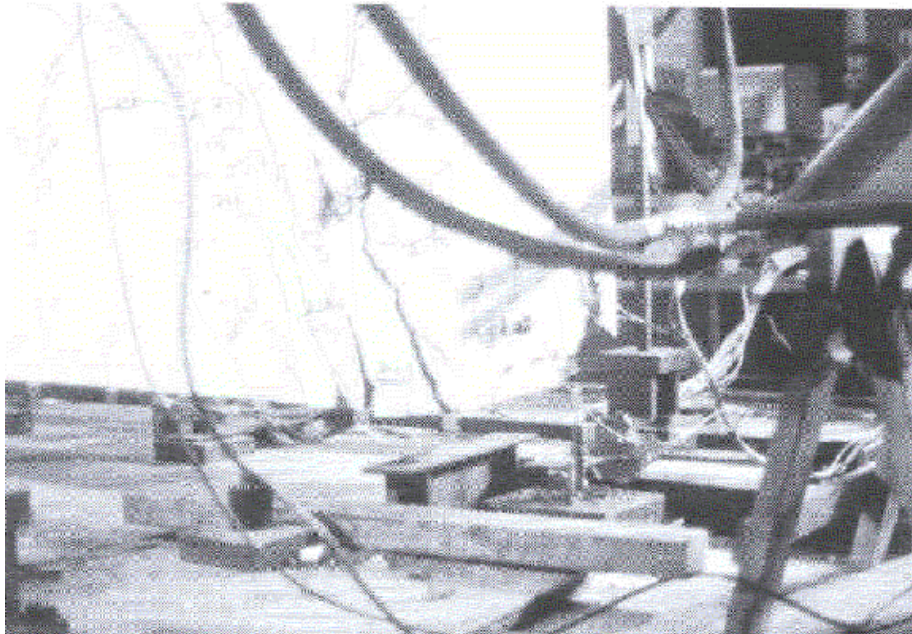
Figure 2.24 Spalling in the Knee Joint of the As-Built Long Specimen(Adapted from Stojadinovic and Thewalt, 1995)

Initial upgraded specimens

In the second part of this study, a retrofit design was developed to improve the strength and deformation capacity of the outrigger knee joint system taking into consideration the observed failure mechanisms of the tested joints. The results of this phase formed the basis for selecting the final upgrade choices. Two upgrade strategies were investigated first: a ductile reinforced concrete upgrade strategy and a strong steel upgrade strategy. The objective of the ductile upgrade strategy was to enhance the deformation and energy dissipation of the knee joint system through flexural hinging in the column during in-plane loading and torsional/flexural hinging of the cap beam under out-of-plane loading. A reinforced concrete jacket cast against the beam and knee joint was used for that purpose. In contrast, the goal of the strong steel upgrade strategy was to enhance the deformation and energy dissipation of the knee joint system through flexural hinging in the column during in-plane and out-of-plane loading. The retrofit procedure consisted of application of 0.5-in. (13-mm) thick A36 flat steel plates around the beam and the joint. Based on the results of the tests, the strong upgrade philosophy was selected to form the final upgrade measure.

Final upgraded specimens

Two strong upgrade strategies were investigated in this third stage: a final concrete upgrade on a long outrigger specimen and a final steel upgrade on one short and one long outrigger specimens.

The final concrete upgrade consisted of a post-tensioned reinforced concrete jacket of two 9-in. (23-cm) thick side bolsters around the beam connecting a half circle

33

bolster around the joint. The column was upgraded using a grouted cylindrical steel casing with a 1-in. (2.5-cm) clearance above the beam. Figure 2.25 shows the upgraded test specimen. Testing showed that the specimen behaved according to the strong upgrade philosophy. The plastic hinge formed in the column, the joint remained virtually intact and the outrigger beam remained in the cracked pre-yield torsion response stage. However, there was a 25% difference in resistance between the longitudinal and the transverse directions. This behavior was related to the bi-directional loading protocol and the difference in the torsional and bending stiffness of the beam. Force-displacement curves for this specimen are shown in Figure 2.26.
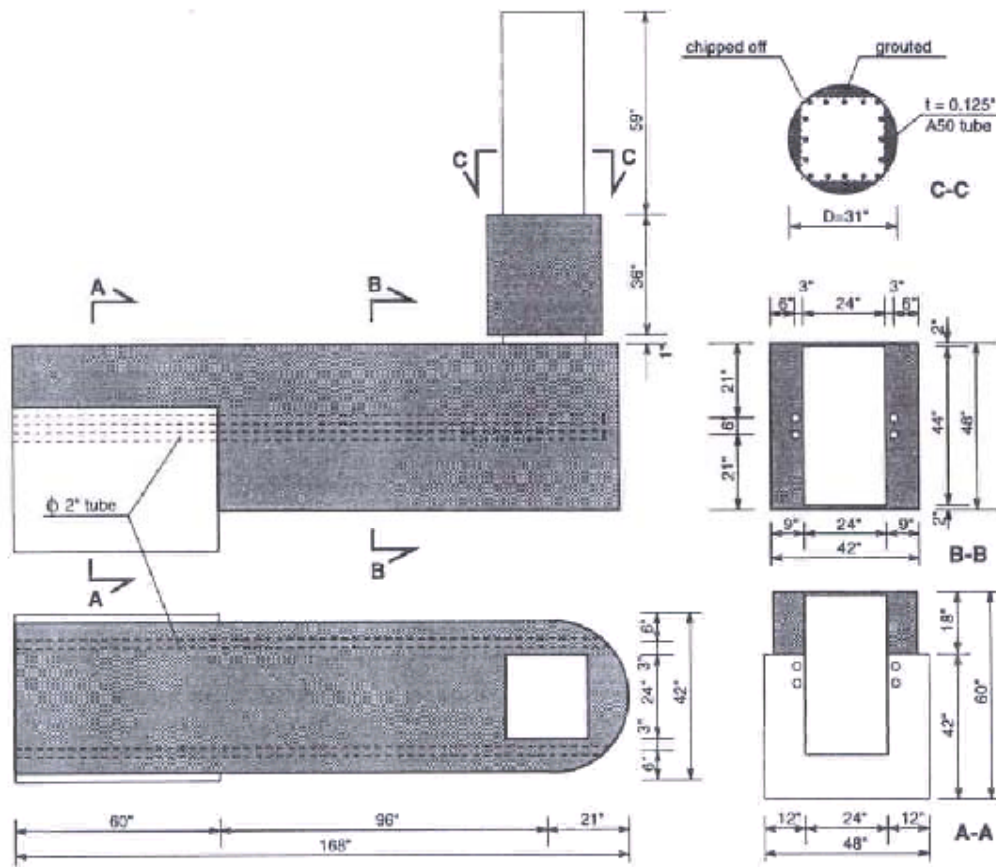
**Figure 2.25 Final Concrete Upgrade Details of the As-Built Long Specimen
(Adapted from Stojadinovic and Thewalt, 1995)**
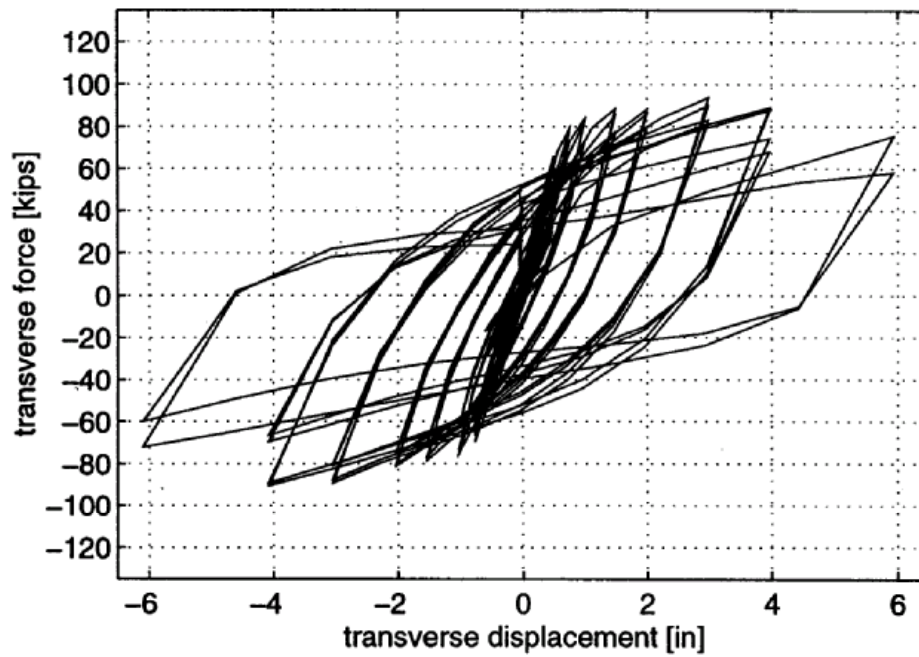
(a)
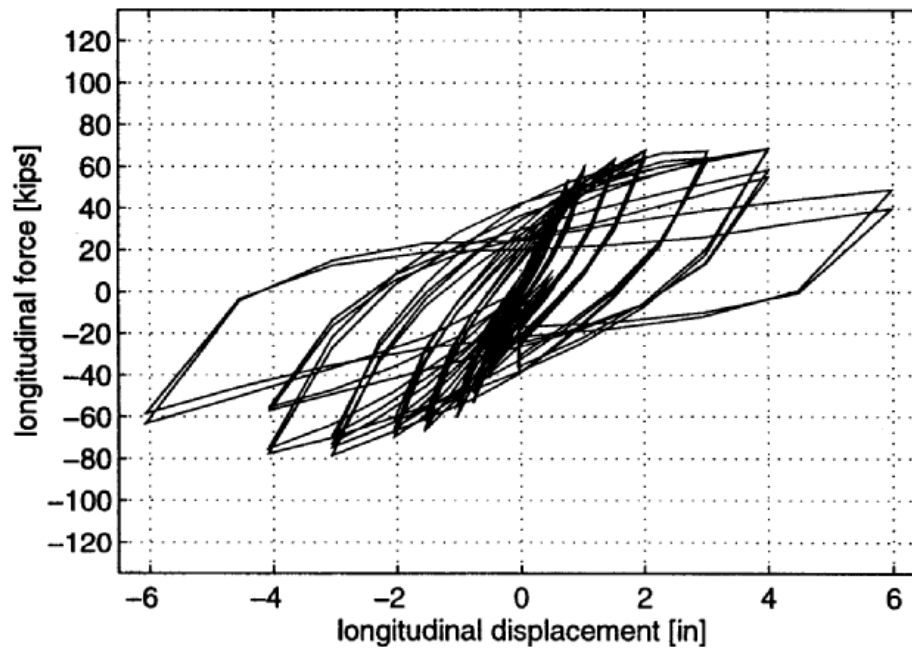
(b)

Figure 2.26 Force-Displacement Responses of the Final Concrete Long Specimen. (a) Transverse Direction (b) Longitudinal Direction. (Adapted from Stojadinovic and Thewalt, 1995)

The steel plate jacket upgrade design was made using 0.25-in. (6-mm) thick A572-50 flat steel plates around the beam with a curved steel plate on the exterior face of the joint. The jacket plates were connected to the as-built beam by high-strength threaded rod through-bars, as shown in Figure 2.27. The column of the specimens was upgraded using a grouted cylindrical steel casing over the first 3.0 ft (0.91 m) with a 1.0-in. (25-mm) clearance above the beam. This upgrading design strategy was tested on two specimens, one with a short outrigger beam and the other one with a long beam. The test results of both upgraded specimens were consistent with the strong upgrade design goals. The column plastic hinge formed at the column joint interface as intended, the ductility of the outrigger knee joint was increased significantly, and the steel jacket provided good confinement to the joint region.

Retrofit conclusions

The study concluded that both of the proposed upgrade strategies, the steel plate jacket and the post-tensioned reinforced concrete jacket, enhanced the deformation and energy dissipation capacity of the outrigger beam knee joint system. The strong upgrade strategy using steel plates was easier to construct than the post-tensioned reinforced concrete. A jacket anchor assembly was suggested by the researchers to transfer the forces from the upgraded outrigger knee joint system to the bridge deck box girder. Therefore, with this retrofit strategy, it is likely to be necessary to strengthen the first cells of the bridge box girder.
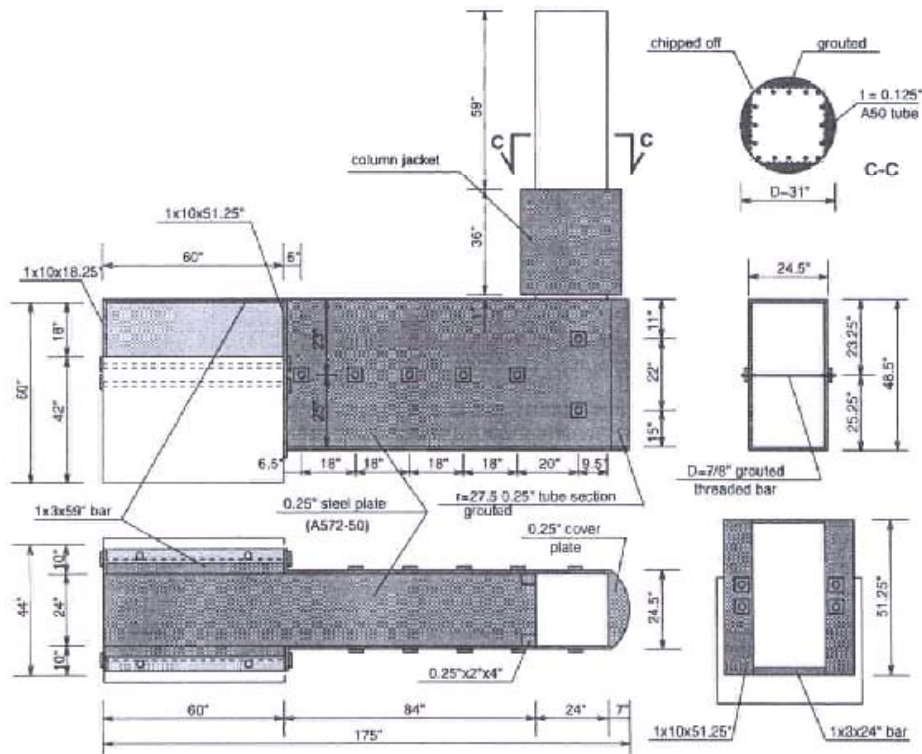
Figure 2.27 Final Steel Upgrade Details of the As-Built Long Specimen (Adapted from Stojadinovic and Thewalt, 1995)

2.4 JOINT DESIGN RECOMMENDATIONS

Current knee joint design procedures are reviewed in this section, including those in ACI 318-02 code provisions (2002), 2004 AASHTO Specifications, Caltrans Seismic Design Criteria (2004) and recommendations developed by Priestley.

2.4.1 ACI 318-02 (2002)

ACI-ASCE Committee 352 provides information to the code-writing committees in the United States on the design of beam-column joints in monolithic reinforced concrete structures for both non-seismic (type 1 joints) and seismic (type 2 joints) areas. The report ACI 352R-91, *Recommendations for the Design of Beam-Column Joints in*

Monolithic Reinforced Concrete Structures, is employed by the ACI 318-02 code provisions (2002) for design and detailing of beam-column joints for normal weight concrete.

For type 2 joints, the recommendations provide guidance only for joints in which the column width is equal to or greater than the beam width and for cases where the beam bars are located within the column core. Connections where the beam bars pass outside the column core are excluded for this type of joints because of a lack of research data on the anchorage of such bars under cyclic loading. However, in highway bridges, the cap beam is frequently of a greater width than the column with some of the longitudinal cap beam reinforcement being developed within the joint outside the core confined by the longitudinal and transverse column reinforcement. Such details were used in some of the outrigger bents in the bridge of this study, the Spokane Street Overcrossing.

Section 4.4.2 of ACI 352R-91 requires that the sum of the nominal moment strengths of column sections above and below a Type 2 joint, calculated using the axial load which gives the minimum column-moment strengths, be at least 1.4 times the sum of the nominal moment strengths of the beam sections framing into the joint along any principal plane. This requirement is intended to produce flexural hinging in the beams than in the columns. Hinging in the beams is normally preferred in the seismic design of moment resisting reinforced concrete building frame structures, whereas in elevated freeway structures the standard practice is to form plastic hinging in the columns. Therefore, these recommendations frequently do not apply to highway bridges.

The basic steps in the design and detailing of beam-column joints based on ACI 352R-91 are as follows: classify the joint according to type and geometry, define the

joint demands and capacity, provide joint confinement and required development length for the reinforcement.

The ACI-ASCE Committee 352 requires that the moment resisting joints be proportioned so that:

$$\phi \, V_n \geq V_u \tag{2.1}$$

where $\phi = 0.85$, V_n = nominal shear strength of the joint, and V_u = the design shear force in the joint. V_u is determined based upon stresses in the longitudinal reinforcement framing into the joint at the member-joint interface of the element first reaching flexural yielding due to lateral, gravity and secondary loads. Typically, the joint design shear force should be based on a stress value of αf_y, where f_y is the specified yield strength of the reinforcing bars and α is a stress multiplier. For type 2 joints, the stress multiplier α should be equal to or greater than 1.25. The factor α accounts for uncertainty in the actual yield strength, which is commonly 10 to 25 percent higher than the nominal value, and the significant increase in steel stress above the actual yield stress due to strain hardening when plastic hinging occurs.

ACI Committee 352 set the strength of the joint as a function of only the compressive strength of the concrete. Experimental observations on joints and deep beams indicated that the shear strength is fairly independent of the volume of transverse reinforcement for lightly reinforced joints and beams. Therefore, the nominal shear strength of the joint can be expressed as:

$$
\begin{aligned}
V_n &= \gamma \sqrt{f_c'} \, (psi) \, b_j h \quad for \, f_c' \leq 6000 \, psi \\
V_n &= \frac{\gamma}{12} \sqrt{f_c'} \, (MPa) \, b_j h \quad for \, f_c' \leq 414 \, MPa
\end{aligned} \tag{2.2}
$$

where b_j is the effective width of column transverse to the direction of shear, f_c' is the

compressive strength of concrete, h is the thickness of the column in the direction of load being considered, and γ is a shear strength factor reflecting confinement at the joint-member interface by the neighboring members (i.e., joint configuration).

The joint configurations defined by the ACI-ASCE Committee 352 are shown in Figure 2.28. They are interior joints having horizontal members framing into all four sides of the joint, exterior joints having either three horizontal members or at least two horizontal members framing into opposite sides of the joint, and corner joints consisting of one or two orthogonal horizontal members framing into the joint. γ values for these configurations are shown in Table 2.1. However, to use Table 2.1, joint classification for each category requires that the horizontal frame member cover at least three-quarters of the width of the column and that the total depth of the shallowest horizontal member not to be less than three-quarters of the total depth of the deepest horizontal member framing into the joint. Otherwise, lower values of γ corresponding to a lower configuration should be used.

Table 2.1 Values of γ for Monolithic Beam-Column Joints

Joint Type	Joint Classification		
	Interior	**Exterior**	**Corner**
2	20	15	12
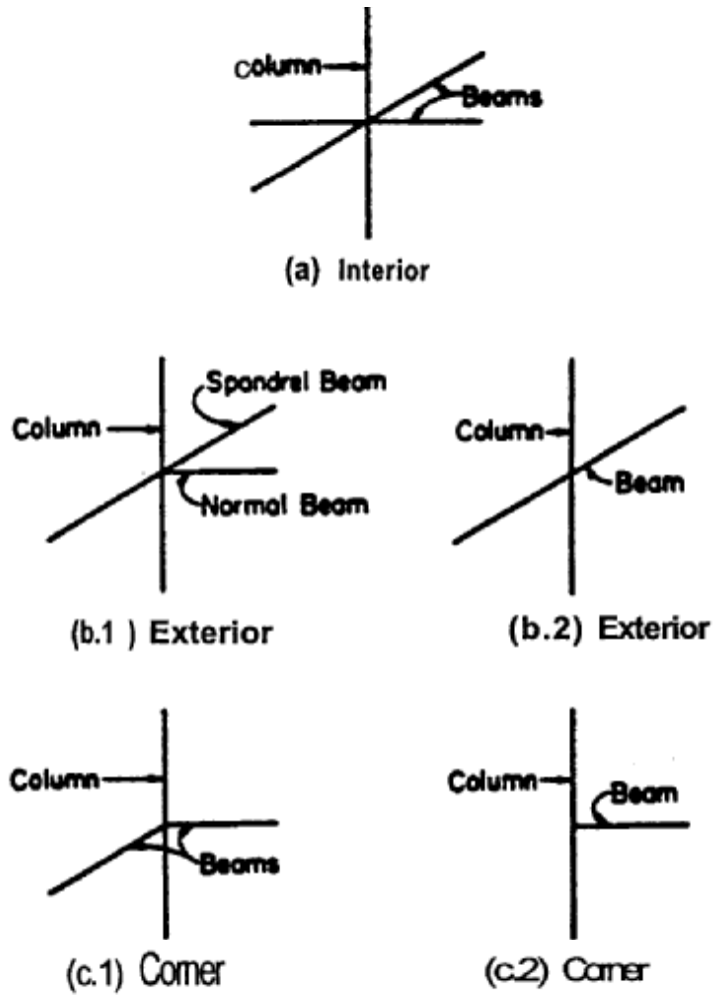
Figure 2.28 Geometric Description of Joints (Adapted from ACI-ASCE Committee 352)

The recommendations of the ACI 318-02 code provisions (2002) for the effective joint width, b_j, for shear calculations are shown in Figure 2.29. These recommendations can also be summarized by the following equations:

$$b_j = b_b + h \qquad (2.3a)$$

$$b_j = b + 2x \qquad (2.3b)$$

where b_b is the effective compression flange width of the beam perpendicular to the direction of forces generating shear, x is the smaller perpendicular distance from the

beam side to the column side, and h is the thickness of the column in the plane of joint

shear calculations. The smaller value of b_j determined from equations 2.3a or 2.3b

should be used.
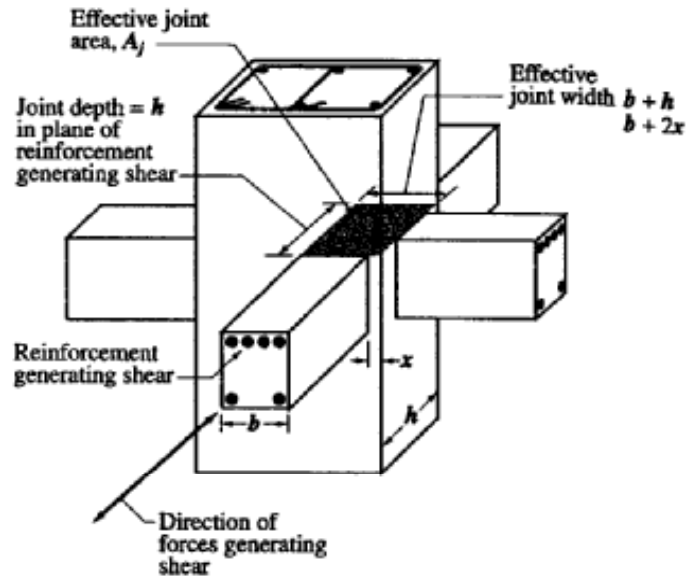
Figure 2.29 Determination of Effective Joint Width (Adapted from ACI 318-02, 2002)

From the previous discussion, it can be determined that for knee joints, the focus

of this study, the shear strength factor γ is equal to 12. Also, for situations where the

outrigger beam width is greater than the column width, the effective joint width is taken

as the column width. Thus, no dispersion of the column axial force into the joint is

considered.

The design philosophy adopted by the ACI-ASCE Committee 352 is that during

anticipated earthquake loading and displacement demands, the joint should be able to

carry the resulting shear forces if the joint concrete is adequately confined and the

longitudinal bars of the members meeting in the joint are well detailed. Thus, the

required transverse reinforcement presented in the ACI 318-02 code provisions (2002) is

not a function of earthquake demand upon the joint. It is clear that the intended function of the transverse reinforcement is to provide enough confinement to the joint region and to prevent buckling of the column longitudinal bars. Therefore, the ACI 318-02 code provisions (2002) provide the following recommendations on joint reinforcement and details:

a) For type 2 joints, the special transverse reinforcement in the column ends must be continued through the beam-column joint. For joints with square or rectangular hoops, the total cross-sectional area of transverse reinforcement, A_{sh}, shall not be less than that required by the following equations:

$$A_{sh} = 0.3(s\, h_c f_c' / f_{yh})\left[(A_g / A_{ch}) - 1\right]$$ (2.4a)

$$A_{sh} = 0.09(s\, h_c f_c' / f_{yh})$$ (2.4b)

where s is the spacing of the transverse reinforcement measured along the longitudinal axis of the column, h_c is the cross sectional dimension of column core area measured center-to-center of confining reinforcement, f_{yh} is the specified yield strength of the transverse reinforcement, A_g is the gross section area of the column framing into the joint and A_{ch} is the cross sectional area of the column measured out-to-out of transverse reinforcement.

b) Lap splices of flexural reinforcement shall not be used within the joints nor within a distance of twice the member depth from the face of the joint.

c) Longitudinal beam reinforcement terminating in a column should be extended to the far face of the confined column core and anchored in tension according to the provisions of ACI 21.5.4 and in compression according to ACI Chapter 12.

d) To substantially reduce slip during the formation of adjacent beam hinging, the

column dimension parallel to the beam reinforcement shall not be less than 32 times the diameter of the largest longitudinal bar.

e) Other recommendations regarding confinement for splices of continuing reinforcement, anchorage of reinforcement terminating at the connection, development length for hooked bars and straight bars in tension or compression are provided in the ACI 318-02 code provisions (2002).

2.4.2 AASHTO Specifications (2004)

The seismic design and detailing of typical highway bridges in the United States is governed by the American Association of Highway and Transportation Officials (AASHTO) Bridge Design Specifications.

In general, AASHTO specifications (2004) require plastic hinges to be ascertained to form before any other failure or instability in the structure. In particular, the specifications permit hinges to form at locations in columns where they can be feasibly inspected and/or repaired. AASHTO (2004) therefore differs from ACI 318-02 recommendations (2002) in which plastic hinges are designed to form in the beams.

AASHTO (2004) requires that the design force for the connection between the column and the cap beam superstructure to be calculated on the basis of inelastic flexural resistance of the column by multiplying the nominal resistance of reinforced concrete sections by 1.30 and that of steel sections by 1.25. These amplified forces may be taken as the extreme seismic forces that the bridge is capable of developing. The nominal shear resistance, V_n, provided by normal-weight aggregate concrete in the joint of a frame or bent in the direction under investigation, shall be less than:

$$V_n = 12.0\sqrt{f_c^{'}}\ (psi)\ bd$$
$$V_n = 1.0\sqrt{f_c^{'}}\ (MPa)\ bd \tag{2.5}$$

where b is the width of the compression face of the member and d is the distance from compression face to centroid of tension reinforcement. Similar to ACI 318-02 code provisions (2002), the specifications assign no contribution to the strength of the joint from the amount of transverse reinforcement, assuming that the minimum amount of confinement is always provided.

For transverse reinforcement for confinement at plastic hinges, the specifications require the column transverse reinforcement to be continued for a distance not less than one-half the maximum column dimension or 15 in. (380 mm) from the column-joint interface into the joint. The main function of this reinforcement is to ensure the same axial load column capacity before and after spalling of the concrete cover and to prevent longitudinal bar buckling. For a rectangular column, the total gross sectional area of rectangular hoop reinforcement, A_{sh}, shall not be less than either equation 2.4a or the following:

$$A_{sh} = 0.12(s\ h_c f_c^{'} / f_{yh}) \tag{2.6}$$

The minimum amount of transverse reinforcement requirements by ACI 318-02 code provisions (2002) and the AASHTO Specifications (2004) are quite similar. Other specifications regarding development and splices of reinforcement will not be presented here, as most of the AASHTO (2004) provisions on this issue are based on ACI 318-02 code provisions (2002) and its attendant commentary. However, AASHTO (2004) requires the development length for all longitudinal steel to be 1.25 times that required for the full yield strength of the reinforcement, see article 5.10.11.4.3.

2.4.3 Caltrans Seismic Design Criteria

The Caltrans Seismic Design Criteria (SDC) specify the minimum design requirements for bridges designed by and for the California Department of Transportation. The SDC are an encyclopedia of new and currently practiced seismic design and analysis methodologies for the design of new bridges in California, focused mainly on concrete bridges. The SDC version 1.3 was released on February 2004 and is the most current criteria.

Section 7.4 of the SDC deals with superstructure joint design. The SDC necessitate moment resisting connections between the superstructure and the column to be designed to transmit maximum forces produced when the column has reached its overstrength capacity including the effects of overstrength shear. This is to ensure elastic behavior of the joint when resisting the column overstrength moments and shears. Therefore, the Caltrans SDC and AASHTO Specification (2004) have the same philosophy in forcing the inelastic behavior into the column region. The overstrength moment is calculated by applying a 20% overstrength magnifier to the plastic moment capacity of the column. The factor is introduced to account for material strength variations between the column and the adjacent members and column moment capacities, which are usually greater than the idealized plastic moment capacity, M_p. The latter is calculated by balancing the areas between the actual and the idealized moment curvature curves beyond the first longitudinal bar yielding point, M_y, as shown in Figure 2.30.

The SDC require all superstructure-to-column moment resisting joints to be proportioned so that the principal tension, p_t, and compression, p_c, stresses be less than those given by the following equations:

$$p_t \leq 12\sqrt{f_c'}\,(psi), p_t \leq 1.0\sqrt{f_c'}\,(MPa) \tag{2.7a}$$

$$p_c \leq 0.25 f_c' \tag{2.7b}$$

In addition, the cap beam width required for adequate joint shear transfer should be at least 24 in. (600 mm) wider than the column dimension in the perpendicular direction. This requirement is different than the current ACI 318-02 (2002) joint design recommendations, which are based on results of tests of connections in which the column width was equal to or greater than the beam width.
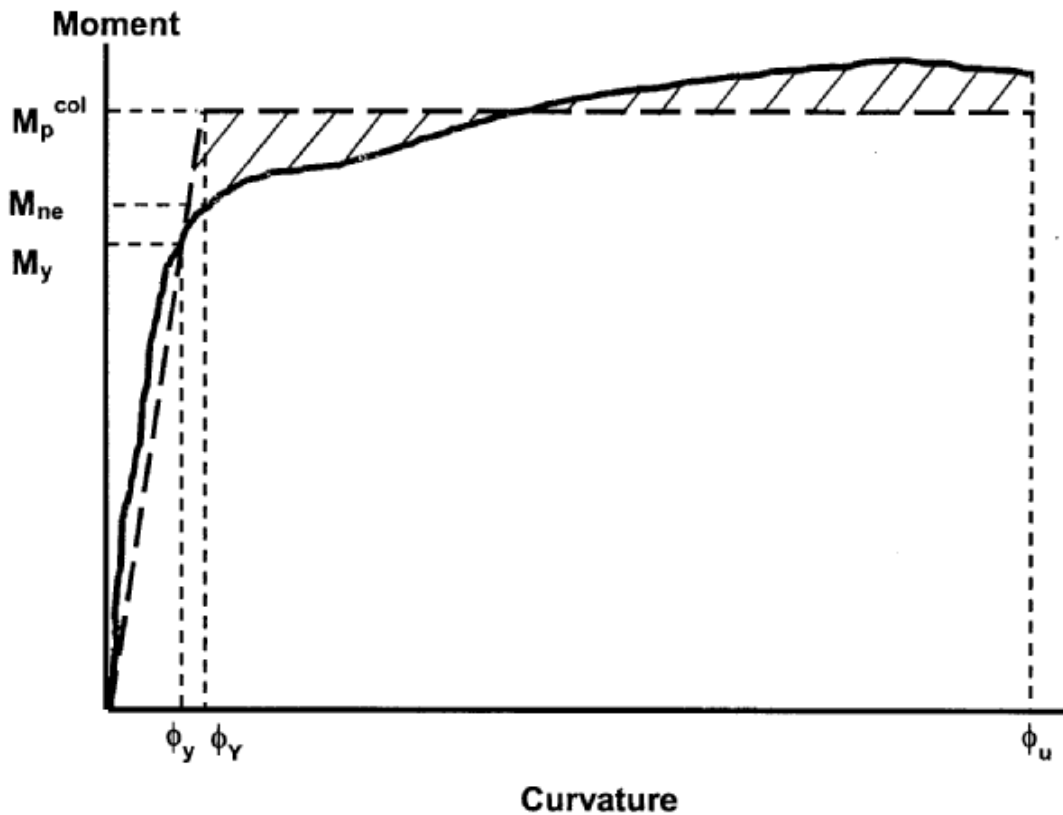
Figure 2.30 Moment Curvature Curve (Adapted from Caltrans, 2001)

The SDC provide recommendations on T-joint shear design, including principal stress definition, minimum joint shear reinforcement and joint shear reinforcement involving vertical stirrups, horizontal stirrups and recommendations on joint transverse

reinforcement and detailing of main column reinforcement extending into the cap beam. However, there are no provisions for design levels of joint shear stress applicable to knee joints except the general principal joint shear requirements presented by equations 2.7a and 2.7b. The SDC consider knee joints as nonstandard elements for which design criteria shall be developed on a project-specific basis.

2.4.4 Recommendations Proposed by Priestley

In an effort to assess the shear strength of existing joints, Priestley reviewed some of the recently developed shear transfer models and proposed recommendations for design of knee joints in new structures. The models were developed for circular columns or rectangular columns with intersecting circular spirals under in-plane loading.

While the ACI 318-02 code provisions (2002) and the AASHTO Specifications (2004) set the joint condition based upon nominal shear stress calculations, Priestley related the behavior of nominally unreinforced knee joints to the principal tension and compression stresses. According to Priestley, joints are unlikely to experience shear distress if the average principal tension stress is less than the cracking strength of the concrete. Additionally, special joint reinforcement contribution to shear strength is ineffective once the nominal principal compression stresses exceed the concrete crushing strength.

Experiments showed that diagonal cracking initiated in nominally unreinforced knee joints when the principal diagonal tension stress was approximately $3.5\sqrt{f_c'}$ psi $(0.29\sqrt{f_c'}$ MPa) (Priestley et al., 1996). However, the joints were able to resist tension

stresses up to $5.0\sqrt{f_c'}$ psi $(0.42\sqrt{f_c'}$ MPa) before brittle joint failure due to alternative concrete mechanisms and residual tension stress within the joint. These principal shear stress values were based on test specimens with circular columns or rectangular columns with intersecting circular spirals under in-plane loading.

Based on the previous test observations, Priestley suggested the following recommendations as minimum joint shear reinforcement for new designs:

a) If $p_t \leq 3.5\sqrt{f_c'}$ psi $(0.29\sqrt{f_c'}$ MPa$)$, joint shear cracking is not expected and horizontal joint reinforcement should be provided to transfer at least 50% of the cracking stress resolved to the horizontal direction by lateral clamping pressure. This thus requires that:

$$\rho_{s,min} = \frac{3.5\sqrt{f_c'}}{f_{yh}} \tag{2.8}$$

where $\rho_{s,min}$ is the minimum required volumetric ratio of transverse reinforcement. For such low levels of principal joint tension stress, no vertical joint reinforcement is required as the column sidebars are assumed to provide for the necessary vertical shear component (Priestley, 1993).

b) If $p_t \geq 5.0\sqrt{f_c'}$ psi $(0.42\sqrt{f_c'}$ MPa$)$, the required amounts of vertical and horizontal shear reinforcement should be determined based upon clear force transfer mechanisms of joint forces from beam to column reinforcement without reliance on the tension capacity of the joint concrete.

c) For intermediate stress levels, $3.5\sqrt{f_c'} \leq p_t \leq 5.0\sqrt{f_c'}\,psi$

$(0.29\sqrt{f_c'} \leq p_t \leq 0.42\sqrt{f_c'}\,MPa)$, linear interpolation between the nominal (case a) and full (case b) design values can be used.

2.5 SUMMARY

Researchers at the University of California at San Diego and the University of California at Berkeley demonstrated the seismic vulnerability of outrigger knee joint systems by testing representative models of outrigger bents that experienced damage during the 1989 Loma Prieta earthquake. Lack of vertical and horizontal joint reinforcement, and low torsional strength of the outrigger beam, were identified as the main weaknesses. Based upon these identified vulnerabilities, retrofit measures were proposed and then tested. The proposed retrofit measures were generally successful in overcoming the identified deficiencies, but their application to existing bridges was reported to be either impractical or they adversely affect the bridge superstructure.

ACI 318-02 code provisions (2002) and AASHTO Specifications (2004) include design guidelines only for reinforced knee joints. Caltrans SDC (2004) considers knee joints as special elements for which design criteria shall be developed on a project specific basis. Design recommendations for existing knee joints are presented in Priestley et al. (1996).

CHAPTER THREE

EXPERIMENTAL PROGRAM

3.1 INTRODUCTION

In this chapter, information pertaining to the prototype selection and the parameters utilized to specify the test specimen details are presented. In addition, material strengths, construction, testing setup, loading protocol, instrumentation and data acquisition for this study are discussed.

3.2 PROTOTYPE SELECTION

The SR99 Spokane Street Overcrossing was designed in 1957, probably based on the 1953 AASHO Standard Specifications for Highway Bridges, which did not include any provisions for seismic design or detailing. Part of the bridge consists of cast-in-place reinforced concrete box girder frames running parallel to the direction of the traffic. The reinforced concrete box girders are supported on forty-three bents, of which twelve have outrigger knee joints. A typical section in the bridge, as shown in Figure 3.1, has three spans supported by integral bents perpendicular to the main frame.

A 2-in. (5-cm) gap through the superstructure is incorporated at the start and end of each section to allow for longitudinal movements within the bridge. In the outrigger bents, this gap carries through the outrigger beams and knee joints. Figure 3.2 shows a representative outrigger bent in the bridge. Columns in the outrigger bents are supported by individual footings, which are supported by nine composite 35-ton (31-metric-ton) capacity piles. The lower portion of the pile is timber, while the upper 10 ft (3.0 m) is

precast concrete. The concrete compressive strength is specified in the original drawings, dated 1957, as $f'c$ = 4000 psi (28 MPa). This value is usually a low estimate of the actual strength expected in the field because of conservative mix design procedures used at the time and the strength gain of concrete with age.
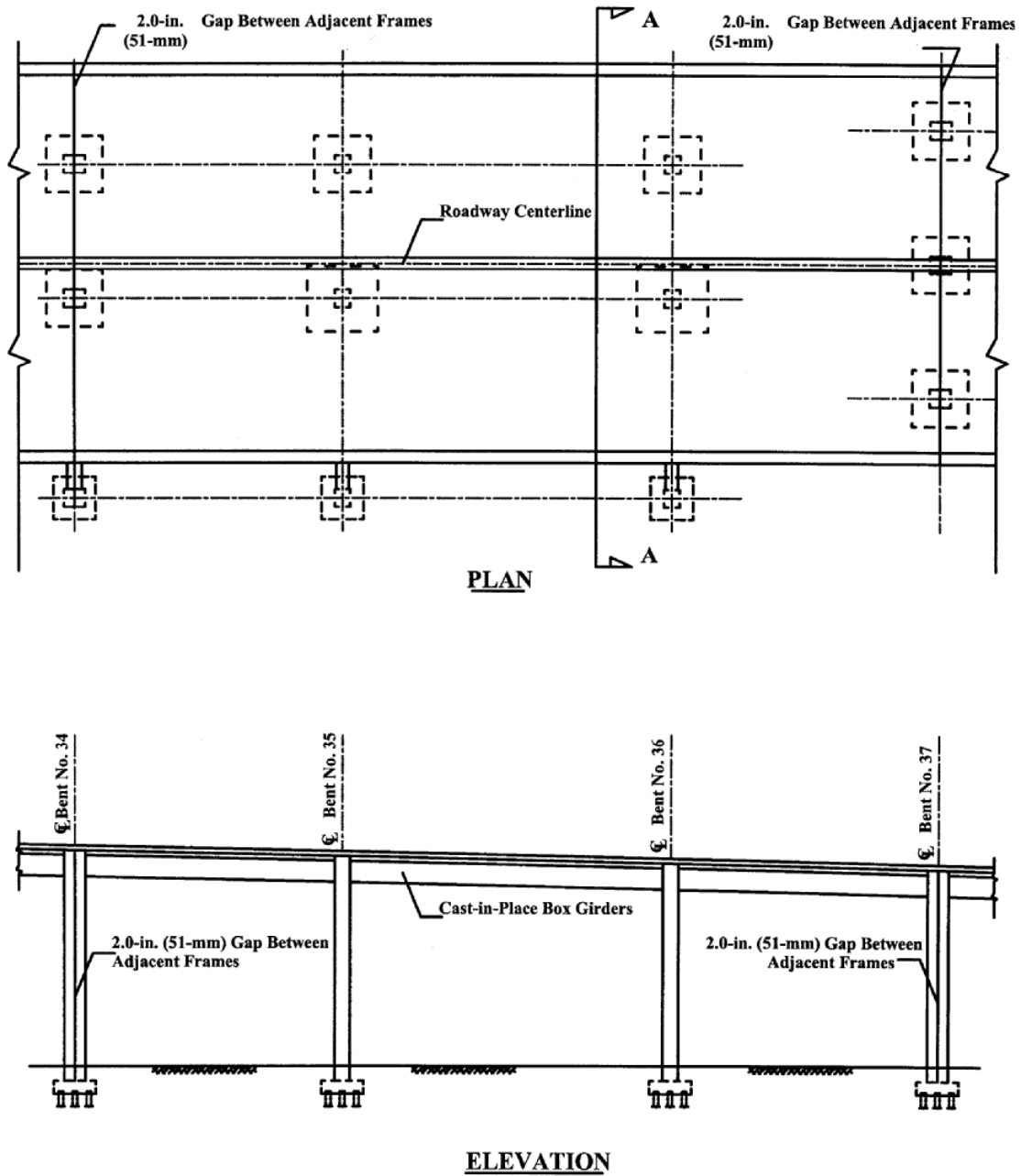
Figure 3.1 A Typical Section in the SR 99 Spokane Street Overcrossing, Plan and Elevation

VIEW A-A
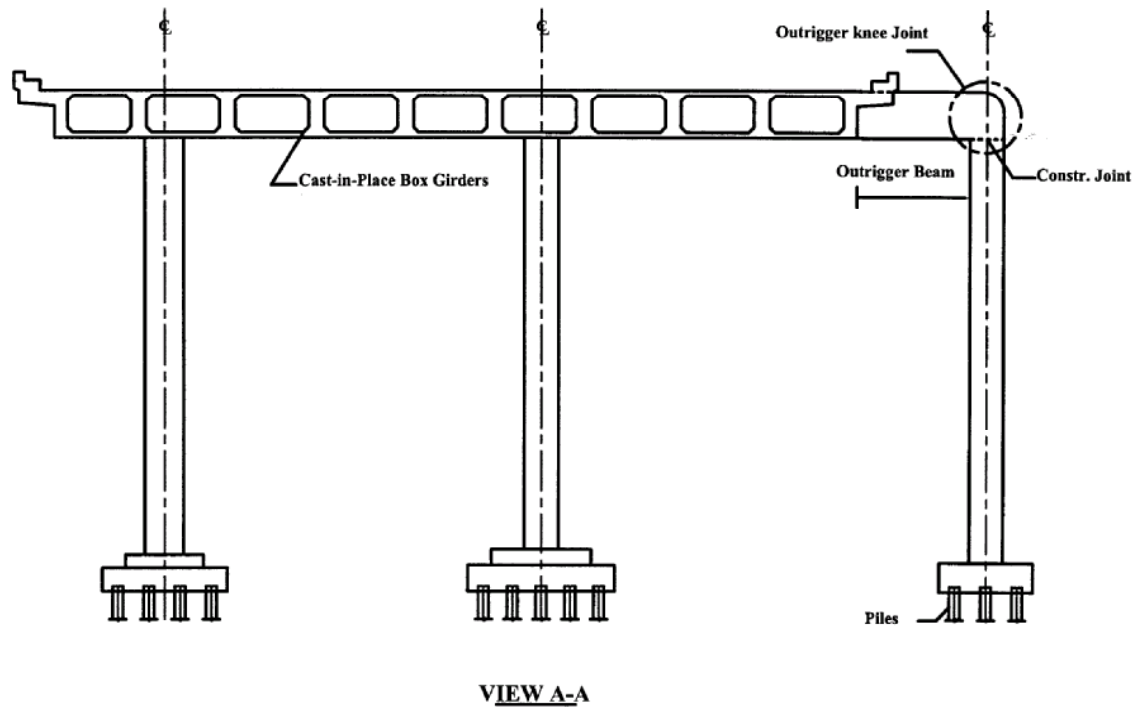
Figure 3.2 A Typical Outrigger Bent in the SR 99 Spokane Street Overcrossing

The columns in the outrigger bents are square or rectangular with heights, measured from the bottom of the outrigger beam to the footing face, of 28.8 ft (8.79 m) to 47.5 ft (14.5 m). The longitudinal steel ratio varies over the length of the column, with most columns having higher steel ratios in the top-third portion than in the lower two-thirds portion. Based on the gross sectional area of the column, the longitudinal steel ratio varies from a minimum of 1.23% to a maximum of 3.95% and from 1.07% to 1.78% in the top one-third and lower two-thirds portion of the column, respectively. Longitudinal reinforcement consists of No. 9 (29 mm), No. 11 (36 mm), No. 14 (43 mm), or No. 18 (57 mm) bars. The columns have No. 3 (9.5 mm) transverse steel bars at 12 in. (305 mm) on center spacing over the entire length, including in the knee joints, with a 1.5 in. (38 mm) clear concrete cover on the sides. The ties are closed stirrups anchored by

90-degree hooks that are not hooked into the column's core. This detail results in a poorly confined column when the concrete side cover over the stirrups spalls off in plastic hinging regions. The axial load levels in the outrigger columns due to the selfweight of the structure range from 0.016 to 0.057 f'c Ag, where Ag is the gross sectional area of the column and f'c is the specified compressive strength of the concrete. This axial load level conforms to WSDOT bridge design standards in 1959, which specified a maximum service axial load level of 0.07 f'c Ag (Jaradat, 1996)

The width of the outrigger beams varies from 2.0 ft (0.61 m) to 4.75 ft (1.45 m) and lengths range from 3.04 ft (0.93 m) to 27.0 ft (8.23 m). Positive flexural reinforcement is provided using No. 11 (36 mm), No. 14 (43 mm), or No. 18 (57 mm) bars, while negative flexural reinforcement is provided using No. 8 (25 mm), No. 9 (29 mm), No. 11 (36 mm), or No. 18 (57 mm) bars. Based on the original drawings of the bridge, the positive reinforcement is cut off at several locations along the length of the beam, while in most cases the negative reinforcement is not terminated. Negative reinforcement is usually in one layer, whereas positive reinforcement is generally distributed over two layers. The steel reinforcement ratio, taken at the beam joint interface section and based on the gross sectional area of the beam, varies from 0.31% to 1.04% and from 0.20% to 1.29% for positive and negative reinforcement, respectively. The positive steel reinforcement ratio varies from 1.04% to 2.52% at the section where the outrigger beam intersects with the superstructure.

Skin reinforcement is provided along the length of the beam using No. 6 (19 mm), No. 7 (22 mm), or No. 8 (25 mm) bars with steel ratios between 0.24% and 0.57%. Beam transverse reinforcement consists of two-legged No. 5's (16 mm) at 24 in. (610 mm)

spacing to four-legged No. 7's (22 mm) at 4 in. (102 mm) spacing open stirrups with 90-degree hooks. The open side of the stirrups is closed with different size U-shaped caps, usually one size smaller and twice larger than the size and the spacing of the stirrups, respectively. In addition, some beams are provided with 45-degree bent-up No. 11 (36 mm), No. 14 (43 mm), or No. 18 bars. The beam hoops usually start at a distance of 1.5 in. (38 mm) to 6.0 in. (152 mm) from the beam joint interface, leaving the joint without any vertical confining reinforcement. The transverse reinforcement in the beam has a 1.0 in. (25 mm) clear concrete cover on the sides and a 4.0 in. (102 mm) and a 2.5 in. (64 mm) clear concrete cover on the top and bottom surfaces, respectively.

The outrigger knee joint has an outside radius of 2.0 ft (0.61 m). Horizontal joint reinforcement consists of No. 3 (9.5 mm) bars at 12 in. (305 mm) spacing as transverse column reinforcement extending for a height of 36 in. (914 mm) into the joint region. No vertical joint reinforcement is present in the joints. The negative flexural reinforcement of the beam is bent parallel to the curved surface of the joint, with a smaller diameter than the outside radius of the joint, and is overlapped with the longitudinal reinforcement in the exterior face of the column in the joint zone. Positive flexural reinforcement of the beam is typically anchored into the joint with a 180-degree hook at the bar end. In some cases it is anchored into the joint with straight bar ends. The outrigger beam side reinforcement usually penetrates the joint and terminates at a distance of about 3 in. (76 mm) to 6 in. (152 mm) from the exterior face of the column. Longitudinal reinforcing bars in the exterior face of the column have 90-degree hooks within the joint and are overlapped with the positive flexural reinforcement of the beam. The longitudinal reinforcement on the other sides of the column are developed into the joint with straight

bar ends that usually terminate below the top beam bars. Figure 3.3 shows a typical as-built reinforcement layout for outrigger knee bents in the Spokane Street Overcrossing.
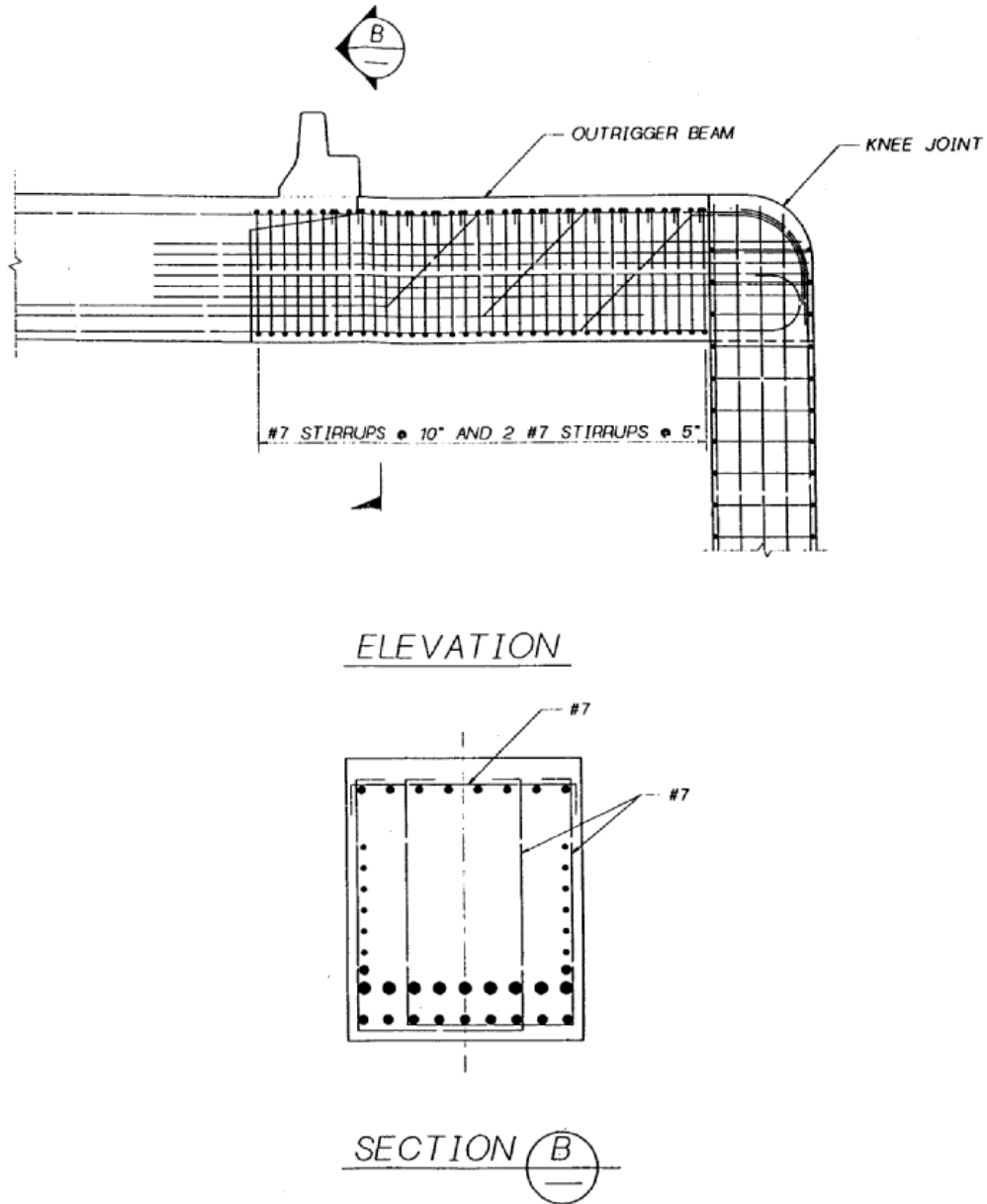
Figure 3.3 A Typical Reinforcement Layout for an Outrigger Bent (Adapted from Zhang et al., 1996)

The WSDOT has implemented a first phase of retrofitting for the Spokane Street Oversrossing, applying steel jackets around the columns. Figure 3.4 shows a typical column jacketing detail for a square column. The jackets are positioned over the entire length of the column with a 2 in. (51 mm) to 4 in. (102 mm) gap between the superstructure soffit and the jacket at the top of the column and with the same gap between the footing and the jacket at the bottom of the column. Columns were upgraded using circular jackets. D-shaped steel jackets were utilized for seismic upgrading of the split columns in order to preserve the split between the column sections. The steel jackets were fabricated from AASHTO M183 structural steel, with thicknesses ranging from 3/8 in. (9.5 mm) to 7/16 in. (11 mm), and the gap between the steel jacket and the existing concrete member was filled by a cement grout.

To select representative prototypes, the twelve outrigger bents of the SR 99 Spokane Street Overcrossing were classified based on the length of the outrigger beam, taken as the distance between the inner face of the column and the outside face of the superstructure. The classification resulted in three main categories: short, medium and long outrigger beams. For each category, the bents were then grouped into regular or split outrigger based on their relative location in the bridge unit (i.e., whether they are intermediate or edge located columns). Table 3.1 shows the prototype classification.
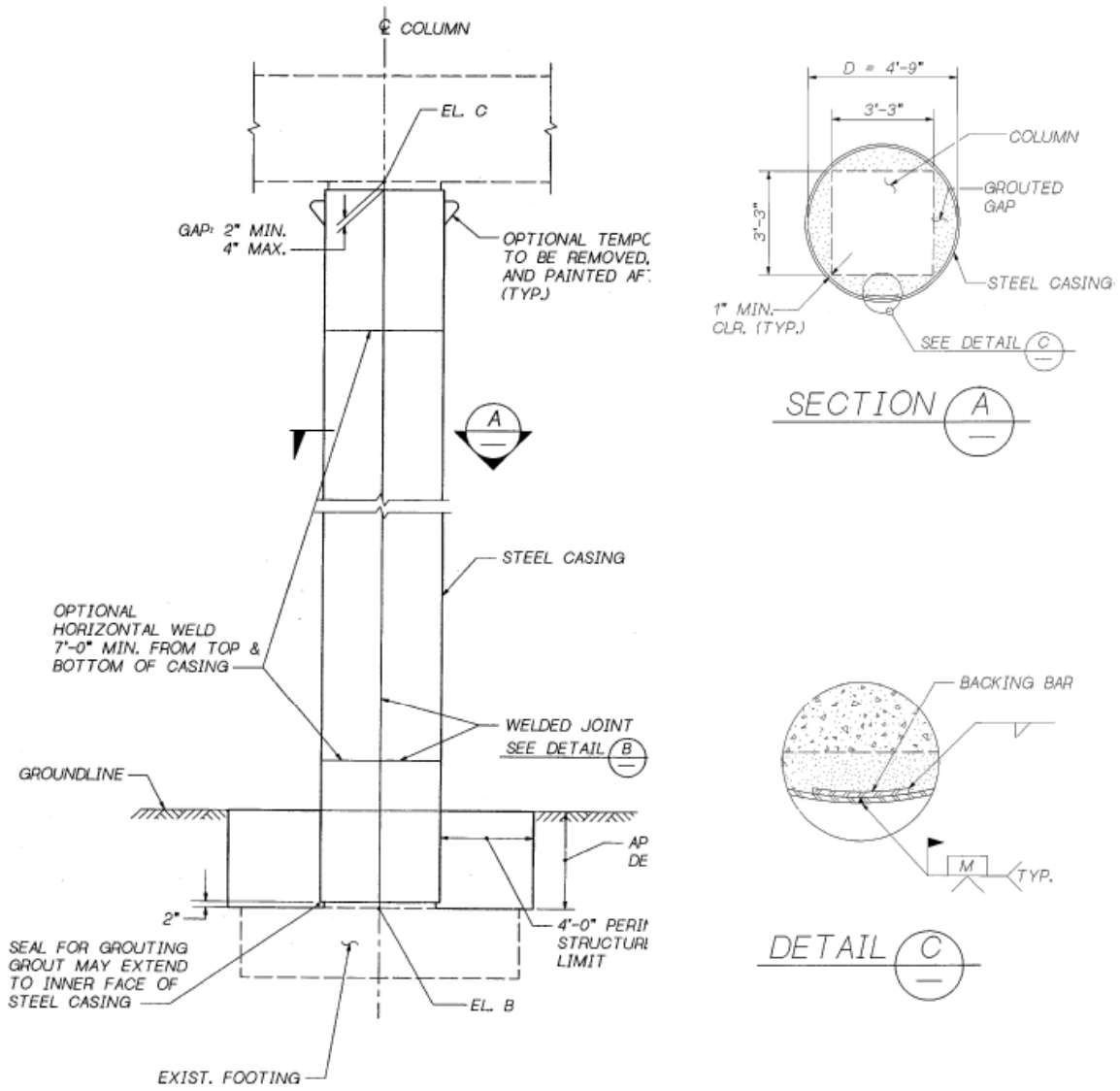
Figure 3.4 Steel Jacket Retrofit Details for a Square Column (from WSDOT)

Table 3.1 Classification of Prototype Bents

Bent No.	Outrigger Beam Length, ft (m)	Relative Location in the Bridge Unit	Classification
Bent 11	3.04 (0.93 m)	Intermediate	Short Regular
Bent 20	4.49 (1.37 m)		
Bent 12	5.28 (1.61 m)		
Bent 42	8.92 (2.72 m)	Intermediate	Medium Regular
Bent 32	9.92 (3.02 m)		
Bent 33	9.92 (3.02 m)		
Bent 35	9.92 (3.02 m)		
Bent 36	9.92 (3.02 m)		
Bent 10	14.6 (4.44 m)		
Bent 34	9.92 (3.02 m)	Edge	Medium Split
Bent 40	14.7 (4.48 m)		
Bent 9	27.0 (8.23 m)	Edge	Long Split

After reviewing several possible candidates and consulting with bridge engineers at the WSDOT, three of the outrigger bents of the SR 99 Spokane Street Overcrossing were selected as prototypes: Bent #20, Bent #36, and Bent #34. Bent #20 was selected to represent bents with short outrigger beams since it has approximately an average beam length value for bents falling in this category. Bent #36 was selected to characterize bents with medium outrigger beams, and Bent #34 represented bents with split outrigger beams and columns. A prototype representing a long split outrigger was not selected due to the limitations in the laboratory facilities and the size of the testing frame. For the purpose of this study, the medium outriggers are henceforth referred to as "long outriggers".

3.3 DIMENSIONAL SCALING

A true model that maintains a complete similarity with the prototype is desirable in all structural models. Usually, the economic and technological conditions preclude a model study that maintains complete similarity with the prototype. For reinforced concrete, modeling the complete inelastic behavior is not an easy task because of the highly inelastic nature of concrete under multi-axial stresses, limited knowledge of the bond characteristics between concrete and the reinforcing elements in the prototype, and the lack of a well-defined failure criterion.

Sabnis and Harris (1999) provide guidelines for the modeling of concrete, masonry, structural steel, and reinforcing bars. They recommended the use of a stress scale factor equal to one to conduct true modeling of reinforced concrete. They conducted many tests on small-scale reinforced concrete specimens, which revealed that the total number of major visible cracks decreases with decreasing the specimen size, while the overall cracking patterns will be similar. Zia et al. (1970) discussed bond similitude requirements in reinforced concrete. For true models, they recommended the use of a stress scale factor of one to ensure that the bond stresses developed by the model reinforcement and the ultimate bond strength of model and prototype reinforcement are identical.

The selection of a model scaling factor for this study took into consideration the characteristics of the existing bridge, the intent to replicate the behavior of the existing and retrofitted knee joint systems as accurately as possible, and the limitations of the laboratory facilities. Based on these considerations, a dimension scale factor (S_F) of three was selected to model the prototype bents.

The relations between model and prototype quantities were determined using a stress scale factor of unity and a dimension scale factor of 3. Table 3.2 shows a summary of the scale factors for different physical quantities (McLean, 1987).

Table 3.2 Summary of Similitude Requirements (Adapted from McLean, 1987)

Quantity	Dimension	Scale Factor for Practical True Model
Stresses	FL^{-2}	1
Strains	---	1
Modulus of Elasticity	FL^{-2}	1
Poisson's ratio	---	1
Mass Density	FL^{-3}	$1/S_F$
Linear Dimension	L	S_F
Displacement	L	S_F
Area	L^2	S_F^2
Concentrated Load	F	S_F^2
Line Load	FL^{-1}	S_F
Pressure	FL^{-2}	1
Moment	FL	S_F^3

3.4 SPECIMEN VARIABLES AND DETAILS

The behavior of the existing and upgraded knee joint systems was investigated using seven one-third scale models subjected to in-plane or out-of-plane forces. Table 3.3 shows the basic features of the seven specimens. The table also includes the designation used to refer to particular specimens throughout the study.

The first phase of testing examined three as-built specimens with two basic beam configurations; the first two specimens containing short outrigger beam, and the third

specimen had a long outrigger beam configuration. The first as-built short specimen was tested under in-plane loading, and the second one was tested under out-of-plane loading. The behavior of the long outrigger specimen was investigated only under the effect of in-plane loading. Retrofit measures were developed based on the observed failure mechanisms as well as the force and deformation capacities obtained from the experiments on the as-built outrigger knee joints and evaluated through testing.

Table 3.3 Test Specimen Designations

Unit No.	Specimen Type	Designation	Upgrade Type	Load Pattern
1	As-built long outrigger	ALI	None	In-plane
2	As-built short outrigger	ASI	None	In-plane
3	As-built short outrigger	ASO	None	Out-of-plane
4	Retrofitted long outrigger	RLI	Steel casing	In-plane
5	Retrofitted short outrigger	RSI	Steel casing	In-plane
6	Retrofitted split long outrigger	RSPLI	Steel casing	In-plane
7	Retrofitted short outrigger	RSO	Steel casing	Out-of-plane

3.4.1 Specimen Configuration

The specimen arrangement was selected to represent the entire length of the prototype outrigger beam, the knee joint and half the length of the column. The length of the column in the test setup models the length of the prototype column up to the inflection point in the bending moment diagram for the columns under lateral loading. Using the software SAP2000 (CSI, 2003), a two-dimensional linear elastic analysis of the bridge bents was performed to determine the location of the inflection point. The results

of the analyses showed that the location of the inflection point ranges from 0.45 to 0.55 of the column's height. Consequently, an average value of 0.50 was adopted and used as the column height in the test setup.

Limits on the weight and ability to handle the test specimens made it necessary to substitute part of the concrete column with a steel section. Therefore, the column length was reduced to 36 in. (914 mm) and was checked to insure that it provided sufficient development length for the scaled longitudinal reinforcement of the prototype columns. The remaining part of the column was an A500 steel tube section designed to remain elastic at the anticipated failure load of the specimen. A group of six, cast-in-place, Grade-8 high strength anchor bolts were placed in the top of the concrete column to transfer the forces from the steel section. The bolts were 12-in. (305-mm) long headed type bolts with 8.5 in. (216 mm) effective embedment length. Confinement of the anchor bolts was achieved by providing the top 15.0 in. (381 mm) of the column with No. 3 (9.5 mm) hoops at 2.25 in. (57 mm) spacing.

Limits on the cost, size, and weight of the specimens prevented complete modeling of the deck and the actual boundary conditions it provides for the outrigger beam. Thus, a stiff anchor block was selected to model the monolithic connection of the beam to the bridge deck. The following Figures 3.5 to 3.7 show the dimensions of as-built short, as-built long and the split long outrigger specimens, respectively.

Steel jackets were applied to the columns in the Spokane Street Oversrossing as a first phase of retrofitting for the bridge implemented by WSDOT. Therefore, the columns in the specimens were retrofitted to replicate the current state of the bridge.

Steel jacket details are discussed separately for each specimen in the specimen reinforcement details section, Section 3.4.2.

Figure 3.5 As-Built Long Outrigger Specimens Dimensions
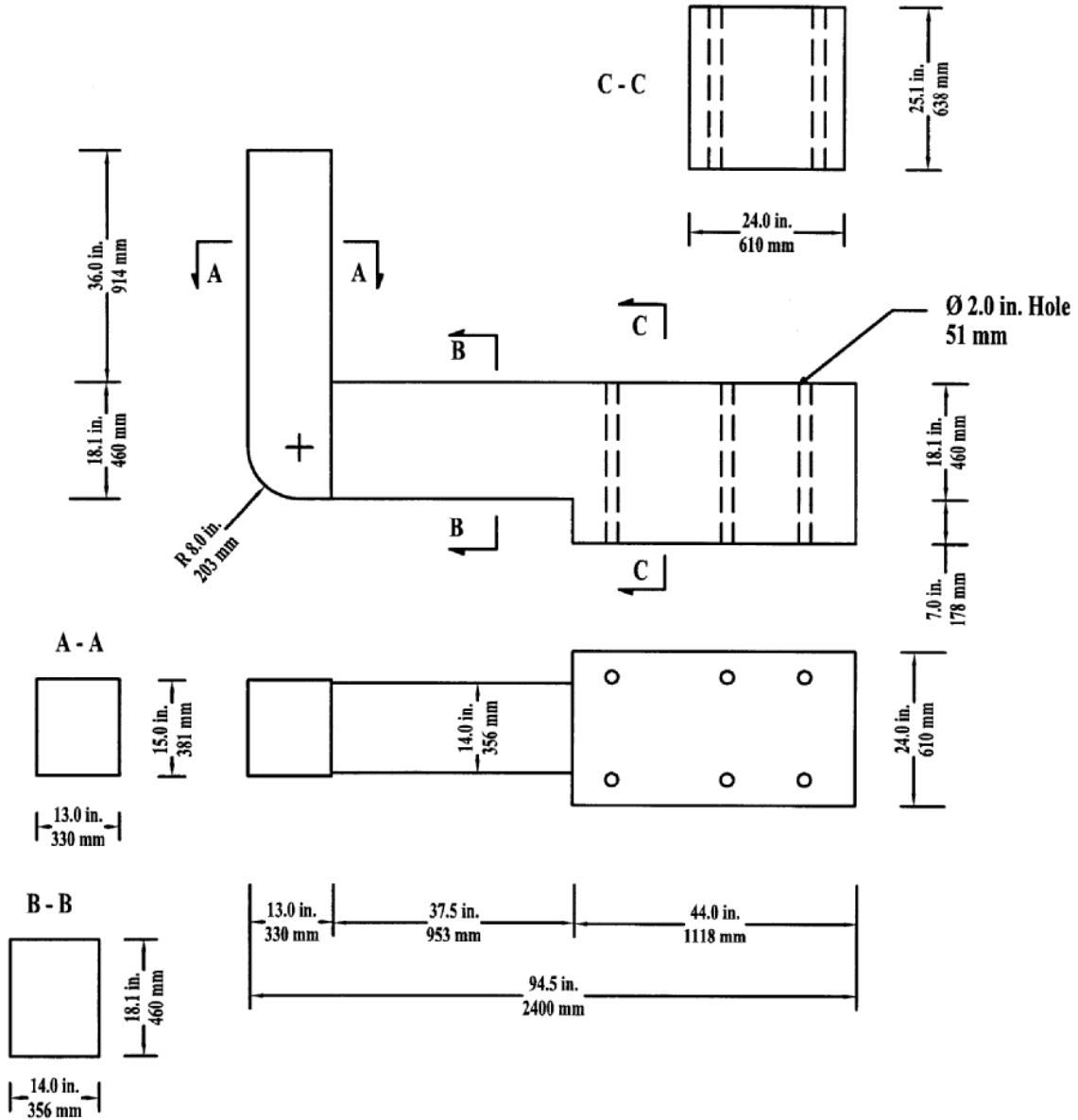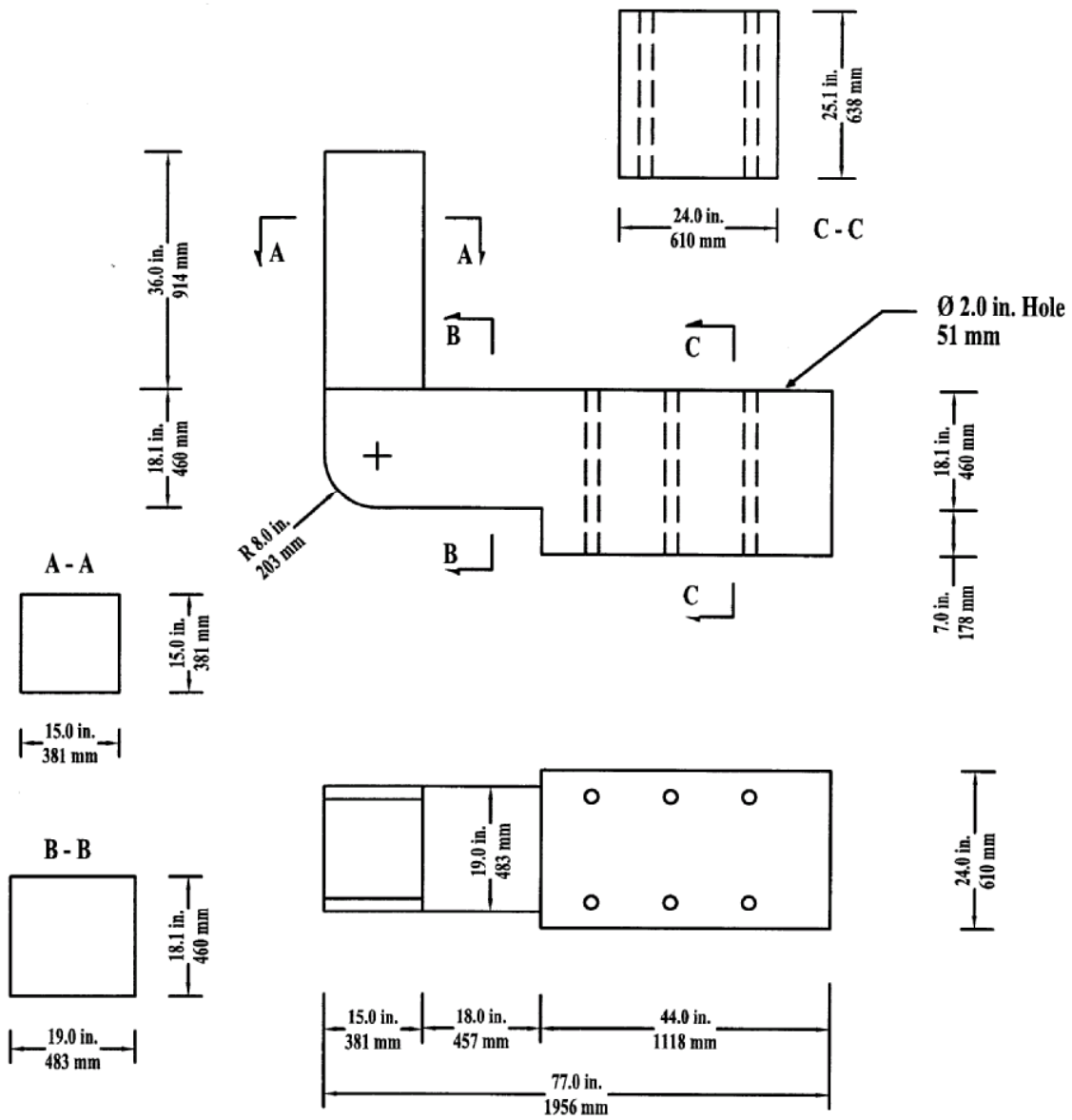
Figure 3.6 As-Built Short Outrigger Specimens Dimensions

65
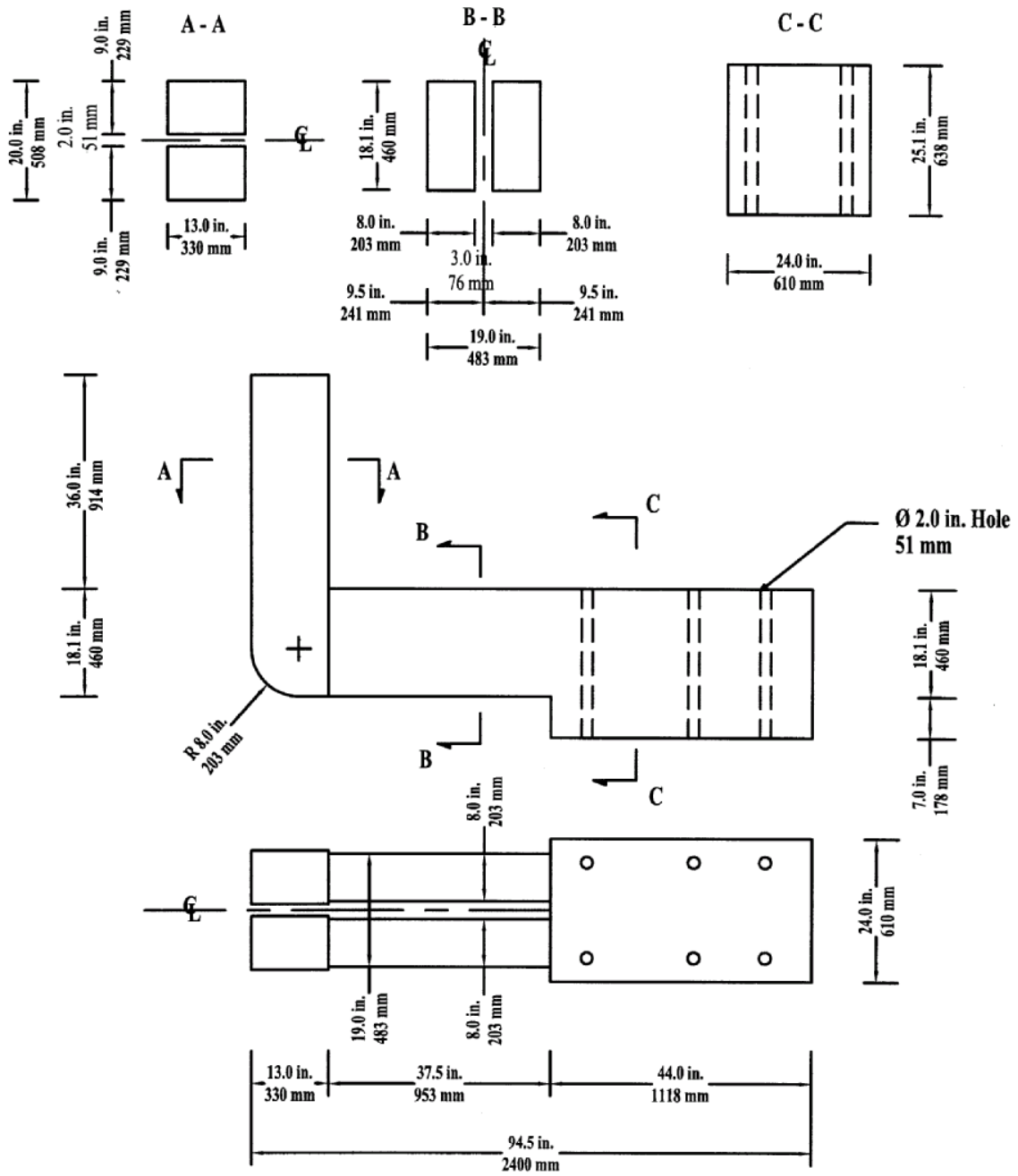
Figure 3.7 As-Built Split Long Outrigger Specimen Dimensions

66

3.4.2 Specimen Reinforcement Details

3.4.2.1 Long Outrigger Specimen

The reinforcement details of the test specimen as-built long outrigger (ALI) were chosen to replicate the as-built bent #36 details as closely as possible. Figure 3.8 shows an overall view of Specimen ALI. A photograph of the test specimen prior to forming is shown in Figure 3.9.

Figure 3.8 Overall View of the As-Built Long Outrigger Specimen

Figure 3.9 As-Built Long Outrigger Specimen Prior to Forming

Figure 3.10 shows the reinforcement details of Specimen ALI. The longitudinal column reinforcement consisted of 22 No. 4 (13 mm) (ρ=2.26%) Grade 40 (276 MPa) bars, which modeled the 22 No. 11 (36 mm) (ρ=1.96%) Grade 40 (276 MPa) bars of the prototype. The difference between the longitudinal reinforcement ratios of the test specimen and the prototype arises from the preservation of the number of reinforcing bars and the difficulty to directly scale the No. 14 (43 mm) bars using a scale factor of 3. The column transverse reinforcement in the model was two 0.25-in. (6.4-mm) diameter undeformed closed stirrups at 5.25 in. (133 mm) spacing, which replicated two No. 3 (9.5 mm) deformed closed stirrups at 12 in. (305 mm) spacing in the prototype. Modeling the transverse reinforcement of the column exactly was not a concern since the columns were retrofitted with steel jackets representing the infield situation.   Horizontal joint

reinforcement in the model consisted of 0.25-in. (6.4-mm) diameter Grade A36 steel bars at 5.25 in. (133 mm) as transverse column reinforcement extending into the joint region.

The outrigger beam longitudinal negative reinforcement consisted of 5 No. 5 (16 mm) Grade 40 (276 MPa) bars that ran the full length of the beam, modeling 6 No. 11 (36 mm) Grade 40 (276 MPa) bars in the prototype. Longitudinal positive reinforcement consisted of 16 No. 5 (16 mm) Grade 40 (276 MPa) bars, which replicated the 18 No. 14 (43 mm) Grade 40 (276 MPa) bars of the prototype. These bars were distributed in three rows with 1.0 in. (25 mm) clear distance between the rows. Beam side reinforcement consisted of 12 No. 3 (9.5 mm) Grade 40 (276 MPa) bars replicating the 14 No. 8 (25 mm) Grade 40 (276 MPa) bars in the prototype. The outrigger beam transverse reinforcement consisted of 4 legged No. 3 (9.5 mm) Grade 40 (276 MPa) U-shaped stirrups with a spacing of 2.25 in. (57 mm), which modeled two No. 7 (22 mm) U-shaped stirrups at 4.0 in. (102 mm) spacing in the prototype. Thus, the ratio of the transverse reinforcement area to its spacing (A_v/s) in the model is 0.20, which is equal to one-third the ratio in the prototype for which (A_v/s)/3 equals 0.20. Hence, the model preserves the transverse shear reinforcement area per unit length. An A36 single cross tie of 0.25-in. (6.4-mm) diameter was then used to close every other stirrup.

As a replication to the existing field situation, the column in the specimen was retrofitted using a circular steel jacket. The steel jacket had a thickness of 3/16 in. (4.8 mm) and was positioned over the entire length of the rectangular concrete column. The gap between the steel jacket and the column was filled out with a high strength grout. A gap of 3/4 in. (19 mm) was provided between the jacket and the beam, which replicated the 2.0-in. (51-mm) gap in the actual retrofit. This gap was provided to ensure enough

space for potential plastic hinging in the column and to avoid the risk of the jacket acting as compression reinforcement by bearing against the beam under large drift ratios. Figure 3.11 shows the dimensions and the details of the steel jacket for Specimen ALI.

The footing reinforcement was kept the same for all test specimens. The footing was connected rigidly to the laboratory floor using six 1.25-in. (32-mm) diameter threaded rods.
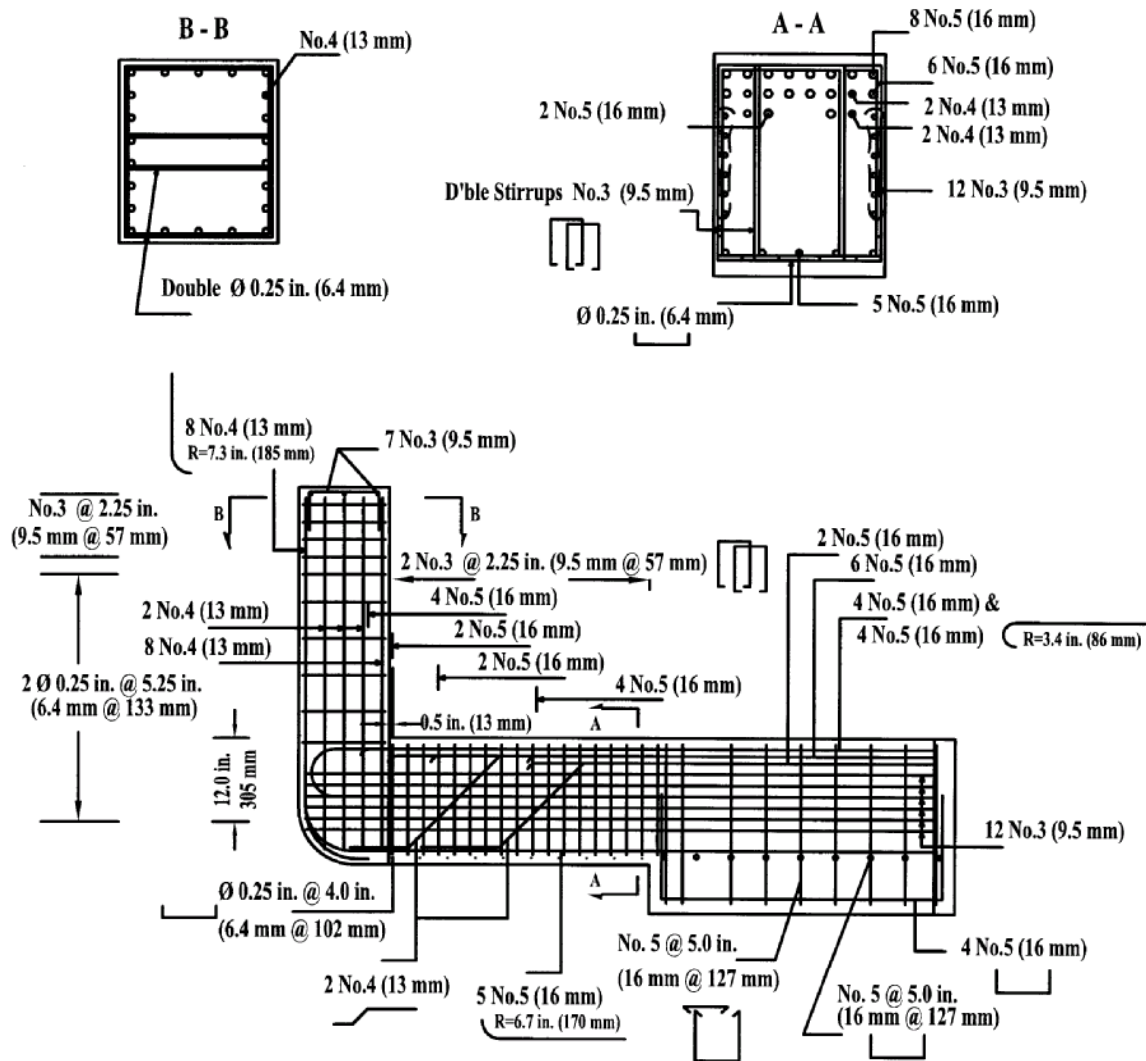
Figure 3.10 As-Built Long Outrigger Specimen Reinforcement Details
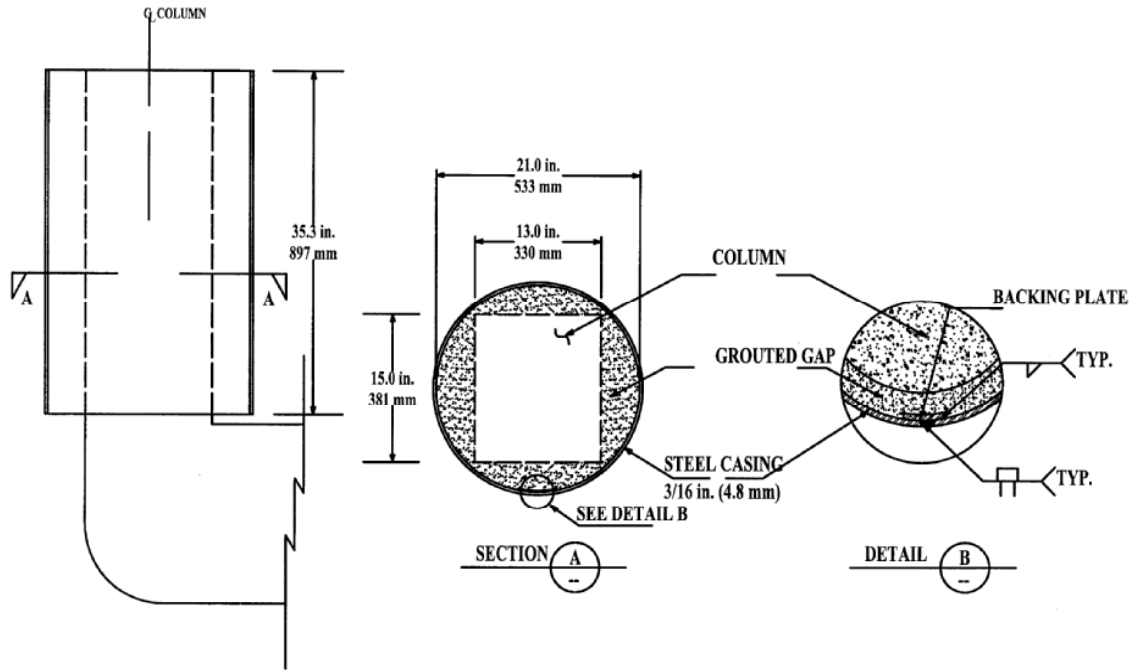
Figure 3.11 As-Built Long Outrigger Column Steel Jacket Retrofit Details

3.4.2.2 Short Outrigger Specimen

The reinforcement details of the test specimen as-built short outrigger (ASI) were chosen to replicate the as-built bent #20 details as closely as possible. Figure 3.12 shows an overall view of Specimen ASI. A photograph of the test specimen prior to forming is shown in Figure 3.13.

Figure 3.14 shows the reinforcement details of Specimen ASI. The longitudinal column reinforcement of Specimen ASI consisted of 26 No. 5 (16 mm) (ρ=3.58%) Grade 40 (276 MPa) bars, which modeled the 28 No. 14 (43 mm) (ρ=3.11%) Grade 40 (276 MPa) bars of the prototype. Similar to Specimen ALI, the longitudinal reinforcement on the exterior face of the column had 90-degree hooks and was lapped to the beam reinforcement within the joint. The column transverse reinforcement in the model was

two 0.25-in. (6.4-mm) diameter Grade A36 undeformed closed stirrups at 5.25 in. (133 mm) spacing, which replicated two No. 3 (9.5 mm) deformed closed stirrups at 12 in. (305 mm) spacing in the prototype. Horizontal joint reinforcement in the model consisted of two 0.25-in. (6.4- mm) diameter Grade A36 undeformed closed stirrups at 5.25 in. (133 mm) as transverse column reinforcement extending into the joint region.

The prototype longitudinal negative beam reinforcement consisted of 10 No. 18 (57 mm) Grade 40 (276 MPa) bars distributed over one layer. Since No. 6 (19 mm) bars, which directly model No. 18 (57 mm) bars, were not available in Grade 40 (276 MPa), it was decided to use No. 5 (16 mm) Grade 40 (276 MPa) bars instead. Thus, the specimen outrigger beam longitudinal negative reinforcement consisted of 14 No. 5 (16 mm) Grade 40 (276 MPa) bars distributed on two layers with 1.0 in. (25 mm) clearance between the layers. The outrigger beam longitudinal positive reinforcement consisted of 20 No. 5 (16 mm) Grade 40 (276 MPa), which replicated the 9 No. 14 (43 mm) and the 9 No. 18 (57 mm) Grade 40 (276 MPa) bars of the prototype. Beam side reinforcement of 12 No. 3 (9.5 mm) Grade 40 (276 MPa) bars modeling the 14 No. 8 (25 mm) Grade 40 (276 MPa) bars in the prototype were added. The beam transverse reinforcement consisted of 4 legged, No. 3 (9.5 mm) Grade 40 (276 MPa) U-shaped stirrups with a spacing of 2.25 in. (57 mm), which replicated two No. 7 (22 mm) Grade 40 (276 MPa) U-shaped stirrups at 4.0 in. (102 mm) spacing in the prototype. A single No. 3 (9.5 mm) Grade 40 (276 MPa) cross tie was also included on the top of every other stirrup.

A circular steel jacket was applied to the column of Specimen ASI as a replication to the existing bridge situation. The details of the steel jacket were the same as for

Specimen ALI, as shown in Figure 3.11, except for the diameter of the jacket, which was increased to 22.0 in. (559 mm).

Figure 3.12 Overall View of the As-Built Short Outrigger Specimen

Figure 3.13 As-Built Short Outrigger Specimen Prior to Forming
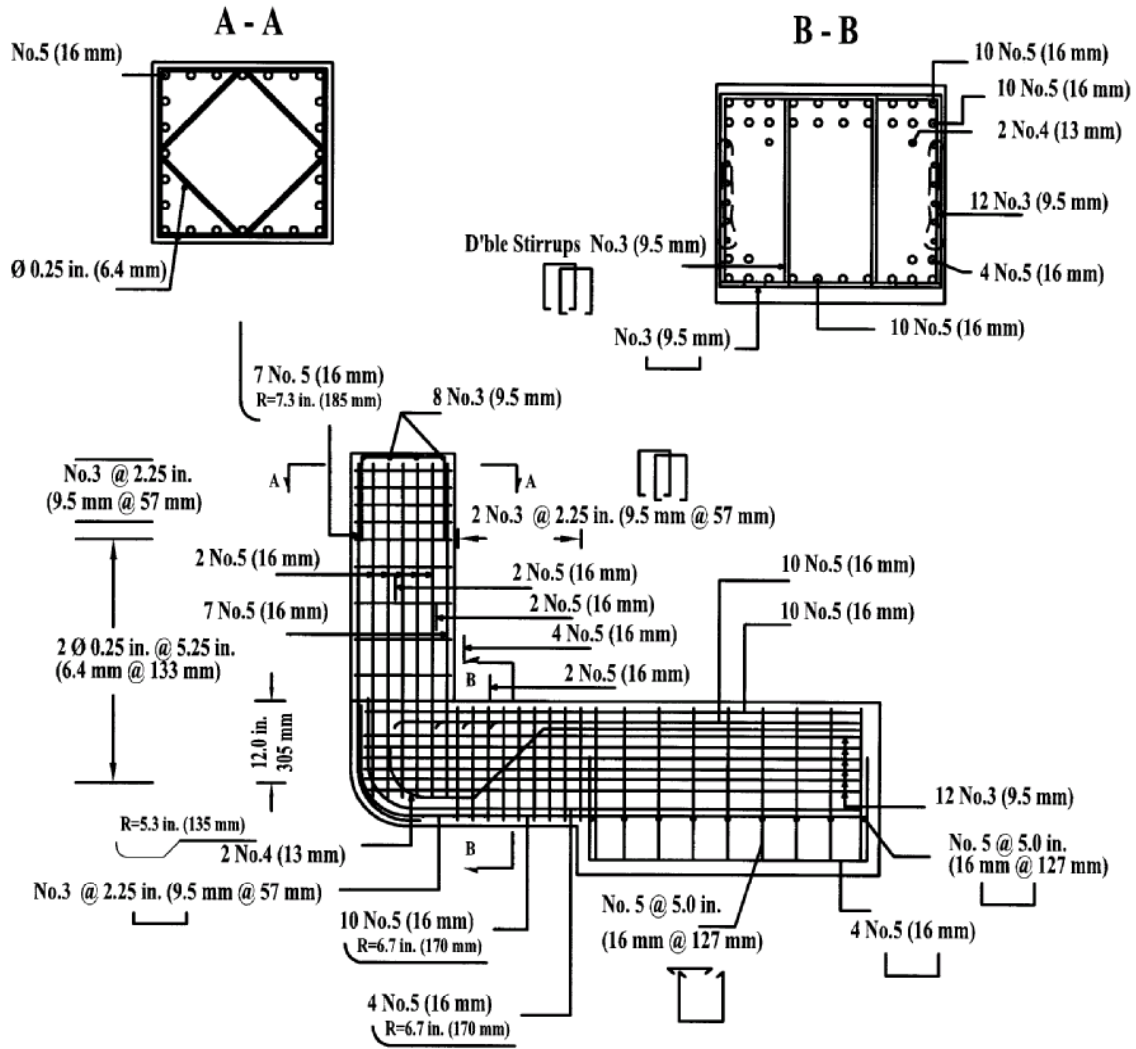
Figure 3.14 As-Built Short Outrigger Specimen Reinforcement Details

3.4.2.3 Retrofitted Long Outrigger Specimen

Construction and reinforcement details of the retrofitted long outrigger specimen were nominally identical to the as-built long outrigger specimen. The retrofit scheme of the outrigger beam and the knee joint was carried out in three steps. First, a ¾-in. (19-mm) gap was provided at a distance of 5.50 in. (140 mm) above the beam-joint interface by removing the existing column jacket and the grout in that region. This gap was extended to the depth of the original column. Second, two clamshell sections made of

A36 steel with 3/16-in. (4.8-mm) thickness and a 24.9-in. (632-mm) diameter were fabricated offsite and welded together in the laboratory using full capacity welding. The clamshell jackets, continuous over the beam, were terminated at a ¾-in. (19-mm) distance from the face of the anchor block. The dimensions and details of the beam and joint jackets of Specimen RLI are shown in Figure 3.15.

The clamshells were fabricated by curving a flat plate to form a pipe section with the required length and radius. The pipe was then cut at a 45-degree angle to the required length to jacket the beam. By rotating the leftover piece (eventually forming the joint jacket) in-plane by 90-degrees, followed by a 180-degree out-of-plane rotation, the piece was then welded to the beam jacket along the 45-degree seam using a full capacity weld forming an elbow shape. The jacket overlapped the existing column jacket above the beam-joint interface with a lip distance of 1.5 in. (38 mm) over the beam jacket. Finally, the difference between the beam and the joint and the steel jacket was filled by high strength grout. Figure 3.16 shows an overall view of Specimen RLI.
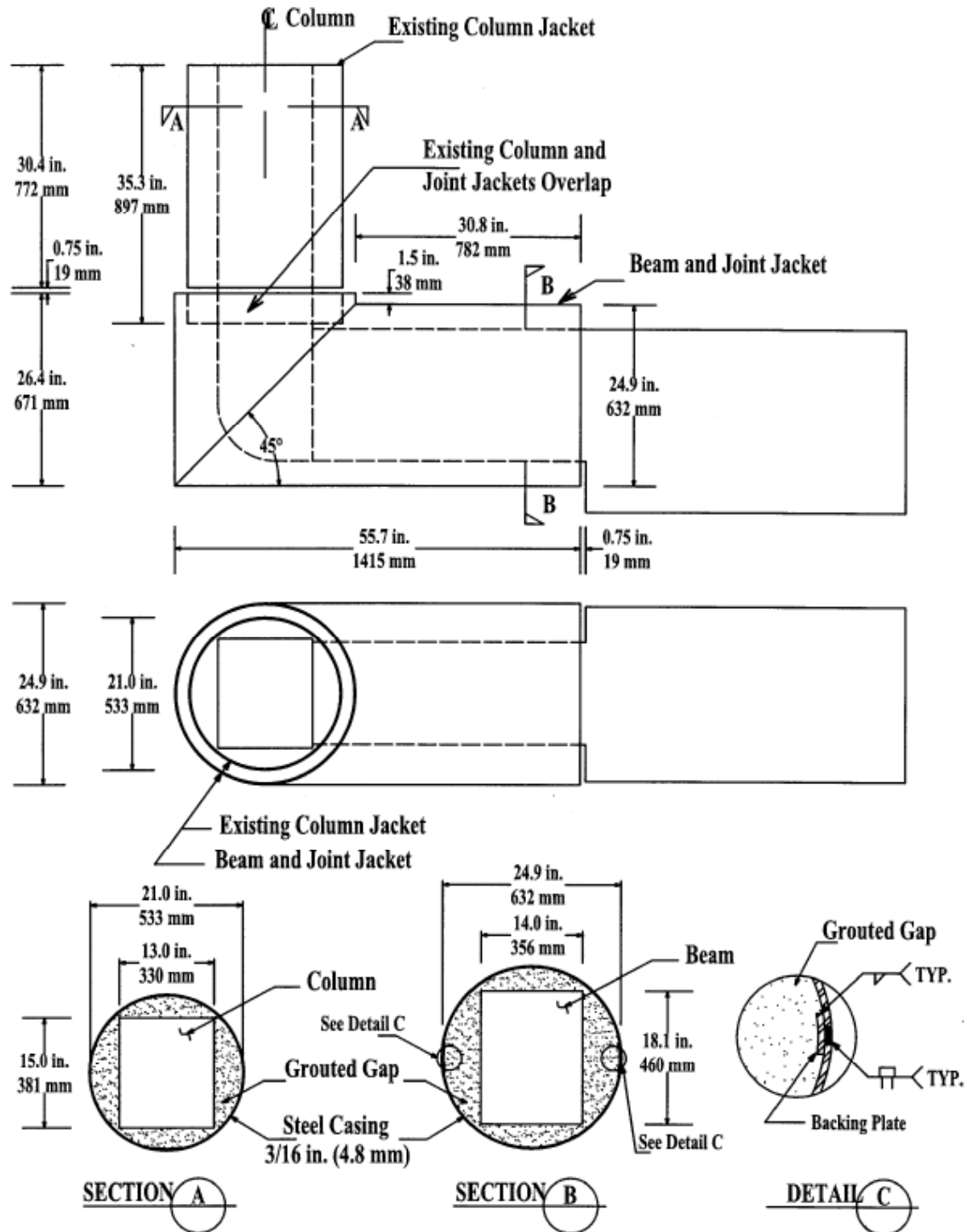
Figure 3.15 Beam and Joint Jackets Details for Specimen RLI

Figure 3.16 Overall View of the Retrofitted Long Outrigger Specimen

3.4.2.4 Retrofitted Short Outrigger Specimens

Construction and reinforcement details of the retrofitted short outrigger specimen were nominally identical to the as-built long outrigger specimen. The retrofit scheme of the outrigger beam and the knee joint was carried out in three steps. First, a ¾-in. (19-mm) gap was provided at a distance of 5.25 in. (133 mm) above the beam-joint interface by removing the existing column jacket and the grout in that region. This gap was extended to the depth of the original column. Second, two clamshell sections made of A36 steel with 3/16-in. (4.8-mm) thickness and 27.4-in. (696-mm) diameter were fabricated offsite and welded together in the laboratory using full capacity welding.

Figure 3.17 shows the details of the retrofit measure. The clamshell jackets continuous over the beam were terminated at a ¾-in. (19-mm) distance from the face of the anchor block. The clamshell jacket was fabricated in the same manner as discussed in the previous section.
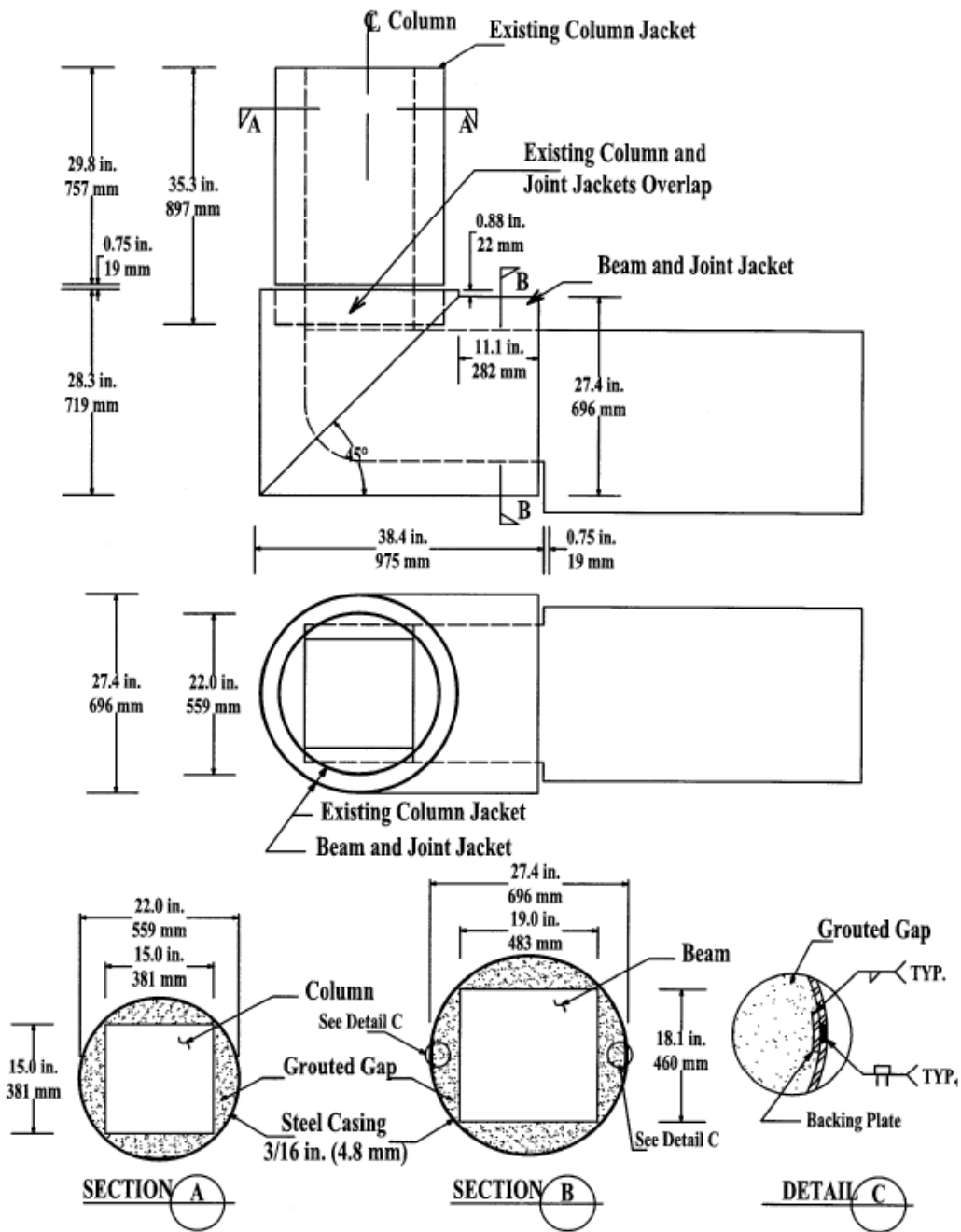
Figure 3.17 Beam and Joint Jackets Details of Specimen RSI and Specimen RSO

The joint jacket intersected with the beam jacket at a 45-degree plane forming an inverted L-shaped section around the beam and the joint. The jacket overlapped the existing column jacket above the beam-joint interface with a lip distance of 7/8 in. (22 mm) over the beam jacket. Finally, the gap between the beam and the joint and the steel jacket was filled by high strength grout. Figure 3.18 shows an overall view of a retrofitted short test specimen.

Figure 3.18 Overall View of the Retrofitted Short Outrigger Specimen

3.4.2.5 Retrofitted Long Split Outrigger Specimen

The reinforcement details of the retrofitted long split outrigger test specimen (RSPLI) prior to retrofitting were chosen to model the as-built bent #34 details as closely as possible. Due to application issues related to the retrofit installation in the scaled split long outrigger specimen, the 2-in. (5-cm) gap in the prototype split columns was not scaled down, and the full gap was incorporated in the specimen. Figure 3.19 shows an overall view of Specimen RSPLI. A photograph of the test specimen prior to forming the columns is shown in Figure 3.20.

Figure 3.19 Overall View of the Retrofitted Split Long Outrigger Specimen
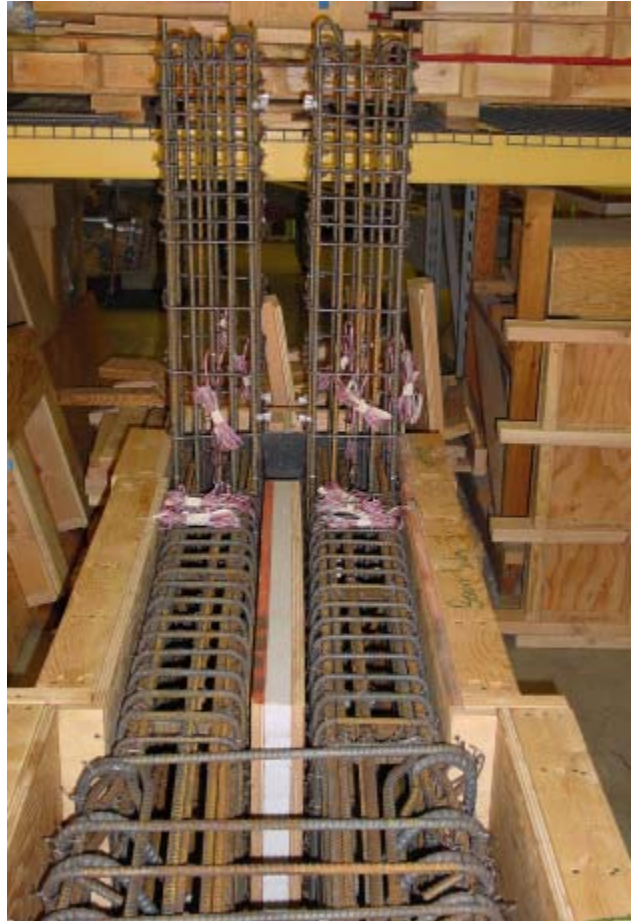
Figure 3.20 Retrofitted Split Long Outrigger Specimen Prior to Column Forming

Figure 3.21 shows the reinforcement details of Specimen RSPLI.   The longitudinal column reinforcement of Specimen RSPLI consisted of 16 No. 3 (9.5 mm) (ρ=1.50%) Grade 40 (276 MPa) bars, which modeled the 16 No. 9 (29 mm) (ρ=1.52%) Grade 40 (276 MPa) bars of the prototype. The column transverse reinforcement in the model was 0.25-in. (6.4-mm) diameter undeformed closed stirrups at 5.25 in. (133 mm) spacing, which replicated No. 3 (9.5 mm) deformed closed stirrups at 12 in. (305 mm) spacing in the prototype. Horizontal joint reinforcement in the model consisted of 0.25-

in. (6.4-mm) diameter Grade A36 steel bars at 5.25 in. (133 mm) as transverse column reinforcement extending into the joint region.

Outrigger beam longitudinal negative reinforcement consisted of 3 No. 4 (13 mm) Grade 40 (276 MPa) bars that ran the full length of the beam. These 3 No. 4 (13 mm) Grade 40 (276 MPa) bars modeled the 3 No. 11 (36 mm) Grade 40 (276 MPa) bars of the prototype. Longitudinal positive reinforcement consisted of 8 No. 4 (13 mm) Grade 40 (276 MPa), which replicated the 5 No. 11 (36 mm) and the 3 No. 14 (43 mm) Grade 40 (276 MPa) bars of the prototype. The 8 No. 4 Grade 40 (276 MPa) bars were distributed in two rows with 1.0 in. (25 mm) clear distance between the rows. 6 No. 3 (9.5 mm) Grade 40 (276 MPa) bars were added on both sides of the beam as a replication to the 10 No. 7 (22 mm) Grade 40 (276 MPa) bars in the prototype. The outrigger beam transverse reinforcement consisted of 2 legged, No. 3 (9.5 mm) Grade 40 (276 MPa) U-shaped stirrups with a spacing of 2.5 in. (64 mm) beginning ¾ in. (19 mm) out from the column face, which replicated one No. 7 (22 mm) U-shaped stirrups at 4.5 in. (114 mm) spacing in the prototype. A single 0.25-in. (6.4-mm) diameter Grade A36 cross tie was also included on the top of every other stirrup.

The retrofit scheme of the outrigger beam and the knee joint was carried out in four steps. First, a ¾- in. (19-mm) gap was provided at a distance of 5.25 in. (133 mm) above the beam-joint interface by removing the existing column jacket, whose details are shown in Figure 3.22, and the grout in that region. This gap was extended to the depth of the original column. The existence of a 2-in. (5-cm) gap between the split columns made it impossible to reach the steel jacket on the inner surface of the columns. Therefore, the existing jacket around the columns was cut along the perimeter of the circular face of the

D-shaped jacket and along the inside surface for the area projecting outside the original concrete column leaving a 3/16-in. (4.8-mm) steel skin behind the column. Second, Grade A36 rectangular steel plates of 3/16-in. (4.8-mm) thickness were attached to the inner faces of the beam and the joint using high strength epoxy. The plate was bent out at a 45-degree angle ahead of the beam-joint interface due to the ½- in. (13-mm) increase in the size of the joint over the beam.
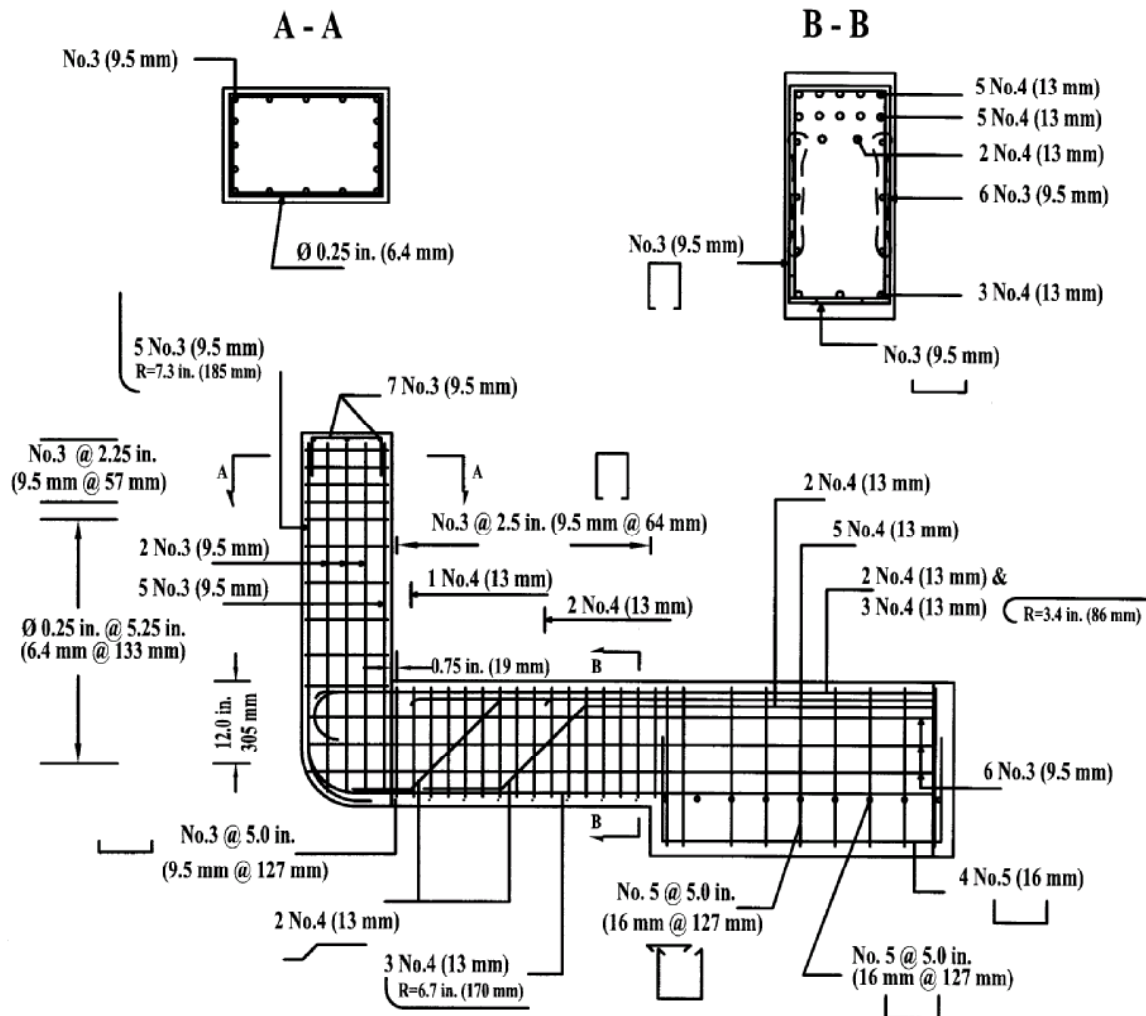
Figure 3.21 Retrofitted Split Outrigger Specimen Reinforcement Details

Again, due to the existing steel jacket around the column above the column-joint interface, the plate was stopped at that location and another rectangular plate projecting 3/16 in. (4.8 mm) (i.e., the thickness of the existing steel plate on the inner of the column) was fillet welded at the shop to the original flat plate. Details of the flat plate are shown in Figure 3.23.

In the third step, clamshell sections made of A36 steel with 3/16-in. (4.8-mm) thickness were fabricated offsite and welded in the laboratory to the rectangular plates on the inner face of the beam and the joint using a full capacity weld, forming a D-shaped section around the beam and the joint. The clamshell jackets continuous over the beam were terminated at a ¾-in. (19-mm) distance from the face of the anchor block. Details of the retrofit measure are shown in Figure 3.24.

The joint jacket intersected with the beam jacket at a 45-degree plane and overlapped the existing column jacket above the beam-joint interface with a lip distance of 1.5 in. (38 mm) over the beam jacket. Finally, the gap between the beam and the joint and the steel jacket was filled by high strength grout. Figure 3.25 shows the construction phases of the retrofit measure around the beam and the joint and details of the retrofit scheme for Specimen ASPLI.
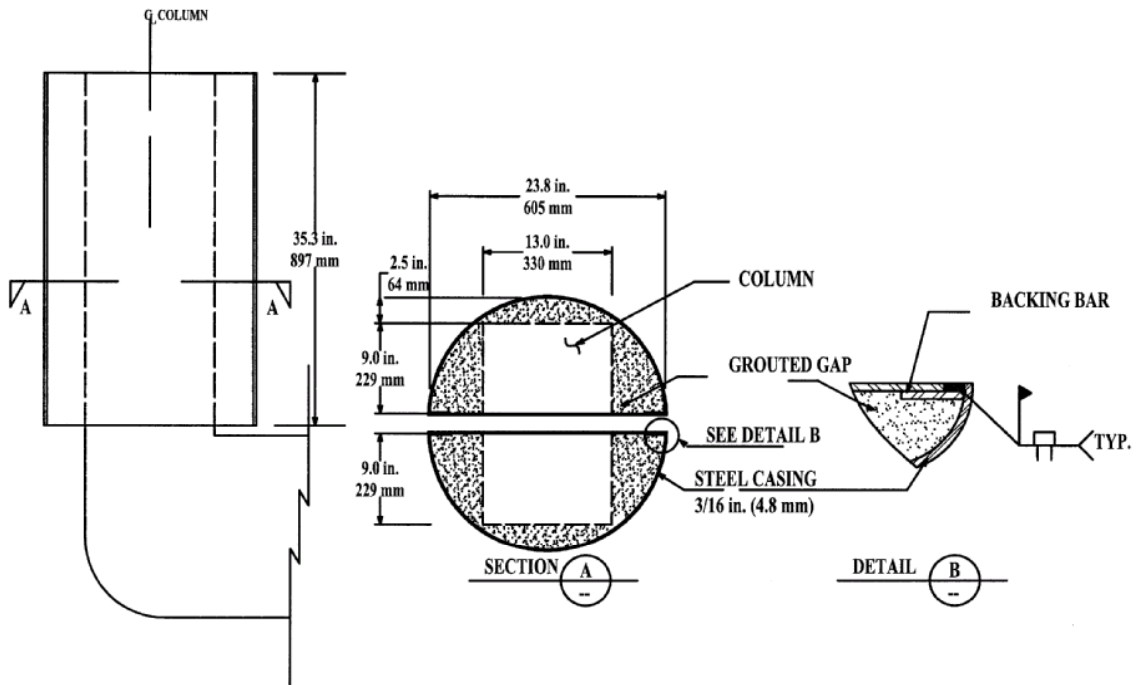
Figure 3.22 Retrofitted Split Long Outrigger Column Steel Jacket Retrofit Details
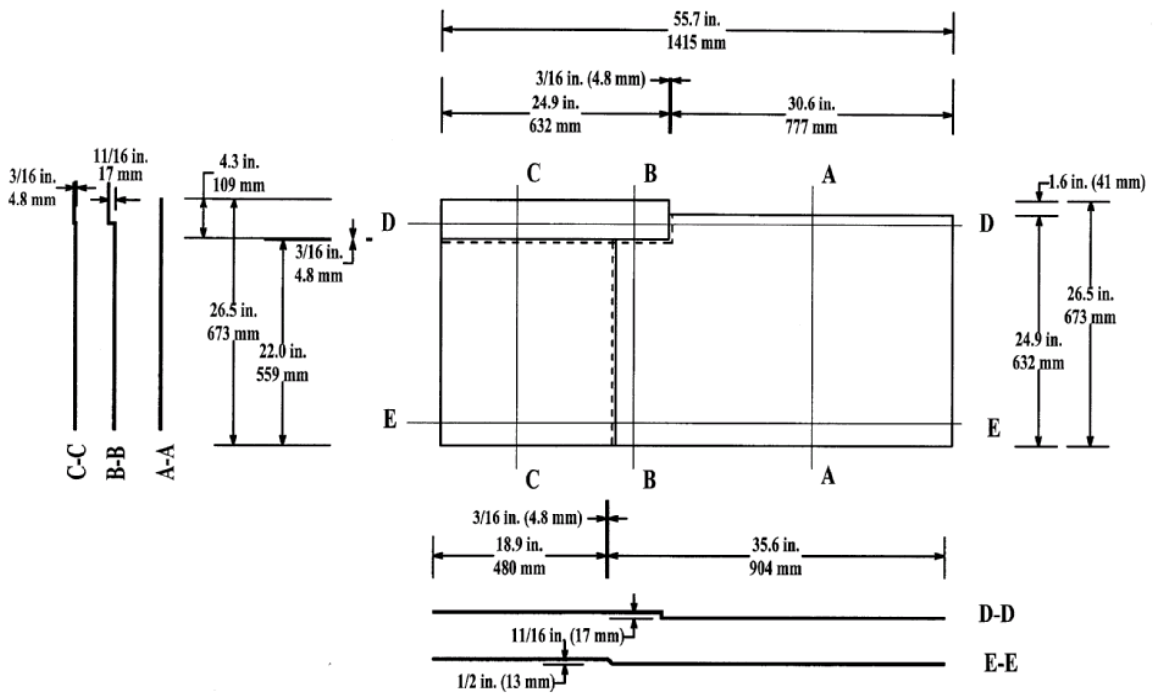
Figure 3.23 Flat Plate Detailing

85
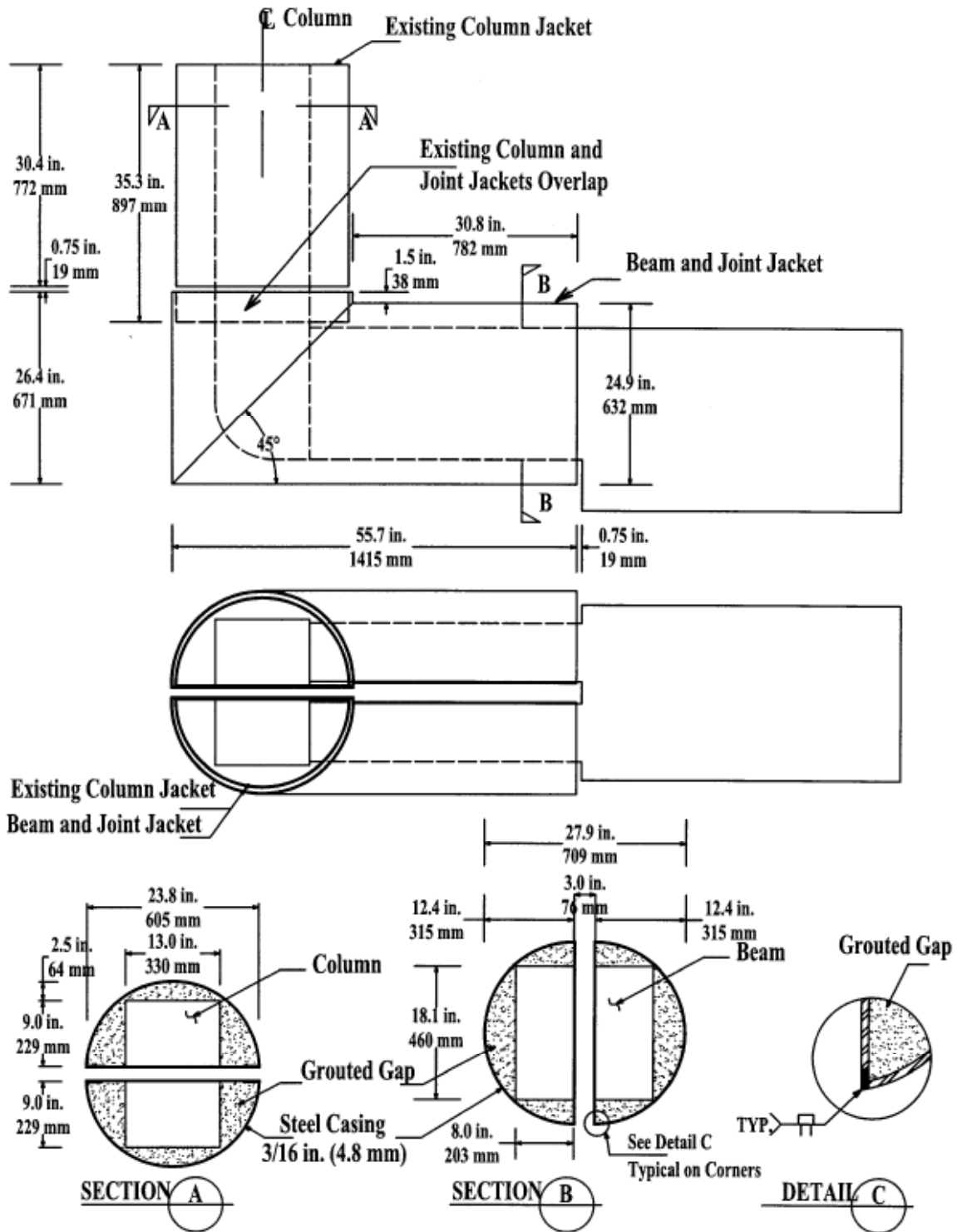
Figure 3.24 Retrofitted Long Outrigger Clamshell Dimensions (Front View)

Figure 3.25 Retrofit Application Around the Beam and the Joint Showing the 3/4 in. (19 mm) New Gap, the Backside Plate and the Final Shape on One Side

3.5 MATERIAL PROPERTIES

3.5.1 Concrete and Grout

The materials used in this study were selected to reflect the materials used in the actual structure as close as possible. A local ready-mix plant supplied concrete with 4000-psi (28 MPa) design compressive strength on two subsequent days. The first pour included casting of the anchor block, the beam and the joint. The second pour was for only the column, resulting in a construction joint at the column-joint interface, as exists in the original bridge.

The concrete mixes consisted of Portland Cement Type I/II with ½ in. (13 mm) maximum size coarse rounded aggregate, sand and superplasticizer. The mixes contained

6 sacks of cement per cubic yard. The grout used for the steel retrofit jacket on the column, beam and joint was a commercial pre-bagged high strength grout.

Concrete strengths were determined based on American Standards for Testing and Materials (ASTM) standards using three 6 in. (152 mm) diameter by 12 in. (305 mm) high cylinders. All cylinders were wet cured and tested after 28 days from casting. Grout strengths were determined using 2 in. (51 mm) diameter by 4 in. (102 mm) high cylinders. Table 3.4 shows the concrete and grout strengths.

Table 3.4 Concrete and Grout Compression Strengths

Section	Age (Days)	Strength, f_c'	
		(psi)	**(MPa)**
Column Concrete	28	4168	28.7
Beam, Joint and Footing Concrete	28	4240	29.2
Grout	3	4578	31.6

3.5.2 Reinforcement and Steel

Standard No. 3 (9.5 mm), No. 4 (13 mm) and No. 5 (16 mm) ASTM A 615 Grade 40 (276 MPa) rebars were used for the beam and column reinforcement. To ensure consistency, bars for each size were obtained from the same mill heat. The column and joint transverse reinforcement desired for modeling the existing ties was not available in standard ASTM bar sizes. Hence, a 0.25-in. (6.4-mm) diameter A36 steel rod was chosen. Coupon tensile tests from randomly selected samples were used to determine the properties of the reinforcing bars and the stress-strain curves. Results are given in Table 3.5 and Figure 3.26.

The retrofit jackets were rolled from 3/16-in. (4.8-mm) thick hot-rolled sheet steel and welded with a continuous full-penetration weld. 1 in. (25 mm) by 12 in. (305 mm) samples were pulled in tension to determine the yield and ultimate strengths. The results are listed in Table 3.5.

Table 3.5 Reinforcement Strengths

Reinforcement Size	Grade	f_y (ksi)		f_{su} (ksi)	
	(ksi)	(ksi)	(MPa)	(ksi)	(MPa)
Dia.= 0.25 in. (6.4 mm) round	36	51.2	353	--	--
No. 3 (9.5 mm) deformed	40	49.3	340	73.6	507
No. 4 (13 mm) deformed	40	53.4	368	87.5	603
No. 5 (16 mm) deformed	40	53.6	370	79.6	549
3/16 in. (4.8 mm) sheet metal	36	50.1	345	--	--
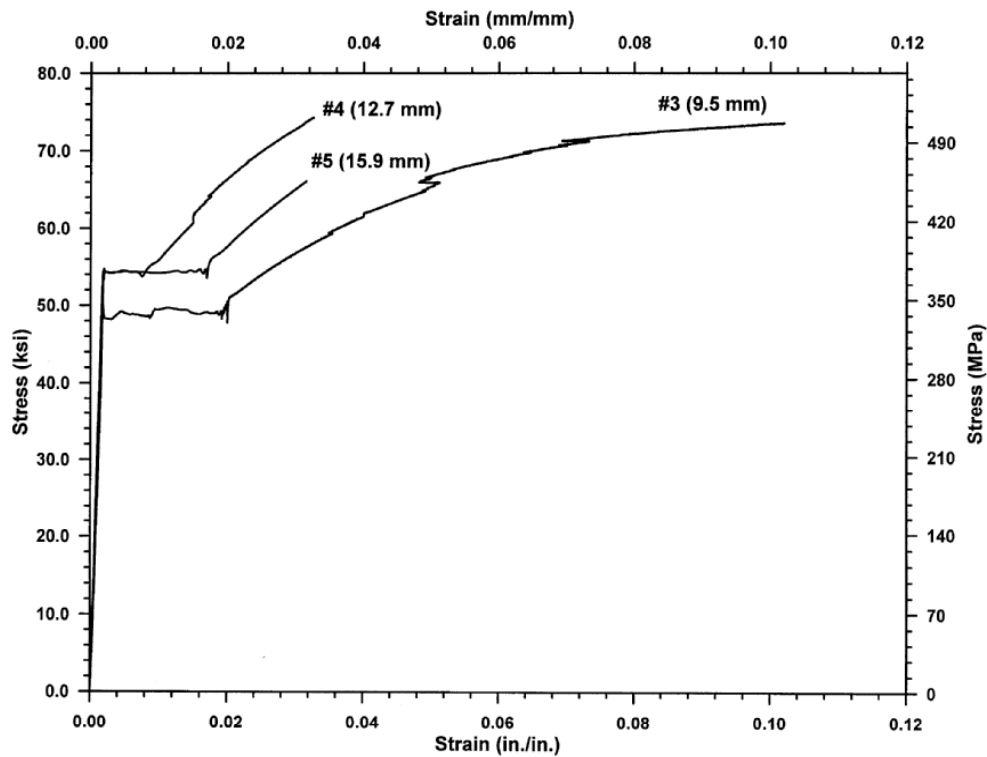
Figure 3.26 Stress-Strain Relationship for Reinforcing Steel

3.6 TESTING PROCEDURES

The selection of the testing procedures should be based on the expected behavior of the existing outrigger knee joints under earthquake loading. A simultaneous bi-directional horizontal motion together with vertical motion of the bridge is expected during an earthquake. However, only the horizontal part of the motion was considered in the present study. Hence, vertical motion of the bridge and its influence on the gravity loads was not modeled.

The effect of the horizontal motion on the outrigger bents can be considered by dividing the motion into two components: in-plane and out-of-plane. The in-plane motion causes in-plane bending of the outrigger beam and column, which results in a change in the axial and shear forces in the column as the outrigger knee joint opens or closes. The out-of-plane component of the bridge motion results in weak-axis bending and torsion of the outrigger beam and bending of the outrigger column. Consequently, it would be more realistic to apply a loading pattern that simulates the effects of the bi-directional motion of the bridge. However, the complex response of previously tested specimens under bi-directional displacement patterns as reported by other researchers (Thewalt and Stojadinovic, 1995), and the need for a bigger loading frame and additional actuators than are currently available, called for a loading pattern that simulates motion in each direction separately. Therefore, the response of the specimens was investigated under in-plane and out-of-plane loading separately.

The loading pattern was divided into a horizontal loading pattern, simulating the earthquake loading, and vertical loading, simulating the column axial load due to the self-weight of the structure and the change in the axial load due to the framing action. As

shown in Figure 3.28, the specimens were tested in an upside-down position with respect to the position of the outrigger knee joint in the real structure. A horizontal 240-kip (1068-kN) capacity actuator reacting against a loading frame was used to apply the horizontal loading pattern. A 200-kip (890-kN) capacity axial load ram provided a constant vertical loading to the top of the column. The application of a constant vertical loading pattern was selected due to the limitations in the laboratory facilities. On one hand, this arrangement will result in inconsistent model and prototype bending moment diagrams, especially for the cap beam bending moments away from the joint region. On the other hand, this configuration is convenient since an evaluation of the behavior of the joint and the members in the vicinity of the joint is the main focus of this study. Furthermore, the application of a constant vertical loading will result in a more definable response of the knee joint system.

Axial load levels of 55 kips (245 kN), 33 kips (147 kN) and 27.5 kips (122 kN) were used for short, long and split outrigger specimens, respectively. These load levels correspond to $0.059 f'_c A_g$, $0.041 f'_c A_g$ and $0.028 f'_c A_g$, respectively. The axial load value for each specimen was determined based on the bridge selfweight load carried by the prototype bent and the change in the axial load due to framing action under opening and closing of the bent. Since the axial load in the testing setup was not varied during testing, a decision was made to model the value of the axial load due to closing which would result in a higher level of demand on the system, providing a more conservative estimation of the overall behavior.

The in-plane setup of test specimens is shown in Figures 3.27 and 3.28. The anchor block of the specimen was fixed to the laboratory strong floor using high strength

1.25-in. (32-mm) diameter anchor rods. The steel tube section was attached to the top of the concrete column through high strength embedded anchor bolts. Two clevises on the lateral load actuator ends were used to position the actuator in place. On one side, the clevis was attached to a bearing plate, then bolted to the loading frame, and the clevis on the other side was bolted to the tube section. The axial load ram was attached to a free-sliding trolley with the swivel being bolted down to the steel plate on top of the tube section.

The out-of-plane setup for the test specimens is shown in Figure 3.29. In general, the specimen location and anchorage to the strong floor were kept the same as for the in-plane case, except for the actuator which was rotated 90 degrees to apply a horizontal force perpendicular to the plane of the specimen. This configuration will result in out-of-plane bending of the knee joint and simultaneous torsion and weak-axis bending of the beam. The axial load level was kept the same, with the axial load ram system being oriented in the same direction of the applied actuator force.

Loading of the test specimens started with the application of the axial load force. The application of the vertical load resulted in a small horizontal force in the actuator, and the horizontal actuator was then moved to a zero force position. Next, the horizontal loading pattern was applied in a quasi-static manner about this point. The horizontal loading was displacement controlled based on a pattern of progressively increasing multiples of 0.5 in. (13 mm) up to a horizontal displacement level of 4.0 in. (102 mm) and with 1.0-in. (25-mm) multiples thereafter. The loading pattern shown in Figure 3.30 was repeated three times for each displacement level. The software XTRACT (Imbsen Software Systems, 2002) was used to perform conventional flexural analysis to assist in

recognizing expected system yielding and ultimate displacements and forces prior to testing.
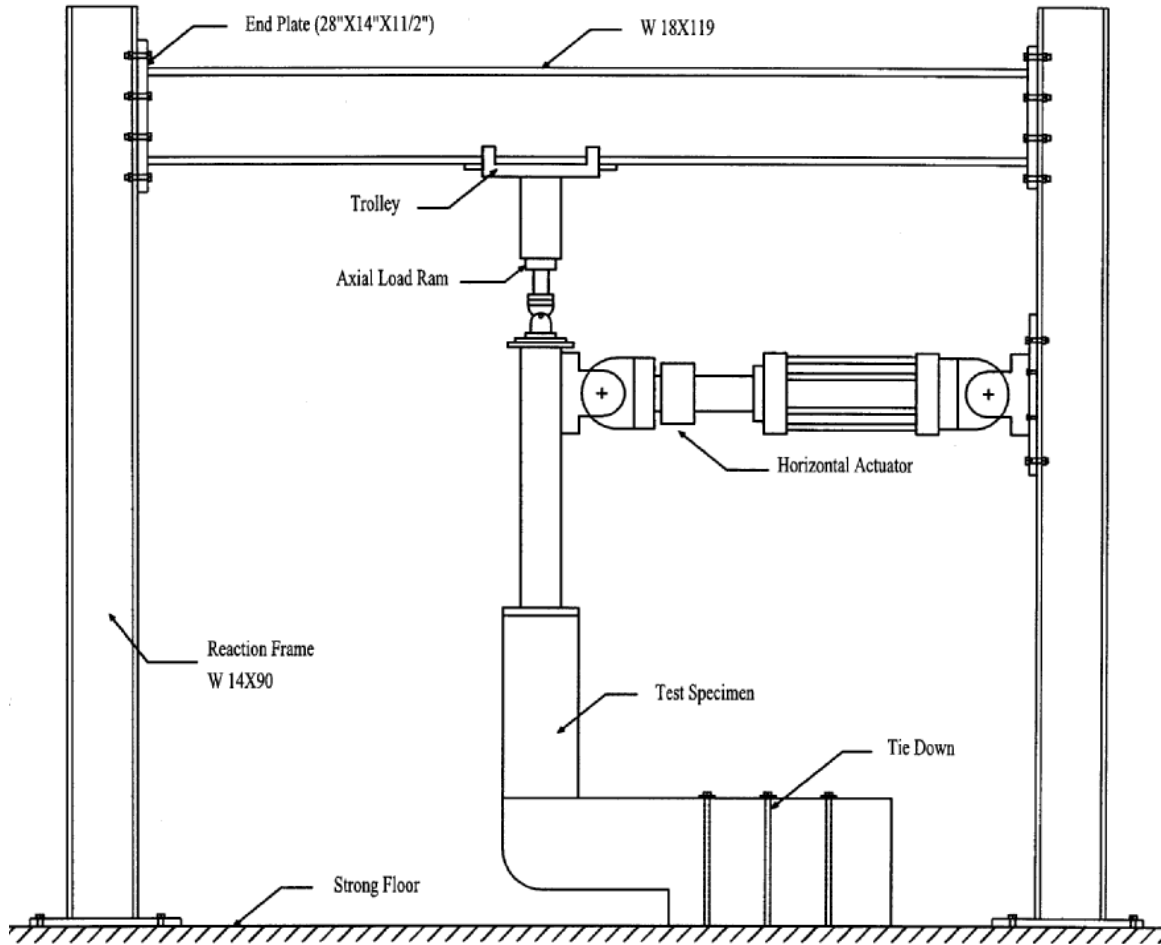
Figure 3.27 Overall In-Plane Test Setup
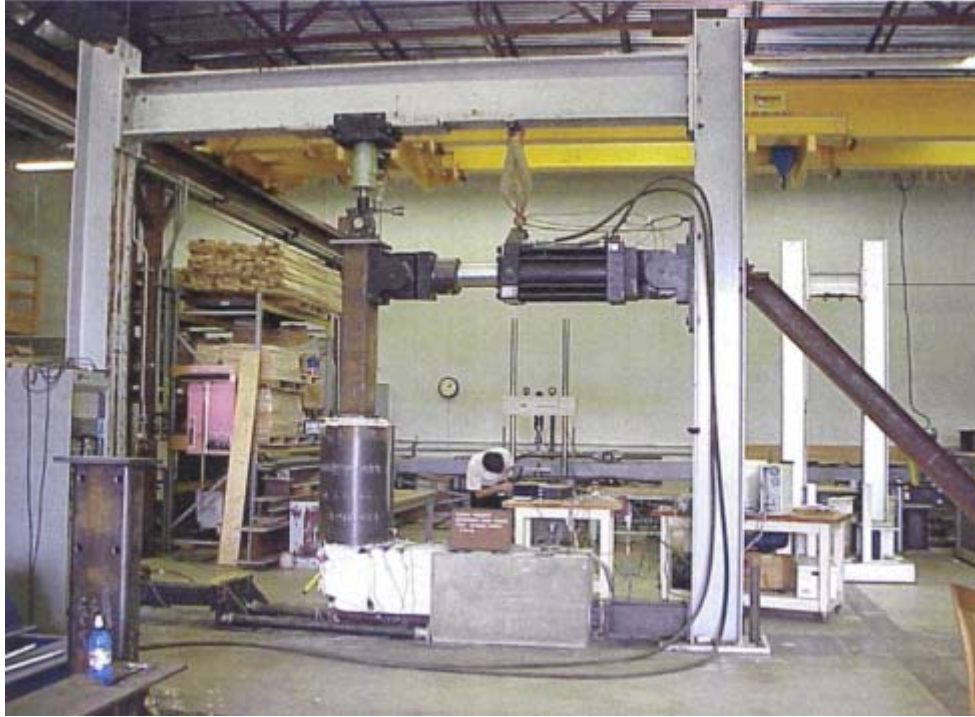
Figure 3.28 Overall In-Plane Test Setup

Figure 3.29 Overall Out-of--Plane Test Setup
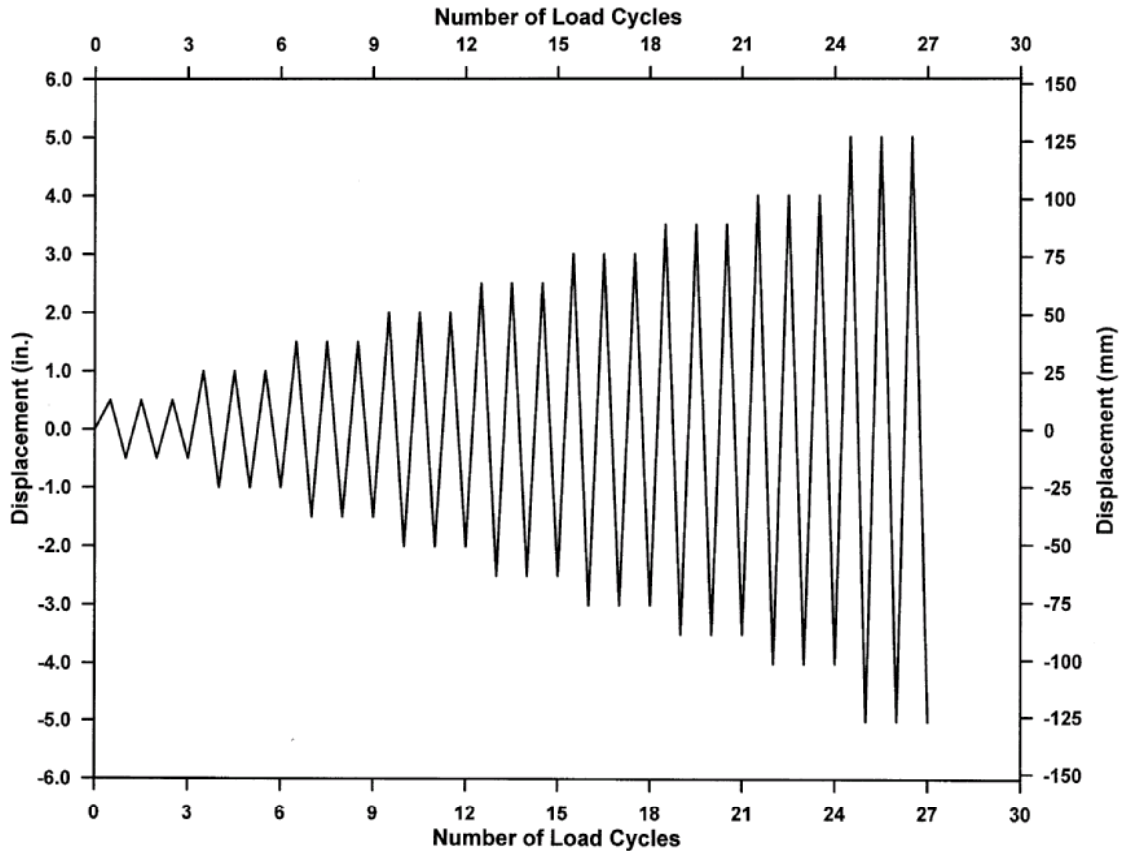
Figure 3.30 Horizontal Loading History

3.7 INSTRUMENTATION

The test specimens were instrumented to capture both global and local events. Between 20 to 35 channels of data were recorded during each test. During each cycle of testing, data was collected using a multi-channel data collection system designed to be remotely operated by a personal computer (PC) based software package, specifically using LABVIEW. Each channel was scanned at one sample per second.

The lateral load was applied using a hydraulic actuator with a travel stroke of ± 10 in. (254 mm). The actuator was controlled using a servohydraulic, closed-loop, MTS system. The horizontal displacement of the actuator, measured at the intersection of the

specimen with the actuator centerline, was determined using a built-in linear displacement potentiometer. A pressure-controlled center-hole ram mounted on a low-friction trolley was used to provide the required axial load to the specimen. The axial load trolley system is shown in Figure 3.31. The vertical displacement of the specimen measured from the outside face of the joint at intersection of the centerline of the outrigger beam and the centerline of the column was captured using a displacement potentiometer.

Figure 3.31 Axial Load Trolley System

Curvatures in the beam and the column in the vicinity of the joint interfaces were determined by measuring the difference in extension of two displacement potentiometers mounted on opposite sides of the member. The extension in the displacement

potentiometers on each side was converted to an average strain over the curvature gage length, referred to as a "cell". The difference in the average strains was divided by the distance between the two linear potentiometers to obtain curvatures. Moment curvature responses were then plotted as the maximum moment within a cell versus the average cell curvature.

Joint panel instrumentation was mounted on both sides of the joint for the as-built in-plane specimens, while the top and one of the beam side faces were instrumented for the as-built out-of-plane specimen. Five displacement potentiometers on each face were attached to the joint/beam to extract the shear mode of deformation, as shown in Figure 3.32. The displacement potentiometers were mounted on threaded rods adjacent to the corners of the joint/beam. Figure 3.33 shows typical displacement potentiometer locations in the as-built specimens tested under in-plane loading, while Figure 3.34 shows those for the as-built specimen tested under out-of-plane loading. A general solution for the multiple modes of deformation in the joint is available for rectangular panels where the displacement potentiometers are oriented parallel to the global reference frame. This is different than the case in this study because of the geometry of the joint. Therefore, it was necessary to derive a general solution for this case. Derivation of the deformation modes for the joint panels of this study is given in Appendix A.

Figure 3.32 View of Joint Panel Instrumentation

Column Cell (P2 - P1)
Beam Cell 1 (P3 - P4)
Beam Cell 2 (P5 - P6)
Joint Panel Instrumentation
Near Side (P7-P8-P9-P10-P11)
Far Side (P12-P13-P14-P15-P16)
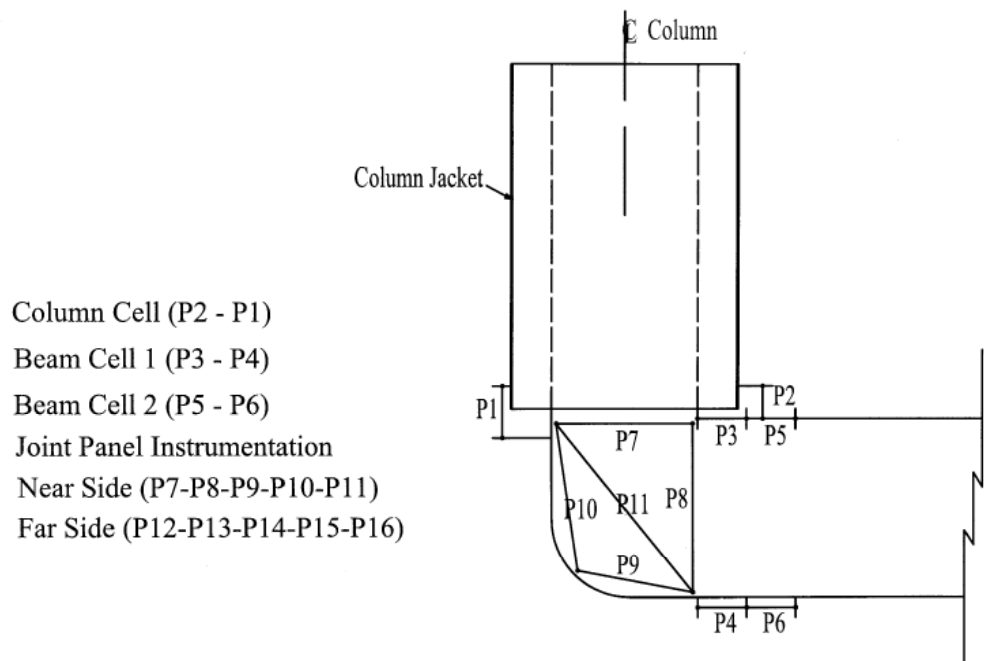
Figure 3.33 Typical Displacement Potentiometer Locations for As-Built Specimens Under In-Plane Loading
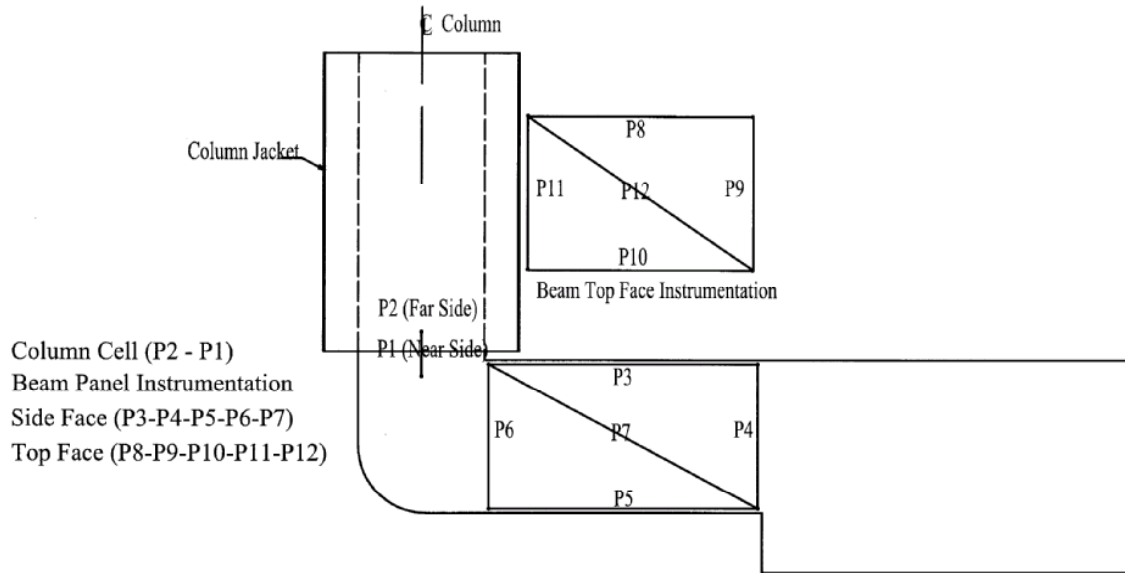
Figure 3.34 Typical Displacement Potentiometer Locations for As-Built Specimen Under Out-Of-Plane Loading

Stresses in selected reinforcement bars and in the steel jackets were measured during testing using strain gages. The gages were mounted on the rebars at the column joint interface and two other locations below the column joint interface, typically 5 in. (127 mm) apart. In a similar manner, a single rebar in the outrigger beam top and bottom reinforcement had strain gages both within the joint and at the beam-joint interface for the in-plane specimens. For the out-of-plane specimens, the beam reinforcement on the top and bottom corners was instrumented at the same previous locations. Strain gages were also mounted to the horizontal joint reinforcement and to the first three stirrups in the beam beyond the beam joint interface. Finally, strain gages were mounted to the steel jackets of the retrofitted specimens around the joint.

Photos of strain gages applied on longitudinal and transverse column and beam rebars are shown in Figure 3.35. Typical strain gage locations in the specimens are shown in Figure 3.36.
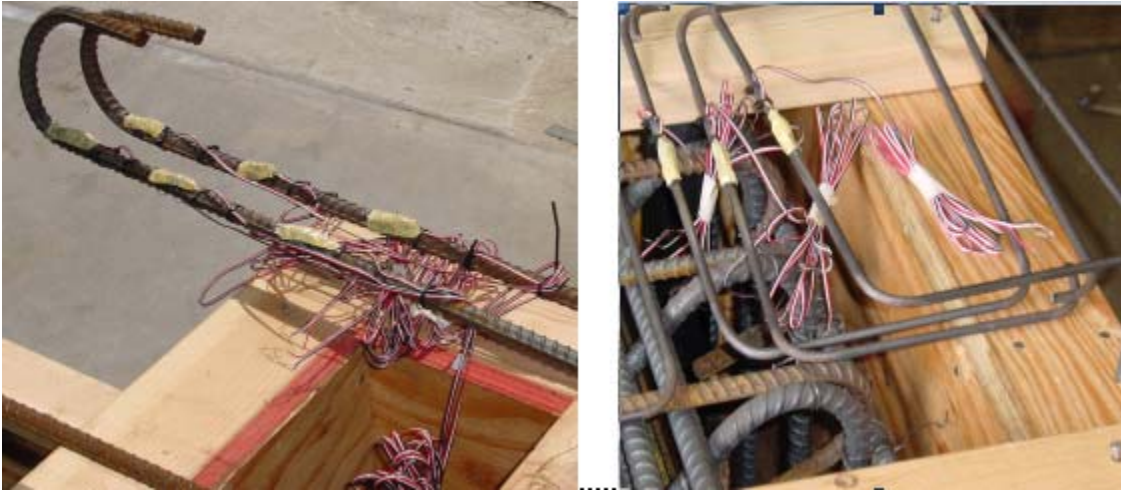
Figure 3.35 Strain Gages Applied to Longitudinal and Transverse Rebars
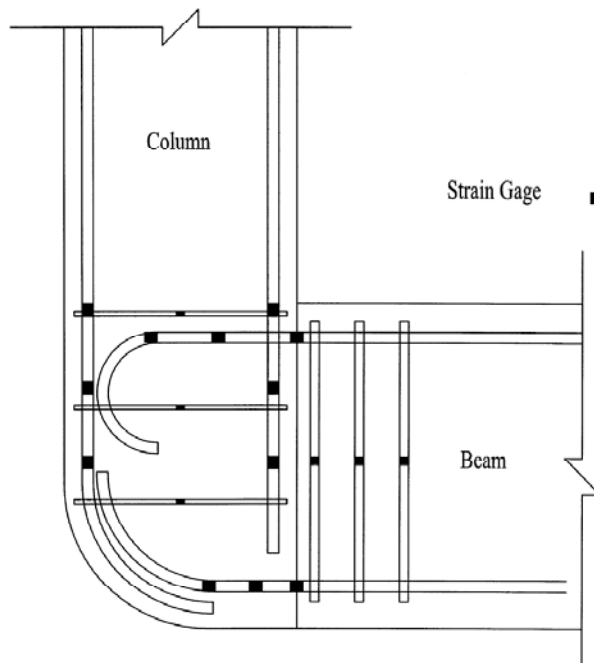
Figure 3.36 Typical Strain Gage Locations

CHAPTER FOUR

EXPERIMENTAL RESULTS AND OBSERVED BEHAVIOR

4.1 INTRODUCTION

This chapter provides details of the experimental results and general observations of specimen behavior. Three as-built specimens were tested first, one with a long and one with a short outrigger beam under in-plane loading, and one with a short outrigger beam under out-of-plane loading. These tests revealed the failure mechanisms as well as the force and deformation capacities of the existing outrigger knee joints. Results were then used to formulate the retrofit measures for the four subsequent specimens: in-plane retrofitted long outrigger, in-plane retrofitted short outrigger, out-of-plane retrofitted short outrigger, and in-plane retrofitted split long outrigger. Evaluations of the observed behavior of the seven specimens and comparisons of performance based on force-displacement response envelopes, specimen ductility and drift, and system capacity and stiffness are then made.

4.2 PROCEDURES FOR EVALUATING SPECIMEN RESPONSE

4.2.1 Equilibrium of Forces

The horizontal actuator force at the top of the column was measured directly during testing. Bending moments at the column-joint interface and at the beam-joint interface were calculated based on static equilibrium of the forces in the system. The trolley friction force and the selfweight of the specimen were evaluated and not considered in the analysis since they were insignificant. Half the horizontal actuator

selfweight, 1.5 kips (67 kN), and second-order effects (P-Δ) were included in the analysis.

In the subsequent representations of the test data, a positive value was used for all actions resulting from closing of the joint, including actuator force, horizontal displacement, bending moments, curvatures and ductilities. Similarly, all actions associated with opening of the joint were assigned a negative value. Horizontal and vertical axial stresses and principal compression and tension stresses were defined as positive when in compression and negative when in tension.

4.2.2 Calculation of Joint Principal Stresses

The procedures employed in this investigation for determining the joint principal shear stresses and joint effective areas for the calculation of the shear and the vertical and horizontal axial stresses under in-plane loading are based on those developed by Priestley (1993).

The stresses developing within a joint under in-plane loading can be divided into three main components: shear stress due to joint shear force (v_j); normal horizontal stress due to the beam axial force (ρ_x); and vertical axial stress due to the column axial force (ρ_y). In this study, for specimens being tested under in-plane loading, the beam axial force was the force in the horizontal actuator and the column axial force was the vertical force provided by the axial load ram. The joint shear force was determined based upon the flexural stress resultants acting at the joint boundary of the member governing the specimen flexure response. Detailed procedures for determining the joint shear force are

discussed by Priestley et al. (1996) and by Ingham (1995). Concisely, the method is based upon joint equilibrium for in-plane response under closing and opening of the joint.

Following determination of the axial and shear forces acting upon the joint for both closing and opening actions, the corresponding stresses are evaluated. Joint horizontal axial stress, ρ_x, was calculated over an effective joint area defined by the beam depth (h_b) and width (b_b) assuming no dispersion of the beam axial force into the column region. Joint vertical axial stress, ρ_y, was calculated over an effective joint area defined based upon spreading of the column axial force into the outrigger beam at 45° in both orthogonal directions. In this case, the area is defined by the column width parallel to the plane of loading plus half the outrigger beam width ($h_c + h_b/2$) and by an effective joint width. The effective joint width is the width taken at the center of the column section allowing for a 45° spread from boundaries of the column section into the cap beam (Priestley et al., 1996). Finally, the effective joint area associated with the shearing stress was taken as the column width parallel to the plane of loading times the effective joint width.

Following the determination of the joint shear stress and horizontal and vertical normal stresses, the maximum joint principal tension, ρ_t, and compression, ρ_c, stresses are calculated based upon the assumption of a uniform stress distribution using a simple Mohr's circle analysis:

$$\rho_c, \rho_t = \left(\frac{\rho_x + \rho_y}{2}\right) \pm \sqrt{\left(\left(\frac{\rho_x + \rho_y}{2}\right)^2 + v_j^2\right)} \qquad (4.1)$$

4.2.3 Prediction of Torsional Capacities

An estimation of the torsional strength of reinforced concrete members with longitudinal steel reinforcement and no transverse reinforcement can be obtained based on various theories for plain concrete sections, including elastic theory, plastic theory and the skew-bending theory (Hsu, 1983). For a more accurate estimation, Hsu (1990) suggested the use of the following equation 4.2 which accounts for the longitudinal steel ratio. The cracking torsional moment (T_{cr}) of a reinforced concrete member can be predicted as:

$$T_{cr} = 6(x^2 + 10)y\sqrt[3]{f_c'}[1.00 + 4(\rho_L + \rho_h)]$$ (4.2)

where x = smaller dimension of the rectangular section, y = larger dimension of the rectangular section, f_c' = compressive strength of the concrete, and ρ_L, ρ_h = volume ratio of longitudinal and hoop steel, respectively, with respect to the gross sectional area.

The torsional cracking moment of the outrigger beam in this study was computed based on the contributions of the concrete and the longitudinal steel only. Contributions from transverse reinforcement were not included because details of the stirrups in the original bridge drawings consisted of U-shaped open stirrups, which will not provide any torsional strength to the section.

4.2.4 Moment-Curvature Response

Conventional flexural analysis of column and beam critical sections was used to predict the response of the test specimens. This analysis included estimates of yield, ideal and ultimate moments, the associated curvatures, and actuator forces. A computer program capable of analyzing reinforced concrete sections, XTRACT version 2.6.2, was

used to compute the cross section moment-curvature response under monotonic loading. The software has the capability to model arbitrary sections by discretizing the section into triangular fibers of user-specified size consisting of user-specified materials.

A typical moment-curvature relationship of a reinforced concrete member under lateral loading is shown in Figure 4.1. The figure also represents a bilinear elasto-plastic moment-curvature approximation for the actual curve. The bilinear curve is characterized by a linear elastic segment passing through the first yield point and extrapolated to the ideal flexural strength. The moment at the first yield point corresponds to the onset of yielding in the extreme tension reinforcement and is termed as the first theoretical yield moment, M_y, with an associated curvature termed as ϕ_y'. The ideal moment strength, M_I, of the section is defined as the nominal flexural strength using measured material properties and corresponding to a 0.004 compression strain in the extreme fibers of the concrete or a 0.015 tension strain in the reinforcement, whichever occurs first (Priestley, 2003). The curvature associated with M_I is termed as ϕ_y. The second segment of the curve connects the M_I and the ϕ_y point to the point of ultimate moment, M_u, and the ultimate curvature, ϕ_u. M_u is defined as the moment at which the ultimate concrete compression strain is developed. This strain limit was computed based on work by Mander (1988) for confined concrete.

Experimental moment-curvature responses for the column critical section were determined and compared to the predicted analysis using XTRACT. Ingham et al. (1994b) suggested that the length over which curvatures are experimentally measured (L_{gage}) be corrected to account for the penetration of the longitudinal column strains into

105

the joint. The correction factor is based upon the recommendations of Priestly et al. (1994). Thus, the corrected curvature cell length (L_{eff}) is given by:

$$L_{eff} \; = \; L_{gage} \; + \; 0.15 f_y \, d_b \quad \text{[} f_y \text{ in ksi]}$$
$$L_{eff} \; = \; L_{gage} \; + \; 0.022 f_y \, d_b \quad \text{[} f_y \text{ in MPa]}$$

(4.3)

where f_y is the yield strength of the longitudinal reinforcement and d_b is the diameter of the longitudinal bars. In this study, beam curvatures were measured, but not reported, because of the small measurements for the beam displacement, which encountered a good amount of signal noise.
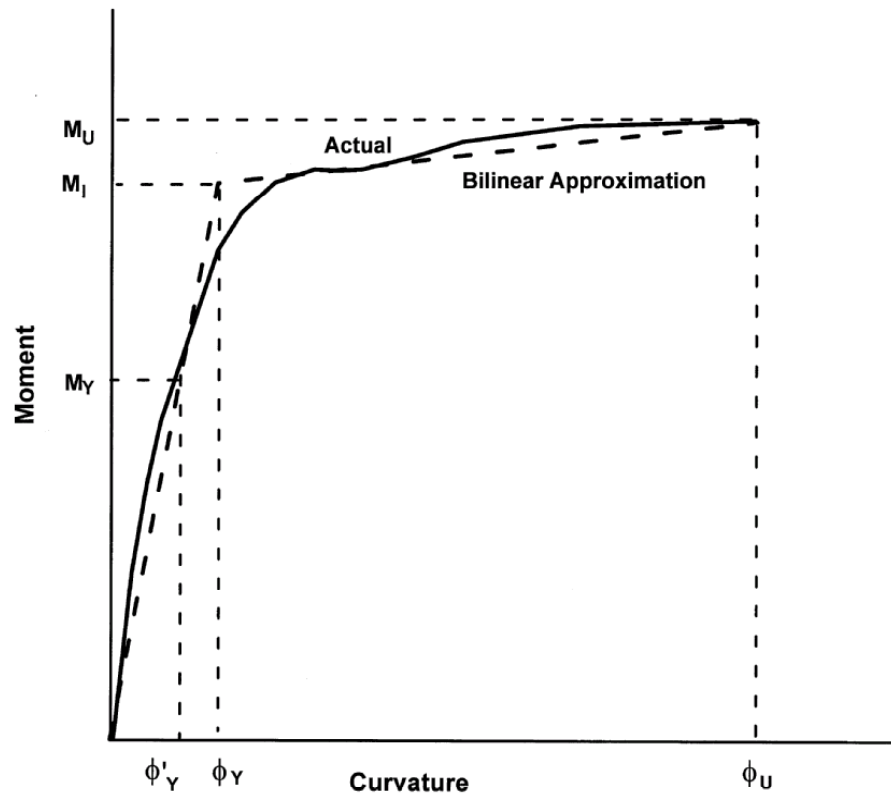
Figure 4.1 Moment-Curvature Relationship and Bi-Linear Approximation

Analysis of the outrigger knee joint system was accomplished using static pushover analysis. The main objective of the analysis was to determine the bilinear

yielding displacement of the system and compare it to the experimental results. This analysis was obtained using the software SAP2000 version 8.2.7. For pushover analysis, nonlinear behavior is typically assumed to occur within frame elements at concentrated plastic hinges. The hinge properties are defined through the definition of the moment-rotation response based on the moment-curvature relationship with an equivalent plastic hinge length (L_p). For steel-encased columns, the equivalent plastic hinge length is calculated based on the recommendations of Priestley (1994) using the following expression:

$$
\begin{aligned}
L_p &= 0.30 f_y \, d_b \ + \ w_g \quad \text{[}f_y \text{ in ksi]} \\
L_p &= 0.044 f_y \, d_b \ + \ w_g \quad \text{[}f_y \text{ in MPa]}
\end{aligned}
\tag{4.4}
$$

where w_g = width of the gap between the column casing and the beam surface for the as-built specimens or the joint jacket for the retrofitted specimens.

4.2.5 Displacement Ductilities

Displacement ductility (μ_Δ) is defined as the ratio of the ultimate lateral displacement of the outrigger knee joint system (Δ_u) to the yield displacement of the member controlling the flexural behavior (Δ_y). Thus:

$$
\mu_\Delta = \frac{\Delta_u}{\Delta_y}
\tag{4.5}
$$

The ultimate displacement used for ductility calculations is typically defined as the displacement corresponding to a 20% drop in the lateral capacity from the maximum value.

Challenges in calculating the displacement ductility for outrigger knee joint systems arise because of different methods for defining the yield displacement. In order to evaluate the sensitivity and reliability with respect to defining the yield displacement, three different ways were considered in this study. Two are based on experimental data, and the other one is based on nonlinear frame analysis. The yield displacement values from each approach were then compared.

Experimentally-determined yield displacements are favored by researchers over the theoretical yield displacement method. Two methods can be used in the experimental approach: strain gage data and force-displacement curves. Yield displacement can be extracted directly from strain gage data by finding the displacement corresponding to the yield strain of the bars in the beam or the column. This approach was utilized by Stojadinovic and Thewalt (1995) to obtain yield displacements for the outrigger knee joint systems of their study. Reliability of this method can be affected by two major factors. First, the expected strain gage survival rate is affected by issues during construction and testing, and the second factor is associated with failure mechanisms in the joint region whereby reinforcement in one member can reach its yield strength prior to the test specimen attaining the theoretical yield strength. For this situation, force displacement curves can be used to obtain the yield displacement as follows: initially, the actuator force, F_y, corresponding to first theoretical yield of the member controlling the flexure behavior in either direction, is determined based on moment-curvature analysis of the critical section of the member. Next, the displacement corresponding to F_y intersecting the force-displacement curve termed, as Δ'_y, is found. The yield

displacement of the system is then found by extrapolating Δ'_y to the ideal flexure strength, M_I, using the following equation:

$$\Delta_y = \frac{M_I}{M_y} \Delta'_y$$ (4.6)

The force displacement curves method was used by Ingham et al. (1994a and 1994b) to determine yield displacements of outrigger knee joints. However, problems can arise with this approach when the specimen is not able to attain its theoretical yield strength in the required direction, in which case nonlinear analysis must be performed to determine the bilinear yield displacements. The bilinear yield displacement can be obtained by a static pushover analysis. This method is usually used as a preliminary step to predict the experimental yield displacement. Yield displacements obtained by this method are highly dependant on the assumed plastic hinge length, moment-curvature relationship of the critical flexure member, and the cross sectional properties of the members in the system.

For older outrigger knee joints built with no or little seismic detailing, as was the case in this investigation, different failure mechanisms may occur in the opening and closing directions, e.g., hinging of the column in the closing direction and hinging of the outrigger beam in the opening direction. Therefore, the outrigger knee joint systems of this study had different yield displacements in the closing than in the opening direction, resulting in different displacement ductilities in both directions. For newly designed or retrofitted bridges, the target is to have a failure mechanism through hinging in the column in the closing and opening of the joint, and one yield displacement value can be adopted for the outrigger knee joint system in both directions.

Table 4.1 presents a comparison of the yield displacement obtained using the three different methods for the outrigger knee joint specimens of this study tested under in-plane loading. The table shows that yield displacements obtained from force-displacement curves are in good agreement with those reported from strain gages. Thus, yield displacements of an outrigger knee joint system can be determined by one of these approaches and checked with results obtained form a different one.

Yield displacements were not reported for the out-of-plane specimen due to the performance of the test specimen. Early torsion cracking of the beam due to poor transverse reinforcement made it impossible to produce torsion hinging in the beam reinforcement. In addition, the ultimate actuator force level that was attained during testing was less than the yield load for the beam or the column reinforcement. Displacement ductilities are therefore not reported.

In this study, experimental yield displacements based on force-displacement curves were adopted whenever a specimen was able to attain its ideal strength. Otherwise, bilinear yield displacements based on pushover analysis were used. Experimental yield displacements were adopted for the as-built short and the long outrigger specimens under in-plane loading in the closing direction. Bilinear yield displacements were adopted in the opening direction since both of the specimens were not able to attain the theoretical yield strength. A single experimental yield displacement value was adopted for all the retrofitted specimens under in-plane loading since hinging in the column formed in both directions. This yield displacement represents an average value of the experimental yield displacements in both directions.

110

Table 4.1 Comparison of Yield Displacements

Specimen	Force –Displacement Test Curves		Bilinear Displacement		Strain Gages	
	Opening in. (mm)	Closing in. (mm)	Opening in. (mm)	Closing in. (mm)	Opening in. (mm)	Closing in. (mm)
As-built long	--[1]	1.07 (27.2)	0.80 (20.3)	1.18 (30.0)	--[3]	1.02 (25.9)
Retrofitted long	0.80 (20.3)	0.80 (20.3)	0.75 (19.1)	0.78 (19.8)	--[3]	0.79 (20.1)
As-built short	--[1]	1.50 (38.1)	0.90 (22.9)	1.24 (31.5)	0.95 (24.1)	1.42 (36.1)
Retrofitted short	1.09 (27.7)	1.09 (27.7)	0.91 (23.1)	1.04 (26.4)	--[3]	1.07 (27.2)
Retrofitted Split	0.78 (19.8)	0.78 (19.8)	--[2]	--[2]	--[3]	0.66 (16.8)

[1] Specimen failed to attain the ideal strength in this direction.
[2] Pushover analysis was not performed due to modeling issues of the flat plate behind the column (see Section 4.4.2, discussion on moment curvature response of Specimen RSPLI.)
[3] No readings were obtained from the strain gages.

4.3   AS-BUILT   SPECIMENS   -   GENERAL   BEHAVIOR   AND   FAILURE   MECHANISMS

4.3.1 As-Built Specimens Under in-Plane Loading

Specimen ALI

The as-built long outrigger specimen represented a portion of bent #36 in the Spokane Street Overcrossing. Compared to current earthquake-resistant design practice, the confinement and detailing of the joint, as well as the beam and the column reinforcement meeting in the joint, are unsatisfactory. Consequently, a failure mechanism within the joint was expected for Specimen ALI.

Testing of Specimen ALI started with the application of a 33-kips (147-kN) vertical force to simulate the scaled prototype dead load and the increase in the axial load due to frame closing action of the joint. The application of the vertical load resulted in a small force in the horizontal actuator, and the horizontal actuator was then retracted to produce zero load in the actuator. Cycled testing was conducted about this point.

While cycling at a displacement level of ±1.0 in. (±25 mm), a vertical crack associated with opening moments developed at the beam-joint interface. Actuator forces of 13.7 kips (60.9 kN) and −10.3 kips (-45.8 kN) were recorded at this displacement level in the closing and opening direction, respectively. Shear cracks in the joint started to develop at a displacement level of ±1.5 in. (±38 mm) combined with vertical cracking in the top corner of the joint resulting from straightening of vertical hook extensions of the bottom beam reinforcement within the joint. With repeated cycling at this displacement level, there was some widening and extension of the vertical crack at the beam-joint interface, indicating the onset of some slipping and yielding of the top bars of the beam. Maximum actuator forces of 16.7 kips (74.3 kN) and −11.5 kips (-51.2 kN) were recorded at this displacement level in the closing and opening directions, respectively. Figure 4.2 shows the joint region at this point of testing.

During cycles to ±2.0 in. (±51 mm) displacement level, there was additional joint shear cracking, with the existing joint cracks becoming wider. Some hairline flexural cracks at the bottom face of the beam were observed while cycling in the closing direction. The vertical crack on the beam-joint interface opened more on repeated cycling, particularly during opening of the joint. Signs of bond splitting cracks along the beam and column reinforcement within the joint became obvious at the last opening cycle

as cracks formed in the same plane where the beam bottom reinforcement and column rebars were hooked together and overlapped within the joint. These cracks started to extend beyond the beam-joint interface towards the beam and terminated at the column-joint interface. The largest measured actuator force at this displacement level in the closing direction was 17.8 kips (79.2 kN) and -11.9 kips (-52.9) in the opening direction showing, thus, a slight increase over the actuator forces in the previous stage. A picture of the joint at the end of this displacement level is shown in Figure 4.3.
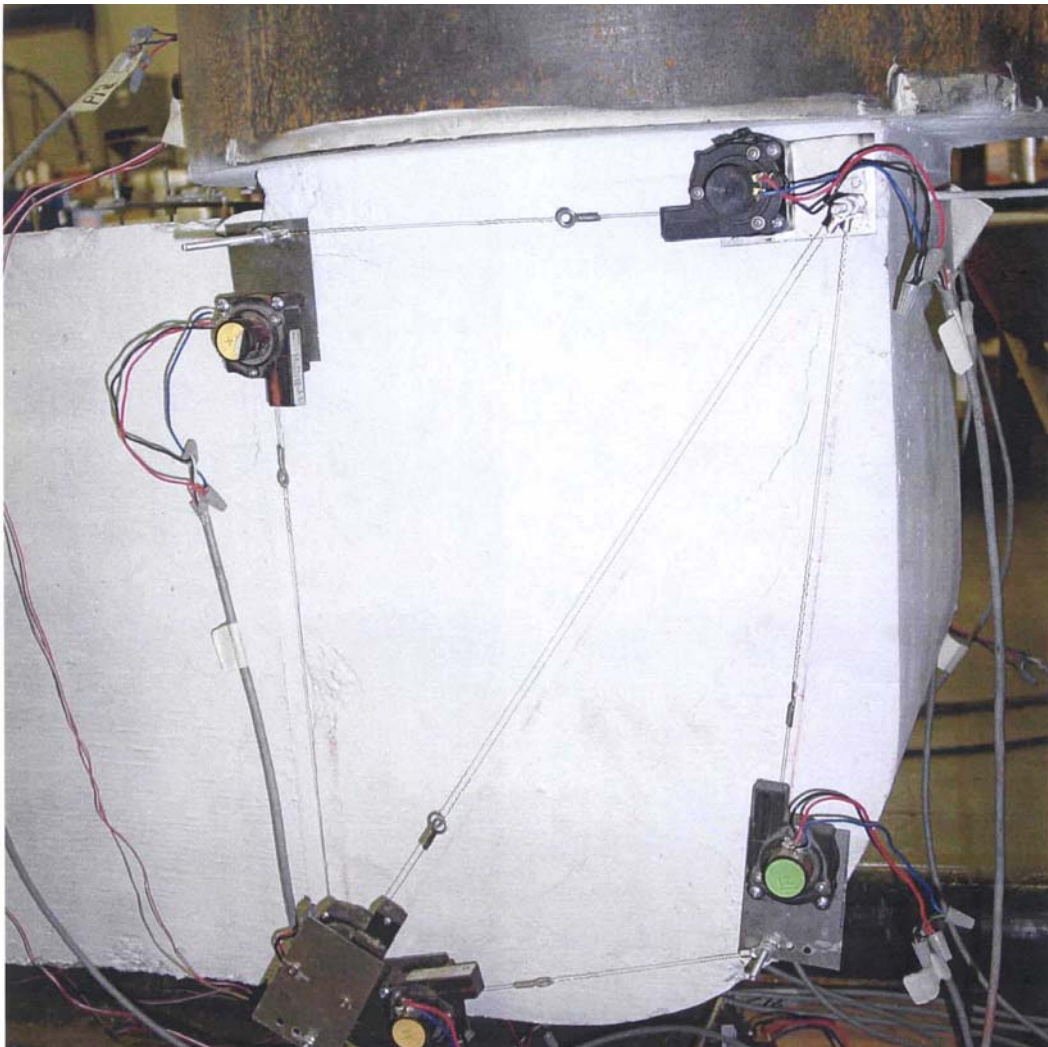
Figure 4.2 Specimen ALI at the End of 1.5-in. (38-mm) Displacement Level
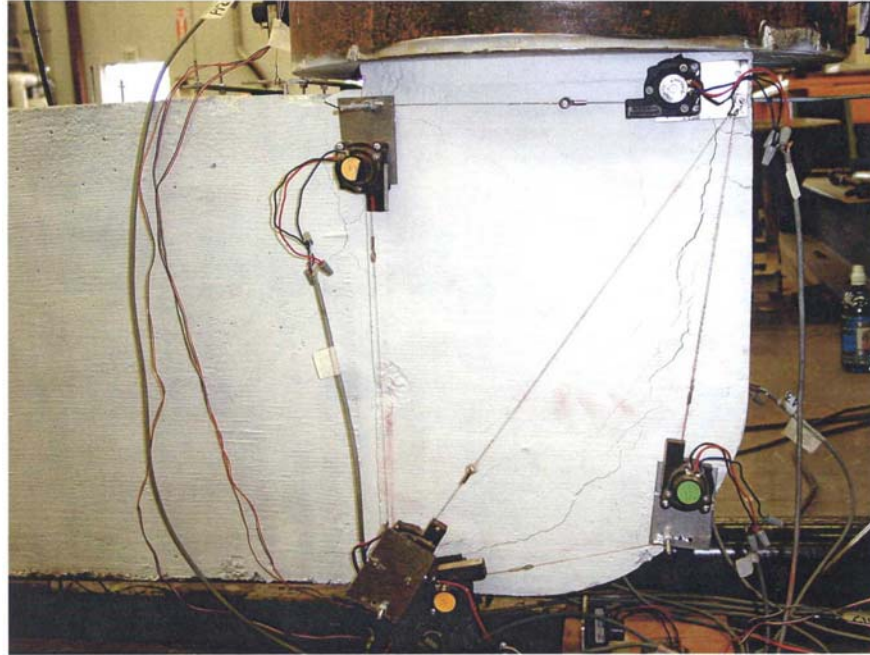
Figure 4.3 Specimen ALI at the End of 2.0-in. (51-mm) Displacement Level

During cycling to a displacement level of ±2.5 in. (±64 mm), additional joint shear cracks developed along with further opening of the existing shear and splitting cracks within the joint. Horizontal splitting cracks on the back face of the joint were clearly visible. The vertical crack at the beam-joint interface became wider. In the closing direction, the maximum measured actuator forces were 17.7 kips (78.7 kN), 16.2 kips (72.1 kN) and 14.8 kips (65.8 kN) following the first, second and third cycles of loading, respectively. This deterioration in the strength supported the physical observation of the widening of the shear and splitting cracks in the joint with repeated cycling. The largest actuator force in the closing direction was −11.0 kips (-48.9 kN), which is less than that recorded in the previous cycles. Pictures of the joint at the end of this displacement level are shown in Figures 4.4 and 4.5.
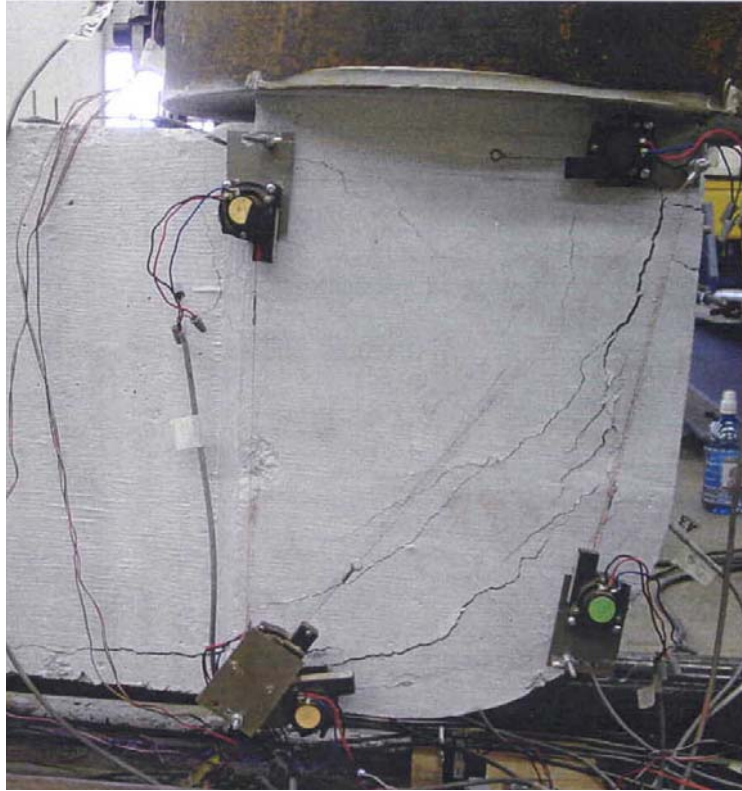
Figure 4.4 Specimen ALI at the End of 2.5-in. (64-mm) Displacement Level
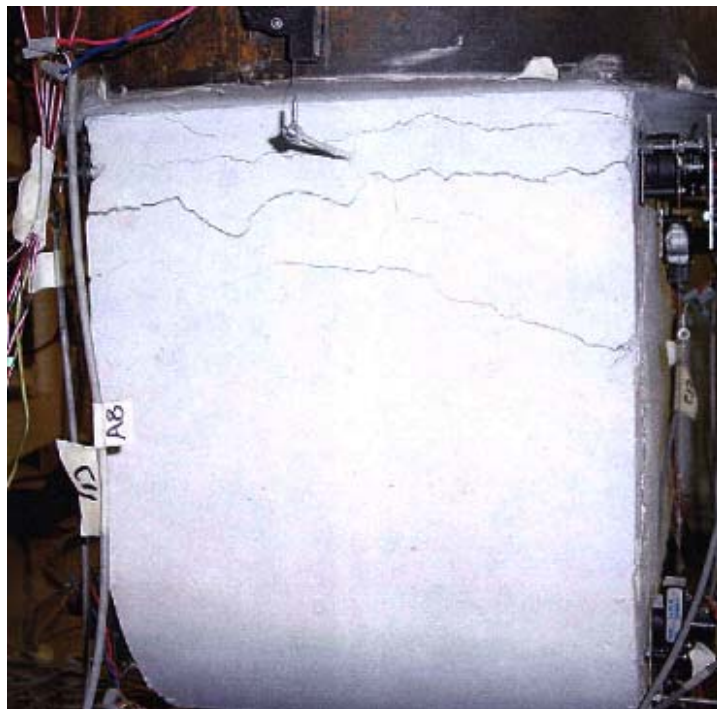
Figure 4.5 Back Face of the Joint in Specimen ALI at the End of 2.5-in. (64-mm) Displacement Level

During cycles to ±3.0 in. (76 mm) displacement level, the column hook extensions became visible as concrete at the curved side of the joint face spalled off at a displacement level of 2.19 in. (56 mm). Joint shear distress was also noticeable at this displacement level prior to the bond splitting cracks. In addition to the physical degradation of the joint strength, degradation of the system can be seen by comparing the maximum actuator forces to those of the previous cycles. Maximum forces of 7.1 kips (31.6 kN) and –8.7 kips (-38.7 kN) were recorded in the closing and opening direction at the end of the first cycle, respectively. This is equivalent to a 60% and 21% decrease in the strength in the closing and opening direction, respectively. Testing was stopped following the second closing cycle to this displacement level. At the end of testing, the specimen was still capable of sustaining the applied axial load. Figures 4.6 and 4.7 show the damage to the test specimen at the completion of the test.
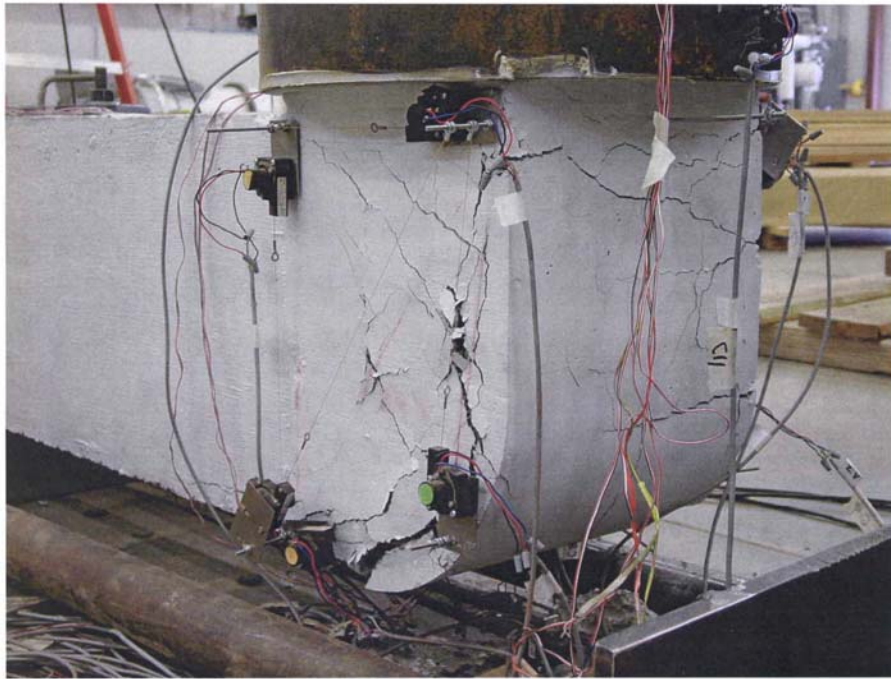
Figure 4.6 Shear Distress to the Joint in Specimen ALI
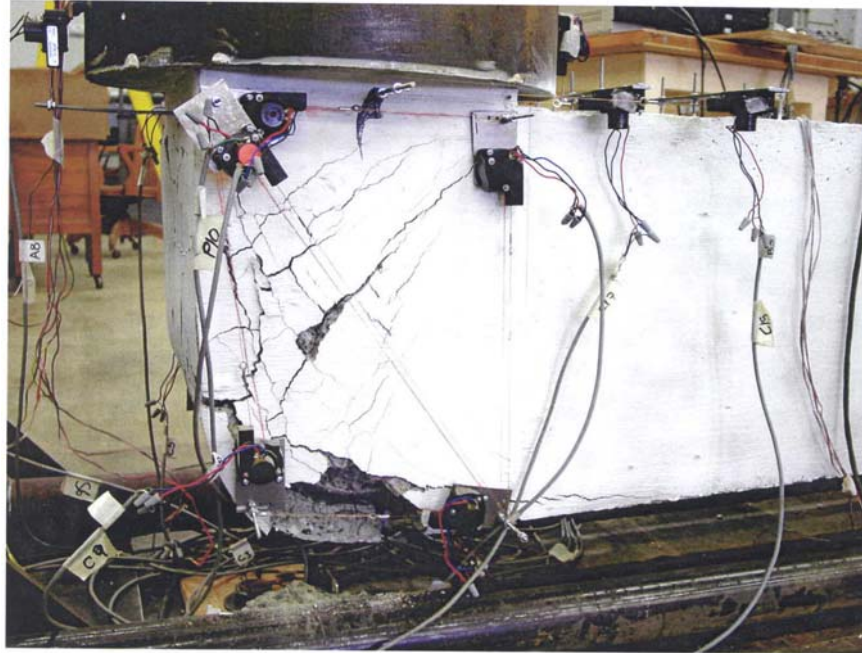
Figure 4.7 Bond Splitting Failure of the Column Rebars in the Joint Region

The actuator force-horizontal displacement history for Specimen ALI is shown in Figure 4.8. The values of the actuator force corresponding to yielding moment, F_Y, and ideal moment, F_I, are shown in the figure. The ideal and yield moment values were calculated based on plastic hinging in the column section at the column-joint interface for the closing direction. In the opening direction, the moment values were based on hinging in the outrigger beam at the beam-joint interface. Figure 4.8 indicates that the test specimen was able to attain the ideal strength in the closing direction, but failed to attain even the yield strength in the other direction. Therefore, experimental ductilities were determined for the closing direction, while bilinear yield displacements were defined for the opening direction based upon the results of a static pushover analysis. The experimental yield displacement for Specimen ALI in the closing direction was 1.07 in.

(27.2 mm), and the bilinear yield displacement in the opening direction was 0.78 in (19.8 mm).

The shape of the force-displacement history shows narrowing of the curves near the origin, referred to as pinching, due to cracking of the joint concrete and degradation of the overall performance of the joint. The specimen was able to withstand displacements up to 2.5 in.(64 mm) in both directions before the abrupt drop in the actuator force while looping to close the joint to 3.0 in. (76 mm) displacement level, as shown in Figure 4.8. Specimen ALI was able to attain a maximum ductility level of 2.8 at a drift ratio of 3.4% in the closing direction and a ductility of -3.8 at a drift ratio of -3.4% in the opening direction.
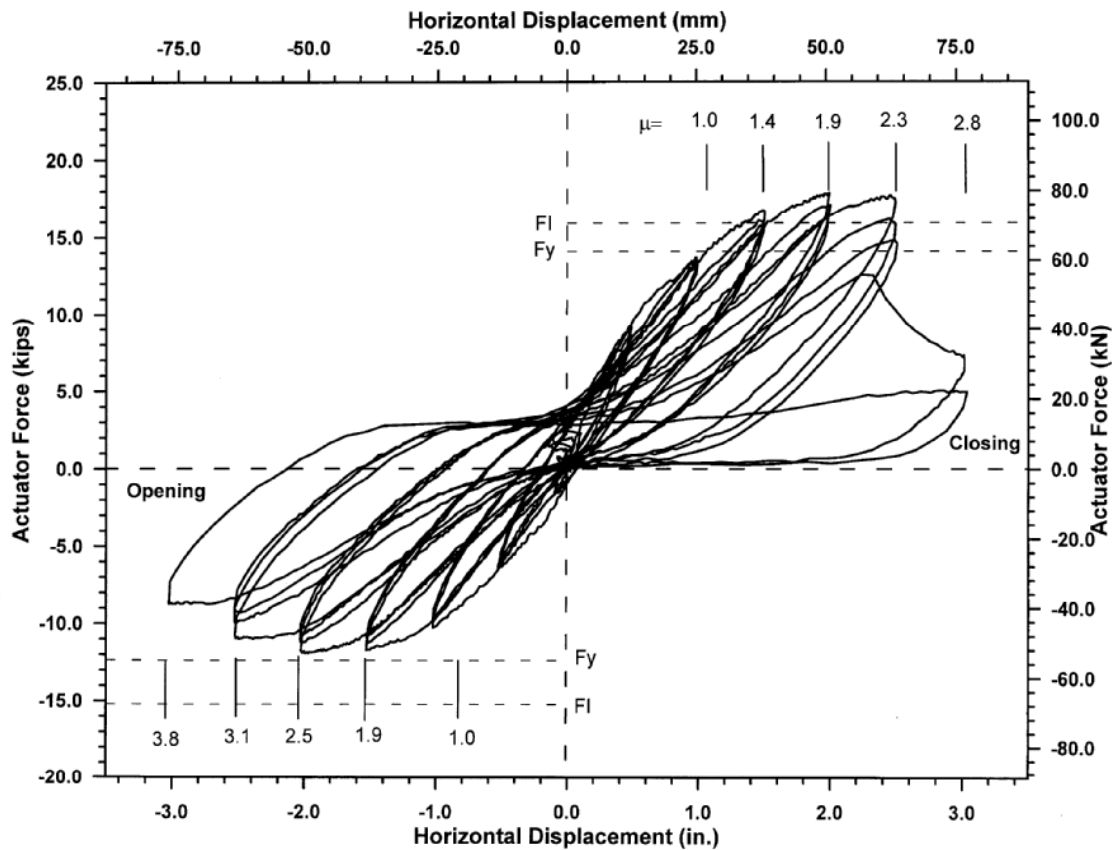
Figure 4.8 Actuator Force-Horizontal Displacement History for Specimen ALI

118

Figure 4.9 shows the experimental and the predicted moment-curvature responses in the column plastic hinge region. The experimental moment curvature plots the average measured curvature against the maximum moment. Figure 4.9 reveals that the column yield moment was attained in the closing direction but was never attained in the opening direction. This finding was also noticed in the force-displacement history, where the specimen was able to attain the yield and ideal strength in the closing direction. The ultimate curvature in the opening direction as shown in Figure 4.9 is larger than that in the closing direction, indicating a different behavior than was anticipated since beam hinging was expected in the opening direction. The increase in the ultimate column curvature in the opening direction was believed to occur as a result of large horizontal joint splitting cracks developing on the back face of the joint.

Figure 4.9 Column Moment-Curvature Response for Specimen ALI

Figure 4.10 presents the history of the joint principal tension stress versus the actuator horizontal displacement. The principal tension stress was calculated using a simple Mohr's circle analysis and an effective joint width, as discussed in Section 4.2.2. The observed behavior of the joint at different stages of the test can be linked to the principal tension stress history. Diagonal cracking was observed in the joint region when the principal tension stress reached $6.2\sqrt{f_c'}$ psi ($0.52\sqrt{f_c'}$ MPa) in the opening direction and $5.5\sqrt{f_c'}$ psi ($0.46\sqrt{f_c'}$ MPa), in the closing direction. Maximum principal tension stresses of $7.3\sqrt{f_c'}$ psi ($0.61\sqrt{f_c'}$ MPa), and $6.2\sqrt{f_c'}$ psi ($0.52\sqrt{f_c'}$ MPa), were recorded in the joint in the opening and closing direction, respectively, before failure. The nominal shear stress value corresponding to the largest principal tension stress of $7.3\sqrt{f_c'}$ psi ($0.61\sqrt{f_c'}$ MPa) is $7.6\sqrt{f_c'}$ psi ($0.63\sqrt{f_c'}$ MPa).

Figure 4.10 Joint Principal Tension Stress History for Specimen AL1

Specimen ASI

The as-built short outrigger specimen represented a portion of bent #20 in the Spokane Street Overcrossing. The as-built drawings of the bridge from which the test specimen was designed showed inadequate confinement and detailing of the outrigger knee joint when compared to current earthquake-resistant design practice. Consequently, a brittle behavior of the system due to the poor detailing of the joint was expected for Specimen ASI.

Prior to the application of the horizontal loading pattern, Specimen ASI was subjected to a vertical load level of 55 kips (225 kN). This load simulated the scaled bridge selfweight on the bent and the increase in the axial load due to frame closing action of the joint. After the application of the vertical load, the horizontal actuator was adjusted to the zero force position, and cycled testing was conducted about this point.

The earliest noticeable shear cracks on both sides of the joint were observed in the first opening cycle to a displacement level of 1.0 in. (25 mm). These cracks opened when cycling in the opening direction and closed in the closing direction. Maximum actuator forces of 22.0 kips (97.9 kN) and −13.7 kips (-60.9 kN) were recorded at this displacement level in the closing and opening directions, respectively. New joint shear cracks parallel to each other developed during the first two cycles at a displacement level of 1.5 in. (38 mm) due to joint opening. On the third cycle in the joint opening direction, a vertical crack occurred in the top corner of the joint starting at the column joint interface and penetrating beyond the mid-height of the joint. The presence of this vertical splitting crack resulted from straightening of the vertical hook extensions of the bottom beam reinforcement into the joint. This vertical splitting crack connected with an

inclined horizontal splitting crack in the same plane of the beam top reinforcement and a shear crack near the curved side of the joint. Maximum actuator forces of 28.2 kips (125.4 kN) and −15.7 kips (-69.8 kN) were recorded at this displacement level in the closing and opening directions, respectively. Figure 4.11 shows the test specimen joint at the end of loading to this displacement level.
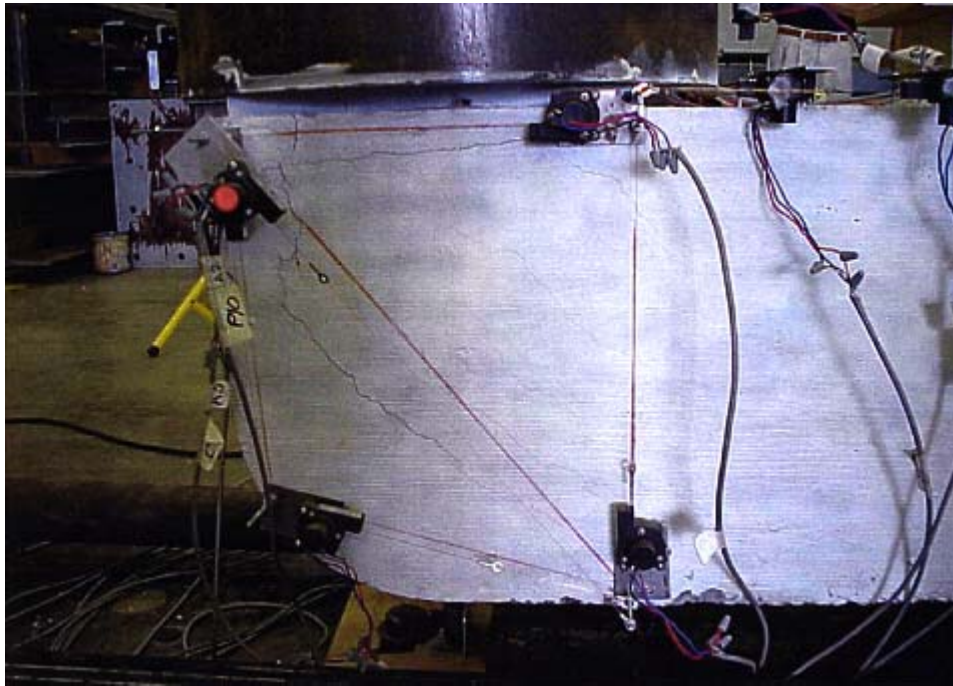
Figure 4.11 Specimen ASI at the End of 1.5 in.(38 mm) Displacement Level

During cycling to ±2.0 in. (±51 mm) displacement level, very little increase in joint cracking developed, but the existing cracks widened. There was an extension of the shear crack near the curved side of the joint into the beam region, suggesting the onset of a bond splitting of the column reinforcement tails hooked into the joint. The resistance of the specimen to transverse joint opening started to decrease on repeated cycling at this displacement level as there was a 24% degradation in the lateral resistance between the

first and the third cycle. The largest measured actuator force in the closing direction was 30.9 kips (137.5 kN) and −14.0 kips (-62.3 kN) in the opening direction showing a slight decrease in the capacity of the system in the opening direction when compared to the maximum actuator forces in the previous stage. Figures 4.12 and 4.13 show pictures of the joint at the end of testing at this displacement level.

At a displacement level of ±2.5 in.(±64 mm), the bond splitting cracks began to widen. New horizontal splitting cracks formed on the back face of the joint with the existing horizontal and vertical splitting cracks getting wider. In the closing and the opening directions, the maximum measured actuator force was 28.5 kips (126.8 kN) and −10.7 kips (-47.6 kN), respectively. This is equivalent to 8% and 24% decrease in the capacity of the system in the closing and opening directions when compared to the previous capacities. Figure 4.14 shows a picture of the joint at the end of this displacement level.
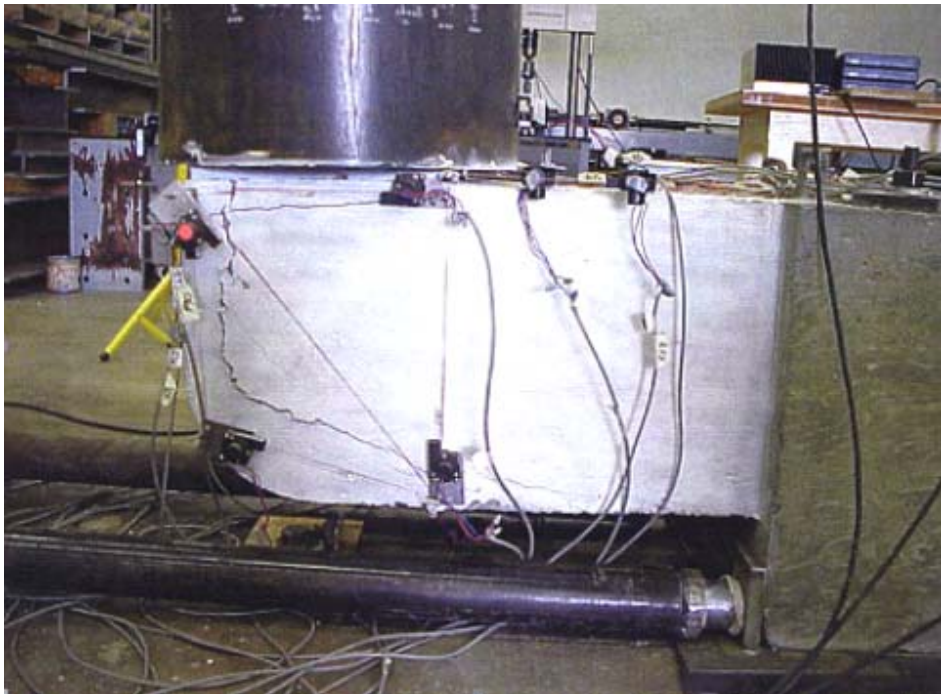
Figure 4.12 Specimen ASI at the End of 2.0 in. (51 mm) Displacement Level

Figure 4.13 Bond Splitting Cracks on the Back Face of Specimen ASI
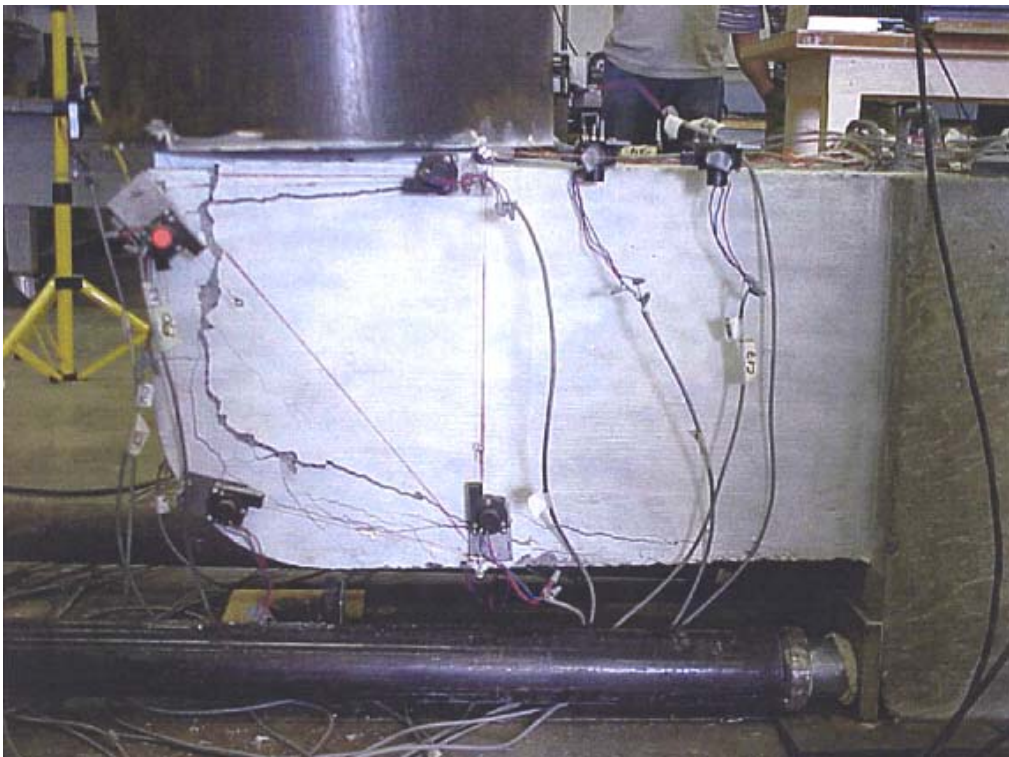
Figure 4.14 Specimen ASI at the End of 2.5 in. (64 mm) Displacement Level

Spalling and splitting of the concrete cover in the top left corner on one of the joint sides happened when cycling in the closing direction to a displacement level of 3.0 in. (76 mm). Some additional spalling of the joint concrete also occurred due to widening of the existing splitting cracks and crushing of the concrete in this region. On the first cycle in the joint opening direction, it was observed that joint splitting cracks extended more into the beam region. These splitting cracks were wide enough that some of the joint reinforcement became visible. On the second cycle in the opening and closing directions, the joint continued to be stable with further widening of the existing cracks. Bond failure of the embedded column and beam rebar hook extensions occurred when cycling to the third cycle in the closing direction at a displacement level of 2.7 in. (69 mm). The column and the beam hook extensions became exposed as concrete along the free perimeter of the joint from both sides spalled off. This spalling is attributable to the poor confinement of the reinforcement, particularly for the reinforcement in the part projecting outside the column area.

At the end of the test, loose concrete around the column hook extensions was removed and one of the column rebars was seen to have slipped approximately 1/8 in. (3 mm). Strength degradation of the system upon repeated cycling is clear when comparing the actuator forces at the end of each cycle. In the closing direction, the measured actuator forces were 23.5 kips (104.5 kN) and 14.2 kips (63.2 kN) following the first and the third cycle, respectively. This is equivalent to a 40% degradation of lateral resistance between successive cycles. The test was stopped following the third closing cycle with the specimen still being able to support the applied axial load. Figure 4.15 shows the damage to the test specimen at the end of the test.

Figure 4.15 Concrete Spalling off as a Result of Splitting Bond Failure of the Column Reinforcement Within the Joint of Specimen ASI

The actuator force-horizontal displacement history is shown in Figure 4.16. The values of the actuator force corresponding to yielding moment, F_Y, and ideal moment, F_I, are shown in the figure. Similar to Specimen RLI, ideal and yield moment values were calculated based on plastic hinging in the column section at the column-joint interface for the closing direction. In the opening direction, these values were computed based on hinging in the outrigger beam at the beam-joint interface. Figure 4.16 indicates that Specimen RSI reached its yield strength but barely attained the ideal strength in the closing direction. The figure also indicates that in the opening direction the specimen failed to attain the yield strength. Hence, bilinear yield displacements were defined for the opening direction based upon the results of a static pushover analysis. The experimental yield displacement for Specimen ASI in the closing direction was 1.48 in.

(37.6 mm), and the bilinear yield displacement in the opening direction was 0.91 in. (23.1 mm).

Figure 4.16 shows that the force-displacement hysteresis loops for Specimen RSI had little pinching up to a displacement level of 2.0 in. (51 mm), after which the curves started to show significant pinching due to cracking of the joint concrete. The abrupt drop in capacity caused by the bond splitting cracks during joint closing to 3.0 in. (76 mm) displacement level is evident in Figure 4.16. Specimen ASI was able to attain a maximum ductility level of 2.0 at a drift ratio of 3.4% in the closing direction and a ductility of -3.3 at a drift ratio of -3.4% in the opening direction.

The experimental and the predicted moment-curvature response for the column plastic hinge region are shown in Figure 4.17. The experimental moment curvature plots the maximum moment against the average measured curvature. Figure 4.17 shows that the column hinge section experienced significant inelastic curvature in the closing direction. This conclusion is consistent with the observations from the force-displacement history where the specimen was able to attain the yield and ideal strength in the closing direction. Figure 4.17 shows that the column hinge section experienced very low levels of curvatures in the opening direction along with low moment values. This supports preliminary theoretical predictions in which column hinging was not expected in the opening direction.
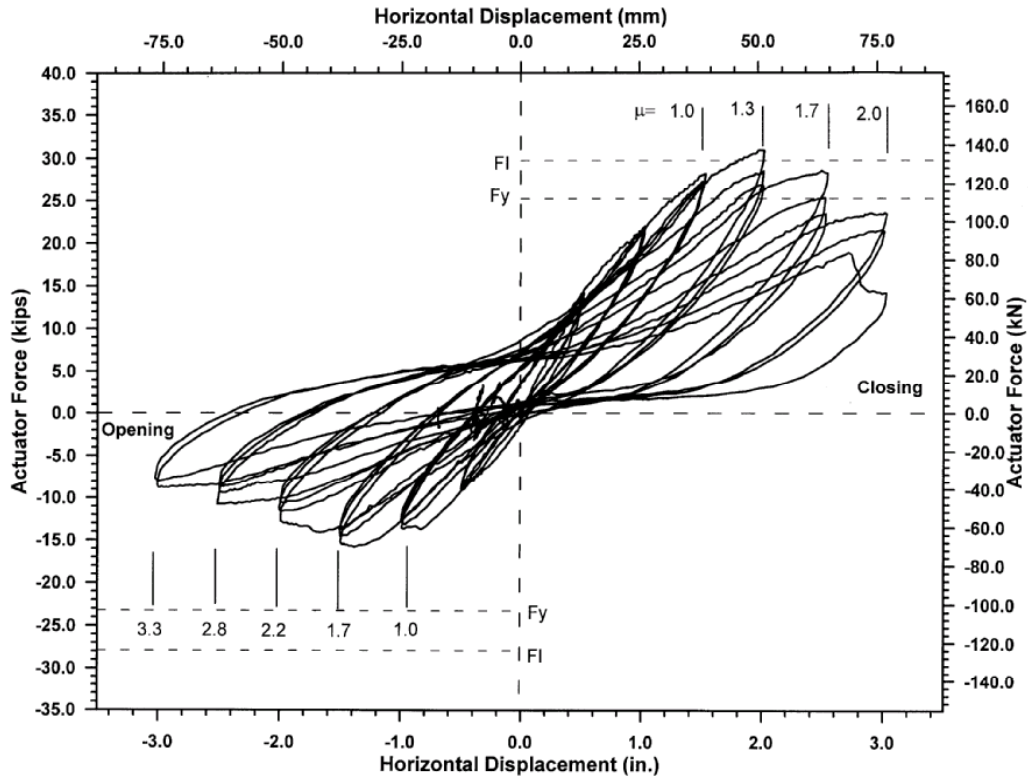
Figure 4.16 Actuator Force-Horizontal Displacement History for Specimen ASI
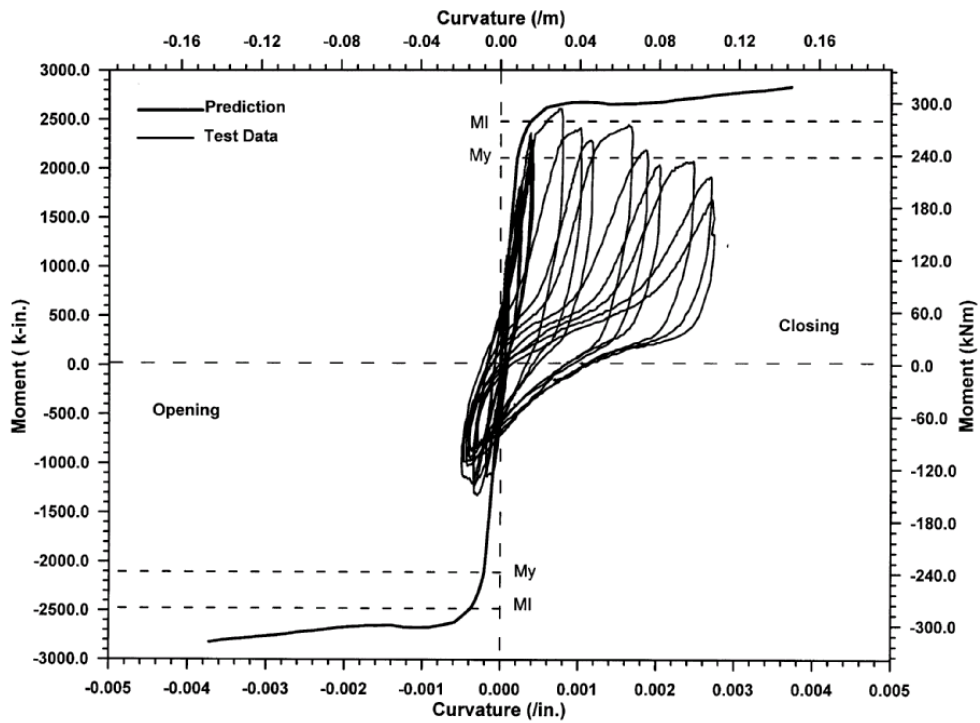
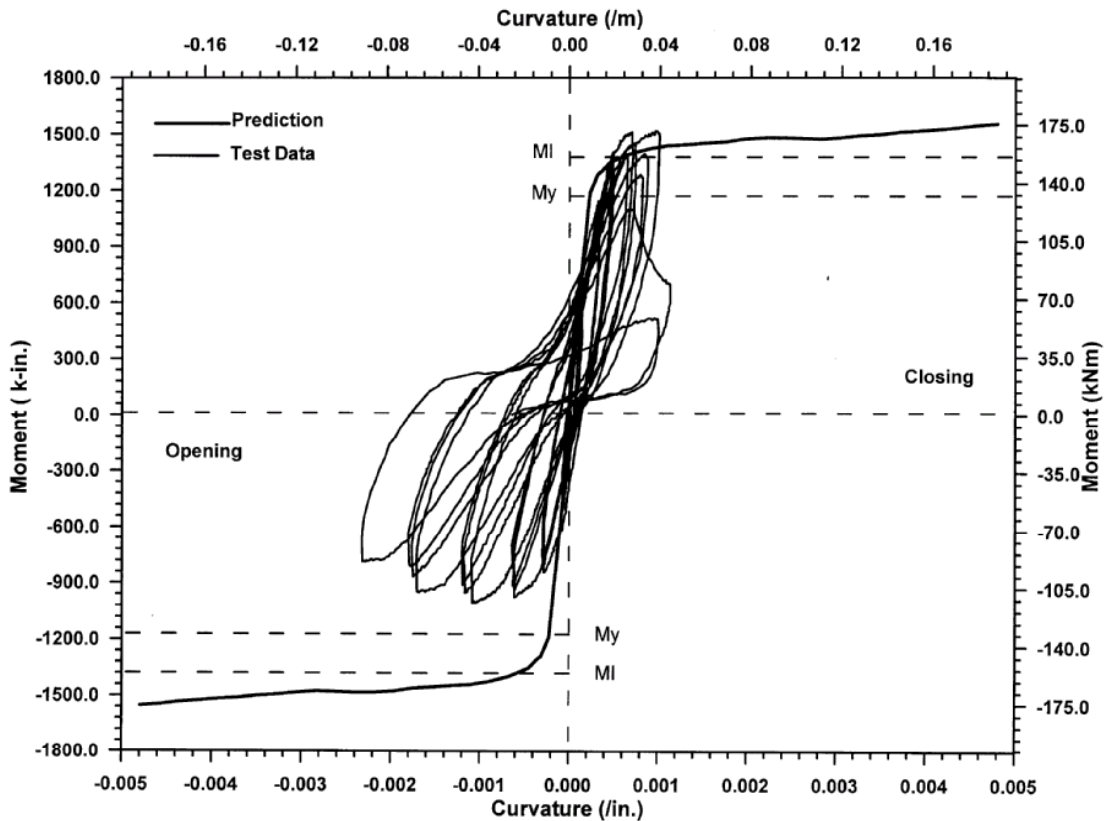**Figure 4.17 Column Moment-Curvature Response for Specimen ASI**

128

The history of joint principal tension stress versus the actuator horizontal displacement is shown in Figure 4.18. The principal tension stress was determined in a similar fashion to that of Specimen ALI. Test observations along with Figure 4.18 show that diagonal joint cracking occurred in the opening direction when the principal tension stress reached $4.9\sqrt{f_c'}$ psi $(0.41\sqrt{f_c'}$ MPa). The maximum principal tension stress was $7.8\sqrt{f_c'}$ psi $(0.65\sqrt{f_c'}$ MPa, before failure in the opening direction and $8.5\sqrt{f_c'}$ psi $(0.71\sqrt{f_c'}$ MPa), before failure in the closing direction. The nominal shear stress value corresponding to the largest principal tension stress of $8.5\sqrt{f_c'}$ psi $(0.71\sqrt{f_c'}$ MPa) is $10.2\sqrt{f_c'}$ psi $(0.85\sqrt{f_c'}$ MPa).
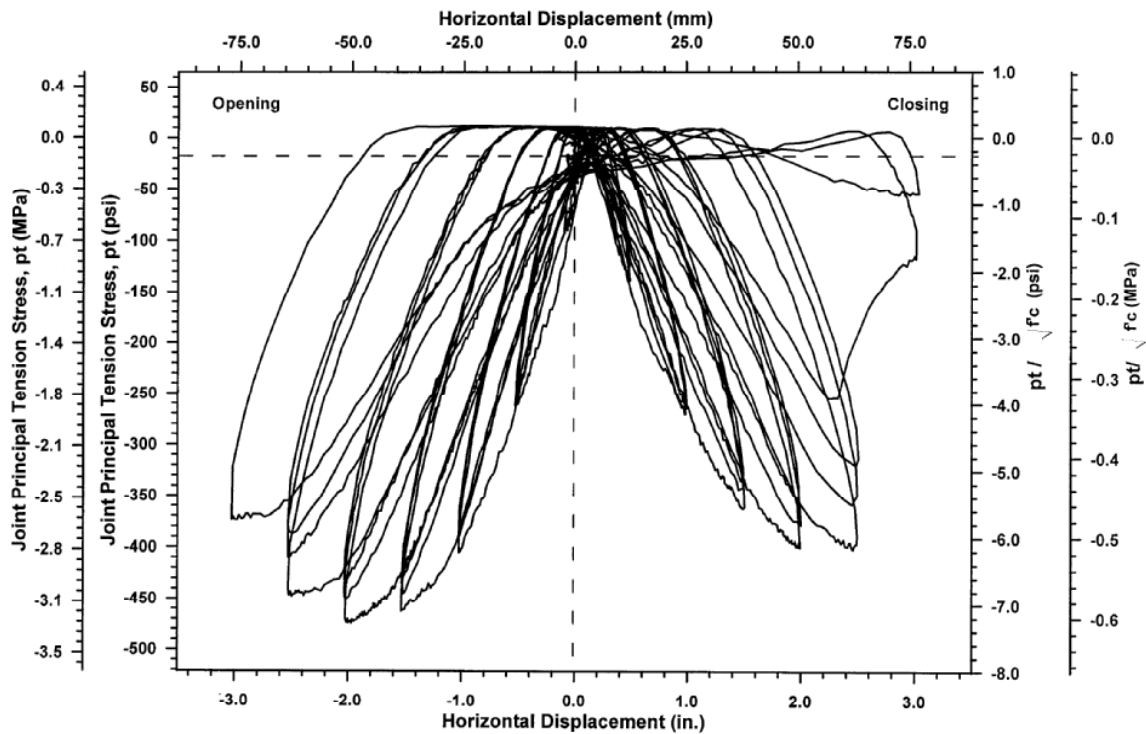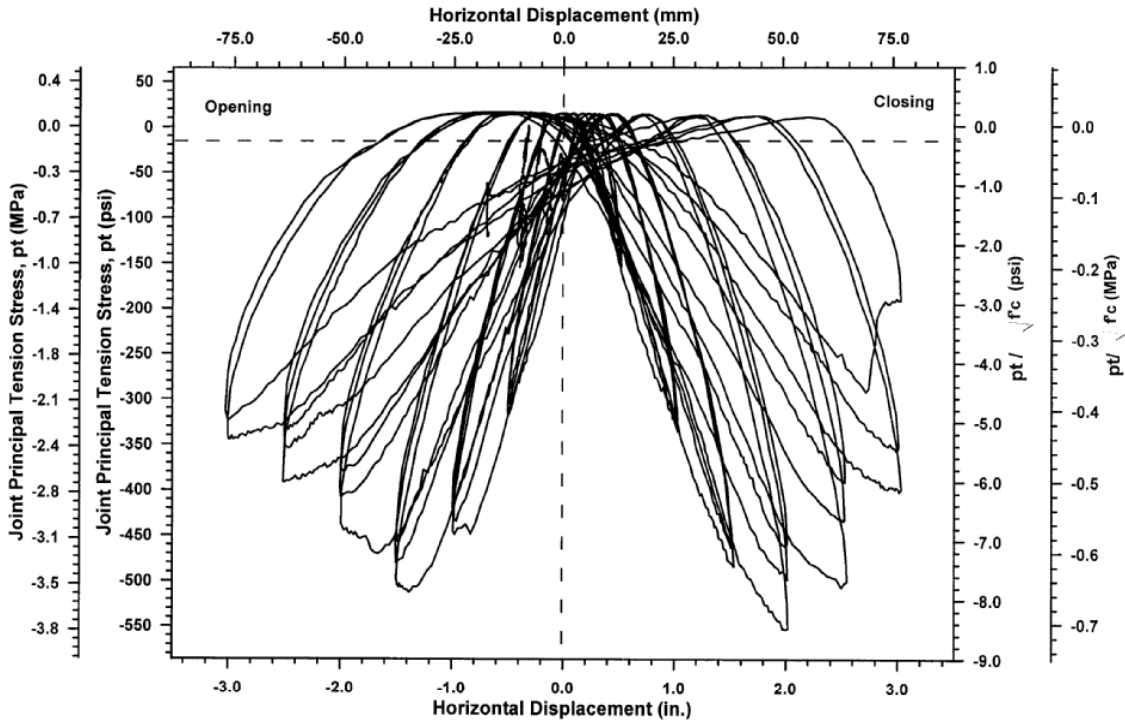

Figure 4.18 Joint Principal Tension Stress History for Specimen ASI

129

4.3.2 As-Built Specimen Under Out-of-Plane Loading

The detailing of Specimen ASO was identical to Specimen ASI. Both of the specimens represented a portion of bent #20 from the Spokane Street Overcrossing. Specimen ASO was subjected to an out-of-plane loading, while Specimen ASI was tested under in-plane loading. The outrigger beam was reinforced transversely using U-shaped stirrups. This form of stirrups with an open side is ineffective in providing any torsional resistance to the section after cracking. As a result, the torsion capacity of the outrigger beam would be expected to be very close to that of a plain concrete member.

The axial load level of Specimen ASO was chosen to be similar to the axial load used in testing Specimen ASI. Thus, testing of Specimen ASO started with the application of a 55-kips (244.7-kN) vertical force. This load value represented the scenario in which the outrigger bent is taken to a large response under in-plane action with a simultaneous movement in the out-of-plane direction. Moreover, this loading facilitates comparison of the behavior of the two specimens.

The first hairline torsional cracks in the outrigger beam were noticed during the second cycle to 0.5 in. (13 mm) displacement level. These cracks were marked after their formation to make them visible, as shown in Figure 4.19. The joint region of the specimen remained unaffected during this displacement level. Horizontal actuator forces of 8.8 kips (39.1 kN) and −7.9 kips (-35.1 kN) were recorded at this displacement level in the pull and push directions, respectively.

Torsional cracks on both faces of the joint with vertical bond split cracks on the back face of the joint developed at a displacement level of ±1.5 in. (±38 mm). The splitting cracks started at the column joint interface and formed at approximately 2 in. (5

cm) away from the edge of the joint. New cracks in the outrigger beam developed with some widening and extension of the existing cracks. Maximum actuator forces of 12.4 kips (55.2 kN) and -13.8 kips (-61.4 kN) were recorded at this displacement level in the pull and push directions, respectively.
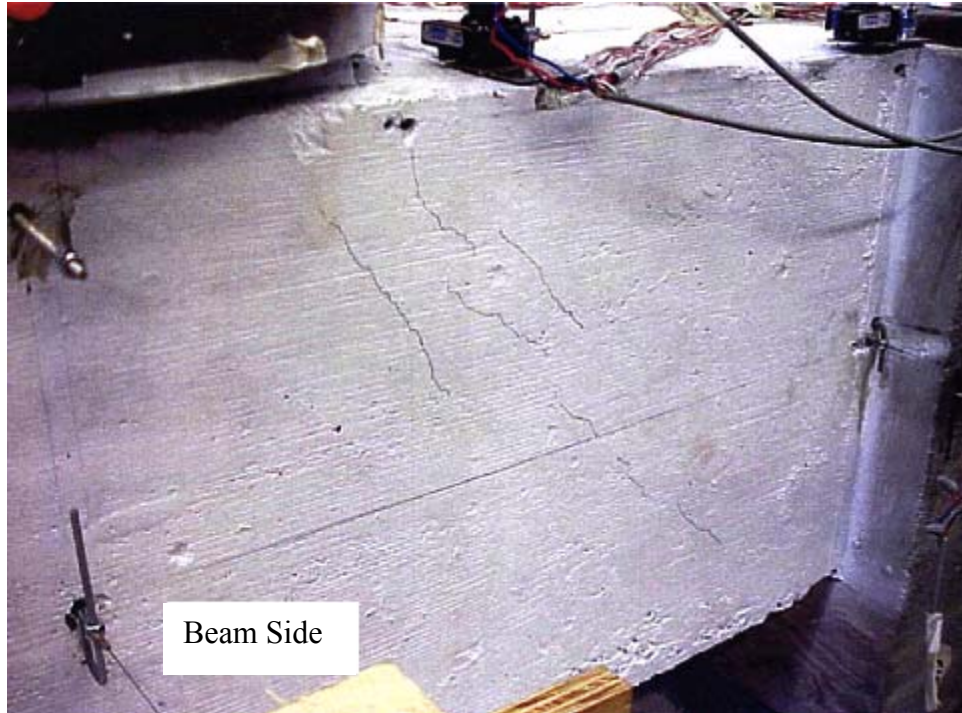
Figure 4.19 Early Torsional Cracking in the Outrigger Beam of Specimen ASO

During cycles to ±2.0 in. (±51 mm) displacement level, there was additional joint and beam torsional cracking, and the cracks formed earlier became wider. The splitting cracks on the back face of the joint started to widen and penetrated along the outside perimeter of the joint. This cracking is attributed to the difference in the stiffness between the joint concrete coinciding with the column area and the joint concrete outside that region. Torsional cracks on the top face of the beam developed. The largest

measured actuator forces during cycles at this displacement level were 13.3 kips (59.2 kN) and −13.9 kips (-61.8 kN) in the pull and push directions, respectively. These values show a 7% and 0.7% increase in the lateral resistance of the system when compared to those for the previous cycles. A picture of the joint at the end of this displacement level is shown in Figure 4.20.
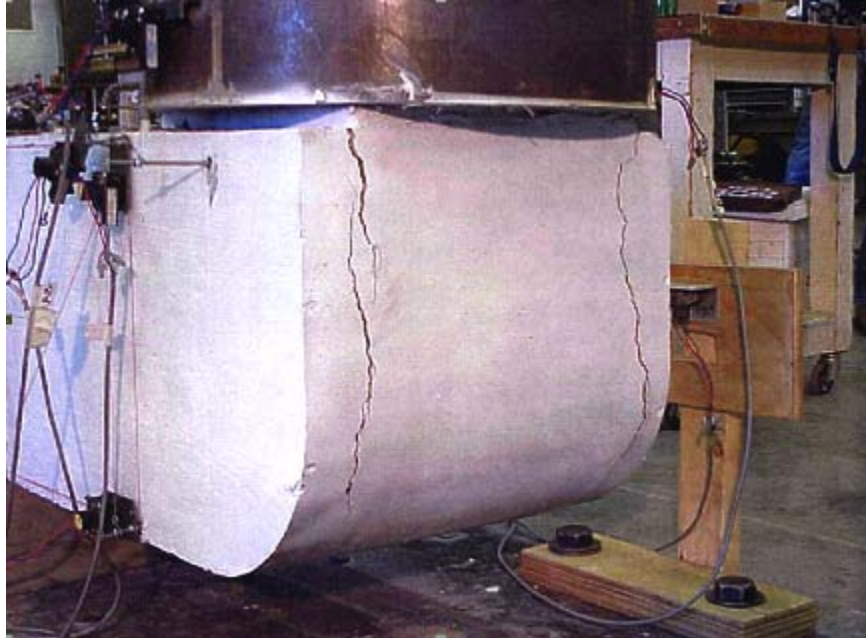
Figure 4.20 Bond Splitting Failure in the Back Face of Specimen ASO

During cycling to a displacement level of ±2.5 in.(±64 mm), further opening of the existing torsional and splitting cracks occurred. Torsional cracks on the sides of the joint linked to cracks in the upper face of the joint area outside the column region. Two existing diagonal cracks, one originating from the left upper corner of the joint and the other one starting from the right upper corner at the beam, increased in size. Furthermore, the width of the splitting cracks on the back face of the joint increased significantly. New horizontal splitting cracks in the outrigger beam formed along the

plane of the bottom reinforcement. These cracks extended beyond the beam-joint interface following the profile of the beam reinforcement as it hooked into the joint region. The horizontal splitting cracks may be due to tension loading of the longitudinal bars caused by shear distortion of the beam section.

After the test was completed, the bottom of the specimen was examined. The bottom face of the beam was found to have large X-shaped torsional cracks linked to the splitting cracks in the bottom face of the joint. The large size of these cracks on this face is due to lack of torsional strength and confinement in the section as a result of using U-shaped stirrups. Figure 4.21 shows the bottom face of the beam after the end of the test. The measured actuator force in the pull direction was 12.7 kips (56.5 kN) and 10.3 kips (45.8 kN) following the first and the third cycles, respectively. This is equivalent to a 19% degradation of lateral resistance between successive cycles. While in the push direction, the measured actuator forces were 11.7 kips (52.0 kN) and 10.4 kips (46.3 kN) following the first and the second cycles, respectively, which is equivalent to a 12% drop in the strength between the two cycles. The test was stopped following the third pull cycle to avoid any damage to the testing apparatus. At the end of the test, the specimen was still able to support the applied axial load. Figure 4.22 shows the damage to the test specimen at the end of the test.
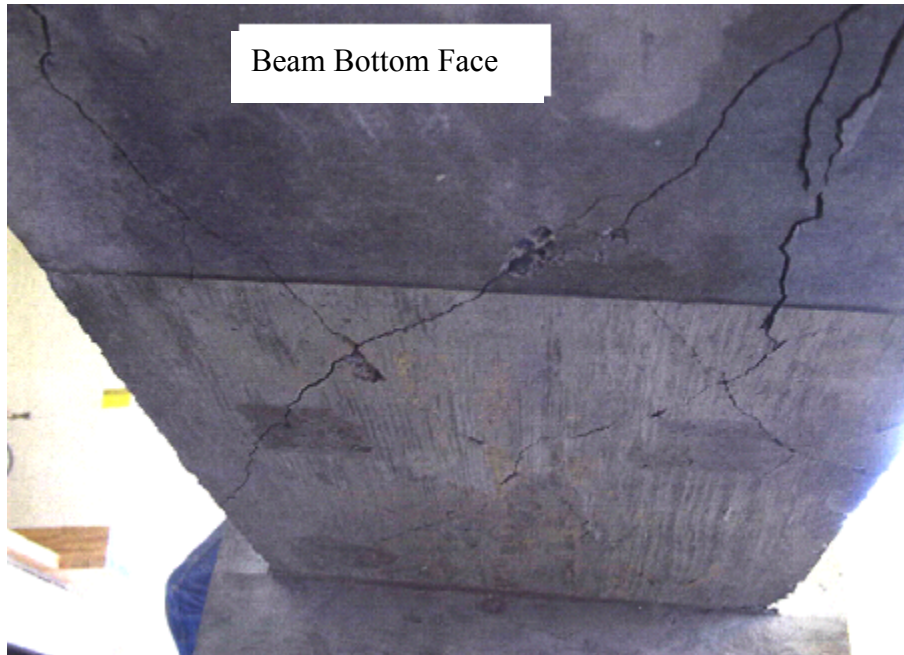
Beam Bottom Face

Figure 4.21 Torsional Cracks on the Bottom Face of Specimen ASO
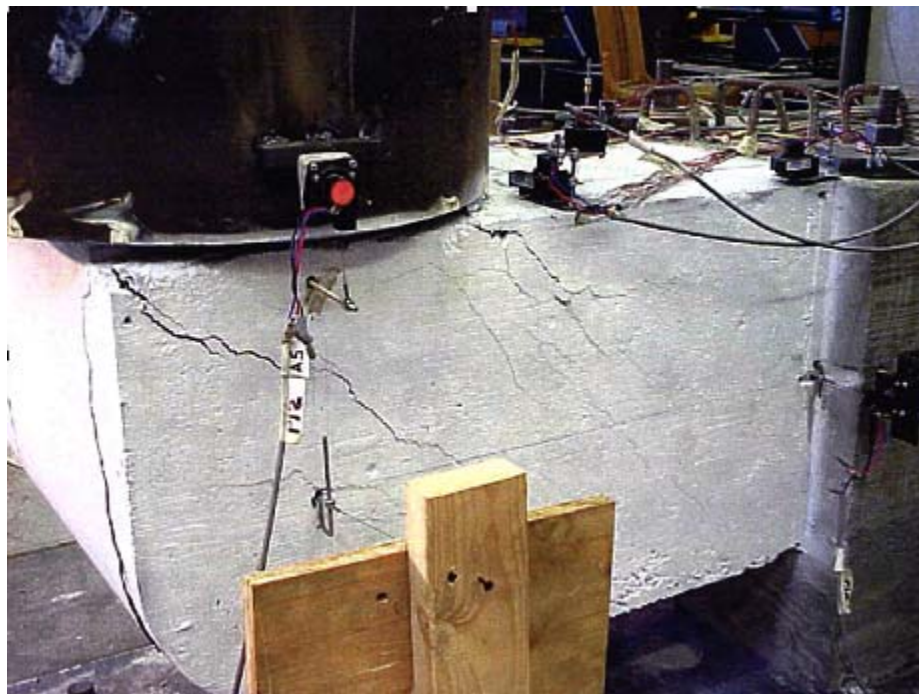
Figure 4.22 Torsional Cracks in the Outrigger Beam and the Joint of Specimen ASO at the End of the Test

The actuator force-horizontal displacement history is shown in Figure 4.23. The value of the actuator force corresponding to the theoretical torsion cracking strength of the outrigger beam, T_{cr}, is shown in the figure. T_{cr} was calculated based on contributions from the concrete and longitudinal steel. Figure 4.22 indicates that the test specimen was able to attain an average ultimate capacity of 1.68 times the theoretical torsion strength in both directions. The fact that the specimen had a stronger response than predicted may be due to the short outrigger beam. The beam developed compression struts that transferred forces directly to the anchor block. Ductilities were not reported for the out-of-plane specimen due to failure mechanism of the specimen, which involved two interacting phenomena - bond splitting and torsion. This interaction makes yielding hard to define.

The hysteresis curves for Specimen ASO were relatively narrow, showing little energy dissipation up to a tip displacement of ±1.0 in. (25 mm). The specimen exhibited some energy dissipation in the subsequent loops along with some pinching in the last loops to 2.5 in. (64 mm) displacement level due to cracking in the beam and splitting bond failure in the joint region. The specimen was able to withstand displacements of up to 2.0 in. (51 mm) in both directions before a reduction in the actuator force, as shown in Figure 4.23, corresponding to a drift ratio of 2.5%. A 3.1% maximum drift ratio was reported in both directions at the end of the test.
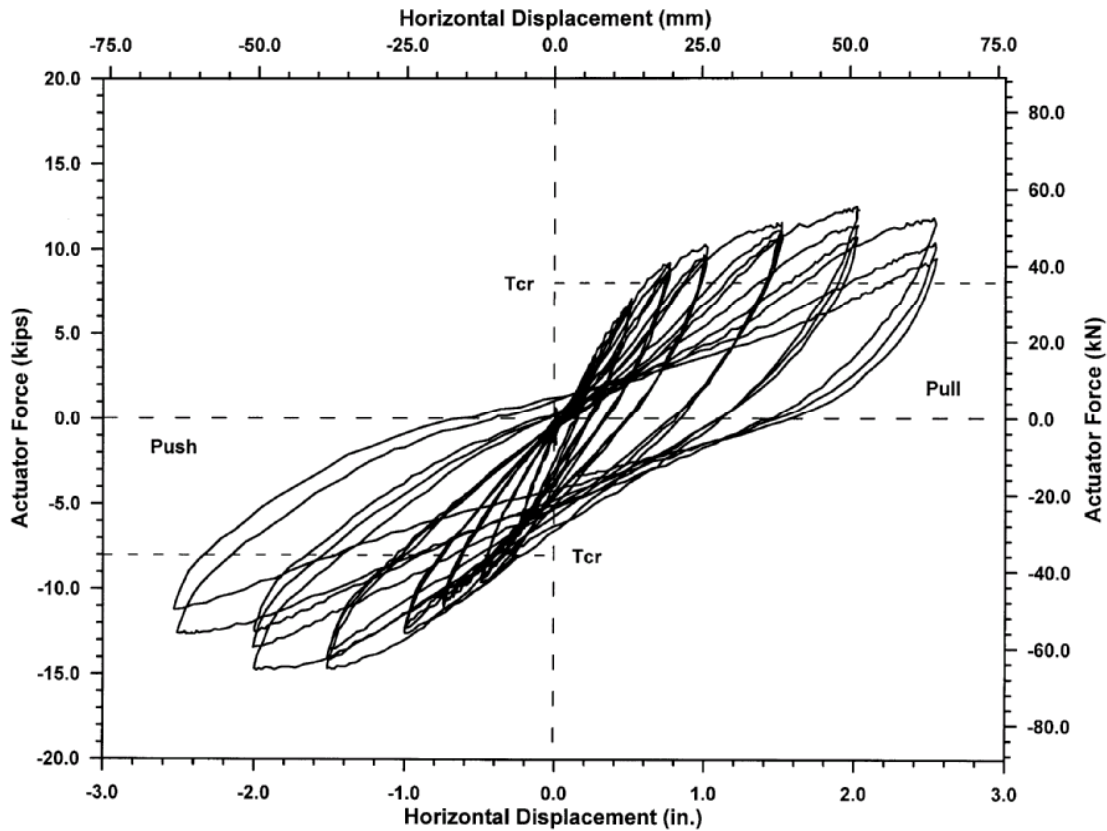
Figure 4.23 Actuator Force-Horizontal Displacement History for Specimen ASO

Figure 4.24 shows the experimental and the predicted column moment-curvature responses in the plastic hinge region. It can be seen from Figure 4.24 that the column yield moment was never attained for either direction of loading. This reduced response of the column hinge region occurred because of the low torsion strength of the beam and the bond splitting failure in the joint region. The moment-curvature history supports the preliminary theoretical predictions, in which the specimen was expected to fail long before forming a clear yielding mechanism in the column critical section.
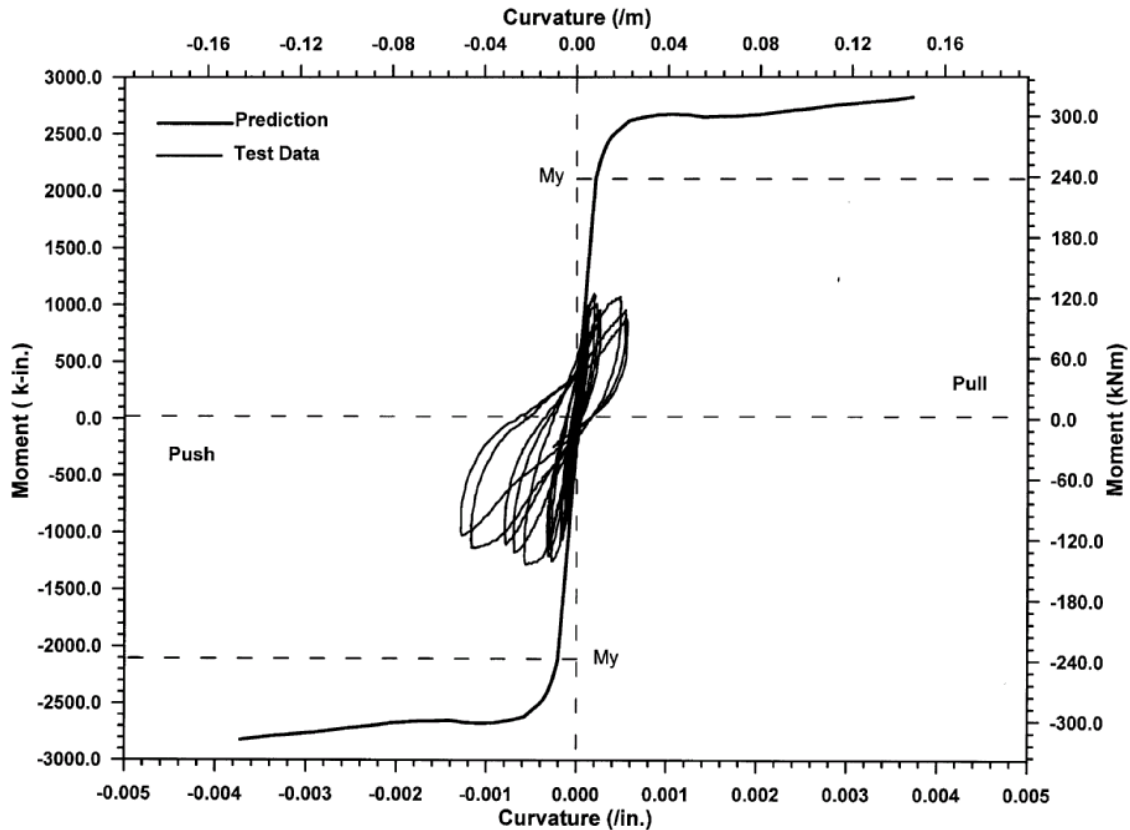
Figure 4.24 Column Moment-Curvature Response for Specimen ASO

4.3.3 Conclusions on As-Built Specimen Performance

In the first phase, three as-built test specimens replicating outrigger bents in the Spokane Street Overcrossing were tested. One specimen had a long outrigger beam and the other one a short outrigger beam; both were tested under in-plane loading. The third specimen had a short outrigger beam and was tested under out-of-plane loading.

In-plane Loading

For in-plane loading, testing showed that the outrigger knee joint system performed poorly with limited energy dissipation capacity due to the performance of the

joint. In the opening direction, both of the test specimens were unable to develop the yield strength of the outrigger beam framing into the joint. The long outrigger and the short outrigger had measured yield flexural strengths that were 96% and 67%, respectively, of the predicted strengths based on conventional flexural analysis. Differences in behavior were related to the detailing of the top longitudinal beam reinforcement embedded into the joint. In the long outrigger specimen, the longitudinal beam reinforcement bars carried into the joint had 180-degree hooks inside the joint, thus providing the required embedment length for the bars. In the short outrigger specimen, the longitudinal beam reinforcement bars carried into the joint had a straight embedment rather than hooks bending into the joint. The other reason for this difference in the measured flexure strength was believed to be due to the increased width of the short outrigger beam over the column width, resulting in some of the beam reinforcement extending into the joint region outside the column core.

In the closing direction, both the long and the short outrigger specimens experienced a loss of strength after developing the ideal strength of the column. This behavior ensured that the column reinforcement was successfully able to develop its yielding strength due to the good anchorage of the column bars within the joint. The two specimens eventually failed in the same manner due to splitting bond failure within the joint region. The column reinforcement hook extensions became exposed as concrete at the curved side of the joint face spalled off while cycling to 3.0 in. (76 mm) displacement level. This failure indicated that the joint was not able to support the diagonal compression strut between the column and the beam compression zones during closing of the joint.

Figure 4.25 shows the actuator force-horizontal displacement envelopes for the long and the short outrigger specimens. Figure 4.25 demonstrates that both of the specimens behaved in a similar manner and had the same trend in both the closing and opening directions. As can be seen in Figure 4.25, the long and the short outrigger specimens failed at the same displacement level, implying an approximately similar drift ratio for both. It also can be seen that the short outrigger specimen showed higher stiffness and load capacities in the closing direction when compared to the similar values for the long outrigger because of the shorter beam and the larger column cross-sectional area and reinforcement. A maximum ductility level of 2.0 and -3.3 for the short outrigger and a 2.8 and -3.8 maximum ductility level for the long outrigger were attained in the closing and opening directions, respectively.

In summary, the existing outrigger knee joints would be expected to fail at a relatively low ductility level of between 2.0 to 2.8.
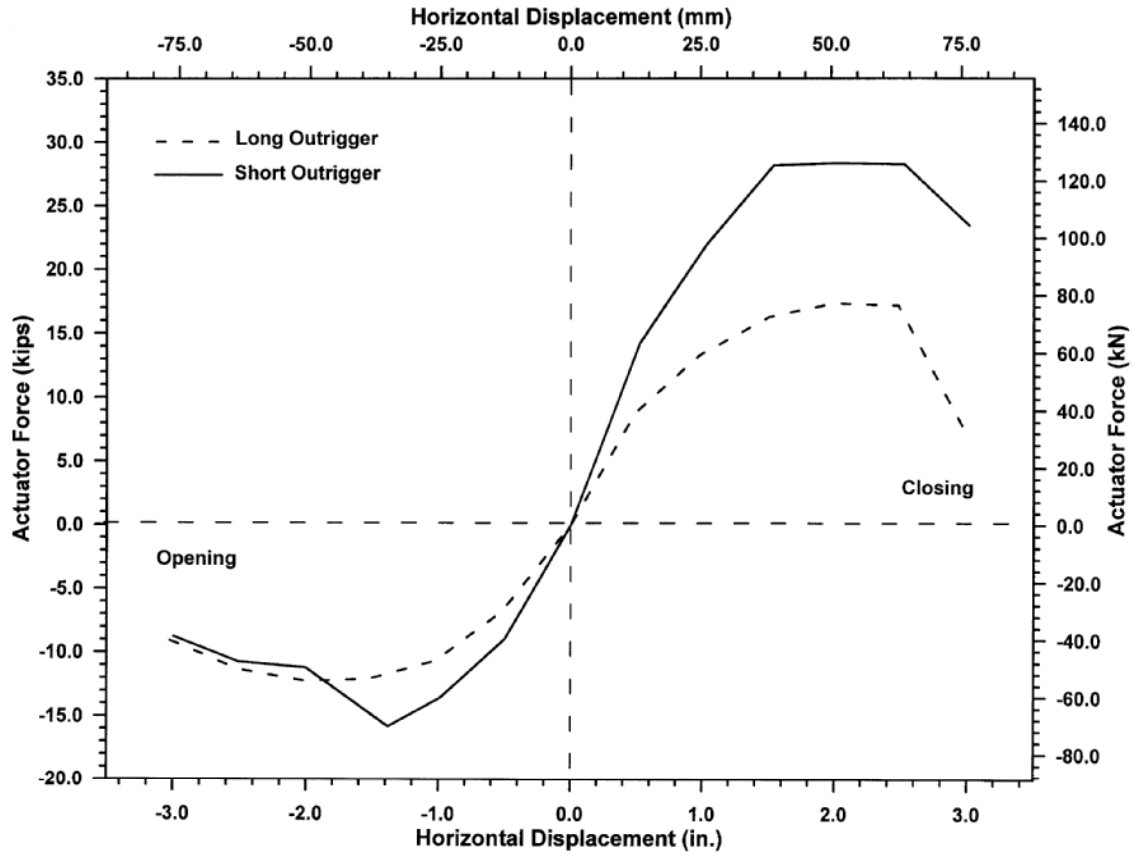
Figure 4.25 Actuator Force-Horizontal Displacement Envelopes for the As-Built Specimens Under In-Plane Loading

Out-of-plane Loading

In the out-of-plane direction, the as-built specimen was able to attain a maximum capacity, on average, 68% higher than the cracking torsion strength in both directions. This substantial increase in the capacity is believed to be due to the behavior of the short outrigger beam transferring forces directly to the anchor block.

The specimen was able to attain a displacement level of 2.5 in. (64 mm) in both directions before the splitting bond failure within the joint region caused by the beam reinforcement.   The out-of-plane specimen was capable of sustaining a drift ratio of approximately 2.5% before degradation of capacity. This value falls in the same range of

140

drift ratios as was obtained for the in-plane specimens, 1.9% to 3.2%, at the point of maximum capacity. Therefore, an average value of 2.5% can be adopted as a drift ratio for the existing outrigger bents in both the in-plane and out-of-plane motions.

4.4 RETROFITTED SPECIMENS – GENERAL BEHAVIOR

4.4.1 Retrofit Strategy and Design Goals

The test on the one-third scale models of the as-built outrigger knee joint systems demonstrated their vulnerability to in-plane and out-of-plane seismic loading. An efficient upgrading of the outrigger knee joint systems is thus needed to elevate the performance of the existing outrigger bents to an acceptable level by current earthquake – resistant design practice.

The main goals of the upgrade strategy are to provide for virtually no damage in the joint region, improve the torsion capacity of the outrigger beam, enhance the deformation and the energy dissipation of the system, be applicable to split outrigger bents, and be feasible to build. These goals were to be achieved by using steel jacketing of the knee joint and the outrigger beam.

Circular steel jackets around the beam and the joint were used to upgrade the short and the long outrigger specimens. The steel jacket formed an inverted L-shaped jacket encasing the beam and the joint. The joint jacket overlapped the existing column jacket. A new ¾-in. (19-mm) gap in the existing column jacket was created by removing the existing column jacket and the grout in that region. This gap was extended to the depth of the original column. The split long specimen was retrofitted in the same manner but with a D-shaped jacket. The retrofit strategy and details were discussed in detail in

Chapter Three. General recommendations for retrofitting existing outrigger joints are given in Chapter Six.

The steel jacket retrofit strategy was selected for the following reasons:

a) In tests on the short and the long outrigger specimens, ultimate cracking patterns and failure mechanisms of the joint indicated the tendency of the beam and the column reinforcement hooks within the joint to straighten. Thus, an external force was necessary to restrain these hooks. This force can be efficiently provided by confining the joint region using a circular steel jacket. Confinement pressure is created as the reaction of the joint jacket to the dilation of the compressed concrete.

b) For the in-plane specimens, a compression diagonal strut developed between the flexural compression forces of the beam and the column reinforcement under opening and closing of the joint. Horizontal and vertical forces are required to transfer and stabilize the transfer of the compression strut to the column and beam flexure tension reinforcement. This can be achieved by providing a circular jacket around the joint.

c) In the in-plane tests, shear distress of the joint was apparent before ultimate bond splitting failure. Consequently, there is a need to increase the shear strength of the joint in the vertical and horizontal directions by providing horizontal and vertical hoops to the joint region. This can be achieved by using a steel jacket around the perimeter of the joint.

d) Under opening moments, the outrigger beam was the member controlling the flexural behavior in the as-built specimens. The standard practice in bridge design is to develop a plastic hinge in the column rather than in the beam. For single level outrigger bents, curvature ductilities within the column plastic hinges will enhance displacement

ductilities. It was determined that additional reinforcement or increasing the cross sectional area of the beam, especially in the joint vicinity, will increase its capacity and therefore force the plastic behavior to be in the column region. The circular steel jacket around the beam will increase its flexural capacity. First, the distance between the resultant compression force in the concrete and the resultant tension force in the rebars of the beam is increased because of the grout between the jacket and the original beam section. Second, the steel jacket will increase the capacity by participating in a composite action with the concrete of the section.

e) In the test of the out-of-plane specimen, torsional cracking developed in the outrigger beam due to poor transverse reinforcement. Therefore, there is a need to have transverse reinforcement to upgrade the torsion capacity of the outrigger beam. The circular steel jacket around the beam is equivalent to continuous hoop reinforcement.

f) A reaction force in the beam jacket would develop due to the confining pressure around the joint. This force has to be restrained either by using through bolts in the outrigger beam or by transferring it back to the anchor block using end plates anchored to the beam jacket on one side and to the anchor block on the other side. It was found that the way in which the steel jacket is assembled around the beam and the joint makes it possible to take the reaction by relying on the grout in the area at the intersection of the beam with the joint jacket. In addition, there is no need to provide any additional restraint to the steel jacket to account for buckling. This issue would have been of more importance if flat plates had been used.

g) A recent experimental study was completed at Washington State University (McLean, El-Aaarag and Rogness, 2001) that investigated the performance of existing

split columns. D-shaped steel jackets were investigated and shown to improve the column performance to an acceptable ductility level. It was suggested that using the same retrofit technique for the split outrigger specimens in this study would meet these goals.

h) A minor consideration was the aesthetics appearance of the outrigger bents after being retrofitted and matching with the existing column steel jacket.

4.4.2 Retrofitted Specimens Under in-Plane Loading

Specimen RLI

The retrofitted long outrigger specimen represents the retrofit of bent #36 in the Spokane Street Overcrossing. Specimen RLI was retrofitted using an inverted L-shaped circular steel jacket around the beam and the joint. With this provided retrofit scheme, the behavior of the specimen was expected to improve significantly. A well-defined failure mechanism for Specimen RLI was expected through hinging in the column gap section.

In order to provide a comparison between the behavior of the as-built and retrofitted specimens, testing and loading setups for Specimen RLI were kept identical to those used for Specimen ALI. Consequently, testing started with the application of a 33 kips (146.8 kN) vertical force. The horizontal actuator was then retracted to produce zero force in the actuator and testing was conducted about this point.

The first visible flexure crack in the column gap region attributable to opening moments was noticed during the first cycle to 2.0 in. (51 mm) displacement level. This crack extended about 2.5 in. (64 mm) inside the gap region. On the cycles to ±2.5 in.

(±64 mm) displacement level, there was a flexure crack on the other side of the column gap region during the first cycle in the closing direction. The length of the crack was about 1.8 in. (45 mm). The cracks on both sides of the column hinge section closed when cycling in the opposite direction. Upon further loading, there was some widening and extension of the existing cracks in the gap area. The column concrete cover within the gap started to spall off at a displacement level of 3.5 in. (89 mm) in both directions. The test was stopped following cycles to 5.0 in. (127 mm) displacement level to avoid any damage to the laboratory loading apparatus.

The test showed that the ¾-in. (19-mm) gap created in the column was functioning properly, as it did not close up in either direction of loading and still had the ability to provide for further rotation of the column in the horizontal plane. Maximum actuator forces of 27.1 kips (120.5 kN) and −23.5 kips (-104.5 kN) were recorded at the end of the test in the closing and opening directions, respectively. Figure 4.26 shows a picture of the test specimen at the end of the test.

The circumferential strains in the joint jacket of Specimen RLI were well below yielding, with a maximum strain of about 27% of the yield strain. This indicates that the provided jacket thickness was adequate.
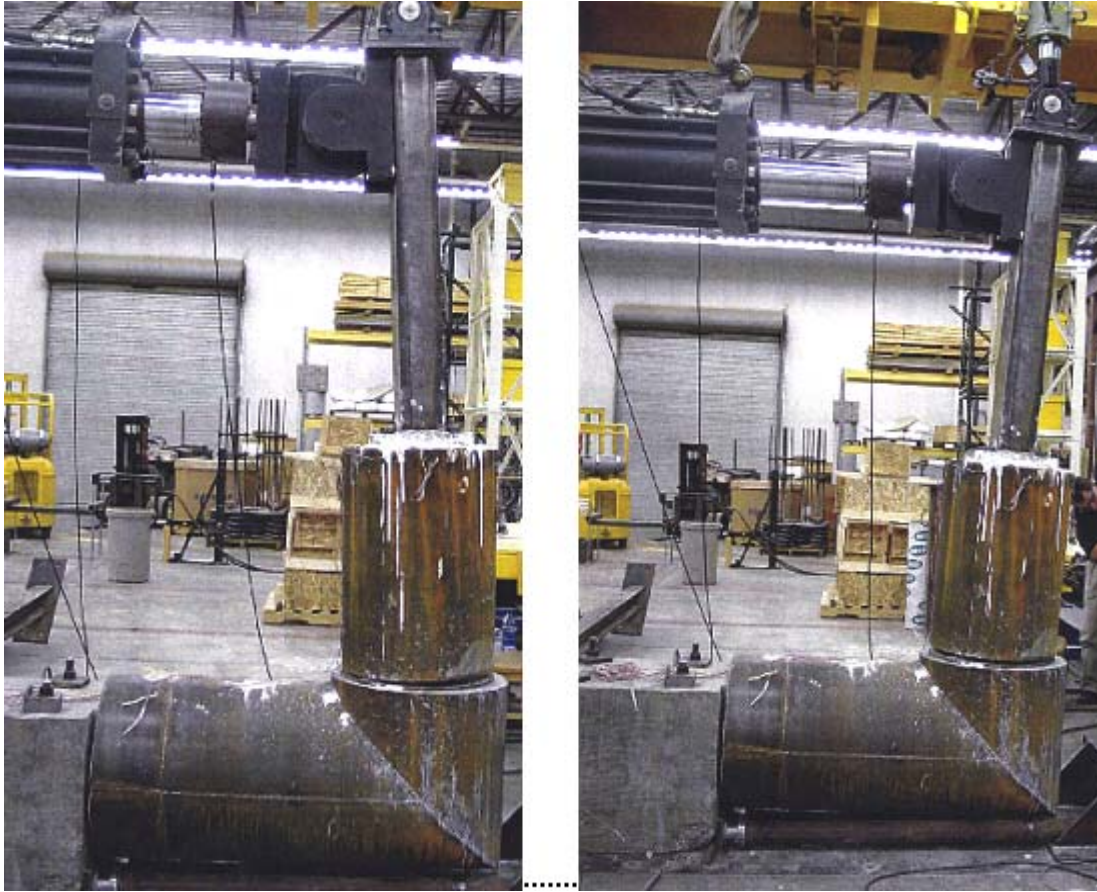
(a) Closing   **(b) Opening**

Figure 4.26 Specimen RLI at Peak Test Displacements

The actuator force-horizontal displacement history for Specimen RLI is shown in Figure 4.27. The values of the actuator force corresponding to yielding moment, F_Y, and ideal moment, F_I, are included in the figure. The ideal and yield moment values were calculated based on plastic hinging in the column section at the ¾-in. (19-mm) new gap for both directions. From Figure 4.27, it can be determined that the maximum actuator force in both the joint-opening and the joint-closing direction reached the calculated ideal moment. Therefore, the experimental yield displacement was determined for the specimen in both directions as discussed in Section 4.2.5. An average value of the yield

displacement in both directions for Specimen RLI was used as the specimen had the same failure mechanism in the opening and closing direction. Thus, the yield displacement was determined as 0.80 in. (20.3 mm).

The hysteresis loops of Specimen RLI were narrow up to 1.0 in. (25 mm) displacement level. After that, the area under the hysteresis loops started to increase implying the onset of a pronounced plastic behavior. Figure 4.27 demonstrates that the specimen exhibited considerable energy dissipation while looping to 5.0 in. (127 mm) displacement level. The specimen was able to achieve a 5.0 in. (127 mm) displacement level without any signs of strength degradation. The maximum achieved actuator force was, on average, 48% higher than the ideal strength. This increase in strength occurs due to strain hardening in the column reinforcement and higher concrete compressive strength affected by the confinement provided by the steel jackets. Specimen ALI was able to attain a maximum ductility level of 6.3 at a drift ratio of 6.7% in both directions. These values represent a lower bound estimation of the ductility, drift and strength capacities for Specimen RLI as testing was stopped at 5.0 in. (127 mm) displacement level before seeing any significant damage to the specimen.

To gain insight into the post-yield behavior, the measured and the computed column moment curvature responses are shown in Figure 4.28. The measured moment curvature plots the average curvature against the maximum moment within the column cell. From Figure 4.28, it is clear that the measured response is higher than the computed response. This behavior may be related to conservative estimation of the ultimate compressive strength of steel-encased concrete. Another observation from the measured response is that there exists a difference in the ultimate curvatures in the closing and the

opening directions, although the failure mechanism was the same in both directions. It is believed that some errors were encountered in the curvature measurements for this specimen due to slipping of the potentiometer fixtures and measuring small displacement levels. It can also be concluded from Figure 4.28 that the specimen was able to attain its yield and ideal strengths in both directions.

Figure 4.27 Actuator Force-Horizontal Displacement History for Specimen RLI

148
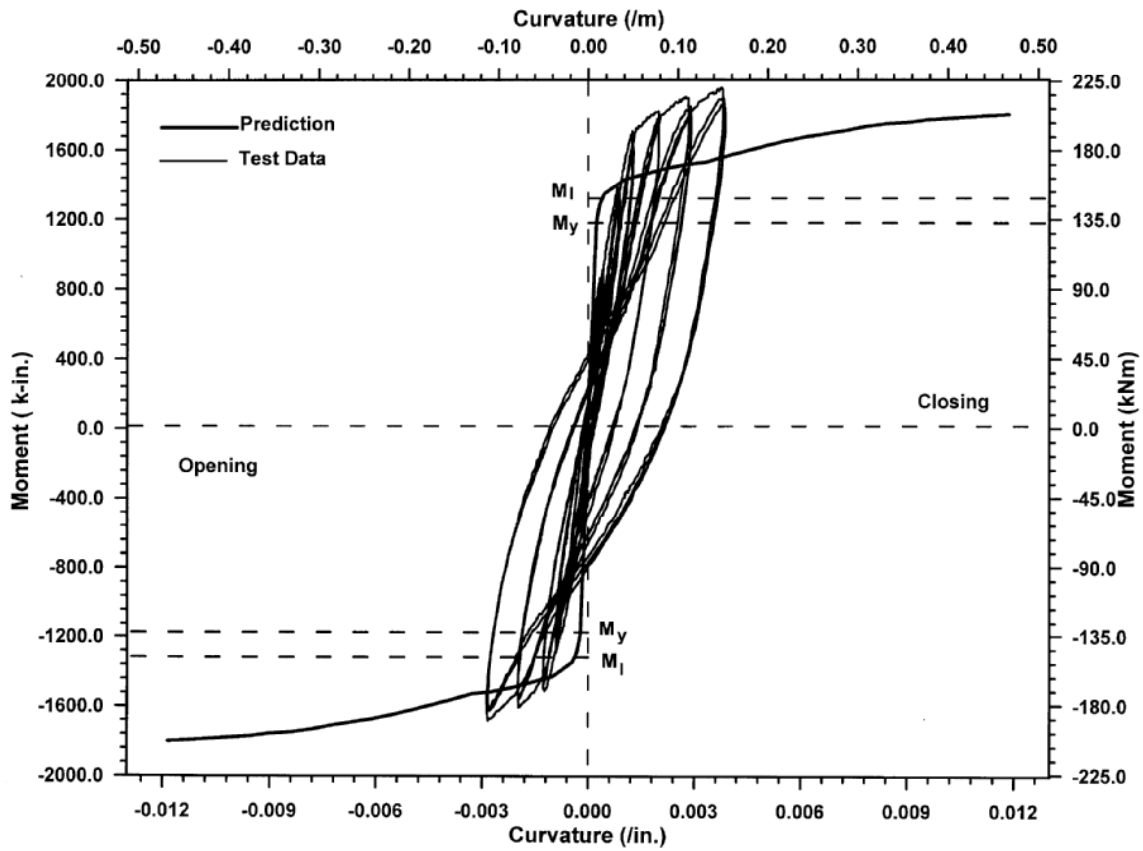
Figure 4.28 Column Moment-Curvature Response for Specimen RLI

Figure 4.29 shows the measured force-displacement hysteresis curves and the predicted force-displacement curve for Specimen RLI. The predicted force-displacement curve was obtained through static pushover analysis using the software SAP2000. The idealized nonlinear finite element model of Specimen RLI is shown in Figure 4.30. All nonlinear behavior was assumed to occur in the column plastic hinge, while the other elements were assumed to remain elastic.

The retrofitted outrigger beam is represented by a single two-dimensional frame element, which passes through the mid-depth of the section. Gross-sectional properties of the beam section before retrofit were used in the analysis. This is to account for the

enhancement of the beam stiffness by the steel jacket. This approximation agrees well with the recommendations of Priestley et al. (1996) on the stiffness enhancement of rectangular columns retrofitted by steel jackets. The beam moment of inertia was 6947 in^4 and the cross-sectional area was 254 in^2.

A rigid end zone for the elements representing the retrofitted knee joint was used since the retrofit measure limits rotation in the joint region. The plastic hinge length, as determined by equation 4.4, was represented by two two-dimensional frame elements. Based on moment curvature analysis of the column plastic hinge section, the effective yield moment and effective yield curvature of the plastic hinge were, 1509 k-in. (171 kN-m) and 0.000289 1/in. (0.0114 1/m), respectively. The plastic hinge section had an ultimate moment strength equals to 1890 k-in. (214 kN-m) and an ultimate curvature equals to 0.012 1/in. (0.47 1/m). The ultimate strength and curvature of the column hinge section were determined using the same confinement pressure as for the retrofitted column part.

Unretrofitted column effective moment of inertia and cross-sectional area were used to define the hinge elements. The hinge element moment of inertia was 1395 in^4 and the cross-sectional area was 99 in^2. A single element was used to represent the retrofitted column. Similar to the retrofitted beam elements, the cross-sectional properties of the retrofitted column were taken as the gross sectional properties of the column before retrofitting. The moment of inertia of the element representing the retrofitted column was 2746 in^4 and the cross-sectional area was 195 in^2. Finally, the steel tube section was modeled as a single element with a moment of inertia equal to 106 in^4 and a cross sectional area equal to 21 in^2.
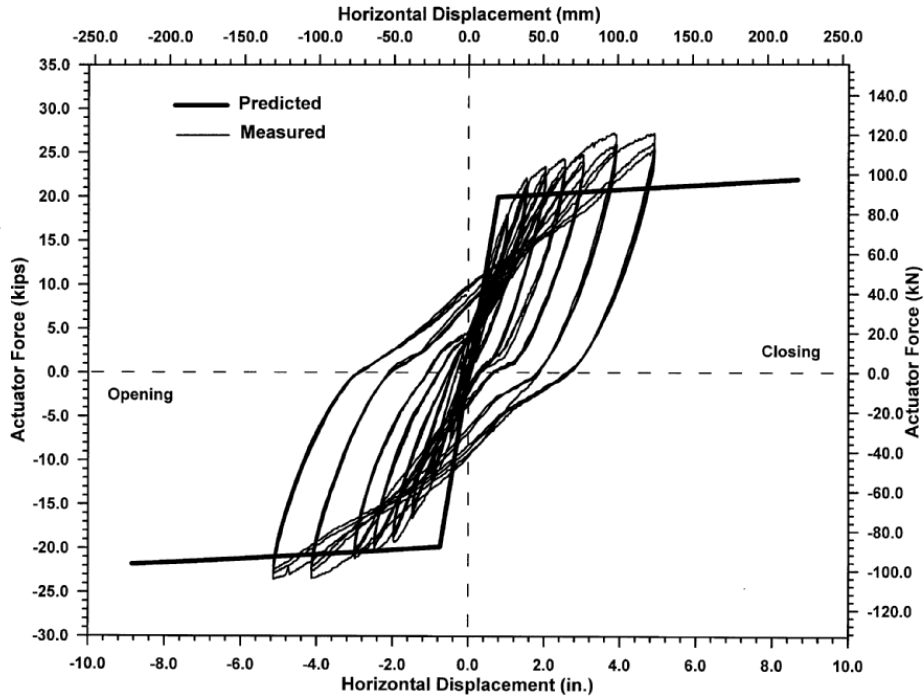
Figure 4.29 Measured and Predicted Behavior of Specimen RLI
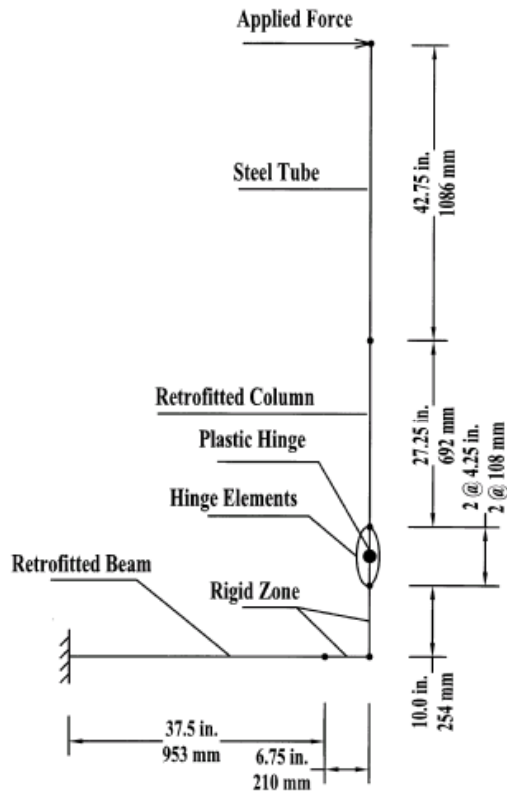
Figure 4.30 Computer Model of Specimen RLI

From Figure 4.29, it can be seen that Specimen RLI has higher measured strength, in both directions, than the predicted strength. The specimen had a strength at the end of testing that is, at the maximum, 23% higher than the predicted strength. This is believed to be a result of the conservative estimation of the ultimate confined compressive strength of the concrete in the hinge region. Therefore, it is suggested that an overstrength factor of at least 25% be included in estimating the ultimate capacity of the plastic hinge for capacity design of the remaining bridge members.

Figure 4.29 shows that the predicted displacement capacity for Specimen RLI was greater than the maximum attained test displacement. Part of the lower experimental estimation of the displacement capacity is due to the early termination of the test at 5.0 in. (127 mm) to avoid damage to the laboratory apparatus. Based on the condition of the column gap section of Specimen RLI at the end of testing, it was clear that the ultimate displacement capacity had not been reached. The good prediction of the behavior of Specimen RLI using a simple finite element model shows that the retrofit scheme can be incorporated in a simplified model assessing the overall bridge response.

Specimen RSI

Specimen RSI was constructed as a companion unit to Specimen ASI and was retrofitted utilizing the same retrofit measures as used for Specimen RLI. The specimen was a model retrofit of bent #20 in the Spokane Street Overcrossing. Testing and loading setups for Specimen RSI were identical to those used for Specimen ASI. Testing started with the application of a 55-kip (244.7-kN) vertical force. This force simulated the scaled prototype dead load and the increase in the axial load due to frame closing action

of the joint. The horizontal actuator was then retracted to the zero force position, and testing was conducted about this point.

On the cycles to ±2.0 in. (±51 mm) displacement level, there was a flexure crack in the joint gap region during the first cycle to close the joint. This crack extended about 2.5 in. (64 mm) inside the gap region. The first visible flexure crack in the opening direction was noticed during the first cycle to 2.5 in. (64 mm) displacement level. The cracks in the hinge region were closing when cycling in the opposite direction. Upon further loading, there was more widening and extension to the existing cracks. Crushing and spalling of the concrete column cover within the gap region started at a displacement level of 4.0 in. (102 mm) in both directions. The test was stopped following cycles to 5.0 in. (127 mm) displacement level to avoid any damage to the actuator and the axial load ram. As previously noted for Specimen RLI, the ¾-in. (19-mm) gap created in the column was functioning as required; it did not close in both directions, and still had the ability to provide for further rotation of the column in the horizontal plane. Maximum actuator forces of 42.3 kips (188.2 kN) and −31.7 kips (-141.0 kN) were recorded at the end of the test in the closing and opening direction, respectively. Figure 4.31 shows damage to the concrete in the gap region at the end of the test.

The strains caused by the confining pressure measured on the surface of the joint jacket of Specimen RSI were well below yielding, as was obtained for the previous retrofitted Specimen ALI. A maximum circumferential strain of about 29% of the yield strain was recorded for a strain gage near the bottom of the joint.
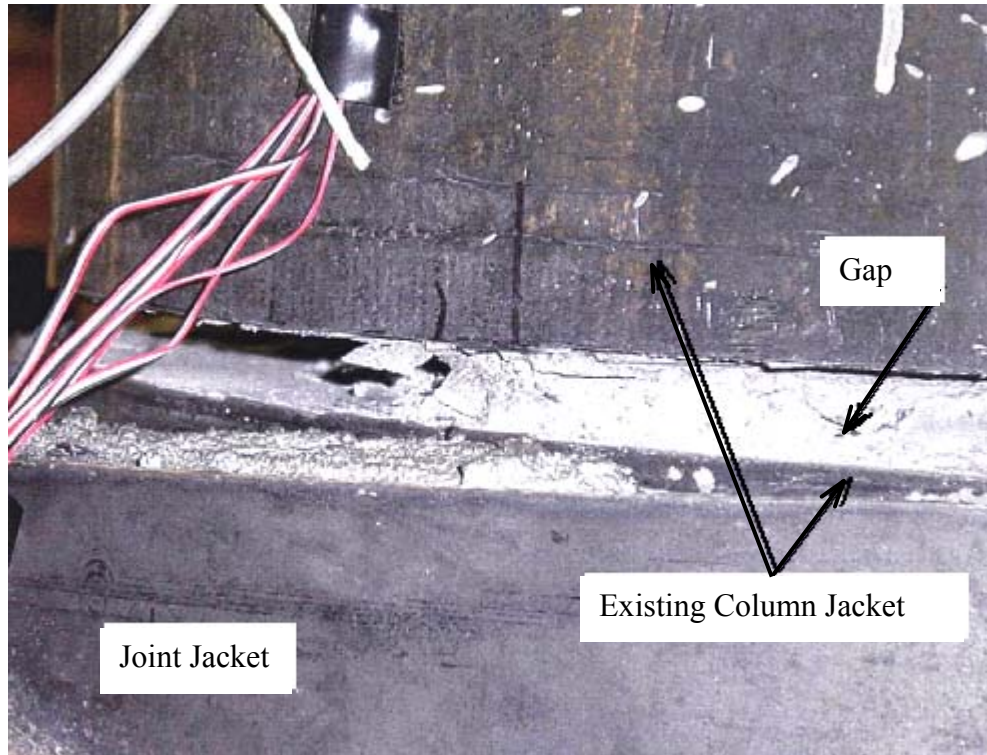
Figure 4.31 Spalling off Concrete at Column Corners for Specimen RSI

Figure 4.32 shows the actuator force-horizontal displacement history for Specimen RSI. The values of the actuator force corresponding to yield moment, F_Y, and ideal moment, F_I, are included in the figure. Similar to Specimen RLI, the yield and ideal moments were calculated based upon plastic hinging in the column region in both directions. From Figure 4.32, the specimen was able to reach the yield strength in both directions, but failed to achieve the ideal strength in the opening direction.

The specimen had a 26% higher capacity in the closing compared to the opening direction. Part of the difference in the ultimate behavior in both directions could be related to unsymmetrical bar locations around the centerline of the section. The additional strength in the closing direction over the ideal strength was due to strain hardening and increased compressive strength of the concrete due to confinement. The

experimental yield displacement for Specimen RSI was determined to be 1.09 in. (27.7 mm).

The force-displacement hysteresis curves for Specimen RSI showed little energy dissipation up to 1.0 in. (25 mm) displacement level. After a few cycles, inelastic deformation was noticed as a result of longitudinal reinforcement yielding. The loops were stable up to the end of the test with some minor pinching at the zero force axis in the closing direction.

Similar to Specimen RLI, Specimen RSI was able to achieve a 5.0-in. (127-mm) displacement level without any signs of strength degradation. Actual ductility, drift and strength capacities will be higher than reported since testing was stopped at 5.0 in. (127 mm) displacement level to avoid damage to the laboratory testing apparatus. Moment-curvature histories for the column gap are shown in Figure 4.33. Curvatures from test data are calculated from the linear potentiometer measurement on both sides of the column, while moments were calculated based on equilibrium of forces at the gap section. Predicted flexural response was computed based on a moment curvature analysis of the column section in the gap region using XTRACT. From Figure 4.33, good agreement can be noticed between the measured and predicted response in the closing direction. The specimen showed a lower calculated ultimate moment and curvature than predicted in the opening direction. By comparing the predicted and the computed response, it can be judged that the retrofit measure was a beneficial upgrade technique, as Specimen RSI was capable of more plastic behavior.
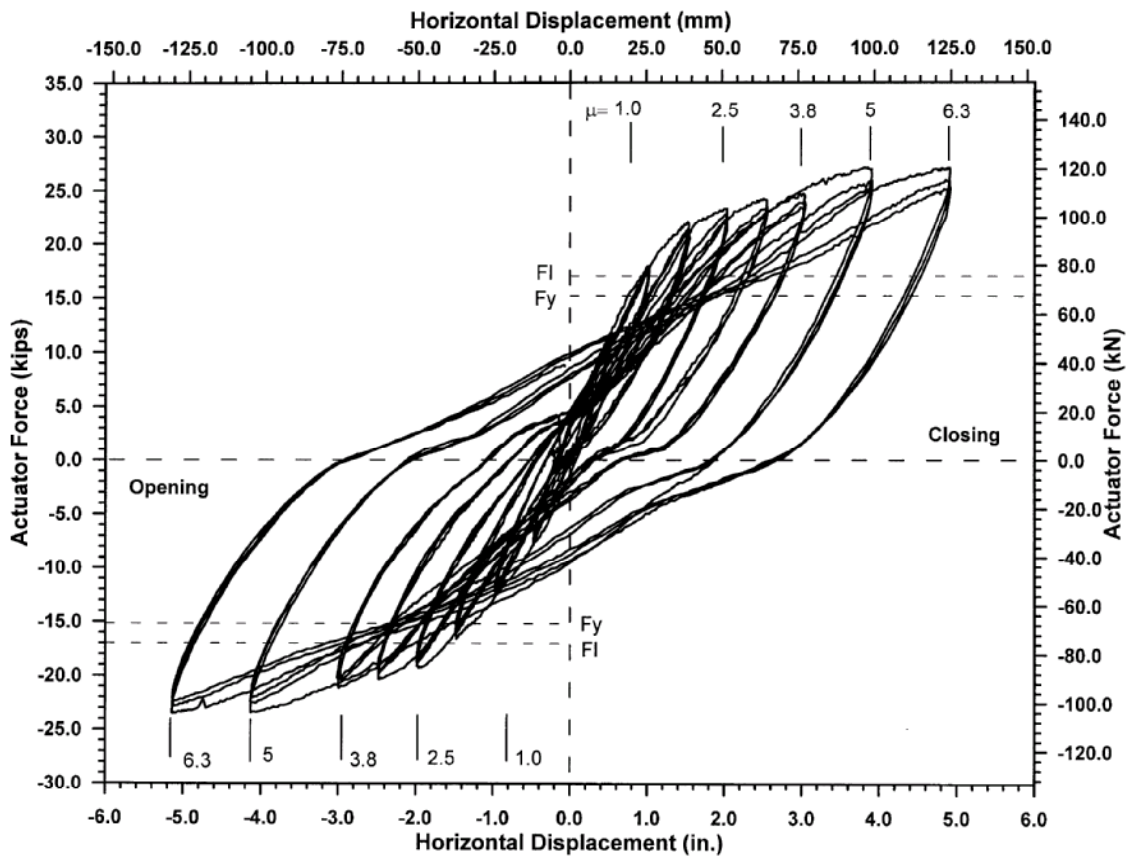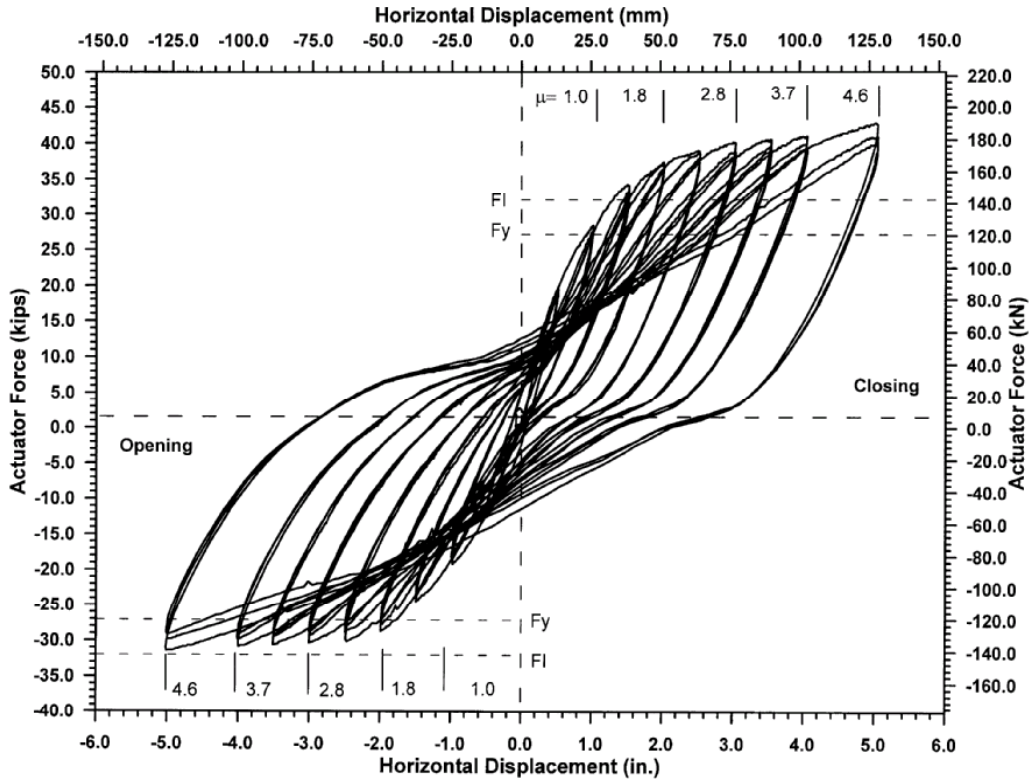
Figure 4.32 Actuator Force-Horizontal Displacement History for Specimen RSI
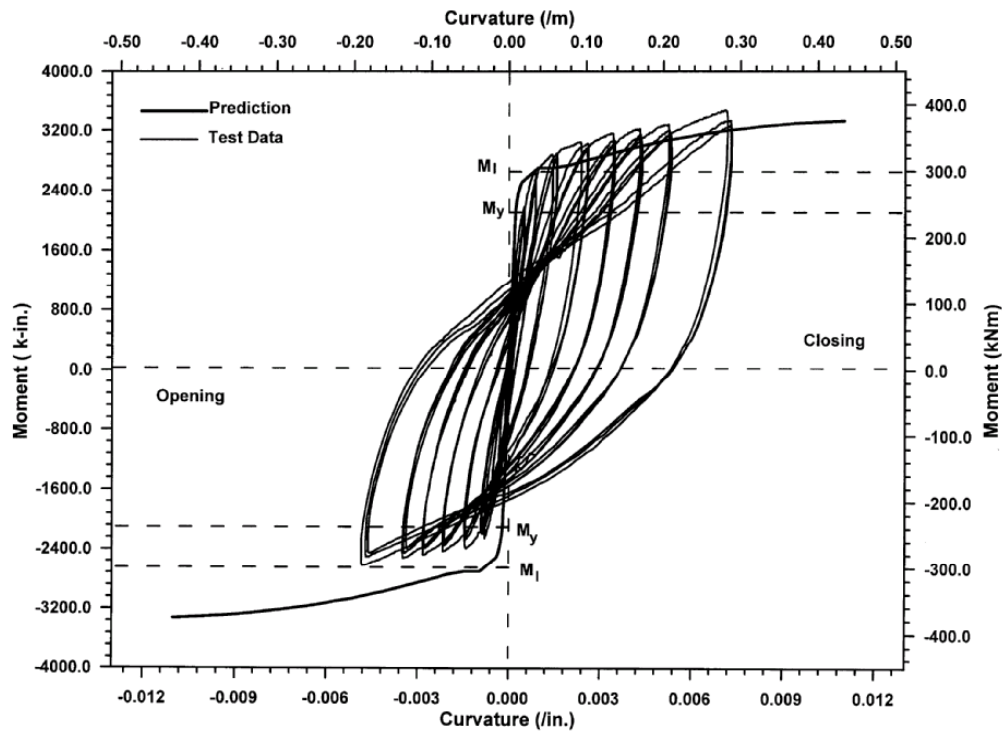
Figure 4.33 Column Moment-Curvature Response for Specimen ASI

156

Specimen RSPLI

Specimen RSPLI is a retrofitted split long outrigger specimen and is a model retrofit of bent #34 in the Spokane Street Overcrossing. Specimen RSPLI was retrofitted using a 90-degree elbow steel jacket with a D-shaped cross section. Based on test observations from previous retrofitted specimens, RLI and RSI, the specimen was expected to experience a failure mechanism through hinging in the column gap region.

Performance of Specimen RSPLI was examined under in-plane loading. Therefore, the testing and loading setup for Specimen RSPLI was identical to that of the other in-plane tests. Testing started with the application of a 27.5-kip (122.3-kN) vertical force to simulate the scaled prototype dead load and the increase in the axial load due to frame closing action of the joint. The horizontal actuator was then retracted to the zero force position, and the testing was conducted about this point.

The earliest signs of flexural cracking in the column gap region were observed in the first cycle to 1.5 in. (38 mm) in the closing direction. Upon further loading, and during the third cycle to 2.0 in. (51 mm) displacement level, a flexure crack formed in the gap region as a result of joint closing. On the cycles to ±2.5 in. (±64 mm) through ±3.5 in. (±89 mm) displacement levels, cracks on both sides of the column hinge experienced more widening and extension.

It was observed during testing that the existing column steel jacket slipped with respect to the new joint jacketing while cycling to the 4.0 in. (102 mm) displacement level, as shown in Figure 4.34. This movement likely happened due to a drop in the original confining pressure around the joint region as a result of out-of-plane bending of the flat side plate on the backside of the joint and the beam. The concrete cover on the

corners of the column started to crush and spall at a displacement level of 4.0 in. (102 mm) in both directions. The test was concluded at the 5.0 in. (127 mm) displacement level to avoid any damage to the laboratory testing apparatus.

The ¾-in. (19-mm) gap created in the column was functioning as expected. The gap did not close in either direction, and it still had the ability to provide for further rotation of the column in the horizontal plane. Maximum actuator forces of 24.2 kips (107.6 kN) and –20.5 kips (-91.2 kN) were recorded at the end of the test in the closing and opening direction, respectively.
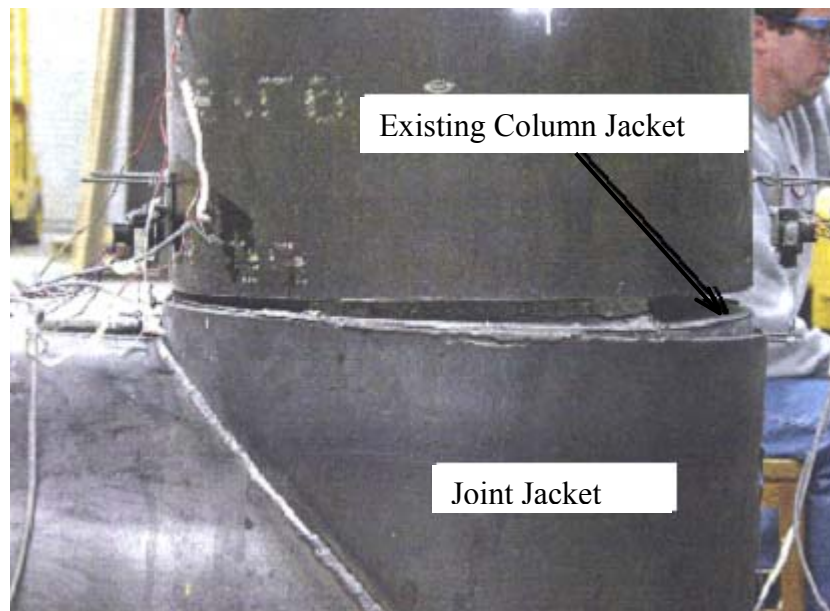
Figure 4.34 Slippage of the Existing Column Jacket Within the Joint Jacket

Circumferential strains recorded on the joint jacket can be taken as indicative of confinement provided to the joint region. Strain gages were positioned on both split knee joints jackets in the Specimen RSPLI with values showing similar behavior. The maximum strain value was measured for a gage located at 5 in. (127 mm) from the top

edge of the joint jacket just before the slippage of the existing column jacket from the joint jacket as 33% of the yield strain.

The actuator force-horizontal displacement history is shown in Figure 4.35. Included in the figure are the actuator forces corresponding to yielding moment, F_Y, and ideal moment, F_I. These values were determined based on plastic hinging in the column section at the ¾-in. (19-mm) new gap for closing and opening directions. In calculations of the yield displacement discussed earlier, the presence of the flat plate on the backside of the split columns contributed to the flexural strength of the section. Unfortunately, strain gages were not provided on these plates to get a precise estimation of this contribution. Therefore, the yield and the ideal actuator force shown in Figure 4.35 represented an average of two values: one characterizing a column section with a flat plate and the other a column section without a flat plate. It is apparent from Figure 4.35 that the maximum actuator force in both the joint-opening and the joint-closing directions reached the calculated ideal moment. Ultimate lateral force in the closing direction was about 15% higher than that of the opening direction. Part of this difference may be related to the flat plate contribution in one direction more than in the other. Experimental yield displacement was determined for the specimen in both directions as discussed in Section 4.2.5. The yield displacement was determined to be 0.78 in. (19.8 mm).

It is evident from Figure 4.35 that the Specimen RSPLI exhibited little energy dissipation up to 1.0 in. (25 mm) displacement level. Thereafter, plastic behavior is demonstrated by the increase in the area enclosed by subsequent loops. The specimen experienced substantial energy dissipation while looping to 4.0 in. (102 mm) and 5.0 in. (127 mm) displacement levels. Strain hardening and confinement effects pushed the

hysteresis loops above the specimen ideal strength. The specimen was able to achieve a 5.0-in. (127-mm) displacement level without any signs of strength degradation. Specimen RSPLI was able to attain a maximum ductility level of 6.4 at a drift ratio of 6.7% in both directions. Similar to the other retrofitted specimens, RLI and RSI, these values represent a lower estimation of the ductility, drift, and strength capacities for Specimen RSPLI, as testing was stopped at a 5.0 in. (127 mm) displacement level before having any significant damage to the specimen.
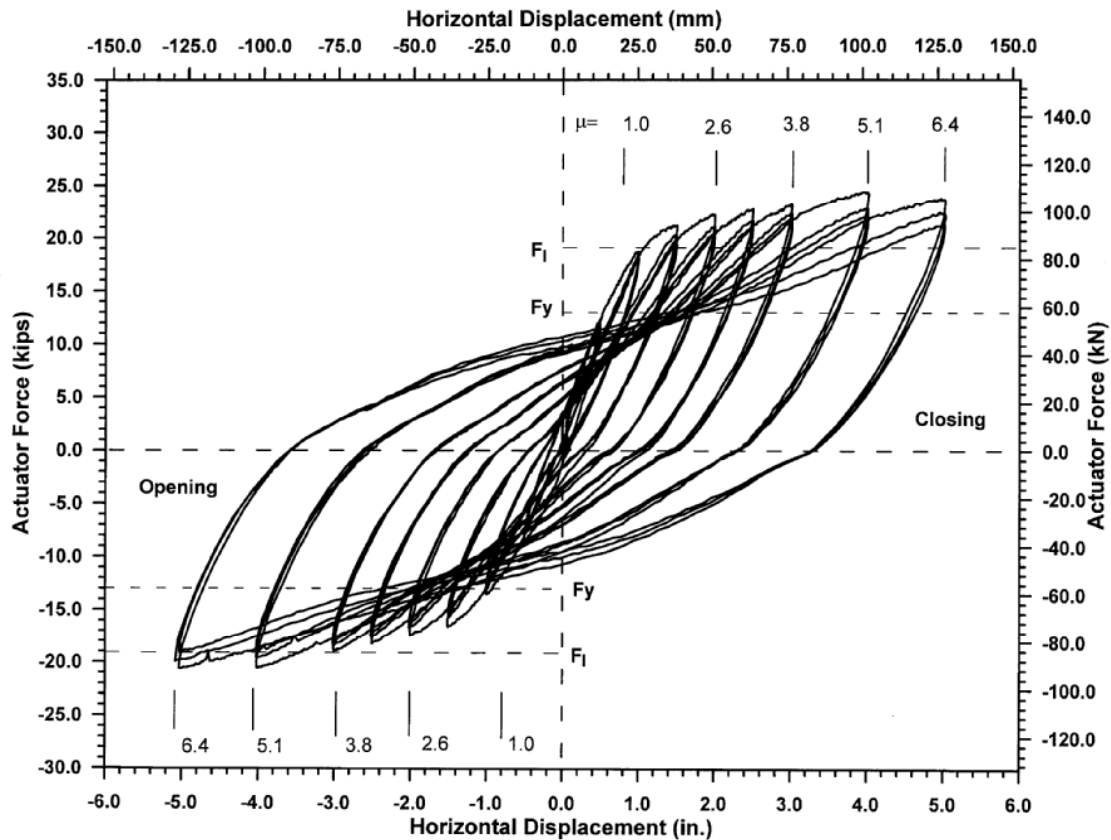
Figure 4.35 Actuator Force-Horizontal Displacement History for Specimen RSPLI

Figure 4.36 shows the measured and the predicted column moment curvature responses for Specimen RSPLI. The measured moment curvature was determined in a

way analogous to that for the previous specimens. Practically, there is no experimental data on the confined concrete strength and the crushing strain for reinforced concrete columns retrofitted using D-shaped sections. Therefore, values were proposed as an input to describe the stress strain curve for confined concrete in the software XTRACT to enable analyses for this study based on taking the average of both the confined concrete strength and the crushing strain for an unconfined concrete section and a section confined with a circular jacket matching the thickness and the diameter of the D-shaped jacket. The predicted moment curvature was averaged again for two cases: first when the flat plate on the backside face of the split column is assumed to completely contribute to the flexural strength, and the other case when it has no contribution.
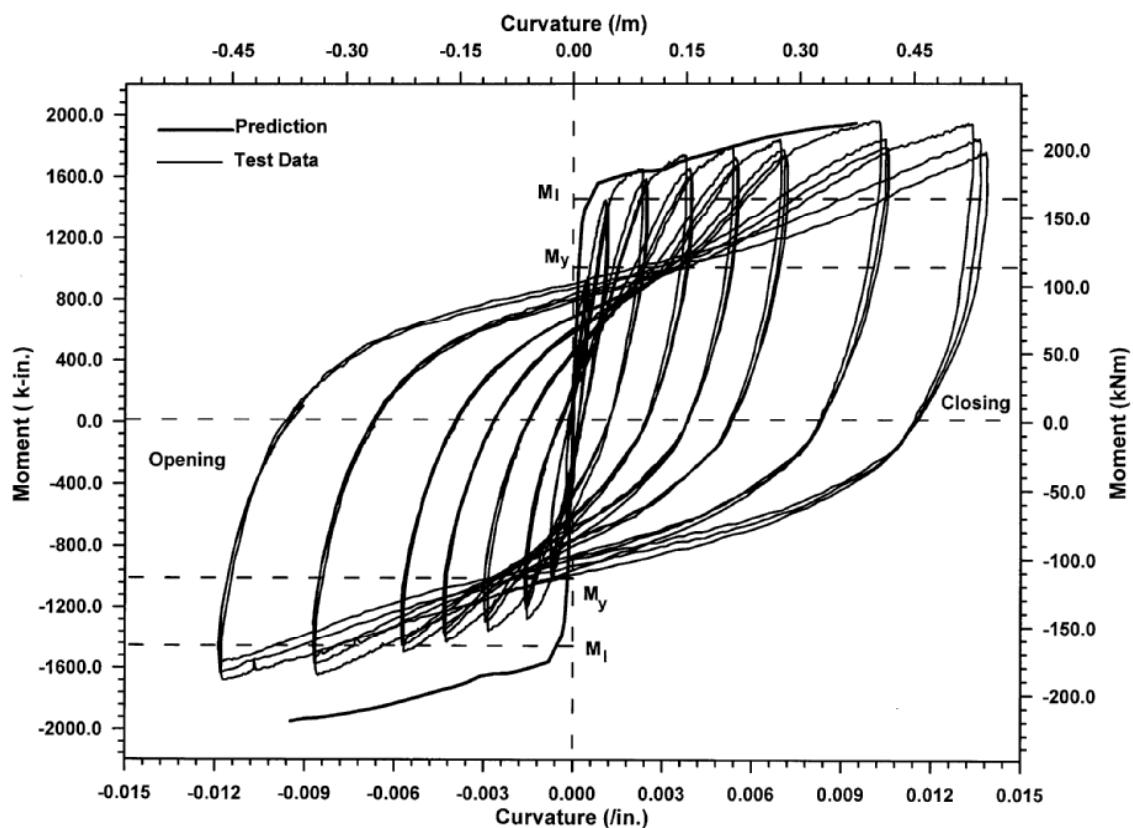
Figure 4.36 Column Moment-Curvature Response for Specimen RSPLI

161

Figure 4.36 shows that Specimen RSPLI achieved its ideal capacity in both directions. An interesting observation is that the measured response in the closing direction compared well to the predicted moment curvature envelope even with the number of approximations made. Higher ultimate curvatures in both directions were measured than were predicted, likely due to slipping of the existing column jacket from the joint jacket.

4.4.3 Retrofitted Specimen Under Out-of-Plane Loading

Specimen RSO was a retrofitted knee joint specimen modeling bent #20 in the Spokane Street Overcrossing. The specimen was retrofitted in the same fashion as Specimen RSI, but was tested under out-of-plane loading. A 55-kip (244.7-kN) vertical load was applied prior to the application of a horizontal loading pattern perpendicular to the plane of the specimen. The circular steel jacket was expected to contribute significantly to the torsional strength and stiffness of the concrete outrigger beam, which in turn would improve the overall behavior of the specimen.

Following cycles to ±0.5 in. (±13 mm) displacement level, there was unanticipated cracking at one of the anchor block corners due to high in-plane torsional demand on the anchor block. The test was stopped, and a new bracing system was provided to support the anchor block and decrease the demand on the anchor bolts. Testing was subsequently resumed.

Testing was stopped following cycles to 3.0 in. (76 mm) displacement level to avoid any damage to the actuator and the axial load ram. This is ½-in. (13-mm) higher than the maximum displacement level in the comparable unretrofitted Specimen ASO.

Observations were made of two critical sections of Specimen RSO during the out-of-plane testing: the new ¾-in. (19-mm) column gap, and the region where the outrigger beam connects to the anchor block. Testing showed no cracking in these sections. The column in the specimen behaved as a cantilever with a fixed support at the knee joint. Consequently, the specimen was expected to experience some cracking in the column gap region if testing were taken to higher responses. Maximum absolute actuator forces of 25.2 kips (112.1 kN) and –28.9 kips (-128.6 kN) were recorded at the end of the test in the pull and push directions, respectively. Figure 4.35 shows Specimen RSO at the end of the test.

The maximum circumferential strains in the joint jacket of Specimen RSO were well below yielding, about 12% of the yield strain.

The actuator force-horizontal displacement history is shown in Figure 4.38. Included in the figure are the actuator forces required to produce the calculated yield moment, F_Y, and ideal moment, F_I, based on column hinging in both directions. It is apparent from the figure that the calculated ideal strength was not reached in either direction due to the test being stopped early, at the 3.0 in. (76 mm) displacement level. In addition, yield strength was not achieved in the pull direction, while barely achieved in the push direction. Experimental yield displacement was not determined for the specimen, and therefore ductilities are not reported.

The hysteresis loops of Specimen RSO show a small increase between subsequent displacement levels. The discontinuity of the hysteresis loops between the ½-in. (13-mm) loops and the subsequent loops was due to the footing damage, addition of bracing, and retesting of the specimen, as discussed earlier. Peak lateral force in the push

direction was about 13% higher than in the pull direction. This difference could be due to a small error in location or alignment of the horizontal actuator or the axial load ram. The specimen was able to achieve a 3.0-in. (76-mm) displacement level at a drift ratio 3.75% without any signs of strength degradation. These values represent a lower estimation of drift and strength capacities as testing was stopped early, without witnessing any damage to the specimen.

Figure 4.37 Specimen RSO at the End of Testing
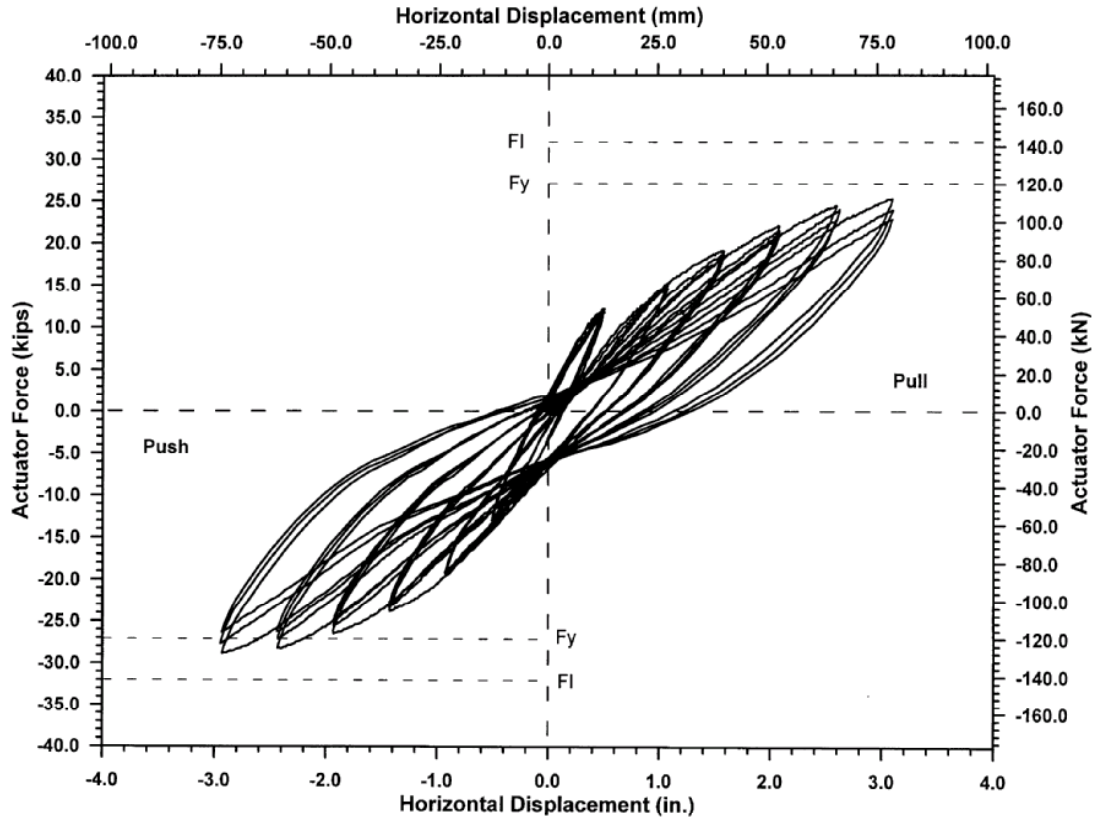
Figure 4.38 Actuator Force-Horizontal Displacement History for Specimen RSO

The measured and the computed column moment curvature responses are shown in Figure 4.39. The measured moment curvature plots the average curvature versus the maximum moment within the column cell. From Figure 4.39, it can be seen that elastic response was evident in the column section during most of the testing phase, and the column had just reached first yield strength at the end of the test. This behavior is also evident from the force-displacement response. Another observation from Figure 4.39 is that the specimen still had the ability to sustain higher load and displacement levels.
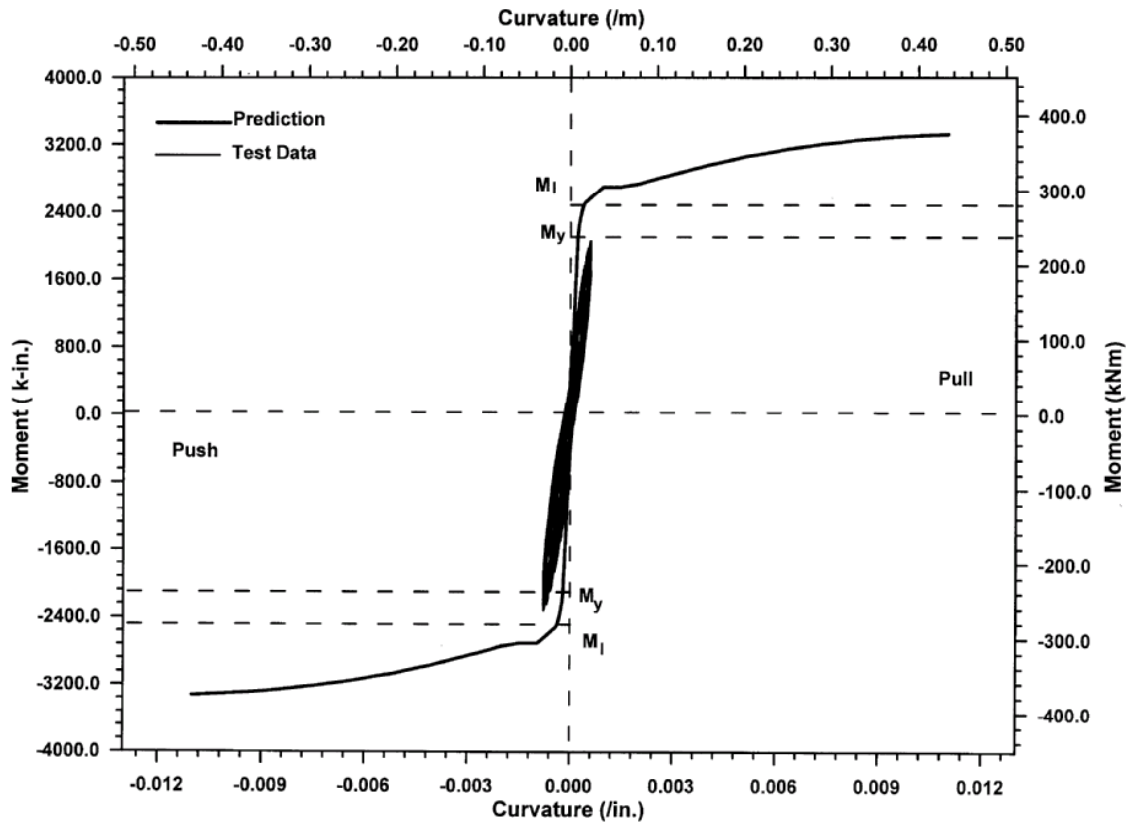
Figure 4.39 Column Moment-Curvature Response for Specimen RSO

4.4.4 Conclusions on Retrofitted Specimen Performance

In the second phase, four retrofitted specimens were investigated: in-plane retrofitted long outrigger, in-plane retrofitted short outrigger, short outrigger, in-plane retrofitted split long outrigger, and out-of-plane retrofitted.

In-plane Loading

The tests on the retrofitted specimens under in-plane loading showed that the proposed retrofit measures successfully achieved the retrofit design goals.   The specimens formed a plastic hinge in the column gap as intended, and they were able to

attain the theoretical yield and ideal strengths of the column hinge section in both directions. In addition, the retrofit measures substantially improved the ductility and the energy dissipation capacities of the upgraded specimens when compared to the behavior of the similar as-built specimens. Ductility levels of 6.3, 4.6, and 6.4 were attained for the retrofitted long outrigger, retrofitted short outrigger, and retrofitted long split outrigger, respectively. These ductility values correspond to the maximum testing displacement level. Higher ductility values would be anticipated if the specimens were tested to higher displacement levels.

In summary, the retrofitted specimens will behave in a ductile manner under in-plane loading, with a ductility level higher than 5.

Out-of-plane Loading

In the out-of-plane direction, the retrofitted short specimen was able to attain the theoretical yield strength of the column hinge section in the push direction. From the test results, it is believed that the retrofitted short specimen would be able to achieve the theoretical yield and ideal strengths in both directions if the test was taken to higher displacement levels. The specimen showed no signs of failure up to the maximum testing displacement level, 3.0 in. (76 mm), with stable force-displacement and energy dissipation behavior in both directions. This improved response of the specimen is due to the composite behavior of the existing outrigger elements and the steel jacket.

Therefore, it can be said that the retrofit measure has satisfied the retrofit design goals in the out-of-plane direction, forcing the hinge to be formed in the column section and increasing the torsional strength of the outrigger beam.

4.5 COMPARATIVE OVERVIEW OF THE TEST RESULTS

A series of seven tests of three as-built and four retrofitted specimens were carried out. In the first phase, two as-built specimens were tested under in-plane loading while the other one was examined under out-of-plane loading. A duplicate of each of the as-built specimens was then retrofitted and tested. The retrofit strategy incorporated the use of circular steel jackets around the beam and the joint. The jacket formed an inverted L-shape casing the beam and the joint. The last specimen represented a retrofit model of a split outrigger bent upgraded using the same retrofit strategy, but with a D-shaped cross section. Benefits of the retrofit measure can be quantified based upon the differences in the behavior between as-built and upgraded specimens. This can be done by comparing the following measures: failure mechanisms, force-displacement response envelopes, ductility, drift, capacity, system stiffness, and specimen energy dissipation.

The measured envelopes of the lateral force-displacement response for as-built specimens are compared with those of the corresponding retrofitted specimens. Force envelopes for the long outrigger and short outrigger specimens under in-plane loading are shown in Figures 4.40 and 4.41, respectively. The following points can be drawn from these figures:

a) The as-built long and as-built short specimens behaved in a brittle way as a result of a bond splitting failure of the column bars within the joint. This behavior is clear from the abrupt drop in the capacity, particularly in the closing direction, shortly after the onset of yielding. The retrofitted specimens exhibited a ductile behavior through a failure mechanism controlled by hinging in the column. From the force-displacement

envelopes, the retrofitted specimens have a long segment of a post-yielding plateau evident of ductile behavior.

b) It can be seen from the figures that a considerable improvement in performance was achieved using the retrofit procedures. For the long and the short specimens, the retrofitted specimens maintained their capacity up to the end of the test with no signs of strength degradation, and they had a maximum strength approximately 50% greater than that of the as-built specimens in the closing direction. In the joint opening direction, the retrofitted specimens developed strengths of approximately twice that of the as-built specimens. This big difference in the opening direction was due to the difference in the member controlling the flexural behavior: the beam in the as-built specimens and the column in the retrofitted specimens.

c) The force-displacement envelopes showed some difference in the elastic stiffness between the as-built and the retrofitted specimens. The difference is related to two factors: the shift in the plastic hinge location and the higher effective sectional properties due to composite action and confinement. This increase in the retrofitted system elastic stiffness over that of the as-built can be argued to have minor influence on the seismic behavior of the structure. Under moderate to strong ground motion earthquakes, the behavior of the bridge is no longer a function of the elastic properties. Of greater importance are the inelastic properties, which are substantially improved by the retrofit measures.
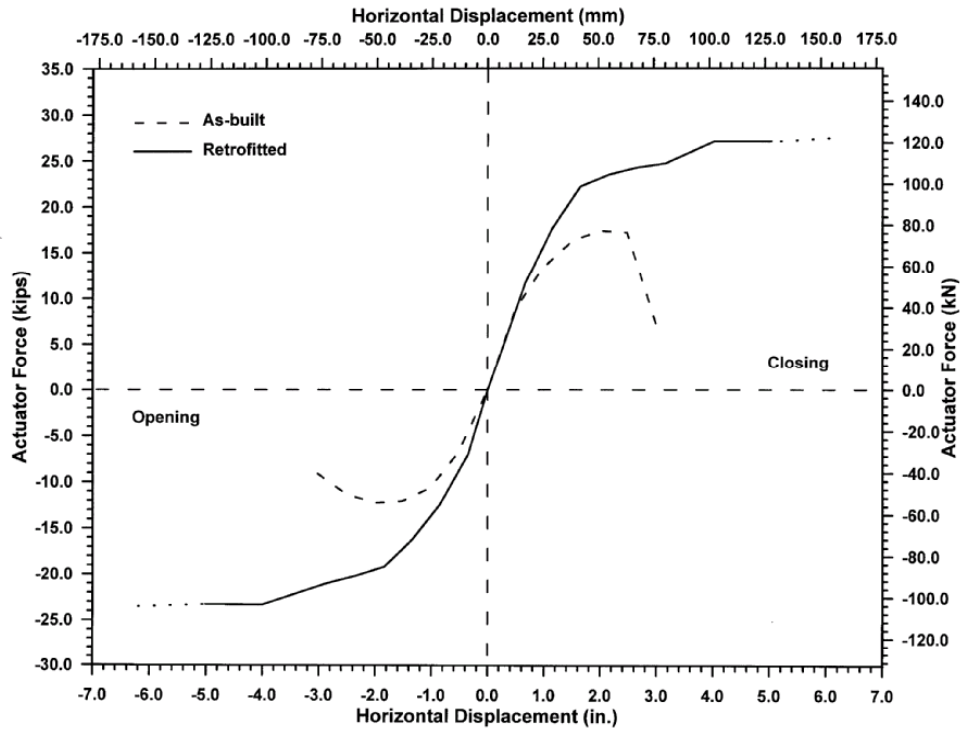
Figure 4.40 Force-Displacement Envelopes For Long Outrigger Specimens Under In-Plane Loading
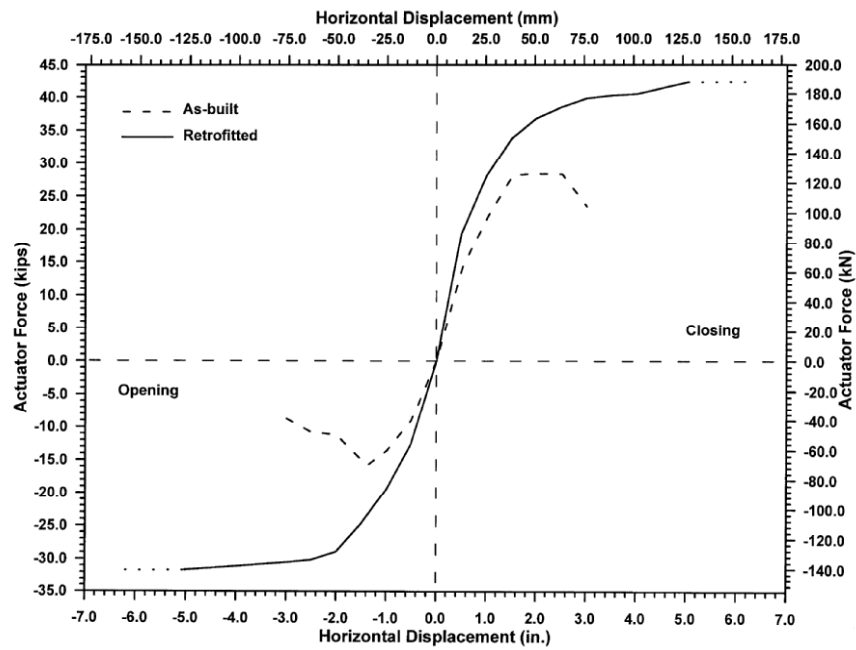
Figure 4.41 Force-Displacement Envelopes For Short Outrigger Specimens Under In-Plane Loading

In recent years, there has been a strong shift in seismic design and retrofit philosophy towards performance-based seismic design. Under such a design philosophy, the primary objective is to design or retrofit structures such that they have a predictable level of damage when subjected to a range of ground motion intensities. Damage to bridge structures may be most directly related to displacements and displacement-related quantities (e.g., ductility and drift ratio). As an example of the benefit of the retrofitting measures, Table 4.2 shows the specimens' displacement ductility and drift ratio in both directions. The displacement ductility and drift ratio of the upgraded specimens are more than twice the ductility of the as-built specimens in the closing direction. Greater improvement would be anticipated if the tests had been conducted to higher displacement levels. For the opening direction, a direct comparison cannot be made due to differences in the failure mechanism. However, the retrofitted specimens achieved higher displacement ductility and drift ratio than the as-built specimens.

Table 4.2 Specimen Ductility and Drift Ratio

Specimen	Closing		Opening	
	Displ. Ductility	Drift (%)	Displ. Ductility	Drift (%)
As-built long outrigger	2.8	3.75	3.8	3.75
Retrofitted long outrigger	6.3[1]	6.7[1]	6.3[1]	6.7[1]
As-built short outrigger	2.0	3.75	3.3	3.75
Retrofitted short outrigger	4.6[1]	6.7[1]	4.6[1]	6.7[1]

[1] These values correspond to the largest test displacement, not to the capacity of the specimens.

Figure 4.42 shows the force-displacement envelopes for the short outrigger specimens under out-of-plane loading. The as-built specimen experienced diagonal

torsion cracking in the outrigger beam and the knee joint during early stages of the test with an ultimate brittle behavior induced by splitting bond failure within the joint region. In reference to the force-displacement envelopes, it is evident that the retrofit measures added significantly to the system capacity and stiffness. In particular, the jacket of the specimen significantly increased the torsion capacity of the beam. The retrofitted specimen reached twice the capacity of the as-built specimen without any sign of strength deterioration. Greater displacement and strength capacities would have been achieved if the retrofitted specimen had been tested at higher response.
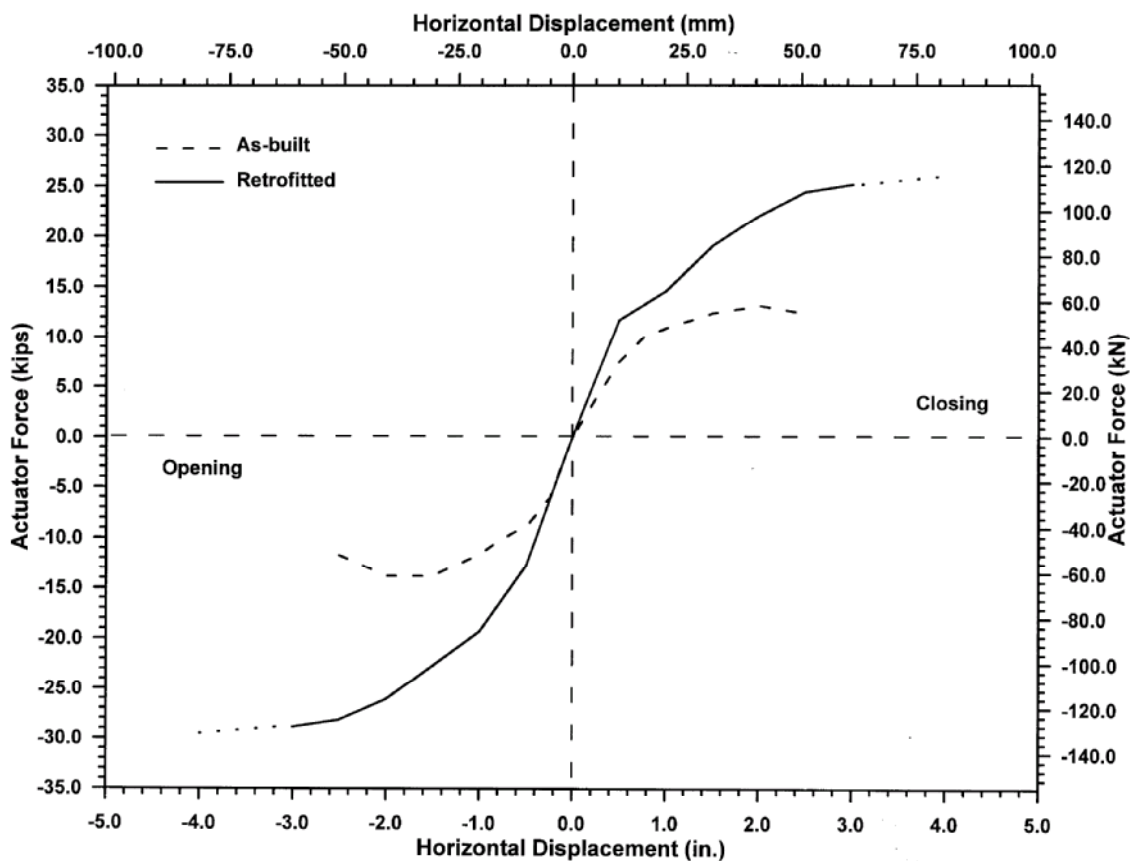
Figure 4.42 Force-Displacement Envelopes For Short Outrigger Specimens Under Out-of-Plane Loading

For a given ground motion, a split outrigger bent in a real bridge will experience approximately the same displacement and half of the seismic force demand on the neighboring bent in the in-plane direction. The split outrigger specimen was able to achieve a ductility of 6.4 and a drift ratio of 6.7% at a 5.0-in. (127-mm) displacement level, which is quite similar to the retrofitted long outrigger specimen.

Apart from enhancing the strength, ductility, and drift ratio, the retrofit measures helped to achieved significant levels of energy dissipation. The areas contained within the hysteresis curves of the retrofitted specimens were higher by several times than those of the as-built specimens.

CHAPTER FIVE

SEISMIC ASSESSMENT OF EXISTING BRIDGE KNEE JOINTS

5.1 INTRODUCTION

Design and detailing guidelines for new reinforced T-joints and reinforced knee joints are available in the ACI 318-02 (2002) code provisions and AASHTO specifications (2004). The 2004 Caltrans Seismic Design Criteria (SDC), released in February 2004 as an update to the 2001 Caltrans SDC, provides a basis for design and detailing of reinforced T-joints, but still considers knee joints as nonstandard elements where design criteria need to be developed on a project-specific basis. Strength and deformation of existing knee joints are discussed in the 1997 National Earthquake Hazard Rehabilitation Program (NEHRP) Guidelines for the Seismic Rehabilitation of Buildings (FEMA-273) for joints subject to in-plane and out-of-plane seismic forces and by Priestley et al. (1996) for joints subject to in-plane seismic forces.

For a given limit state, assessment of existing knee joints can be carried out by comparing the demand actions on the joint with the design requirements presented in FEMA-273 document (1997) and with Priestley's recommendations. In this chapter, an assessment approach based upon the observed behavior and results from the knee joint tests of this study is proposed and compared to the procedures presented in the aforementioned references. A brief summary of the performance of the as-built knee joint systems, particularly the observed failure mechanisms, is presented first followed by a discussion on knee joint assessment limit states and knee joint shear forces and stresses.

5.2 RESULTS FROM TESTS OF EXISTING KNEE JOINTS

Failure mechanisms as well as the force and deformation capacities of existing outrigger knee joints were obtained in this study from tests on one-third scale models of bridge knee joints having similar features to those existing in the Spokane Street Overcrossing. This investigation included three as-built specimens: one with a long and one with a short outrigger beam, both tested under in-plane loading, and the third having a short outrigger beam tested under out-of-plane loading. The main deficiencies of such joint systems are the lack of confinement for both the joint concrete and the main reinforcement of the members meeting within the joint and the poor torsional strength of the outrigger beam.

For existing bridge knee joints under in-plane loading, the tests showed that diagonal shear cracking was initially the main distress in the knee joint under opening and closing of the joint. Eventually, however, complete failure of the joint occurred due to splitting bond failure within the joint region of column and beam reinforcement. The out-of-plane loading on the short outrigger specimen caused diagonal cracking in the knee joint and the outrigger beam at early stages. Upon further loading, the resistance of the knee joint system deteriorated as a result of the significant torsional cracking in the bottom face of the beam with open transverse reinforcement and due to splitting bond failure within the joint region of beam reinforcement.

5.3 JOINT ASSESSMENT LIMIT STATES

Limit states are conditions beyond which a structure or a structural element no longer satisfies the design performance requirements. Priestley and Seible (1991)

characterized three limit states for the seismic design of new bridges and the assessment of existing bridges: the serviceability limit state, the damage control limit state and the survival limit state.

For response to the serviceability limit state, the bridge is required to be serviceable immediately after an earthquake. Damage to non-structural elements may be anticipated, structural elements may reach their flexural strength, limited ductility might be developed, and small cracks that are unlikely to affect durability or the function of the structure may be expected. Thus, existing knee joints based on the requirements of the serviceability limit state should essentially remain fully elastic (Ingham, 1995).

The damage control limit state represents a condition after which the lateral resistance of the bridge diminishes when subject to increasing displacement demand. It is probably the most important limit in terms of seismic assessment since a structure's repairability afterward would be technically infeasible and uneconomical (Priestley et al., 1996). To ensure a reliable performance of the bridge at this limit state, the core concrete in any plastic hinges that develop in the cap beam and/or the column should not need any repair. Consequently, this requires the joints to have strength higher than the maximum strength of the members framing into it (Park and Paulay, 1984). Additionally, the joint contribution to the overall structural deformation in this state should be of a comparable magnitude to the joint contribution to the overall bridge deformation in the elastic range (Ingham, 1995). For existing knee joints, this stipulation demands the joint to remain basically undamaged (Ingham, 1995).

The survival limit state is a condition where the structure is on the verge of experiencing partial or total collapse. The primary concern here is to protect loss of life

through reserving some capacity in the system to withstand the gravity load demands during the strongest ground shaking. Based on this philosophy, existing knee joints should have at least some remaining strength capacity to support the bridge gravity load (Ingham, 1995).

5.4 KNEE JOINT FORCES

Knee joint shear force can be calculated by equilibrium considerations of the flexural stress resultants acting at the joint boundary of the member governing the structure flexural response. For in-plane response, the distribution of forces and stress resultants acting on both joint boundaries under closing of the joint is different than that under opening of the joint (Priestley et al., 1996). Therefore, different equilibrium conditions are considered when calculating the joint shear for each direction.

Figures 5.1a and 5.1b show the forces acting on a knee joint due to closing and opening moments, respectively. In both figures, the following notation is used:

M_b is the outrigger beam moment,

M_c is the column moment,

V_b is the outrigger beam shear force,

V_c is the column shear force,

P_b is the outrigger beam axial force,

P_c is the column axial force,

F is the outrigger beam prestress force (if present),

T_b is the outrigger beam flexural tension stress resultant,

T_c is the column flexural tension stress resultant,

C_b is the outrigger beam flexural compression stress resultant,

C_c is the column flexural tension stress resultant,

a_b is the outrigger beam flexural compression stress block depth,

a_c is the column flexural compression stress block depth,

l_a is the column longitudinal reinforcement embedment length,

h_b is the outrigger beam depth, h_c is the column depth,

d is the effective outrigger beam depth,

V_{jv} is the vertical joint shear force, and

V_{jh} is the horizontal joint shear force.

(a) Closing moment   (b) Opening moment
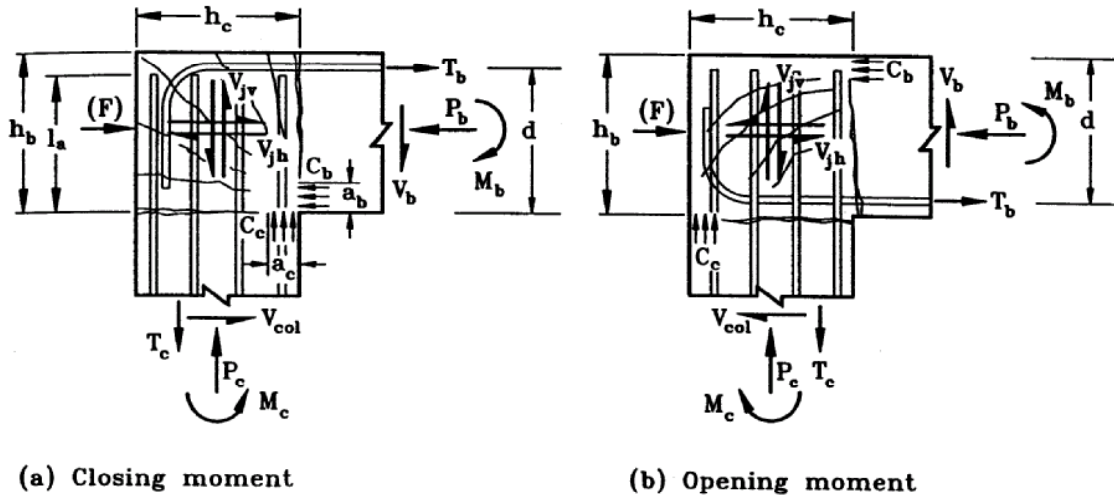
Figure 5.1 Forces Acting on a Knee Joint (Adapted from Priestley et al., 1996)

From Figure 5.1a, the following equilibrium equations can be determined in the closing direction (Priestley et al., 1996).

Beam moment:
$$M_b = T_b(d - \frac{a_b}{2}) + P_b(\frac{h_b}{2} - \frac{a_b}{2}) \tag{5.1}$$

Beam axial force:
$$P_b = F + V_c \tag{5.2}$$

Beam compression force:
$$C_b = T_b + P_b \tag{5.3}$$

Column moment:
$$M_c = M_b + V_b \frac{h_c}{2} - V_c \frac{h_b}{2} \tag{5.4}$$

Column flexural compressive force:
$$C_c = T_c + P_c \tag{5.5}$$

Maximum horizontal joint shear force:
$$V_{jh} = T_b + 0.5F \tag{5.6}$$

Maximum vertical joint shear force:
$$V_{jv} = C_c - P_c \tag{5.7}$$

The equilibrium equations in the opening direction based on Figure 5.1b are:

Beam moment:
$$M_b = T_b(d - \frac{a_b}{2}) + P_b(\frac{h_b}{2} - \frac{a_b}{2}) \tag{5.8}$$

Beam axial force:
$$P_b = F - V_c \tag{5.9}$$

Beam compression force:
$$C_b = T_b + P_b \tag{5.10}$$

Column moment:
$$M_c = M_b + V_b \frac{h_c}{2} - V_c \frac{h_b}{2} \tag{5.11}$$

Column flexural compressive force:
$$C_c = T_c + P_c \tag{5.12}$$

Maximum horizontal joint shear force:
$$V_{jh} = T_b + P_b \tag{5.13}$$

Maximum vertical joint shear force:
$$V_{jv} = T_c + P_c \tag{5.14}$$

When a plastic hinge develops at the column joint interface, the joint horizontal shear force, V_{jh}, can be found, approximately, by assuming that the column overstrength moment, M^o, uniformly diminishes over the full depth of the outrigger beam, as shown in Figure 5.2 (Priestley et al., 1996). Thus:

$$V_{jh} = \frac{M^{\circ}}{h_b} \qquad\qquad (5.15)$$
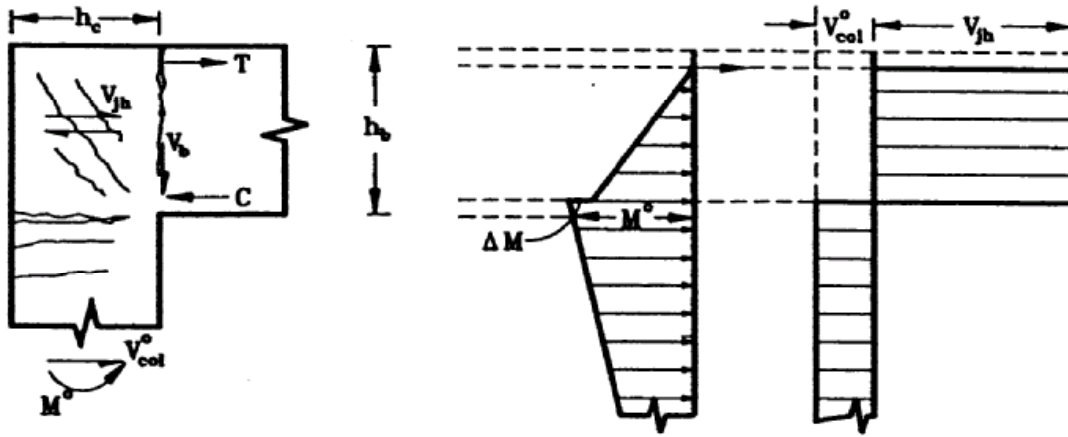
Figure 5.2 Moment and Horizontal Shear Force Distribution in a Knee Joint at Column Overstrength Condition (Adapted from Priestley et al., 1996)

5.5 STRENGTH-BASED ASSESSMENT

5.5.1 Existing Knee Joints

Traditionally, code provisions and design guidelines adopt a nominal joint shear stress level as a parameter for the design of beam-column joints of building frames and bridges. Among those are the current ACI 318-02 code provisions (2002), the FEMA-273 document (1997), and the AASHTO specifications (2004). Other guidelines such as Caltrans SDC (2004) and Priestley's recommendations (Priestley et al., 1996) consider joint principal tension and compression stresses as criteria for joint design. The logic behind using principal stresses rather than nominal shear stresses is that the joint is unlikely to experience shear distress if the average principal tension stress is less than the tensile strength of the joint concrete (Priestley et al., 1996).

The nominal joint shear stress, v_j, can be calculated by dividing the shear force, V_j, determined based on the ultimate flexural capacity of the member controlling the

flexural behavior in the opening and the closing direction, over the effective horizontal joint area, A_j. Thus:

$$\upsilon_j = \frac{V_j}{A_j} \qquad (5.16)$$

Based on FEMA-273 (1997), A_j is defined by a depth equal to the column dimension in the direction of framing and a width equal to the smallest of the column width, the joint depth plus the beam width or twice the smaller perpendicular distance from the longitudinal axis of the beam to the column side. Priestley et al. (1996) defines the effective joint shear area by a depth equal to the column dimension in the direction of framing and a width taken at the center of the column, allowing 45° spread from boundaries of the column section into the cap beam. This definition of A_j is largely based on engineering judgment (Priestley et al., 1996). For comparison, the effective joint area was computed for the as-built long and short outrigger specimens of this study following the definitions in both references. For the as-built long and short specimens, the joint dimensions, depth by width, are 13.0 in. (330 mm) by 15.0 in. (381 mm) and 15.0 in. (381 mm) by 19.0 in. (483 mm), respectively, calculated as defined in both references. Thus, it can be concluded that the effective joint shear area for knee joints where the beam centerline passes through the column centroid is the same based on both FEMA-273 and Priestley's recommendations.

Based on FEMA-273 (1997), the performance of an existing knee joint can be evaluated by comparing the shear stress demand on to the shear stress capacity of the joint, v_n, as described below.

$$\upsilon_n = \gamma\sqrt{f_c^{'}(psi)} = \frac{\gamma}{12}\sqrt{f_c^{'}(MPa)} \qquad (5.17)$$

where γ is a coefficient for joint shear strength based on the volumetric ratio of horizontal confinement in the joint, ρ", as shown in the following table.

Table 5.1 Values of γ for Knee Joint Strength Calculation (Adapted from FEMA-273, 1997)

ρ"	γ
< 0.003	4
≥ 0.003	8

Following Priestley's recommendations, joint principal tension stress is the parameter used to evaluate the performance of an existing knee joint. The joint normal axial and vertical stresses need to be determined in addition to joint shear stress. Using the beam axial force, P_b, the normal horizontal stress, ρ_x, based on Priestley et al. (1996), can be determined by:

$$\rho_x = \frac{P_b}{A_b}$$

(5.18)

where A_b is the outrigger beam gross sectional area. Joint vertical axial stress, ρ_y, is according to the following equation:

$$\rho_y = \frac{P_c}{b_{je}(h_c + 0.5h_b)}$$

(5.19)

where b_{je} is an effective width taken at the center of the column, allowing 45° spread from boundaries of the column section into the cap beam. This is identical to the effective width defined for joint shear area. The joint depth, ($h_c + h_b/2$), used for vertical stress calculations is based upon dispersion of the column axial force into the outrigger

beam at 45° (Priestley et al., 1996). Once the joint shear stress and horizontal and

vertical normal stresses are known, the maximum joint principal tension, ρ_t, and

compression, ρ_c, stresses can be calculated based upon the assumption of a uniform stress

distribution using a Mohr's circle analysis:

$$\rho_c, \rho_t = \left(\frac{\rho_x + \rho_y}{2}\right) \pm \sqrt{\left(\left(\frac{\rho_x + \rho_y}{2}\right)^2 + v_j^2\right)}$$
(5.20)

Using Priestley's recommendations, the performance of the knee joint is then

assessed by comparing the principal tension demand on the joint to the principal tension

stress ranges given in Table 5.2.

Table 5.2 Existing Knee Joint Assessment Based on Priestley et al. (1996)

Principal Tension Stress	Condition
$3.5\sqrt{f_c^{'}(psi)} \leq p_t \leq 5.0\sqrt{f_c^{'}(psi)}$ $0.29\sqrt{f_c^{'}(MPa)} \leq p_t \leq 0.42\sqrt{f_c^{'}(MPa)}$	Joint shear cracking
$p_t \geq 5.0\sqrt{f_c^{'}(psi)}$ $p_t \geq 0.42\sqrt{f_c^{'}(MPa)}$	Joint failure

The stress values presented in the Table 5.2 are based on work done by Ingham,

Priestley and Seible (1994a) on existing knee joint systems with rectangular columns

where a maximum joint principal tension stress of approximately $5.8\sqrt{f_c^{'}}$ psi ($0.48\sqrt{f_c^{'}}$

MPa) was achieved before joint failure. This corresponds to a nominal shear stress of

about $8.0\sqrt{f_c^{'}}$ psi ($0.66\sqrt{f_c^{'}}$ MPa). Later on, Ingham (1995) proposed a slightly different

limiting joint principal tension stress of $6.0\sqrt{f_c'}$ psi $(0.50\sqrt{f_c'}$ MPa), beyond which joint failure occurs.

Results from this study on the tests of the as-built specimens under in-plane loading provided the opportunity to review the values proposed by Priestley et al. (1996) and update them if appropriate. The values presented by Priestley et al. (1996) were based upon a single test on an as-built specimen with nominally unreinforced knee joint under in-plane loading.

Table 5.3 summarizes the joint principal tension stresses and the related joint condition obtained from testing on the as-built long and short outrigger specimens under in-plane loading. Principal tension stresses correspond to the minimum anticipated in the closing and the opening directions.

Table 5.3 Joint Principal Tension Stresses for the As-Built Long and Short Specimens

Specimen	Principal Tension Stress	Condition
As-built long	$5.5\sqrt{f_c'}\,psi(0.46\sqrt{f_c'}\,MPa)$	Joint shear cracking
	$6.2\sqrt{f_c'}\,psi(0.52\sqrt{f_c'}\,MPa)$	Joint failure
As-built short	$4.9\sqrt{f_c'}\,psi(0.41\sqrt{f_c'}\,MPa)$	Joint shear cracking
	$7.8\sqrt{f_c'}\,psi(0.65\sqrt{f_c'}\,MPa)$	Joint failure

Based on the results presented above, the following principal tension stress values are proposed to assess the joint condition, as shown in Table 5.4. To be conservative, principal tension stress values of $4.5\sqrt{f_c'}$ psi $(0.38\sqrt{f_c'}$ MPa) and $6.0\sqrt{f_c'}$ psi $(0.50\sqrt{f_c'}$ MPa)

were set as limits beyond which joint shear cracking and joint failure, respectively, are expected.

Table 5.4 Proposed Principal Tension Stress Values for Knee Joint Assessment

Principal Tension Stress	Condition
$4.5\sqrt{f_c'}\,psi \leq p_t \leq 6.0\sqrt{f_c'}\,psi$ $0.38\sqrt{f_c'}\,MPa \leq p_t \leq 0.50\sqrt{f_c'}\,MPa$	Joint shear cracking
$p_t \geq 6.0\sqrt{f_c'}\,psi$ $p_t \geq 0.50\sqrt{f_c'}\,MPa$	Joint failure

The threshold principal tension stresses proposed for knee joint assessment based upon results from this study, shown in Table 5.4, are higher than those proposed by Priestley, shown in Table 5.2. The difference in the values is believed to be due to the presence of longitudinal side reinforcement in the joint region as beam skin reinforcement extended into the joint. In the knee joint test conducted by Ingham et al. (1994a), which formed the basis for Priestley's recommendations for existing knee joint assessment, the beam side reinforcement was terminated at the beam joint interface. Therefore, it is suggested that knee joints with no side reinforcement be assessed based upon the threshold principal tension stresses proposed by Priestley, as given in Table 5.2. For other cases, in which the beam skin reinforcement is fully developed into the joint region and the longitudinal reinforcement ratio is close to those present in the tested specimens in this study, $\rho=0.45\%$, the principal tension stresses in Table 5.4 may be used.

5.5.2 Existing Outrigger Beams

Testing of the short outrigger beam specimen under out-of-plane loading highlighted the vulnerability of the outrigger beam when subject to combination of bending, torsion and shear stresses. The initial cracking pattern on the outrigger beam's surfaces in the joint vicinity, which developed at nearly at a 45-degree angle, indicates that formation of these cracks happened primarily due to shear and torsion stresses. In this section, a principal tension stress is suggested as a limit to the onset of cracking in the beam. In addition, an ultimate torsional strength value is proposed as a multiple of the torsional cracking strength for short outrigger beams.

The following discussion outlines the procedures that were followed to come up with the principal tension stress limit value. According to the ACI 318-02 code provisions (2002), the torsional shear stress of a plain concrete member can be estimated based on the thin-walled tube, space truss analogy. Using this analogy, members with solid prismatic sections are idealized as thin-walled tube sections with a finite wall thickness, t, within which the torque is resisted by the shear flow, q, as shown in Figure 5.3. The shear flow, q, is treated as a constant at all points around the periphery of the member. The relationship between the external applied torque, T, and the shear flow can be obtained by summing the moment contributions of the shear flow in each wall about the axial center of the wall. Thus,

$$T = 2qA_o \qquad (5.21)$$

where A_o is the area enclosed by the shear flow path. The corresponding shear stress, τ_t, for a tube wall thickness, t, assuming a constant shear stress distribution over the wall is:

$$\tau_t = \frac{q}{t} = \frac{T}{2A_o t} \qquad (5.22)$$

186
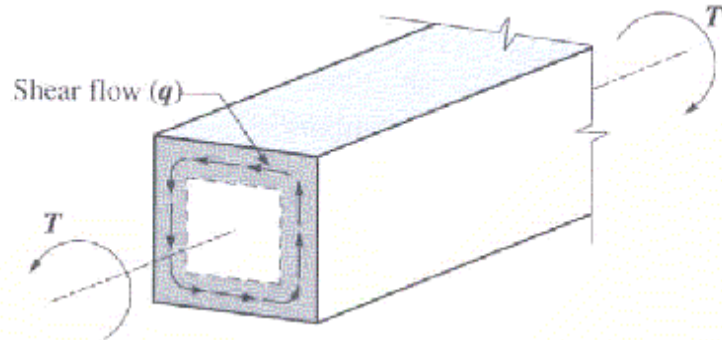
Figure 5.3 Thin-Walled Tube Idealization of a Rectangular Solid Section (Adapted from ACI 318-02, 2002)

Based on ACI 318-02 code provisions (2002), a reasonable estimate of the quantity, $2A_o t$, can be taken as the ratio of the square of the gross concrete area section, A_{cp}, to the perimeter of the full concrete section, p_{cp}. Considering this value, equation 5.22 becomes:

$$\tau_t = T \frac{p_{cp}}{A_{cp}^2} \tag{5.23}$$

For members subject to shear forces only, the nominal shear stress, τ_v, due to a shear force, V, can be obtained by:

$$\tau_v = \frac{V}{b_w d} \tag{5.24}$$

where b_w is the width of the section and d is the distance from the extreme compression fiber to centroid of the longitudinal tension reinforcement.

The maximum shear stress for a solid member subject to shear and torsion forces can be computed as the square root of the sum of the squares of the nominal shear stresses due to torsion, τ_t, and shear, τ_v (Nilson et al., 2003).

$$\tau = \sqrt{\tau_v^2 + \tau_t^2} \tag{5.25}$$

187

Based on the previous discussion, Table 5.5 shows the principal tension stress at which cracking in the outrigger beam was experimentally observed.

Table 5.5 Proposed Principal Tension Stress Values for Outrigger Beam Assessment

Principal Tension Stress	Condition
$p_t = 6.0\sqrt{f_c'}\ psi$ $p_t = 0.50\sqrt{f_c'}\ MPa$	Outrigger beam cracking

As was presented previously in Chapter Four, the existing outrigger beam in this study was able to attain an ultimate torsional strength capacity that was 68%, higher, on average, than the cracking torsion strength in both directions, T_{cr}, before the longitudinal resistance of the knee joint system started to diminish. T_{cr} was computed based on the work of Hsu (1990) using equation 4.2. Consequently, a value of 1.5 T_{cr} is proposed as a conservative estimate of the ultimate torsional strength, T_n, of an existing outrigger beam.

$$T_n = 1.5\ T_{cr} = 1.5 \left[T_{cr} = 6(x^2 + 10)y\sqrt[3]{f_c'}[1.00 + 4(\rho_L + \rho_h)] \right] \qquad (5.26)$$

where x = smaller dimension of the rectangular section, y = larger dimension of the rectangular section, f_c' = compressive strength of the concrete, and ρ_L, ρ_h = volume ratio of longitudinal and hoop steel, respectively, with respect to the gross sectional area.

5.6 DEFORMATION-BASED ASSESSMENT OF EXISTING KNEE JOINTS

The common practice in seismic analysis of concrete bridges is to use rigid links to model the joints between the connecting elements. This inappropriate representation

of the joint overestimates the stiffness values (Priestley et al., 1996), which in turn leads to inaccurate assessment of the overall displacement demand of the bridge under seismic loading. Analytical bridge models that account for joint deformation characteristics are more reliable for seismic assessment, as the contribution of the joint deformations to the global displacement of the bridge is included.

Based on FEMA-273 (1997), joint shear strain is an acceptable parameter for characterizing the general deformation of existing joints. The shear strain parameter was also used by Priestley (1993) to describe existing knee joints deformation behavior. Figure 5.4 shows the principal tension stress versus joint shear strain proposed by Priestley (1993) for existing knee joints. The shear strain value that corresponds to a principal tension stress before joint cracking occurs, $3.5\sqrt{f_c'}$ psi ($0.29\sqrt{f_c'}$ MPa), is 0.00015. This shear strain is determined by dividing the principal tension stress value by the elastic shear modulus of the concrete, G_C, assuming a Poisson's ratio of 0.2. The shear strain value corresponding to a principal tension stress before joint failure happens, $5.0\sqrt{f_c'}$ psi ($0.42\sqrt{f_c'}$ MPa), is 0.0007. The latter value of the shear strain is computed by dividing the principal tension stress by the cracked shear modulus of the joint concrete, rG_C, where r is the ratio of the relative stiffness of column bars to the elastic shear modulus of the concrete. Thus, r, is determined by the following equation:

$$r = \frac{\rho_l E_s}{G_C}$$
(5.26)

where ρ_l is the column longitudinal reinforcement ratio, and E_s is the modulus of elasticity of the column rebars.
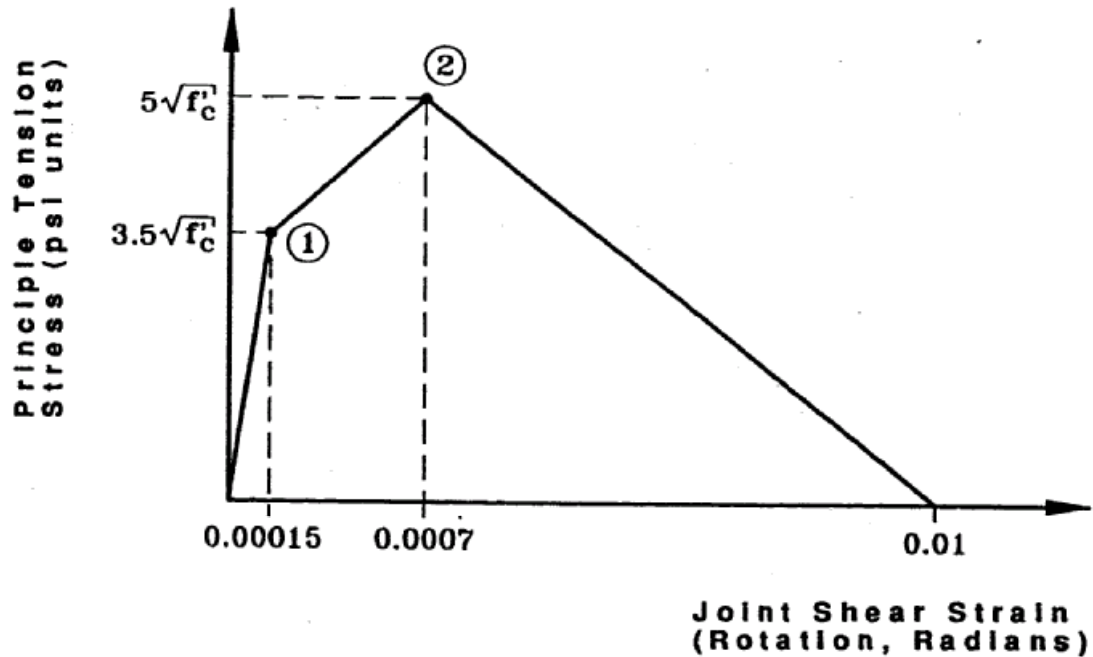
Figure 5.4 Proposed Failure Mechanism for Existing Knee Joints (Adapted from Priestley, 1993)

In this study, new shear strain values are proposed based upon experimental results of the as-built specimens under in-plane loading. The reason for suggesting new shear strain values is that the values proposed by Priestley were found to be reasonably conservative when they were compared to the measured response of an as-built knee joint specimen tested by Ingham, Priestley and Seible (1994a), (Priestley, 1993). The knee joint in the tested unit achieved shear strain values of approximately 0.003 and 0.002 in the closing and the opening directions, respectively, before degradation in the lateral resistance of the specimen, corresponding to limit 2 in Figure 5.4.

Table 5.6 summarizes the measured average shear strain values, γ_j, and the related joint condition obtained from testing the as-built long and short outrigger specimens

190

under in-plane loading in this study. Average shear strains correspond to the minimum value measured in the closing and the opening directions.

Table 5.6 Joint Shear Strain for the As-Built Long and Short Specimens

Specimen	Joint Shear Strain, γ_j. (radians)	Condition
As-built long	0.0014	Joint shear cracking
	0.0059	Joint failure
As-built short	0.0006	Joint shear cracking
	0.0011	Joint failure

Based on the measured strains presented in Table 5.6, the joint shear strains given in Table 5.7 are proposed for assessing existing joints condition.

Table 5.7 Proposed Joint Shear Strain Values for Knee Joint Assessment

Joint Shear Strain, γ_j (radians)	Condition
0.0005	Joint shear cracking
0.001	Joint failure

Note the significant variation in the test values of joint shear strains for the as-built specimens, as shown in Table 5.6. Further research is needed to evaluate this variation.

CHAPTER SIX

RETROFIT RECOMMENDATIONS FOR OUTRIGGER KNEE JOINTS

6.1 INTRODUCTION

This chapter provides retrofit guidelines to improve the seismic performance of outrigger knee joints in existing bridges. First, a review is made of the vulnerabilities and possible failure modes in outrigger knee joints, identifying and characterizing the main factors that influence the different modes of failure. This is followed by a discussion of the steel jacket thickness required to develop a well-controlled ductile hinging mechanism in the columns, the requirements to establish a stable joint force transfer mechanism between the column and the beam reinforcement in the closing and the opening directions, and recommendations to avoid potential failure modes in the joint region and the neighboring elements. Finally, design and detailing guidelines for the retrofit of outrigger knee joints, for both regular and split outrigger bents, are proposed.

6.2 KNEE JOINT FAILURE MODES

Previous experimental research has investigated the failure mechanisms of joints in reinforced concrete building frame structures and in bridges. Tests carried out on joints under in-plane monotonic and seismic loading revealed four possible modes of failure in knee joints: compression failure, anchorage failure, splitting failure, and tension crack failure. Descriptions of each potential mode of failure follow.

(Compression Failure) Crushing Failure

In knee joints under closing moments, failure may occur due to crushing of the concrete struts in the joint, as shown in Figure 6.1, and/or in the concrete at the inner corner of the joint where the compression stress resultants of the beam and the column meet. Such a failure mode is of primary concern in knee joints with large principal compression stresses, which generally develop in prestressed knee joints and knee joints with sufficient shear reinforcement (Sritharan and Ingham, 2003).

Figure 6.1 Crushing Failure Mode in a Knee Joint (Adapted from Sritharan and Ingham, 2003)

Anchorage Failure

The longitudinal beam and column reinforcement entering the joint are required to extend a distance that is sufficient to develop their yield strength at the face of the joint. This anchorage length is usually constrained by the dimensions of the joint core,

which seldom permit development of the steel rebars by straight embedment alone, especially for the beam reinforcement. Therefore, anchorage at the bar's end is usually provided by means of a 90º hook.

In the event that the anchorage length of the bar is insufficient, the tensile stresses in the surrounding concrete will be large enough to cause cracking, thereby resulting in slip of the bars with respect to the adjacent concrete or even pull-out failure of the bars. In the event of anchorage failure, the fixity of the members meeting at the joint will be adversely affected, which in turn will reduce the lateral strength of the structure and cause larger deflections. With this type of failure, visible damage to the joint may be not apparent, as shown in Figure 6.2 (Sritharan and Ingham, 2003).
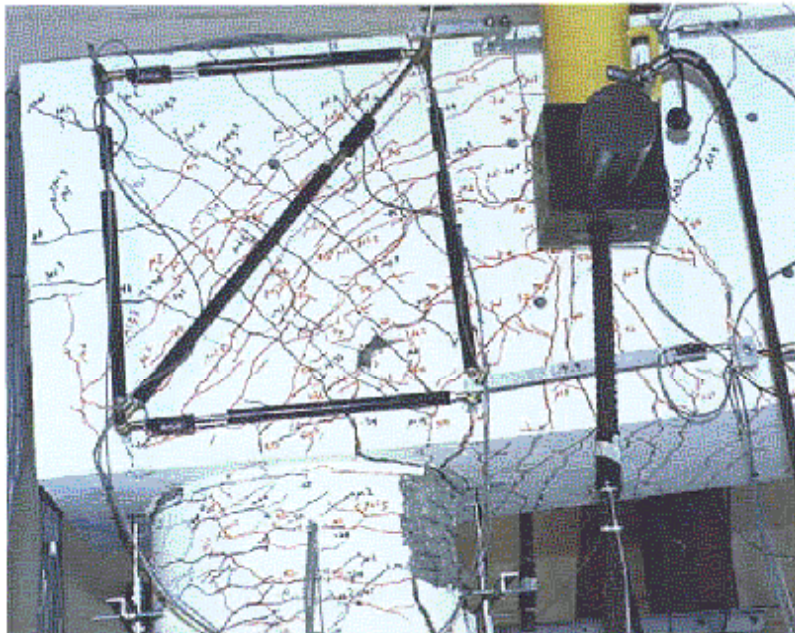
Figure 6.2 Anchorage Failure Mode in a Knee Joint (Adapted from Sritharan and Ingham, 2003)

Splitting Failure

Splitting failure is of primary concern in knee joints under both closing and opening of the joint. Under closing action, the tension force in the beam bars can be transferred by bond to the column bars only if the lap splice is contained with adequate confinement reinforcement, as shown in Figure 6.3. Otherwise, lateral concrete tension stresses will develop below the hook causing splitting of the concrete. The hooks tend to straighten, and joint failure occurs. In the opening direction, the risk of splitting failure arises if the joint has light transverse reinforcement and the beam bottom bars are anchored by straight bar extensions into the joint. With such detailing, there is nothing to resist the horizontal and vertical components of the compression strut between the column and the beam compression blocks. These forces will wedge-off the outside corner of the joint, and the anchorage for the column bars is thus lost (Priestley et al., 1996). This is shown in Figure 6.4.
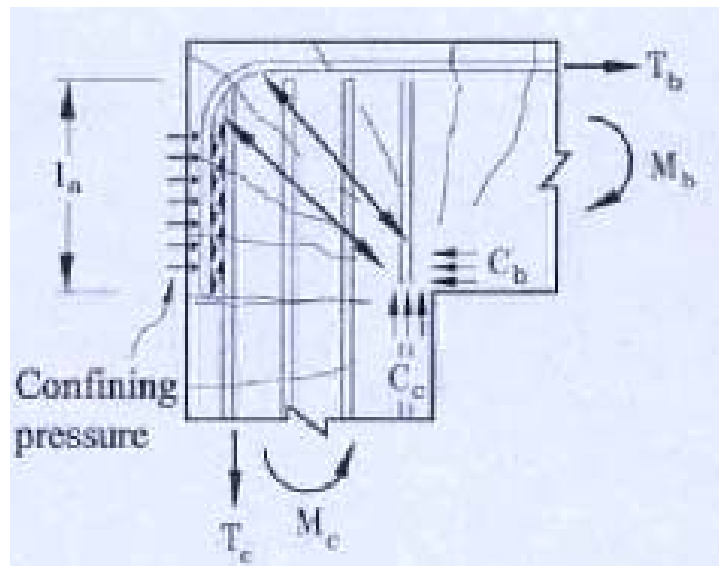
Figure 6.3 Force Transfer by Bond in a Lap Splice With Adequate Confining Pressure (Adapted from Sritharan and Ingham, 2003)
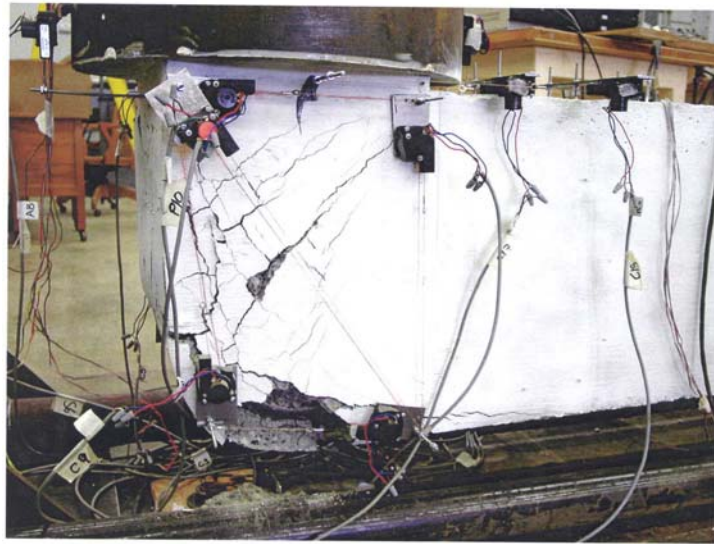
Figure 6.4 Bond Splitting Failure Mode in a Knee Joint

Tension Crack Failure

The tension stress distribution and the corresponding cracking pattern in a knee joint subject to opening actions are shown in Figure 6.5. Cracking of joints loaded in this manner occurs when tensile stresses in a knee joint exceed the tensile strength of the concrete within the joint. Failure of the joint may happen if the joint experiences large values of tensile stresses (Kramer and Shahrooz, 1993).
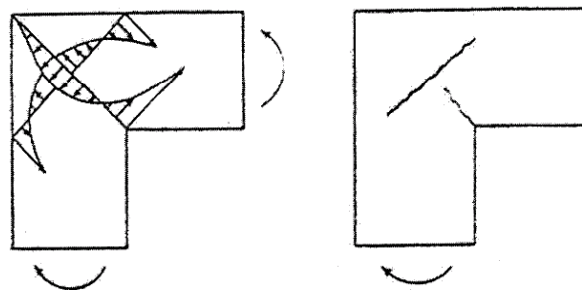
Figure 6.5 Tensile Stress Distribution and Associated Cracking Pattern
http://best.umd.edu/publications/stm.pdf

6.3 RETROFIT DESIGN CRITERIA

6.3.1 Retrofit to Provide Force Transfer Through the Joint

Analysis of the force transfer from beam to column using equilibrium equations based on the assumption of isotropic material behavior of concrete knee joint is only valid prior to cracking (Priestley et al., 1996). Cracking of the concrete, which occurs when principal tension stresses exceed the joint concrete tension strength, along with the inelastic behavior of both the concrete and the reinforcement embedded in the joint, make the analysis of the force flow through the joint more difficult. Therefore, a rational evaluation of the force flow through knee joints is required.

Closing moments

The approach presented here follows the approach by Priestley (1993) to determine the required horizontal stirrups for knee joints with circular columns subject to closing actions. The approach is modified where needed to address the case for knee joints with rectangular columns retrofitted by a steel jacket.

Under closing of the joint, the column tension force is directly transferred into a diagonal strut, D, within the joint region on the assumption that sufficient confining steel is provided to equilibrate the horizontal force, F_h, as shown in Figure 6.6.

For rectangular columns with equally distributed reinforcement on all faces or with concentrated reinforcement along the outer faces parallel to the axis of bending, the centroid of the column tension steel can be approximately assumed at an effective depth of $0.85h_c$, as determined from section analysis utilizing the software XTRACT. Based on work by Priestley (1993), the centroid of the tension force transfer can be assumed to act

at a height of $0.7l_a$ to allow for strain penetration, where l_a is the embedment depth of the column reinforcement into the joint region. Then, the required clamping force, F_h, that equilibrates the vertical component of the diagonal strut, D, can be computed by taking the sum of the moments about the centroid of the column compression block, $a_c/2$.

$$F_h = \frac{T_c\left(0.85h_c - \dfrac{a_c}{2}\right)}{0.7l_a} \qquad (6.1)$$
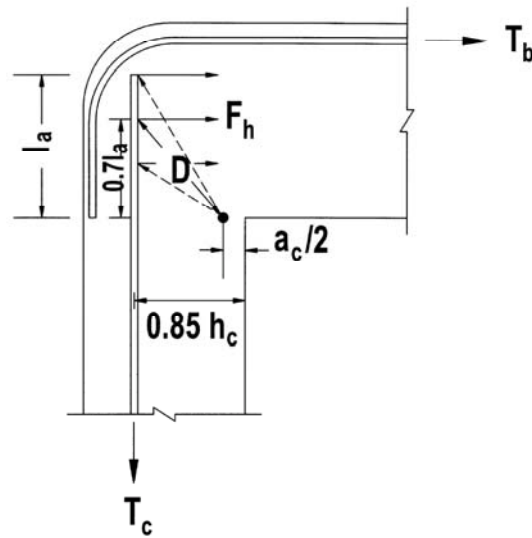
Figure 6.6 Transfer of Column Tension Force to Diagonal Compression Strut

According to Priestley (1993), F_h can be assumed to be uniformly distributed over the top 60% of the column embedment length l_a. Thus, the clamping force that can be provided by a circular steel jacket of a thickness t_c, yield strength f_{yh}, and a length of $0.6l_a$ is given by:

$$F_h = 2t_c(0.6l_a)f_{yh} \geq \frac{T_c\left(0.85h_c - \dfrac{a_c}{2}\right)}{0.7l_a} \qquad (6.2)$$

198

With simplification:
$$t_c \geq \frac{1.19 T_c \left(0.85 h_c - \dfrac{a_c}{2}\right)}{l_a^2 f_{yh}}$$ (6.3)

Equation 6.3 may be further simplified by assuming that $a_c/2$ equals $0.15 h_c$. This assumption is based upon section analysis of rectangular columns with the same longitudinal steel arrangement as mentioned previously and using the software XTRACT. Thus:

$$t_c \geq \frac{0.83 T_c h_c}{l_a^2 f_{yh}}$$ (6.4)

The tension force in the column bars, T_c, in equation 6.4 can be determined precisely by a section analysis, such as can be performed using the software XTRACT. Alternatively, T_c can be taken as the tension force corresponding to 50% of the column longitudinal steel area at yield (Priestley, 1993). This is a reasonable approximation since the column bars on the compression side of the neutral axis are well anchored in the diagonal compression strut (Priestley et al., 1996). An overstrength factor of 1.3 is introduced in equation 6.5 to account for strain hardening of the column reinforcement. Thus,

$$t_c \geq \frac{0.83 \times 1.3 \times 0.5 \rho_l A_{col} f_y h_c}{l_a^2 f_{yh}}$$ (6.5)

or
$$t_c \geq \frac{0.54 \rho_l A_{col} h_c}{l_a^2} \frac{f_y}{f_{yh}}$$ (6.6)

An additional mechanism can be relied on to transfer the column tension force into a diagonal strut in the joint if the top beam steel is extended down to the bottom of

the beam. Such detailing will help in transferring the tension force in the outer column bars by bond to the tails of the beam bars given that the beam steel area is adequate, as shown in Figure 6.7. For this situation, Priestley (1993) suggested that 50% of the column tension force, T_c, be carried to the beam bars by bond and the other 50% be transferred by a clamping force. Consequently, the thickness of the steel jacket given by equation 6.6 can be reduced by ½:

$$t_c \geq \frac{0.27 \rho_l A_{col} h_c}{l_a^2} \frac{f_y}{f_{yh}} \tag{6.7}$$
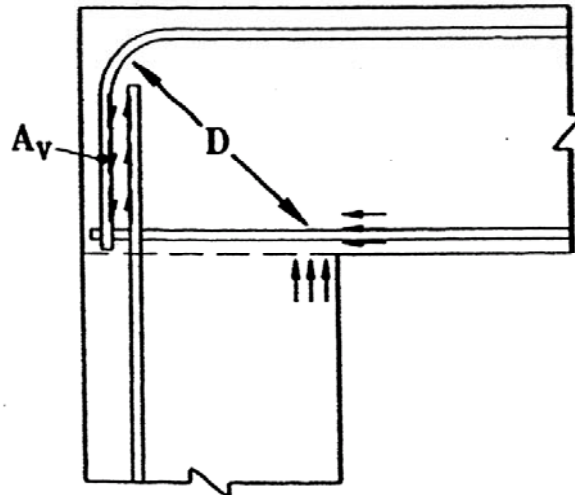
Figure 6.7 Transfer of Column Tension Force by Bond to Beam Steel (Adapted from Priestley, 1993)

Opening Moments

When a knee joint is subject to opening moments, an arch cracking pattern develops between the compression zones of beam and column. This was evident during tests on the nominally unreinforced knee joints under in-plane loading conducted in this study and that conducted by Ingham (1995). A potential failure mechanism of nominally unreinforced knee joints under opening moments is of concern when the column

reinforcement is terminated below the beam compression force, as is the case in most knee joints in older bridges. Concrete covering the column reinforcement can split off the joint through the initiation of a horizontal crack at the top level of the column rebars, as shown in Figure 6.8 (Priestley, 1993).
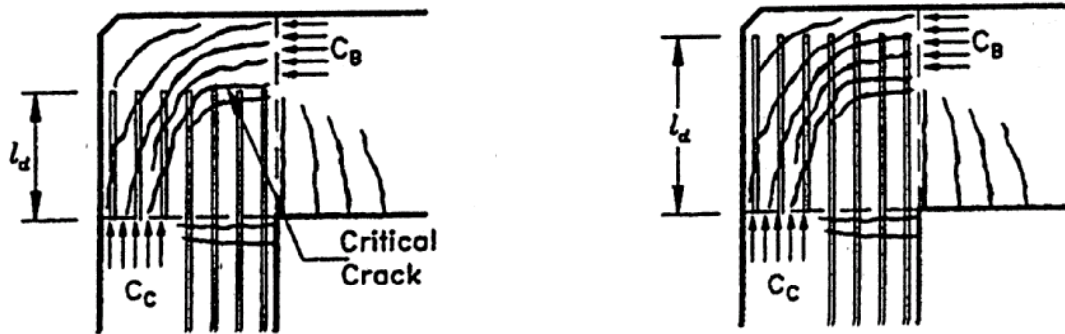
Figure 6.8 Cracking Pattern Under Opening of the Joint for Insufficient and Sufficient Embedment Rebar Lengths (Adapted from Ingham, 1995)

To avoid this kind of failure, Priestley (1993) proposed three mechanisms to transfer the column tension force into a diagonal strut, D, between the beam and the column compression forces. Knee joint reinforcement for each mechanism is shown in the following figure.
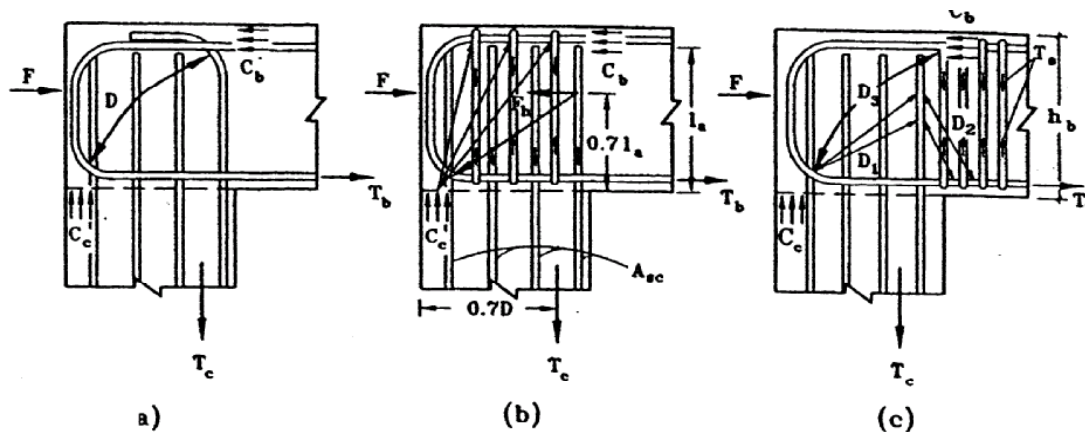
Figure 6.9 Knee Joint Reinforcement Under Opening Moments (Adapted from Priestlety et al., 1996)

201

In the first mechanism shown in Figure 6.9a, the column reinforcement adjacent to the beam is bent over the joint to provide the required vertical component to C_b. The second reinforcement scheme incorporates the use of vertical joint reinforcement to transfer part of the column tension force, T_c, by bond up to the top of the joint, as shown in Figure 6.9b. In the last alternative, vertical reinforcement is provided outside the joint in the outrigger beam to support the formation of a diagonal compression strut outside the joint, as shown in Figure 6.9c. The third force transfer mechanism was employed in this study to determine the required thickness of the beam-joint steel jacket. This third mechanism was selected because the first reinforcement scheme can be utilized only for new designs, and the second alternative results in large amounts of vertical joint reinforcement (Priestley, 1993). The following discussion summarizes the approach followed by Priestley (1993) to determine the reinforcement needed to satisfy the force transfer mechanism in the third arrangement. This approach is then extended to address the use of circular jackets around the beam and the joint.

As shown in Figure 6.10, anchorage of the column bars adjacent to the beam is provided by struts D_1 and D_2. The vertical component of strut D_2, equal to T_s, provides the required force to balance the main strut D_3 from C_b towards C_c. T_s is provided by placing stirrups within a distance $h_b/2$ in the beam region from the beam joint interface in addition to that required for shear. Priestley et al. (1996) recommended that 50% of the tension force in the column, $0.5T_c$, should be transferred by this mechanism, half of which is transferred through strut D_1 and the other half via strut D_2. The tension force carried by the beam stirrups is then $T_s = 0.25T_c$. T_c can be approximated as $0.5A_{sc}f^o_{yc}$, where A_{sc} is column longitudinal reinforcement area and f^o_{yc} is the overstrength stress in

the column bars, which includes strain hardening and yield overstrength (Priestley et al., 1996).
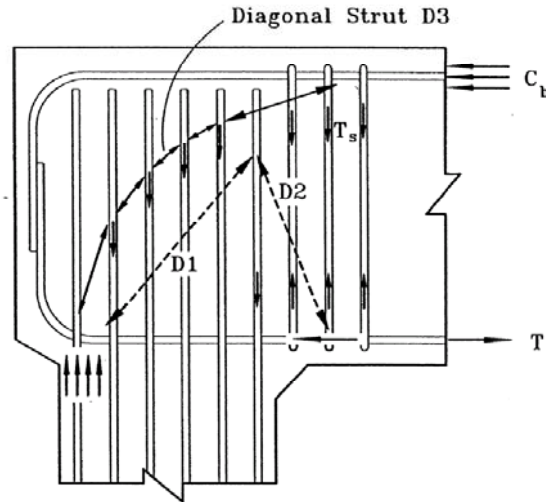
Figure 6.10 Force Transfer Mechanism In a Knee Joint Under Opening Moment (Adapted from Priestlety et al., 1996)

This approach can be extended to deal with circular jackets by equating the tension force in the steel jacket at yield over a length of $h_b/2$ with the required vertical component force, T_s. Thus:

$$T_s = 2t_b \frac{h_b}{2} f_{yh} = 0.125 A_{sc} f_{yc}^o \qquad (6.8)$$

with simplification:
$$t_b \geq \frac{0.125 A_{sc}}{h_b} \frac{f_{yc}^o}{f_{yh}} \qquad (6.9)$$

where t_b is the required jacket thickness around the beam in the joint vicinity.

To ensure bond transfer of the top reinforcement, vertical stirrups are to be provided in the joint area. These stirrups are designed to resist a total force equal to 50%

of T_s (Priestley et al., 1996). Again, this recommendation can be extended to address the situation in which the joint is reinforced with a circular jacket rather than vertical stirrups. In the case of a circular jacket, the vertical force, $0.5T_s$, results in a bending force in the beam jacket, compression on the top face, and tension on the bottom face. Assuming that the vertical force acts at the centroid of the column, the resulting moment at the beam joint interface equals $0.5T_s h_c/2$. The force created in the jacket, F, can be computed by resolving the moment into a tension and a compression component couple over the depth of the steel jacket, that is, the diameter of the jacket. Thus:

$$F = \frac{0.0625 A_{sc} f^o_{yc} h_c}{2D} \qquad (6.10)$$

To support this force, the joint jacket is extended below the bottom of the beam jacket. The required joint jacket thickness can be calculated by equating F with the force provided by the lip length of the joint jacket (i.e., the portion below the bottom of the beam jacket) at yielding. For a lip distance of 6 in. (150 mm), the required thickness is equal to:

$$6(2 f_{yh} t_{o1}) = \frac{0.0625 A_{sc} f^o_{yc} h_c}{2D} \qquad (6.11)$$

with simplification:
$$t_{o1} = \frac{A_{sc} h_c}{380D} \frac{f^o_{yc}}{f_{yh}} \qquad (6.12)$$

Note that the recommendation on the lip distance was obtained from tests on the retrofitted knee joints of this study.

The requirements of equation 6.12 are not onerous, and other equations will, for most cases, control the design of the jacket thickness. Note also that the compression component of the moment in the steel jacket is not considered here as it is counteracted

by the horizontal component of the strut D_1. If vertical stirrups were utilized for the joint design instead of circular jackets, it would be required to provide additional beam bottom reinforcement to sustain the mechanism discussed here. The additional reinforcement for the horizontal component of the strut D_1 is discussed in detail by Priestley (1993).

Priestley et al. (1996) recommended providing horizontal reinforcement to the joint that is able to resist 50% of the clamping force required in the closing direction. This is to counteract the outward thrust resulting from the difference in the horizontal components of struts D_1 and D_2. Thus:

$$t_{o2} \geq \frac{0.14 \rho_l A_{col} h_c}{l_a^2} \frac{f_y}{f_{yh}} \tag{6.13}$$

This requirement is already satisfied by equation 6.7 when designing the joint jacket for the closing direction mechanism.

In conclusion, for a dependable force transfer mechanism in the opening direction, the steel jacket thickness around the beam and the joint should satisfy the greatest thickness required from equations 6.9, 6.12, and 6.13.

6.3.2 Retrofit to Provide Anchorage of Column Longitudinal Steel

Development length may be defined as the distance over which a bar must be bonded to develop the stress in the bar at the overstrength capacity of the member. This length is dependent upon a number of factors, including bar diameter, tensile strength of the concrete and lateral confinement stress around the bar.

Lateral confinement enhances the development of reinforcement by restraining the dilation of the splitting cracks around the bars. Results of experiments on confined bars in elements under seismic loading showed that much shorter development lengths

are needed in confined conditions than for unconfined conditions (Paulay and Priestley, 1992). In knee joints, confinement for column bars adjacent to the beam is provided by the surrounding concrete and transverse reinforcement in the beam itself. For column bars on the other faces, transverse reinforcement should be provided.

According to Priestley et al. (1996), the amount of transverse reinforcement required to transfer the column bar stress to the concrete by shear friction can be obtained by equating the clamping force provided to each bar by hoops distributed over an anchorage length of l_a, as shown in Figure 6.11, to the overstrength bar capacity. For circular columns, the clamping force provided to a bar by a single hoop of area A_h and stress f_s is equal to $A_h f_s 2\pi/n$, while the overstrength bar capacity is $A_b f^o_{yc}$ where A_b is the bar area, fs is equal to 0.0015 times the modulus of elasticity of the steel bars, and n is the number of column longitudinal bars. Assuming a coefficient of shear friction, μ, equal to 1.4, the required area of transverse reinforcement, A_h, can be determined by the following equation (Priestley, 1993):

$$\mu \frac{A_h f_s 2\pi}{n} \frac{l_a}{s} = A_b f^o_{yc} \qquad (6.14)$$

(a) Column with n bars   (b) Section A-A
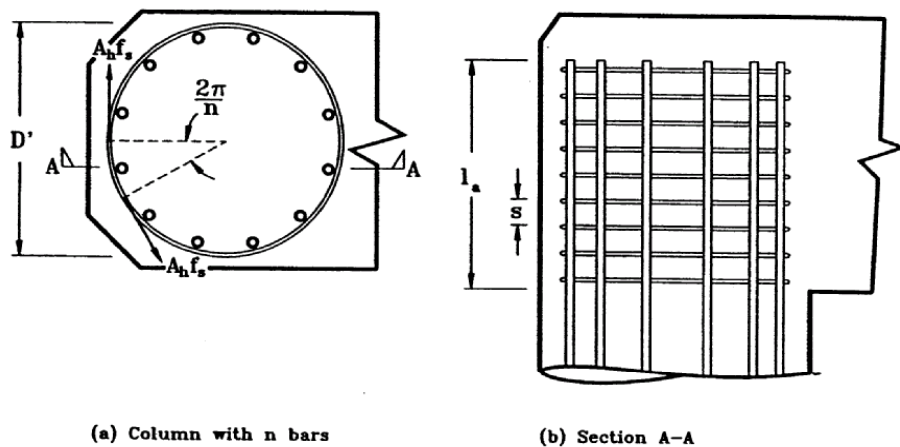
Figure 6.11 Anchorage by Lateral Confinement (Adapted from Priestley et al., 1996)

Equation 6.14 can be modified to address rectangular columns confined by a steel jacket using the same methodology developed by Priestley. The clamping force provided to a bar by a steel jacket of thickness t and stress f_s over a length of l_a is equal to $tl_a 2\pi/n$. Note that the clamping force here represents an average value rather than an exact value, as the case in circular columns, because the $2\pi/n$ term in the clamping force expression is not the same for every segment in a rectangular column, as shown in Figure 6.12. Thus, equation 6.14 then can be expressed as:

$$\mu t f_s l_a \frac{2\pi}{n} = A_b f_{yc}^o \qquad (6.15)$$

Setting μ to 1.4 as proposed previously, expressing nA_b as A_{sc}, and rounding up coefficients, equation 6.15 can be rewritten as:

$$t \geq \frac{0.11 A_{sc} f_{yc}^o}{f_s l_a} \qquad (6.16)$$
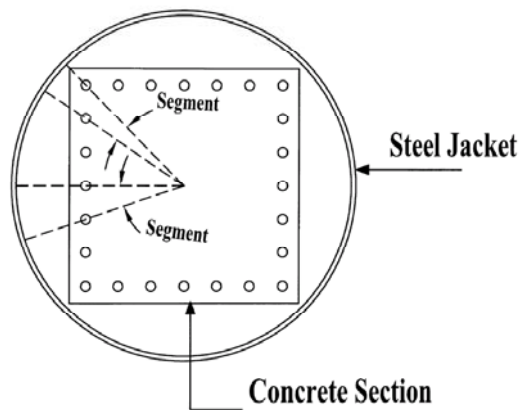
Figure 6.12 Rectangular Column Confined by a Steel Jacket

6.3.3 Retrofit for Flexural Ductility Enhancement

Plastic hinge zones provide deformation and energy dissipation capacity to structural systems. The ability of a plastic hinge to sustain large inelastic rotations and curvatures is a function of the level of confinement pressure provided. A number of studies have been conducted on older bridge columns to investigate the effectiveness of retrofit techniques on flexural ductility and flexural integrity of column lap splices. The retrofit techniques include steel jacketing, reinforced concrete jacketing and composite-material jackets involving fiberglass and carbon fiber. Among those, steel jacketing is the most commonly used technique for retrofitting deficient concrete columns.

Research by Priestley and Seible (1991) has shown that the steel jacketing is a very successful method of retrofitting reinforced concrete columns. The technique, which was originally developed for circular columns, used two half-shells of steel plate rolled to a radius that is 0.5 in. (13 mm) to 1.0 in. (25 mm) larger than the column radius and site welded along the vertical seams (Buckle and Friedland, 1995). Typically, a 2.0-in. (51-mm) gap is provided between the jacket and the neighboring member (e.g., footing or beam) to avoid the possibility of the jacket acting as a compression reinforcement by bearing against the supporting member at large drift angles. The difference between the jacket and the column is then grouted with a cement grout after flushing with water. Usually, partial height jackets are used to improve the hinge and/or splice region performance. The jacket provides the deficient area in the column with the necessary confinement by acting as passive confinement. That is, a reaction is created in the steel jacket due to lateral expansion of the compressed concrete as a result of high axial compression strains or the tensioned concrete as a function of dilation of lap splices

under incipient splice failure.

For rectangular columns, circular or elliptical steel jackets are recommended over rectangular steel jackets (Priestley et al., 1996). Rectangular steel jackets provide confinement to the section through the bending action of the jacket sides, which is significantly more flexible than the circumferential continuous tension action in circular or elliptical sections.

Priestley et al. (1996) developed equations for the design of circular and elliptical steel jackets. For confinement of plastic hinge regions, the equation basically relates the volumetric confinement ratio to the required plastic curvature of the critical section in the column. A conservative material-dependent relationship between ultimate compression strain and volumetric ratio of jacket confinement was then employed to solve for the jacket thickness, t_j:

$$t_j = \frac{0.18(\varepsilon_{cm} - 0.004)Df_{cc}'}{f_{yj}\varepsilon_{sm}}$$ (6.17)

where ε_{cm} = the maximum compressive strain required in the hinge, D = the jacket diameter, f_{cc}' = the confined concrete compressive strength, f_{yj} = jacket yield strength and ε_{sm} = jacket strain at maximum stress. Design charts for required steel jacket thickness for circular columns are given in Figure 6.13 as functions of column longitudinal reinforcement ratio and axial load ratio. The figure was constructed for Grade 40 (276 MPa) and two common longitudinal bar sizes and for A36 steel jacketing based upon extreme deformation requirements (an approximate total drift of 5%).
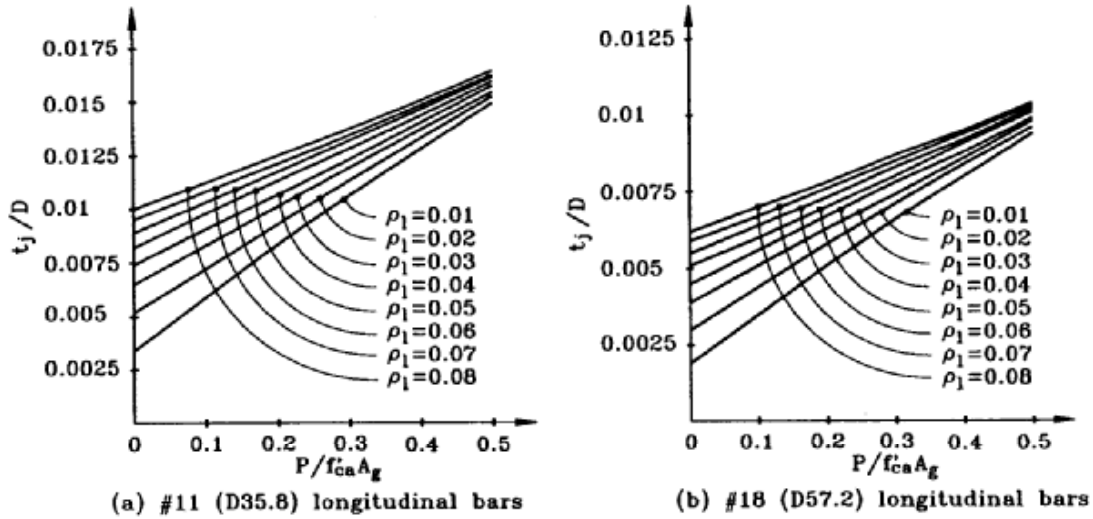
Figure 6.13 Steel Jacket Thickness to Provide a Plastic Drift of 4.5% in a Circular Column (Adapted from Priestley et al., 1996)

6.3.4 Retrofit for Anchorage of Beam Reinforcement

Under closing of the joint, the tension force in the beam reinforcement extending into the joint region results in radial stresses on the concrete below the bend, as shown in Figure 6.14 (Priestley, 1993). In such a case, the beam hook extensions will bend out unless adequate restraint to these bars is provided. Priestley (1993) suggested providing the joint with horizontal reinforcement that is capable of restraining the beam hook extension at the plastic moment capacity of the beam bars. The joint horizontal reinforcement is distributed over a length of $12d_b$, where d_b is the diameter of the beam bar. Assuming no contribution from the concrete cover, the force, F_R, required to restrain one bar is equal to (Priestley, 1993):

$$F_R \geq \frac{1.3\pi d_b^2 f_y}{120} \tag{6.18}$$

210

Extending this approach to joints retrofitted using circular jackets, the required restraining force for n number of beam hooks can be supplied by a steel jacket of thickness, t_j, and a length of $12d_b$. Thus:

$$2f_{yh}t_j(12d_b) \geq \frac{1.3\pi d_b^2 f_y}{120} n \qquad (6.19)$$

simplifying and approximating numbers yields:

$$t_j \geq \frac{nd_b}{700} \frac{f_y}{f_{yh}} \qquad (6.20)$$
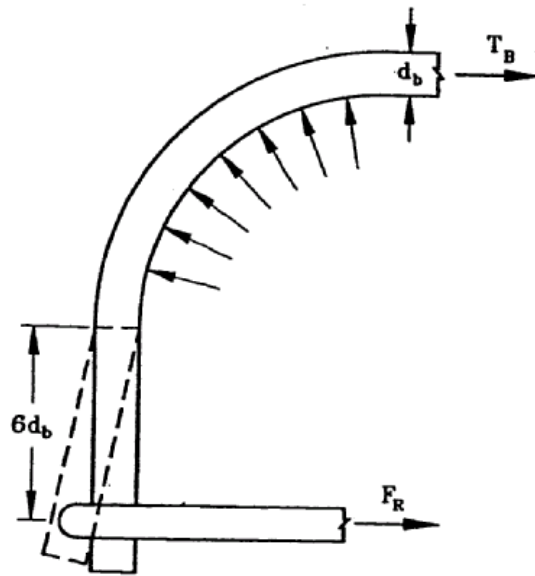
Figure 6.14 Beam Hook Extension Restraint (Adapted from Priestley, 1993)

6.3.5 Retrofit of Outrigger Beam

Under out-of-plane loading, an outrigger beam is subjected to bending, torsion and shear forces. When the magnitudes of two or more of the forces are relatively large, the effects under combined loading must be considered in the design. Design procedures

for members under combined loading generally are in the form of nondimensionalized interaction equations based on the strength of the section. For designing reinforced concrete members under combined loading, Hsu (1983) proposed the following interaction equation:

$$\frac{M}{M_o} + \left(\frac{T}{T_o}\right)^2 R + \left(\frac{V}{V_o}\right)^2 R \le 1 \tag{6.21}$$

where M, T and V are the moment, torsion and shear design forces, respectively; M_o, T_o and V_o are the pure bending, torsion and shear strengths of the member, respectively; and R is the ratio of the tensile and compressive forces in the beam at yield.

Equation 6.21 can be used to determine the required beam steel jacket thickness to carry the beam loads. Demand forces on the most critical outrigger beam section should be computed based upon the overstrength capacity of the column hinge section. Bending, torsion and shear strengths of the reinforced concrete beam with circular steel jacket can be calculated assuming composite action of the existing beam section and the steel jacket.

Based on work by Priestley et al. (1996), the shear strength contribution of a circular steel jacket, V_{sj}, used for retrofitting purposes can be computed by the following equation:

$$V_{sj} = \frac{\pi}{2} t_j f_{yj} D \cot\theta \tag{6.22}$$

where t_j is the thickness of the jacket, f_{yj} is the yield strength of the jacket, D is the diameter of the jacket, and θ is the angle of the critical inclined flexure shear cracking to the column axis taken as 35˚.

In torsion, the torsion moment contribution of a circular steel jacket can be computed using the thin tube analogy. From Hsu (1983), the torsion yield contribution of

the jacket, T_{jy}, is:

$$T_{jy} = 2A_j t_j f_{yj}$$ (6.23)

where A_j is the area enclosed within the centerline of the jacket. Shear and torsion strengths of the existing reinforced beam section are not discussed here as they are presented explicitly in the ACI 318-02 code provisions (2002).

Finally, in bending, the strength capacity of the beam section after retrofitting can be determined using moment capacity analysis, easily obtained using software such as XTRACT.

6.4 SUMMARY OF OUTRIGGER KNEE JOINT SYSTEM RETROFIT DESIGN

The purpose of the seismic upgrade of the outrigger bents is to eliminate any possible failure mechanism in the knee joint and in the outrigger beam, presuming that the column in the outrigger bent has already been retrofitted, and to enhance the ductility and the energy dissipation capacity of the system under in-plane and out-of-plane loading. The retrofit measures proposed in this study incorporate the use of an elbow-shaped steel jacket around the beam and the joint region. The following discussion provides for the design and detailing of the steel jacket around the beam and the joint.

Regular outrigger bents

1.   *Scope*: The retrofit measures presented here are applicable to outrigger bents with columns and beams of similar size sections. For other cases, the approach will lead to two jackets, the column jacket and a jacket over the beam and the joint, that are different in size.

2.   ***Design forces***:   Component demand forces should be determined based on the development of the overstrength capacity of the column hinge section in each direction. The overstrength capacity can be obtained from a section analysis of the column hinge section using characteristic material strengths and including the effect of confinement on the strength of the concrete. The characteristic yield strength can be taken as $1.1f_y$ and $1.3 f_c'$ for the steel and the concrete, respectively (Priestley et al., 1996). A strength reduction factor of $\phi = 1.0$ may be used in the design process since demand actions are determined based on conservative material properties (Ingham and Sritharan, 2003).

3.   ***Column retrofit***:   The plastic hinge location at the top of the column should be located at a distance of 1/3 of the larger column side dimension below the beam-joint interface or 6 in. (150 mm) below the beam jacket, whichever is larger, as shown in Figure 6.15. This limit on the plastic hinge location is introduced so as to locate the hinge as close as possible to the maximum moment location while at the same time provide enough lip distance for the joint. The purpose of the lip is to provide a reaction area for the compression strut between the column and the beam reinforcement. For outrigger bents with jacketed columns, the gap is provided by removing the existing column jacket and grout to the depth of original column. For new retrofits, the column jacket is terminated at the appropriate location. A gap width of 2 to 4 in. (50 to 100 mm) is recommended in order to prevent contact between the jackets at large drift ratios and to avoid excessive flexural strength enhancement of the plastic hinge region.

4.   ***Beam-joint retrofit***:

   a. The beam-joint jacket is constructed from two clamshell-sections fabricated offsite and field welded together with a full capacity weld. The clamshells are

fabricated by formulating a pipe section through curving a flat plate to the required radius and length that covers both the beam and the joint. The pipe is then cut at a 45-degree angle to the required length to jacket the beam. The remaining part of the pipe (eventually forming the joint jacket) is rotated 90-degrees in-plane and 180-degrees out-of-plane to form an elbow shape together with the beam jacket. The two pieces are then welded together using a full capacity weld. The resulting final shape of the jacket is shown in Figure 6.16.
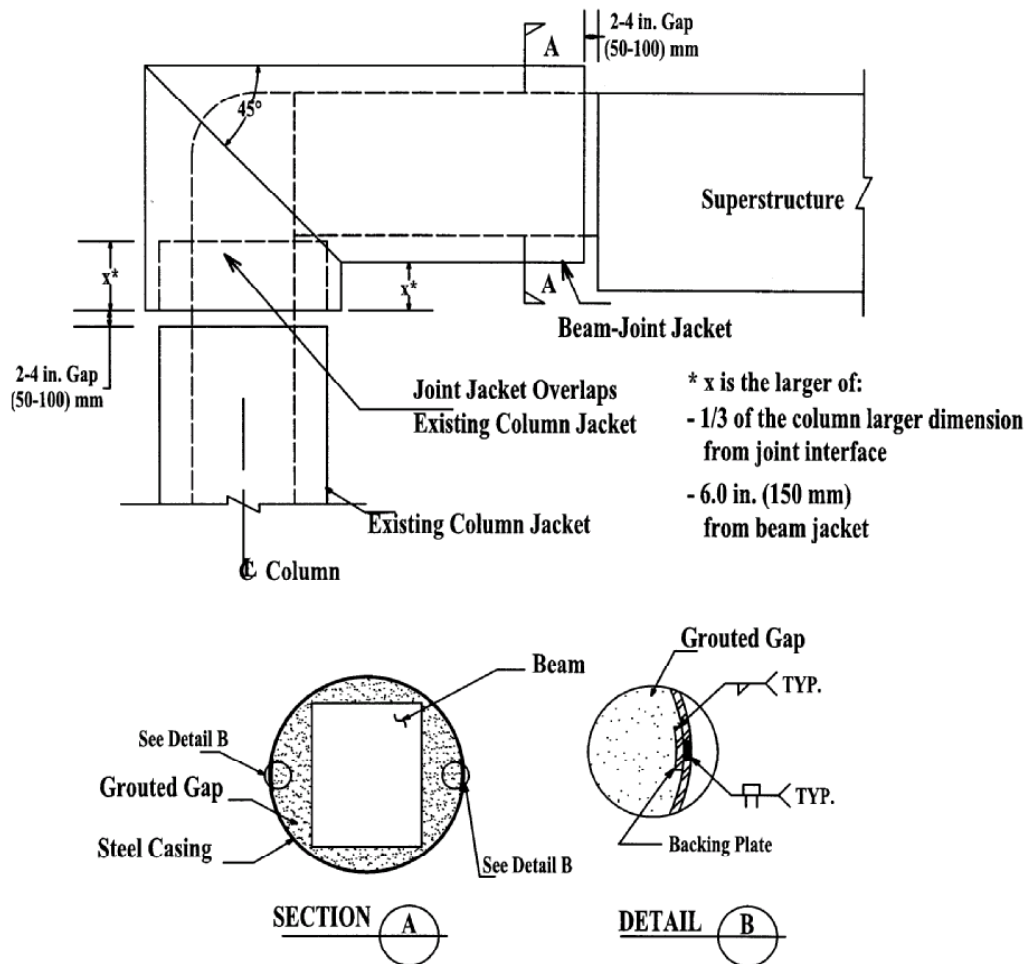
Figure 6.15 Steel Jacket Retrofit Details
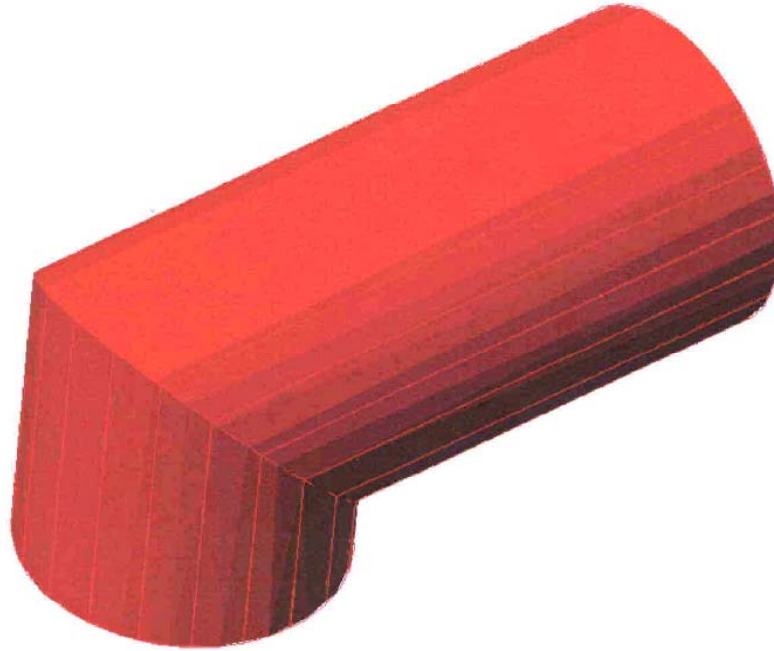
Figure 6.16 Isometric shape of the Beam-Joint Steel Jacket

b. The shape and size of the jacket are determined based on the shape and size of the beam section. For optimal strength, confinement and use of the materials, circular steel jackets are recommended for beams with square sections or rectangular sections with approximately the same side lengths, while elliptical jackets are recommended to encase beams with oblong rectangular sections. For circular or elliptical jackets, the size of the jackets can be reduced by chipping off the corners of the beam.

c. The beam jacket may overlap any existing column jacket above the hinge location, as shown in Figure 6.15. A gap of 2 to 4 in. (50 to 100 mm) should be maintained between the beam jacket and the superstructure to prevent contact at large drift angles.

d. The space between the jacket and the joint and the beam is filled with a high-strength, non-shrinkage grout.   The grouting sequence is a function of the

construction procedures and the type of the grout used. The sequence of grouting should be selected so as to insure complete filling of the void spaces.

5.   *Jacket thickness*: The thickness of the jacket is chosen as the largest of:

a.   The thickness of the existing column jacket.

b.   The thickness that enables a stable force transfer mechanism between the column and the beam in the closing and the opening directions using equation 6.7 is for closing of the joint and equations 6.9, 6.12 and 6.13 are for the opening direction. The requirements of part (a) or part (b) will, most likely, control the required jacket thickness.

c.   The thickness necessary for providing sufficient confinement for anchorage of the column rebars into the joint, equation 6.16.

d.   The thickness that generates an effective confinement pressure around the column joint interface equal to that provided by the column jacket over the hinge location, equation 6.17.

e.   The thickness required for anchorage of beam reinforcement, equation 6.20.

f.   The thickness needed to assure that the nominal capacity of the upgraded beam is greater than the ultimate demand on the beam taking into consideration the interaction of bending, shear and torsion forces, equation 6.21.

6.   *Connection to superstructure*: The connection of the retrofitted outrigger knee joint system to the bridge superstructure should be evaluated. Some retrofitting may be needed to ensure transfer of the forces from the upgraded outrigger bents to the bridge superstructure.   The ultimate forces transferred to the bridge superstructure from the upgraded outrigger knee joint systems can be quantified based on the ultimate capacity of

the column hinge. An overstrength factor of at least 25% is recommended in estimating the ultimate capacity of the plastic hinge for capacity design of the connection.

Split outrigger bents

The guidelines developed for regular outrigger bents can also be utilized to upgrade split outrigger bents:

1. ***Scope***: Same as for regular outrigger bents.

2. ***Design forces***: Same as for regular outrigger bents.

3. ***Column retrofit***: Similar to regular outrigger bents, the plastic hinge location at the top of the column should be located at the larger of: 1/3 of the larger column side dimension below beam-joint interface or 6 in. (150 mm) below the beam jacket, as shown in Figure 6.17. For split outrigger bents with existing column jackets, the gap is provided by removing the circular part of the existing D-shaped column jacket and grout to the depth of the original column. Additionally, the flat plate on the inner surface of the column in the gap hinge region should be cut off to the depth of the original column. For new retrofits, the column jacket is terminated at the appropriate location. The width of the gap is recommended to be between 2 to 4 in. (50 to 100 mm).

4. ***Beam-joint retrofit***:

    a. The beam-joint jacket is a D-shaped steel jacket consisting of a clamshell-section and a flat plate of the same thickness. The flat plate is adhered to the back face of the beam and the joint, using high-strength epoxy, and then field welded to the clamshell with a full capacity weld. A picture of a clamshell section is shown in Figure 6.18.
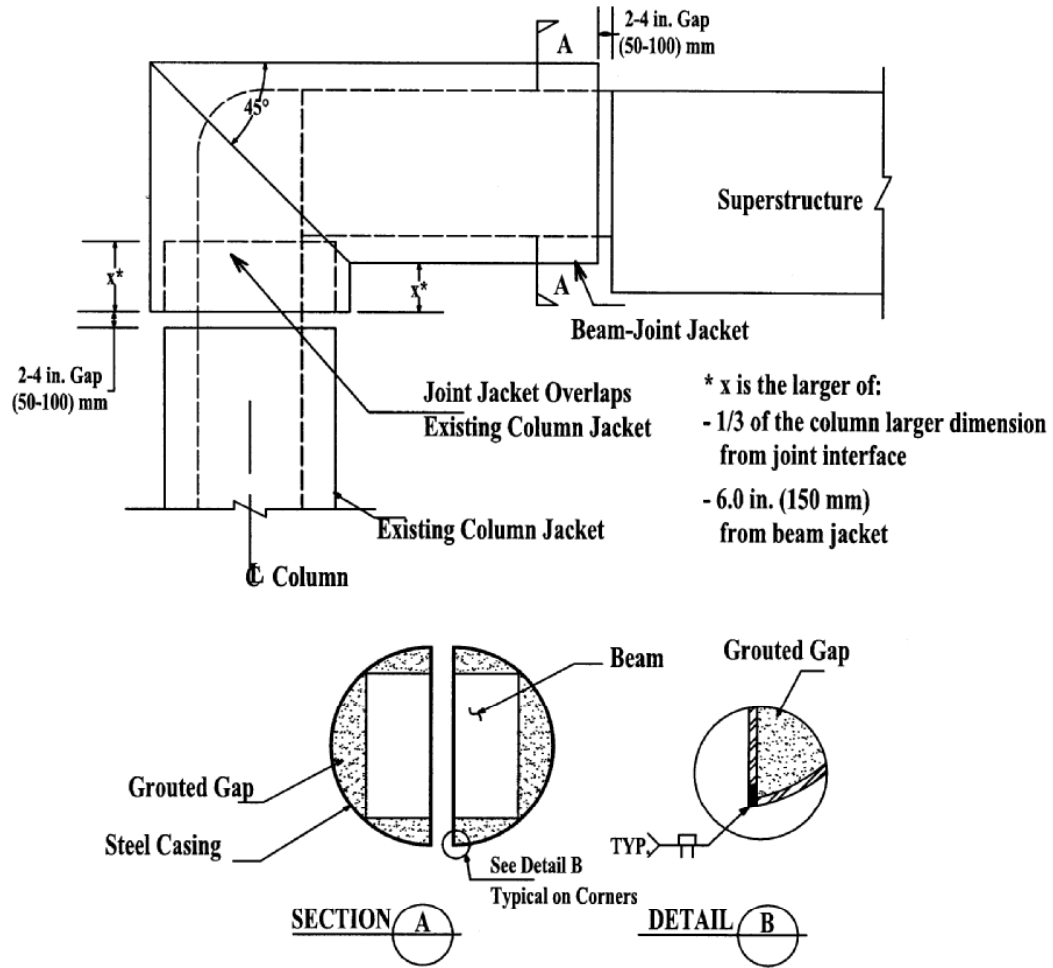
Figure 6.17 Steel Jacket Retrofit Details

Figure 6.18 A Picture of the Clamshell Used in the Retrofit of the Beam-Joint

b. The flat plate on the inner face of the beam should be bent out at a 45-degree angle ahead of the beam joint interface to account for any increase in the size of the joint over the beam. Due to the existing steel jacket being behind the column, the plate behind the joint is cut off at the column joint interface level.   Another rectangular plate projecting out a distance equal to the thickness of the existing plate behind the column is fillet welded at the shop to the big plate. A picture of a flat plate with these details is shown in Figure 6.19.
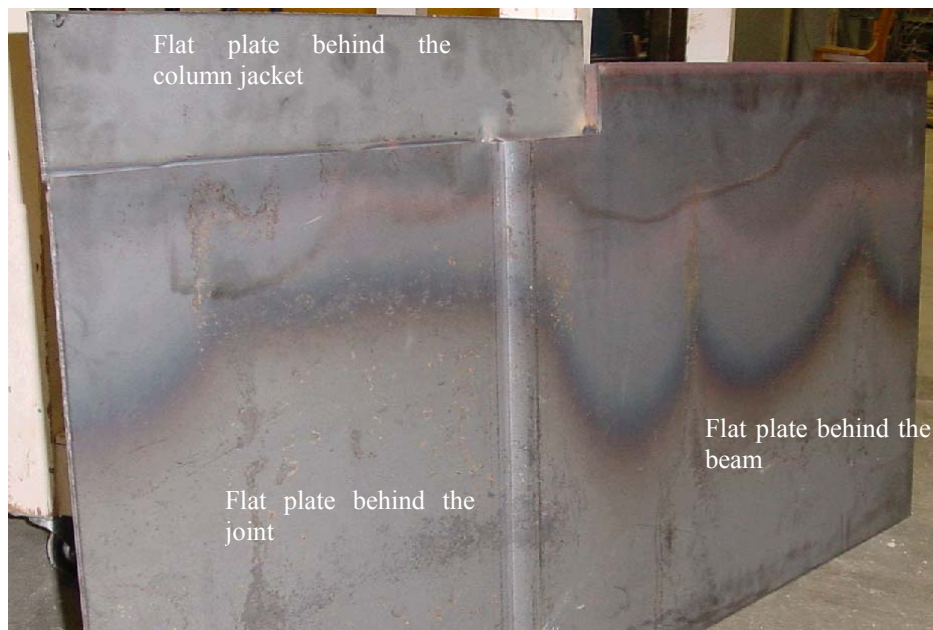
Figure 6.19 A Picture of the Flat Plate Used in the Retrofit of the Beam-Joint

c. The size of the jacket is determined based on the size of the beam section. The diameter of the circular part in the D-shaped casing can be reduced by chipping off the corners of the beam.

d. Similar to regular outrigger bents, the beam jacket may overlap existing column jackets above the hinge location, as shown in Figure 6.17. A gap of 2 to 4 in. (50 to

100 mm) should be maintained between the beam jacket and the superstructure.

e. The space between the jackets and the joint and the beam is filled out by a high-strength, non-shrinkage grout. The grouting sequence should provide for complete filling of the void spaces.

5. *Jacket thickness*: Same as for regular outrigger bents.

6. *Split gap*: It is required to maintain at least a gap of ½ in. (15 mm) between the split outrigger after retrofit to account for any longitudinal movement in the adjacent bridge specimens.

7. *Connection to superstructure*: Same as for regular outrigger bents.

CHAPTER SEVEN

SUMMARY, CONCLUSIONS AND RECOMMENDATIONS

7.1 SUMMARY

The 1989 Loma Prieta, California earthquake highlighted the seismic vulnerability of outrigger knee joints, not only in older bridges but also in relatively new bridges designed to then-current seismic design practice. The 2001 Nisqually, Washington earthquake produced additional evidence of the seismic vulnerability of older knee joint systems where the earthquake caused cracking to outrigger beams and knee joints in the Alaskan Way Viaduct and in the Spokane Street Overcrossing. In both seismic events, the problem areas in outrigger knee bents were identified as the very light transverse reinforcement in knee joints, the lack of vertical stirrups within the joint, poor detailing of the reinforcement, and low torsion strength of the outrigger beam. Under a significant earthquake, these deficiencies could result in a brittle failure in the outrigger knee joint systems, thereby resulting in a catastrophic failure in the bridge.

In this study, seven knee joint specimens were tested under simulated seismic loading. These specimens were one-third scale models of selected outrigger bents in the Spokane Street Overcrossing and represented the entire length of the prototype outrigger beam, the knee joint, half the length of the column, and an anchor block simulating the monolithic connection of the beam to the superstructure. The primary objectives of the study were to define the vulnerabilities of outrigger bents under seismic in-plane and out-of-plane loading and to develop appropriate retrofit measures for outrigger knee joints that address the identified deficiencies.

A literature review of the current knowledge about the behavior of outrigger knee joints under cyclic loading and retrofitting techniques was performed. Although a number of retrofit measures for knee joints have been developed by previous researchers, the application of these schemes to existing outrigger bents is often impractical, either due to obstruction problems from the bridge superstructure or because the schemes are affected by the increased demand on the bridge from the upgraded knee joint bents.

In the first phase of this study, three as-built specimens with two basic beam configurations were examined. The first two specimens contained a short outrigger beam, and the third specimen had a long outrigger beam. Two of the as-built specimens were tested under in-plane loading, and the third was tested under out-of-plane loading. The specimens were subjected to a displacement-controlled horizontal loading pattern applied in a quasi-static manner along with a constant vertical loading. The as-built specimens exhibited poor behavior with failure at low ductility levels.

Following testing of the as-built specimens, retrofit measures were developed based on the observed vulnerabilities and failure mechanisms. The goal with the retrofit design was to enhance the energy and ductility capacities of the outrigger knee bents by developing a well-controlled plastic hinge in the column. To examine the effectiveness of the selected retrofit measure, another four specimens were constructed, retrofitted and tested. Three of the specimens were retrofitted by circular steel jacketing around the joint and the beam, two under in-plane loading, and the third under out-of-plane loading. The fourth retrofitted specimen was a model of a split outrigger bent upgraded by D-shaped steel jacketing and was tested under in-plane loading. In all these specimens, the retrofit jacket formed an elbow shape around the beam and the joint and overlapped the existing

column jacket. At the intended hinge location, a gap below the joint jacket was introduced by removing the steel jacket and the grout to the depth of the original column. Testing showed enhanced performance of the upgraded specimens that satisfied the retrofit design goals.

The observed behavior of the knee joints in the as-built specimens was evaluated with respect to the joint principal tension stress levels. Threshold stress values describing the expected condition of the joints with similar steel arrangement to those present in the Spokane Street Overcrossing were proposed. The values were compared to those proposed by Priestley (1993).

Finally, design guidelines for retrofitting outrigger knee bents were suggested, including for knee joints in split bents. The guidelines include recommendations on the jacket thickness required to form a stable force transfer mechanism between the beam and the column and to prevent any potential failure mechanisms in the knee joint and connections members. Recommendations for detailing of the jacket were presented.

7.2 CONCLUSIONS

The experimental test results of this study indicate that outrigger bents with reinforcement details typical of those present in the Spokane Street Overcrossing will likely perform poorly in a significant earthquake event. Tests carried out on specimens with short and long outrigger beams representing as-built conditions showed that shear cracks will form in the joint region at low displacement levels. Failure will happen as a result of bond splitting of the column reinforcement hook extensions within the joint due to inadequate confinement, thereby resulting in a system with low ductility and energy

dissipation capacities. The existing outrigger knee joint systems can be expected to have a maximum ductility level in the range of 2.0 to 2.8. In the case of out-of-plane motion in the longitudinal direction of the bridge, the outrigger beams will experience cracking at low displacement levels. Bond splitting failure of beam reinforcement in the joint due to inadequate confinement along with the low torsional strength of the beam will result in the potential for failure of the system. Test results indicate that the existing knee joint systems with short outriggers will attain a capacity that is approximately 50% higher than the torsion cracking strength of the beam.

Circular and D-shaped steel jacketing around the beam and the joint of regular and split outrigger bents, respectively, prevented bond splitting failure of the column bars within the joint and increased the torsional strength of the outrigger beam. The steel jackets were effective in improving the displacement ductility, drift, strength and energy dissipation capacities of the system under in-plane and out-of-plane loading when compared to the response of the as-built specimens.

Results from this research showed that the proposed threshold principal tension stress values for seismic assessment of unreinforced knee joints are somewhat higher than those developed by Priestley (1993) due to the beam side reinforcement extending into the joint. Therefore, for knee joints where the beam side reinforcement is fully developed into the joint region and having a longitudinal steel ratio around 0.45%, seismic assessment may be conducted based upon the threshold values proposed in this study. For cases where the beam side reinforcement terminates at the joint interface, values developed by Priestley (1993) should be utilized.

7.3 SEISMIC ASSESSMENT RECOMMENDATIONS

Joint principal tension stress was linked to the joint condition of the as-built specimens under in-plane loading. Joint principal tension stress is determined based on a simple Mohr's circle analysis as discussed by Priestley et al. (1996). Principal tension stress values of $4.5\sqrt{f_c'}$ psi ($0.38\sqrt{f_c'}$ MPa) and $6.0\sqrt{f_c'}$ psi ($0.50\sqrt{f_c'}$ MPa) were set as limits beyond which joint shear cracking and joint failure, respectively, are expected.

For outrigger beams with reinforcement details typical to those present in the Spokane Street Overcrossing, a principal tension stress value of $6.0\sqrt{f_c'}$ psi ($0.50\sqrt{f_c'}$ MPa) is the limit after which torsion cracking in the beam can be expected. The principal tension stress is determined based on contributions from shear and torsion stresses. The ultimate capacity of the outrigger beams, T_n, can be taken as:

$$T_n = 1.5 T_{cr} \tag{7.1}$$

where T_{cr}, is the cracking torsional strength of the beam determined based on work by Hsu (1990), which is given by:

$$T_{cr} = 6(x^2 + 10)y\sqrt[3]{f_c'}[1.00 + 4(\rho_L + \rho_h)] \tag{7.2}$$

where x = smaller dimension of the rectangular section, y = larger dimension of the rectangular section, f_c' = compressive strength of the concrete, and ρ_L, ρ_h = volume ratio of longitudinal and hoop steel, respectively, with respect to the gross sectional area. For the existing outrigger beams which are transversely reinforced with U-shaped stirrups, ρ_h should be taken as zero.

7.4 RETROFIT RECOMMENDATIONS

The results from this research provide guidelines for designing and detailing the steel jacket for regular and split outrigger bents with columns and beams of similar size sections. Circular steel jackets were used for regular bents and D-shaped jackets were utilized for split outrigger bents. The steel jacketing is effective in eliminating possible failure mechanisms in the knee joint and in the outrigger beam in addition to enhancing the ductility and the energy dissipation capacity of the system under in-plane and out-of-plane loading. The thickness of the jacket should satisfy the requirements to establish a stable joint force transfer mechanism between the column and the beam reinforcement and to prevent potential failure modes in the joint region and connecting elements. The beam-joint jacket should be the greatest of the thickness requirements discussed in the following paragraphs.

A required steel jacket thickness to establish a reliable force transfer mechanism between the column and the beam reinforcement in the closing and the opening directions was developed in this study. For closing events, the required joint jacket thickness, t_c, is given by:

$$t_c \geq \frac{0.27 \rho_l A_{col} h_c}{l_a^2} \frac{f_y}{f_{yh}} \tag{7.3}$$

where ρ_l is the column longitudinal reinforcement ratio, A_{col} is the column gross sectional area, h_c is the depth of the column parallel to loading direction, l_a is the column embedment length, f_y is the yield strength of the column reinforcement, and f_{yh} is the yield strength of the jacket.

For opening events, the required jacket thickness, t_{o1}, is:

$$t_{o1} = \frac{A_{sc} h_c}{380D} \frac{f^o_{yc}}{f_{yh}} \tag{7.4}$$

where A_{sc} is column longitudinal reinforcement area, f^o_{yc} is the overstrength stress in the column bars as defined by Priestley et al. (1996), and D is the diameter of the beam-joint jacket. It is also required for opening events that the jacket thickness, t_b, around the beam in the joint vicinity be:

$$t_b \geq \frac{0.125 A_{sc}}{h_b} \frac{f^o_{yc}}{f_{yh}} \tag{7.5}$$

The required joint jacket thickness, t, to avoid anchorage failure of the column longitudinal bars is given by:

$$t \geq \frac{0.11 A_{sc} f^o_{yc}}{f_s l_a} \tag{7.6}$$

The required joint jacket thickness, t, to restrain the beam hook extensions is given by:

$$t_j \geq \frac{n d_b}{700} \frac{f_y}{f_{yh}} \tag{7.7}$$

where n is the number of beam hooks to be restrained and d_b is the diameter of the beam bar.

For flexural ductility enhancement, the required steel jacket thickness can be computed by equations developed by Priestley et al. (1996) for application to retrofitting columns.

The demand forces on the beam-joint steel jacket should be determined based on the development of the overstrength capacity of the column hinge section in each direction. For the beam section, this should take into consideration the interaction of

bending, shear and torsion forces.

For regular and split outrigger bents, the plastic hinge location at the top of the column should be located at a distance of 1/3 of the larger column side dimension below the beam-joint interface or 6 in. (150 mm) below the beam jacket, whichever is larger. For outrigger bents with jacketed columns, the gap is provided by removing the existing column jacket and grout to the depth of original column. For new retrofits, the column jacket is terminated at the appropriate location. The width of the gap is recommended to be between 2 to 4 in. (50 to 100 mm).

For both regular and split outrigger bents, the beam jacket may overlap any existing column jacket above the hinge location. A gap of 2 to 4 in. (50 to 100 mm) should be maintained between the beam jacket and the superstructure. The space between the jackets and the joint and the beam is filled out by a high-strength, non-shrinkage grout. For split outrigger bents, it is required to maintain at least a gap of ½ in. (15 mm) between the split outrigger after retrofit to provide for longitudinal movement between the adjacent bridge units.

The connection of the retrofitted outrigger knee joint system to the bridge superstructure was not addressed in this study. However, the connection should be evaluated to ensure transfer of the forces from the upgraded outrigger bents to the bridge superstructure. An overstrength factor of at least 25% is recommended in estimating the ultimate capacity of the column plastic hinge for capacity design of the connection.

REFERENCES

AASHTO (2004). *AASHTO Standard Specifications for Highway Bridges*, American Association of State Highway and Transportation Officials, Washington, D.C.

ACI 318-02 (2002). *Building Code Requirements for Structural Concrete (ACI 318-02) and Commentary (ACI 318R-02)*. American Concrete Institute, Detroit, MI.

ACI-ASCE Committee 352 (1985). "Recommendations for design of beam-column joints in monolithic reinforced concrete structures." *ACI Journal*, 82/923):266-283

ACI-ASCE Committee 352 (1991). "Recommendations for design of beam-column joints in monolithic reinforced concrete structures (ACI 352R-91),." American Concrete Institute, Farmington Hills, MI.

Caltrans (2001). "Caltrans Seismic Design Criteria (SDC) Version 1.2," California Department of Transportation, Sacramento, California.

Caltrans (2004). "Caltrans Seismic Design Criteria (SDC) Version 1.3," California Department of Transportation, Sacramento, California.

Cook, D. R., Malkus, S. D., Plesha, E. M., and Witt, J. R. (2002). "Concepts and Applications of Finite Element Analysis," *John Wiley & Sons*, Inc. New York.

CSI (2003). *SAP2000 Analysis Reference*, Computers and Structures, Inc., Berkeley, CA.

EERI (1990). *Loma Prieta Earthquake Reconnaissance Report,* Earthquake Spectra, Supplement to Vol. 6, Earthquake Engineering Research Institute.

FEMA (1997). *NEHRP Guidelines for the Seismic Rehabilitation of Buildings, FEMA 273*; Federal Emergency Management Agency, Washington, D.C.

Filiatrault, A., Uang, C., Folz, B., Chrstopoulous, C., and Gatto, K. (2001). "Reconnaissance Report of the February 28, 2001 Nisqually (Seattle-Olympia) Earthquake," *Rep. No. SSRP 2001/02*, University of California, Berkeley, San Diego.

Housner, G. W. (Chairman) (1990). "Competing Against Time," *Report To The Governor George Deukmejian From The Governor's Board Of Inquiry On The 1989 Loma Prieta Earthquake,*" State of California, Office of Planning and Research.
Hsu, T. T. (1983). "Torsion of Reinforced Concrete," *Van Nostrand Reinhold Company Inc.* New York.

Hsu, T. T. (1990). "Shear Flow Zone in Torsion of Reinforced Concrete," *ASCE Journal of Structural Engineering,* 116(11), 3206-3226.

Imbsen Software Systems (2002), XTRACT: cross-sectional X structural Analysis of Components Analysis Reference, Sacramento, CA.

Ingham, J. (1995). "Seismic Performance of Bridge Knee Joints," Ph.D. Dissertation, The Department of Structural Engineering, University of California, San Diego.

Ingham, J. M., Priestley, M. J .N., and Seible, F. (1994a). "Seismic Performance of Bridge Knee Joints – Volume I," *Rep. No. SSRP 94/12*, University of California, Berkeley, San Diego.

Ingham, J. M., Priestley, M. J .N., and Seible, F. (1994b). "Seismic Performance of Bridge Knee Joints – Volume II," *Rep. No. SSRP 94/17*, University of California, Berkeley, San Diego.

Ingham, M. J., and Sritharan, S. (2003). "Application of Strut-and-Tie Concepts to Concrete Bridge Joints in Seismic Regions," *PCI Journal* 48(4), 66-90.

Jaradat, O. A. (1996). "Seismic Evaluation of Existing Bridge Columns," Ph.D. Dissertation, Department of Civil and Environmental Engineering, Washington State University.

Kramer, S. L., and Eberhard, M.O. (1995). "Seismic Vulnerability of the Alaskan Way Viaduct: Final Summary Report," Report No. WA-RD 363.4, Washington State Department of Transportation, Olympia.

Kingsley, G. R., Seible, F., and Priestley, M. J. N. (1994). "The U.S.-TCCMAR Five-Storey, Full Scale Reinforced Masonry Resaerch Building Test: Part II, Design, Construction and Testing," *Rep. No. SSRP 94/02*, Structural Systems Research, University of California, San Diego, La Jolla, California

Kramer, D. A. and Shahrooz, B. M. (1993)."Cyclic Response of Composite Beam-Column Knee Connections." *Rep. No. UC-CII 93/01*, Cincinnati Infrastructure Institute, University of Cincinnati, Cincinnati, Ohio.

Mander, J. B., Priestley, M. J. N., and Park, R. (1988). "Observed Stress-Strain Behavior for Confined Concrete," *ASCE Journal of Structural Engineering,* 114(8), 1827-1849.

McLean, D. I. (1987). "A Study of Punching Shear in Arctic Offshore Structures," Ph.D. Dissertation, Department of Civil Engineering, Cornell University.

McLean, David I., El-Aaarag, Moein H., and Rogness, Paul D. (2001). "Retrofit of Split Bridge Columns," Report No. WA-RD 363.4, Washington State Department of Transportation, Olympia.

Megget, L. M. (2000). "The Seismic Design and Performance of Reinforced Concrete Beam-Column Knee Joints," *12th World Conference on Earthquake Engineering*, Upper Hutt, New Zealand, CD ROM Paper No. 1058.

Nilson, H. A., Darwin, D., and Dolan, C.W. (2003). "Design of Concrete Structures," *McGraw-Hill College.*

Park, R., and Paulay, T. (1984). "Joints in Reinforced Concrete Frames Designed for Earthquake Resistance," *Rep. No. 84-9*, Department of Civil Engineering, University of Canterbury, Christchurch, New Zealand.

Paulay, T., and Priestley, M. J. N. (1992). "Seismic Design of Reinforced Concrete and Masonry Buildings," *John Wiley and Sons, Inc.*

Priestley, N. M. J. (1993). "Assessment and Design of Joints For Single-Level Bridges with Circular Columns," *Rep. No. SSRP 93/02*, University of California, Berkeley, San Diego.

Priestley, M. J .N. (2003). "Myths and Fallacies in Earthquake Engineering, Revised," *IUSS Press.*

Priestley, M. J. N., and Seible, editors. (1991). "Seismic Assessment and Retrofit of Bridges," *Rep. No. SSRP 91/03*, Department of Applied Mechanics and Engineering Seinces, University of California, San Diego, La Jolla, California

Priestley, M. J. N., Seible, F., Benzoni, G. (1994). "Seismic Performance of Circular Columns with Low Longitudinal Steel Ratios," *Rep. No. SSRP 94/08*, Structural Systems Research, University of California, San Diego, La Jolla, California

Priestley, M. J. N., Seible, F., and Calvi, G. M. (1996), " Seismic Design and Retrofit of Bridges," *John Wiley & Sons*, Inc. New York.

Priestley, M. J. N., Seible, F., Xiao, Y., and Verma, R. (1994). "Steel Jacket Retrofitting of Reinforced Concrete Bridge Columns for Enhanced Shear Strength – Part 2: Test Results and Comparison with Theory," *ACI Structural Journal* 91(4), 394-405.

Roberts, J. E. (1996). "US Perspectives on Seismic Design of Bridges," *Eleventh World Conference on Earthquake Engineering*, Acapulco, Mexico, CD ROM Paper No. 2109.

Sabnis, G. M., and Harris, H. G. (1999). *Structural Modeling and Experimental Techniques*. CRC Press LLC, Boca Raton, Florida.

Stojadinovic, B. and Thewalt, C. R. (1995)."Upgrading Bridge Outrigger Knee Joint Systems." *Rep. No. UCB/EERC-95/03*, Earthquake Engineering Research Center, University of California, Berkeley, California.

T. Y. Lin International, (2001). "Alaskan Way Viaduct: Report of the Structural Sufficiency Review Committee," June 28, 2001.

Wallace, J. W., McConnnell, S. W., and Gupta, P. (1996). "Cyclic Behavior of RC Beam-Column Joints Constructed Using Conventional and Headed Reinforcement," *Eleventh World Conference on Earthquake Engineering*, Acapulco, Mexico, CD ROM Paper No. 655.
Wood, Harry O. (1993) Preliminary report on the Long Beach earthquake. BSSA 23:2 pp.44-56.

Zia, P., White, R. N., and Van Horn, D. A. (1970). "Principles of model Analysis, in models for Concrete Structures," ACI Special Publication SP 24, *American Concrete Institute,* pages 19-39.

Zhang, H., Knaebel, P. J., Coffman, H.L., VanLund, J.A., Kimmerling, R.E., and Cuthbertson, J.G. (1996). "Seismic Vulnerability Study of the SR 99 Spokane Street Overcrossing," Washington State Department of Transportation, Olympia.

APPENDIX

APPENDIX A: JOINT PANEL DEFORMATION

Joint panel modes of deformation for non-rectangular joints can be derived using the same methodology for deriving the strains of a 4-node planar isoparametric element as discussed by Cook et al. (2002). The non-rectangular joint in the actual Cartesian coordinates (x,y) is mapped to an apparent rectangular joint in the natural coordinates (ξ,η) as shown in Figure A1.
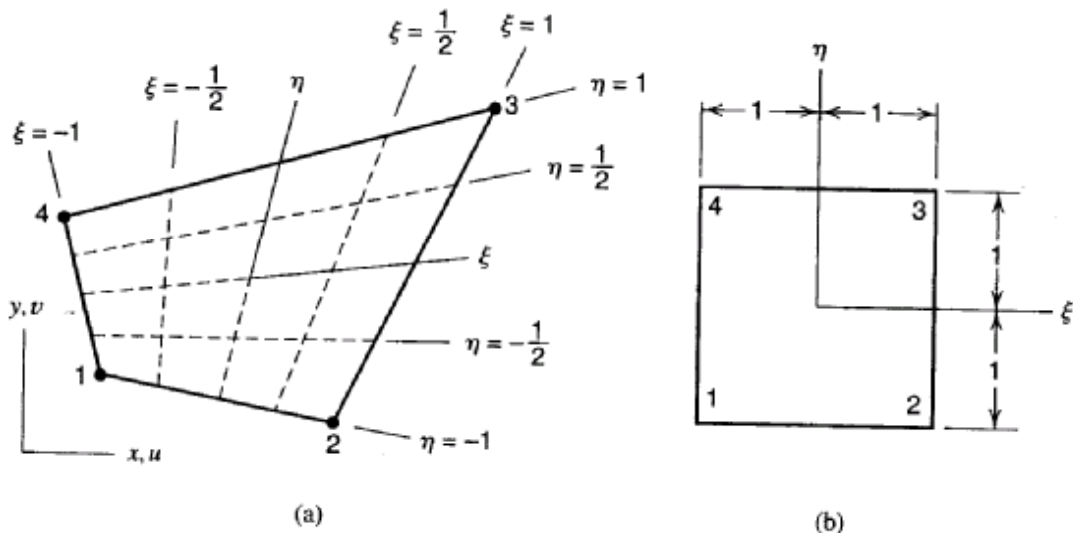

Figure A1 (a) Non-rectangular Joint in Cartesian Space. (b) The Same Joint Mapped into Natural Space (Adapted from Cook et al., 2002)

The coordinates of a 4-node joint in natural coordinates (ξ,η) can be expressed in terms of the actual Cartesian coordinates of the joint as:

$$\begin{Bmatrix} x(\xi,\eta) \\ y(\xi,\eta) \end{Bmatrix} = \begin{bmatrix} N_1 & 0 & N_2 & 0 & N_3 & 0 & N_4 & 0 \\ 0 & N_1 & 0 & N_2 & 0 & N_3 & 0 & N_4 \end{bmatrix} \begin{Bmatrix} x_1 \\ y_1 \\ x_2 \\ y_2 \\ x_3 \\ y_3 \\ x_4 \\ y_4 \end{Bmatrix} \tag{A1.1}$$

where N_1, N_2, N_3 and N_4 are shape functions from Lagrange interpolations:

$$N_1 = \frac{1}{4}(1-\xi)(1-\eta) \tag{A1.2}$$

$$N_2 = \frac{1}{4}(1+\xi)(1-\eta) \tag{A1.3}$$

$$N_3 = \frac{1}{4}(1+\xi)(1+\eta) \tag{A1.4}$$

$$N_4 = \frac{1}{4}(1-\xi)(1+\eta) \tag{A1.5}$$

Similarly, the displacement field (u,v) in the natural coordinate space can be expressed in terms of the actual displacement field in Cartesian coordinates as:

$$\begin{Bmatrix} u(\xi,\eta) \\ v(\xi,\eta) \end{Bmatrix} = \begin{bmatrix} N_1 & 0 & N_2 & 0 & N_3 & 0 & N_4 & 0 \\ 0 & N_1 & 0 & N_2 & 0 & N_3 & 0 & N_4 \end{bmatrix} \begin{Bmatrix} u_1 \\ v_1 \\ u_2 \\ v_2 \\ u_3 \\ v_3 \\ u_4 \\ v_4 \end{Bmatrix} \tag{A1.6}$$

The linear strain-displacement relationship is given by:

$$\begin{Bmatrix} \varepsilon_x \\ \varepsilon_y \\ \gamma_{xy} \end{Bmatrix} = \begin{Bmatrix} u_{,x} \\ v_{,y} \\ u_{,y}+v_{,x} \end{Bmatrix} \tag{A1.7}$$

where ε_x is the strain in the x direction, ε_y is the strain in the y direction, and γ_{xy} is the shear strain. Derivatives of u and v with respect to x and y are not available directly since u and v are functions of ξ and η. Displacement derivatives can be obtained using the chain rule:

$$\frac{\partial u}{\partial x} = \frac{\partial \xi}{\partial x}\frac{\partial u}{\partial \xi} + \frac{\partial \eta}{\partial x}\frac{\partial u}{\partial \eta}$$

$$\frac{\partial u}{\partial y} = \frac{\partial \xi}{\partial y}\frac{\partial u}{\partial \xi} + \frac{\partial \eta}{\partial y}\frac{\partial u}{\partial \eta}$$

(A1.8)

Reorganizing equation A1.8 in a matrix form:

$$\begin{Bmatrix} u_{,x} \\ u_{,y} \end{Bmatrix} = \begin{bmatrix} \xi_{,x} & \eta_{,x} \\ \xi_{,y} & \eta_{,y} \end{bmatrix} \begin{Bmatrix} u_{,\xi} \\ u_{,\eta} \end{Bmatrix}$$

(A1.9)

Equation A1.9 is not available, but the inverse is. Then:

$$\begin{Bmatrix} u_{,\xi} \\ u_{,\eta} \end{Bmatrix} = \begin{bmatrix} x_{,\xi} & y_{,\xi} \\ x_{,\eta} & y_{,\eta} \end{bmatrix} \begin{Bmatrix} u_{,x} \\ u_{,y} \end{Bmatrix}$$

(A1.10)

$$\begin{Bmatrix} u_{,\xi} \\ u_{,\eta} \end{Bmatrix} = [J] \begin{Bmatrix} u_{,x} \\ u_{,y} \end{Bmatrix}$$

(A1.11)

where [J] is called the Jacobian matrix. From equation A1.1, the Jacobian matrix [J] can

be written as the following:

$$[J] = \begin{bmatrix} \Sigma N_{i,\xi}\, x_i & \Sigma N_{i,\xi}\, y_i \\ \Sigma N_{i,\eta}\, x_i & \Sigma N_{i,\eta}\, y_i \end{bmatrix}$$

(A1.12)

Taking the derivatives of the shape functions with respect to ξ and η, the Jacobian matrix

[J] is then equal to:

$$[J] = \frac{1}{4}\begin{bmatrix} -(1-\eta) & (1-\eta) & (1+\eta) & -(1+\eta) \\ -(1-\xi) & -(1+\xi) & (1+\xi) & (1-\xi) \end{bmatrix} \begin{bmatrix} x_1 & y_1 \\ x_2 & y_2 \\ x_3 & y_3 \\ x_4 & y_4 \end{bmatrix}$$

(A1.13)

The Jacobian matrix [J] in equation A1.13 can be computed for any joint shape given ξ

and η. Then, equation A1.9 can be rewritten as:

$$\begin{Bmatrix} u_{,x} \\ u_{,y} \end{Bmatrix} = [J]^{-1} \begin{Bmatrix} u_{,\xi} \\ u_{,\eta} \end{Bmatrix}$$

(A1.14)

Similarly for displacement v:

$$\begin{Bmatrix} v_{,x} \\ v_{,y} \end{Bmatrix} = [J]^{-1} \begin{Bmatrix} v_{,\xi} \\ v_{,\eta} \end{Bmatrix} \qquad (A1.15)$$

Denoting $[J^{-1}]$ as Γ, then:

$$[\Gamma] = [J]^{-1} = \frac{1}{|J|} \begin{bmatrix} J_{22} & -J_{12} \\ -J_{21} & J_{11} \end{bmatrix} \qquad (A1.16)$$

where $|J|$ is the determinant of the Jacobian matrix calculated by the following equation:

$$|J| = \det J = J_{11}J_{22} - J_{21}J_{12} \qquad (A1.17)$$

The deformations of the joint in the Cartesian coordinates can therefore be expressed as:

$$\begin{Bmatrix} u_{,x} \\ u_{,y} \\ v_{,x} \\ v_{,y} \end{Bmatrix} = \begin{bmatrix} \Gamma_{11} & \Gamma_{12} & 0 & 0 \\ \Gamma_{21} & \Gamma_{22} & 0 & 0 \\ 0 & 0 & \Gamma_{11} & \Gamma_{12} \\ 0 & 0 & \Gamma_{21} & \Gamma_{22} \end{bmatrix} \begin{Bmatrix} u_{,\xi} \\ u_{,\eta} \\ v_{,\xi} \\ v_{,\eta} \end{Bmatrix} \qquad (A1.18)$$

Note that the derivatives of the displacement field in the natural coordinates system (ξ,η) is:

$$\begin{Bmatrix} u_{,\xi} \\ u_{,\eta} \\ v_{,\xi} \\ v_{,\mu} \end{Bmatrix} = \begin{bmatrix} N_{1,\xi} & 0 & N_{2,\xi} & 0 & N_{3,\xi} & 0 & N_{4,\xi} & 0 \\ N_{1,\eta} & 0 & N_{2,\eta} & 0 & N_{3,\eta} & 0 & N_{4,\eta} & 0 \\ 0 & N_{1,\xi} & 0 & N_{2,\xi} & 0 & N_{3,\xi} & 0 & N_{4,\xi} \\ 0 & N_{1,\eta} & 0 & N_{2,\eta} & 0 & N_{3,\eta} & 0 & N_{4,\eta} \end{bmatrix} \begin{Bmatrix} u_1 \\ v_1 \\ u_2 \\ v_2 \\ u_3 \\ v_3 \\ u_4 \\ v_4 \end{Bmatrix} \qquad (A1.19)$$

Combining equations A1.18 and A1.19, the deformations of the joint in Cartesian coordinates becomes:

238

$$
\begin{Bmatrix} u_{,x} \\ u_{,y} \\ v_{,x} \\ v_{,y} \end{Bmatrix} = \begin{bmatrix} \Gamma_{11} & \Gamma_{12} & 0 & 0 \\ \Gamma_{21} & \Gamma_{22} & 0 & 0 \\ 0 & 0 & \Gamma_{11} & \Gamma_{12} \\ 0 & 0 & \Gamma_{21} & \Gamma_{22} \end{bmatrix} \begin{bmatrix} N_{1,\xi} & 0 & N_{2,\xi} & 0 & N_{3,\xi} & 0 & N_{4,\xi} & 0 \\ N_{1,\eta} & 0 & N_{2,\eta} & 0 & N_{3,\eta} & 0 & N_{4,\eta} & 0 \\ 0 & N_{1,\xi} & 0 & N_{2,\xi} & 0 & N_{3,\xi} & 0 & N_{4,\xi} \\ 0 & N_{1,\eta} & 0 & N_{2,\eta} & 0 & N_{3,\eta} & 0 & N_{4,\eta} \end{bmatrix} \begin{Bmatrix} u_1 \\ v_1 \\ u_2 \\ v_2 \\ u_3 \\ v_3 \\ u_4 \\ v_4 \end{Bmatrix}
$$

(A1.20)

Note that the deformations can be evaluated at any point in the joint region. For average values, equation A1.20 is evaluated at the centroid of the apparent element (i.e., at ξ and η equal to zero). Note also that the displacement field of the joint, u_1 to u_4 and v_1 to v_4, is not directly recorded through testing. Instead, relative displacements are measured between the nodes. In such a case, the displacement field can be determined by the method of virtual work for trusses. Relative displacement measurements between the joints can be considered as fabrication errors in the members of the truss.

Joint panel deformations, as shown in Figure A2, can be extracted from the general equation A1.20. The first mode is a pure shear mode corresponding to γ_{xy}. The second and the third modes are vertical and horizontal curvature modes, respectively. The fourth and the fifth modes are horizontal and vertical extensions modes corresponding to ε_x and ε_y, respectively.
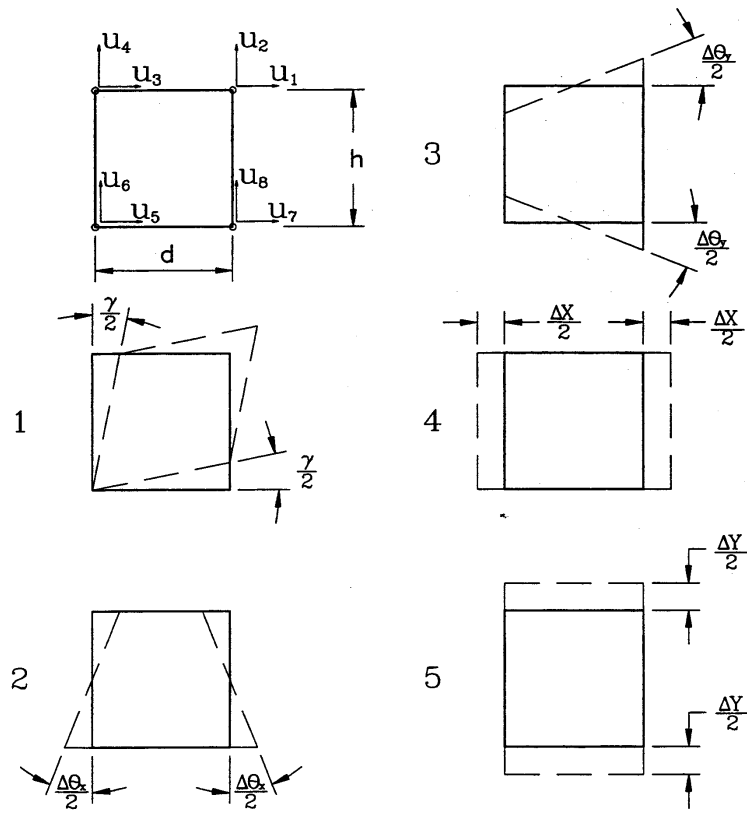
Figure A2 Joint Panel Deformations (Adapted from Kingsley et al., 1994)